AN ABSTRACT OF THE THESIS OF

D. A. McGregor for the degree of Doctor of Philosophy in Mathematics presented on May 26, 2016.

Title: Compatible Discretizations for Maxwell's Equations with General Constitutive Laws

Abstract approved: _____

Vrushali A. Bokil and Nathan L. Gibson

In this thesis we construct compatible discretizations of Maxwell's equations. We use the term compatible to describe numerical methods for Maxwell's equations which obey many properties of vector Calculus in a discrete setting. Compatible discretizations preserve the exterior Calculus ensuring that the divergence of the curl and the curl of a gradient are zero in a discrete setting. This compatibility of discretizations with the continuum Maxwell's equations guarantees that the numerical solutions are physically meaningful.

We focus on the construction of a class of discretizations called Mimetic Finite Differences (MFD). The MFD method is a generalization of both staggered finite differences and mixed finite elements. We construct a parameterized family of MFD methods with equivalent formal order of accuracy. For time-dependent problems, we exploit this non-uniqueness by finding parameters which are optimal with respect to a certain criteria, for example, minimizing dispersion error. Dispersion error is a numerical artifact in which individual frequencies in a wave propagate at incorrect speeds; dominating the error in wave problems over long time propagation.

The novelty of this work is the construction of an MFD discretization for Maxwell's equations which reduces dispersion error for transient wave propagation in materials that

are modeled by a general class of linear constitutive laws. We provide theoretical analysis of these new discretizations including an analysis of stability and discrete divergence. We also provide numerical demonstrations to illustrate the theory.

In addition to applications in the time domain we consider equilibrium Magnetohydrodynamic (MHD) generators. MHD generators extract power directly from a plasma by passing it through a strong magnetic field. Used as a topping cycle for traditional steam turbine generator, MHD offers a theoretical thermal efficiency of 60% compared to 40% of traditional systems. However, this technology has high life cycle costs due to equipment failure. One source of failure is arcing: the formation of high density currents which damage the generator. In this work we develop, analyze, and simulate a model of these generators. We use these simulations to show the viability of detecting electrical arcs by measurements of their magnetic fields outside of the generator.

Compatible Discretizations for Maxwell's Equations with General Constitutive Laws

by

D. A. McGregor

A THESIS

submitted to

Oregon State University

in partial fulfillment of
the requirements for the
degree of

Doctor of Philosophy

Presented May 26, 2016
Commencement June 2016

Doctor of Philosophy thesis of D. A. McGregor presented on May 26, 2016

APPROVED:

Co-Major Professor, representing Mathematics

Co-Major Professor, representing Mathematics

Chair of the Department of Mathematics

Dean of the Graduate School

I understand that my thesis will become part of the permanent collection of Oregon State University libraries. My signature below authorizes release of my thesis to any reader upon request.

D. A. McGregor, Author

ACKNOWLEDGEMENTS

The work herein was supported by a number of individuals and agencies. Great thanks must be given to my advisors Dr. Vrushali Bokil and Dr. Nathan Gibson whose support cannot be understated. I would also like to thank Dr. Rigel Woodside the National Energy Technology Laboratory who invited us to work on the MHD project and who supported my work for three years. I am indebted to Dr. Vitaliy Gyrya, my collaborator and mentor at the Los Alamos National Laboratory, who supervised my work for three summers and introduced me to the Mimetic Finite Difference method. Also at Los Alamos I would thank Dr. Marco Manzini and Dr. Konstantine Lipnikov who hosted me and provided excellent advise and support. I would also like to thank my friend and colleague Dr. Timothy Costa for many long conversations during our time at OSU. Finally this work has been supported by the National Science Foundation Grant # 0811223, by National Energy Technology Grant RES1100426/015, and by the T-5 group of the Los Alamos National Laboratory.

TABLE OF CONTENTS

Page

1 INTRODUCTION 1

1.1 Introduction to Transient Maxwell's Equations 3

1.2 Introduction to Magnetohydrodynamic Generators 11

1.3 Outline 13

1.4 Resulting Publications 14

1.5 Notation 14

2 ELECTROMAGNETIC MODELS 16

2.1 Electricity 16

2.2 Magnetism 19

2.3 Maxwell's Equations 21

2.3.1 Linear Media 23
2.3.2 The Debye Model 24
2.3.3 Drude-Lorentz Model 25
2.3.4 Generalized Polarization Laws 26
2.3.5 Generalized Ohm's Law 28

2.4 Sobolev Spaces 29

3 MIMETIC FINITE DIFFERENCES IN TWO DIMENSIONS 34

3.1 2D DeRham Complices 34

3.2 Preliminaries for Meshes 36

3.3 Discrete Spaces and Primal Operators 37

3.4 Reconstruction and Accuracy 42

3.5 Inner Products 58

3.6 MFD Construction on Rectangular Meshes 66

3.7 Adjoint Operators 72

TABLE OF CONTENTS (Continued)

Page

3.8 Exact Sequence Property 74

4 MFD DISCRETIZATIONS FOR MAXWELL'S EQUATIONS 79

4.1 Semi Discrete MFD Formulations of Maxwell's Equations 79

4.1.1 Transverse Electric Maxwell's Equations in Free Space 80
4.1.2 Transient Maxwell's Equations in a Linear Polarization Media ... 83

4.2 Time Integration 86

4.3 Fully Discrete Approximations for Transient Maxwell's Equations 91

4.3.1 Efficient Treatment of Inner Product Matrices 93
4.3.2 Discrete Gauss' Law and Continuity Equation 96

4.4 Numerical Demonstration of Continuity Equation 100

5 DISPERSION ANALYSIS AND M-ADAPTATION 105

5.1 Introduction to Dispersion Analysis 105

5.2 Continuum Fourier Analysis 106

5.3 Continuum dispersion relations 111

5.3.1 Dispersion Relation for Scalar Wave Equation 113
5.3.2 Dispersion Relation for Maxwell's Equations in Vacuum 113
5.3.3 Dispersion Relation for Maxwell's Equations in Conductive Media 115
5.3.4 Dispersion Relation for Maxwell's Equations in Debye Media 116
5.3.5 Dispersion Relation for Maxwell's Equation in Cold Isotropic Plasma 118

5.4 Discrete Fourier Analysis 119

5.4.1 Dispersion Analysis for MFD Discretizations of Maxwell's Equations 123
5.4.2 M-Adaptation for Free Space 131
5.4.3 Necessary and sufficient conditions for M-adaptation 135
5.4.4 M-adaptation fails for Time Averaged Schemes 138
5.4.5 Dispersion Analysis for the ETMFD 139
5.4.6 M-adaptation for the ETMFD 140

TABLE OF CONTENTS (Continued)

Page

5.5 Numerical Demonstrations of Dispersion Analysis 142

5.5.1 L^2 and Dispersion Errors for Free Space 142
5.5.2 L^2 and Dispersion errors for Cold Isotropic Plasma 147
5.5.3 Numerical Anisotropy in Free Space 150
5.5.4 Numerical Anisotropy in Debye Media 157
5.5.5 Numerical Anisotropy in Collisionless Cold Plasma 158

6 VON NEUMANN STABILITY ANALYSIS FOR M-ADAPTED MFD 161

6.1 Preliminaries 161

6.2 Stability Analysis for M-adapted MFD 163

6.3 Numerical Demonstration of Stability 169

6.3.1 Free Space 169
6.3.2 Linear Polarization Media 171

7 MAGNETOHYDRODYANMIC GENERATORS 173

7.1 Equilibrium Generators 175

7.1.1 Generator Geometry 176
7.1.2 Model Formulation 178

7.2 Well Posedness of Elliptic Electromagnetic Problems 187

7.2.1 Well-Posedness of Electric Currents 188
7.2.2 Well Posedness of Magnetostatics 191

7.3 Heuristic Arcing 194

7.3.1 Magnetic Fields and Parameterized Currents 195
7.3.2 Back-powered Channel with Artificial Conductivities 197

7.4 3D Currents in Equilibrium Generators 201

8 CONCLUSIONS 208

8.1 Open Probems 209

TABLE OF CONTENTS (Continued)

Page

BIBLIOGRAPHY 214

LIST OF FIGURES

Figure		Page
2.1	A simple illustration of the effects of an electric field on a Debye Material	24
3.1	Hilbert complex for discrete spaces.	38
3.2	A commuting diagram relating discrete spaces and their reconstructions.	44
3.3	Local degrees of freedom for the cell f. Arrows on edges represent the orientation of our edges.	67
4.1	By resolving $\mathbb{W}_{\mathscr{E}}^{-1}$ using conjugate gradients to a tolerance of 10^{-15} we produce a discrete charge density $\rho_h^n = \widetilde{\mathrm{div}}_h \mathbf{E}_h^n$ which is pointwise on the order of 10^{-15} for divergence free initial conditions. Over time L^2 norm of ρ_h^n stays bellow 10^{-30} for divergence free initial data. Subfigure (a) shows the charge density $\lvert\rho_h^n\rvert$ at time 2.5 with log scale coloring while subfigure (b) shows the L^2 norm of the field.	102
4.2	(a) We present the difference L^2 divergence error for initial conditions which are not divergence free. (b) we show the quantity $\lVert\rho_h^n\rVert_{L^2}$ at our lowest resolution $h = 2^{-7}$. Charge appears to be conserved throughout computation	102
5.1	Three cells used to assemble the contributions after multiplication by a uniform matrix.	126
5.2	L^2 errors for $\mathbf{E}$ and B for a first order formulation of m-adapted MFD discretization. Errors appear super-quadratic but bellow theoretical estimates	145
5.3	Dispersion errors for $\mathbf{E}$ and B for a first order formulation of m-adapted MFD discretization. Errors appear super-quadratic but bellow theoretical estimates	146
5.4	Using a second order formulation of MFD we recover theoretically optimal errors.	147
5.5	Relative L^2 errors for Experiment 2.	151
5.6	Relative dispersion errors for Experiment 2.	151

Figure Page

5.7 (a) comparison of dispersion errors of the m-adapted MFD and the Yee scheme as a function of angle of propagation θ. Model parameters are $c = 1, k = 4$ solutions are calculated at 12 and 24 points per wavelength. (b) a comparison of dispersion errors for three aspect ratios. Here $c = 1, k = 4$ and we chose 48 h to such that there were 48 points per wavelength. 153

5.8 Yee scheme and M-adapted MFD propagating a radially symmetric pulse in free space generated by initial conditions $\mathbf{E} = 0$ and $B(0) = \mathrm{e}^{-100|\mathbf{x}-(3,3)^T|^2}$ on $[0, 6]^2$. We chose $c = 1$ and $\nu = \frac{1}{2}$. We performed time integration until $T = 2.5$. (a) shows the Yee Scheme and (b) shows the m-adapted MFD 154

5.9 Same experiment as Figure 5.8 but coloring by $\log_{10} |H|$. 154

5.10 We present the amplitude of the discrete field B_h along the circle of radius 2.54 centered at $(3, 3)$. We compute a reference solution with $h = 2^{-11}$ using the M-adapted MFD. 156

5.11 Point-wise relative error of the M-adapted MFD and Yee scheme along the circle of radius 2.54 centered at $(3, 3)$. 156

5.12 We illustrate numerical anisotropy for a Debye medium. (a) shows the amplitude of the electric field along the circle of radius 0.8 centered at (3,3). (b) shows the relative error compared to a reference solution. 158

5.13 We demonstrate levels of numerical anisotropy for a collisionless cold plasma. (a) shows the amplitude of the electric field along the circle of radius 2.01 centered at (3,3). (b) shows the relative error compared to a reference solution. 159

6.1 We show $\|\mathbb{G}^n\|$ for 10 angles of propagation in $(0, 2\pi)$ for 12 and 48 points per wavelength of resolution at $\nu = \frac{1}{2}$. In both cases the norm of the matrix is bounded. The slower rate of oscillation in the higher resolution graph is due to the smaller time steps necessitated by higher resolution. . 170

6.2 Here we show the magnitude of $E_x(0, 1/2)$ for a Fourier mode on $[0, 1]^2$. As we increase ν past the stability condition the method becomes unstable resulting in exponential growth in the solution after a period of seeming stability. 171

Figure Page

6.3 Here we show the maximum of $|\beta_1|$ when $r = \mathrm{i}b$, $\min\{\nu_x, \nu_y\} = \frac{1}{2}$, and $\alpha \in \{1, 1/2, 2\}$. This suggests that the condition $|\Delta t \mathrm{Im}(r)| \ll 1$ may be overly restrictive as the method should be stable for relatively poor resolution of a given mediums resonance frequency. 172

6.4 Illustrates that the norm of the amplification matrix stays bounded over a large number of time steps. Here the Courant number is chosen as $\min\{\nu_x, \nu_y\} = \frac{1}{2}$, $h = 10^{-2}$, and k is chosen so that there are 12 points per wavelength. Ten directions of propagation are chosen in each plot with angle $\theta \in (-\pi/2, \pi/2)$. Note that the norms of the matrix powers stay bounded, although the value of this bound depends upon material parameter r as well as mesh parameter α. 172

7.1 Here we show three prototypical MHD generator configurations – (a) a Faraday channel, (b) a Hall channel, and (c) a segmented Faraday Generator. Pink areas denote the channel which contains the working fluid. Yellow areas are the conductors. Black lines represent wiring connections and resistors. The resistive parts of the casing are not pictured. 177

7.2 We show a cross section of a segmented Faraday channel. Boundaries, interfaces, and subdomains are labeled. 178

7.3 Analysis of the sensitivity of the induced magnetic flux density to the three current density parameters: J_m, s, and θ. 197

7.4 Temperature profiles for a back-powered channel: (a) is the profile along the centerline of the channel while (b) temperature profile across the channel. 199

7.5 Conductivity profiles in the case of no arcing (a) and heuristic arcing (b). Figure (b) shows the $\log_{10}(\sigma)$. 199

7.6 Current densities and streamlines in a back-powered channel. 15 A are added by in the left wire while the right wire is grounded at 0 V. This figure shows a heuristic arc at both electrodes. 200

7.7 Magnetic field measurement configuration for the back-powered channel. 200

Figure Page

7.8 Sensitivity of magnetic fields to σ_a in a back-powered channel. First column is component x, second is component y, third is component z. Rows represent sensors moving counter clockwise starting opposite the wire. 202

7.9 Normalized values on an line in the x direction centered in the channel. (Left) We show temperature, x component of velocity, and gas density. (Right) We show the x component of the Lorentz Force and heat flux. ... 204

7.10 Noramlized values on a line in the y direction centered in the channel. (Left) We show x and y components of velocity. (Right) we show gas density, the xx component of effective conductivity, temperature, and heat flux. 204

7.11 Surface coloring is the voltage while stream lines are current paths. Note concentration of currents at edges of electrodes. 206

7.12 3D current path in end region eddy. Vortical structures may reduce efficiency do to Joule heating 207

7.13 Normalized current densities $|\mathbf{J}|/\max|\mathbf{J}|$ at fluid-electrode interface. Current densities concentrated at the edges of the electrode rather than being uniformly distributed. Further the heat source Q appears to concentrate where $\mathbf{J}$ is concentrated suggesting that the Joule heating is dominant in the boundary region. 207

LIST OF TABLES

Table		Page
1.1	Common notation.	15
4.1	Divergence errors for a free space problem with non-zero divergence initial data. Errors appear to converge at order h^3.	104
5.1	Relative L^2 errors for a first order formulation of the MFD and Yee Schemes.	144
5.2	Relative dispersion errors for a first order formulation of the MFD and Yee Schemes.	145
5.3	Relative errors for a vector wave formulation of the MFD and Yee Schemes.	146
5.4	Relative L^2 Errors for Experiment 2.	150
5.5	Relative Dispersion Errors for Experiment 2.	151
7.1	Boundary conditions for an equilibrium MHD generator.	186

For Jillian

COMPATIBLE DISCRETIZATIONS FOR MAXWELL'S EQUATIONS WITH GENERAL CONSTITUTIVE LAWS

1 INTRODUCTION

The focus of this thesis is on the development of models and discretization techniques for Maxwell's equations motivated by the need to solve challenging problems arrising in electromagnetics. **Maxwell's Equations** are a system of partial differential equations which relate electric fields, electric currents, and magnetic fields to one another. They are named for James Clerk Maxwell, a Scottish physicist who combined the previous works of Faraday and Ampére into a cohesive theory. In essence, Maxwell's equations state that electric fields will wrap around a time varying magnetic field, while magnetic fields wrap around time varying electric fields and currents. In vacuum, this behavior can be reduced to linear wave propagation, c.f. [25].

Maxwell's equations are not complete and must be combined with **Constitutive Laws** which govern the response of the material to the electromagnetic field. In essence, these laws will relate various electromagnetic variables to one another. We consider for the most part **Polarization Laws** and a **Generalized Ohm's Law**. A polarization field describes the behavior of a material where molecular charges are bound in a particular configuration and are not free to move throughout the media – for example water, biological tissues, or cold plasmas, c.f. [25]. Generalized Ohm's law relates electrical currents to

both the electric field as well as the magnetic field via, for example, an anisotropic tensor. When coupled with Maxwell's equations, such a system models wave propagation that is very distinct from the pure wave propagation we observe in free space. For example, a Debye material models a relaxing polarization field where molecules of the material align with the electric field and then relax into a charge neutral configuration after it passes. With realistic coefficients, this model is singularly perturbed and exhibits features of both parabolic and hyperbolic systems, c.f. [49].

We consider numerical solutions of such Maxwell models and thus require a discretization of the continuous model. We develop **compatible discretizations** i.e. those which respect continuum properties but in a discrete setting. The foremost such property is the preservation of the Exterior Calculus– i.e. that the image of the curl is exactly the kernel of the divergence and that the image of the gradient is the kernel of the curl. These discretizations generally consider mixed space formulations of the equations – either relying upon grid staggering for electric and magnetic fields, or stated in a more explicit Galerkin form where each variable will be posed in its own function space. The compatible discretizations we develop in this thesis are Mimetic Finite Difference (MFD) Method.

This thesis is composed of roughly two parts. The first part is a more theoretical development of novel MFD discretizations for Maxwell's equations with linear polarization laws in the time domain. The discretizations we develop will focus on removing a troubling numerical artifact from our simulations; dispersion errors. Our second part is a computational investigation of Magnetohydrodynamic Generators in equilibrium. This investigation will be focused on the sensitivity of magnetic fields to destructive arcing. We will develop a model using Maxwell's equations with generalized Ohm's Law, analyze it, and use simulations of the model in order to determine the practicality of detecting the electromagnetic effects of arcing.

1.1 Introduction to Transient Maxwell's Equations

One of the major challenges of numerical approximation of wave propagation is that discretization errors result in waves travelling at non-physical speeds. This non-physical speed depends both on frequency and direction of propagation. The frequency dependence can be understood in that not all frequencies are equally well resolved by a given mesh, resulting in different magnitudes of error for different frequency components. The angular dependence is really a property of the underlying mesh on which we are simulating wave propagation. This error is called **numerical dispersion** and we refer to the angular dependence as **numerical anisotropy**. We refer to these errors as numerical since they are artifacts of a numerical methods. Many physical systems have **phyiscal dispersion**. In particular, linear polarization models describe **dispersive media** and this frequency dependence of wave speed is a *feature* of the model and a property of the medium.

Numerical dispersion error results in a number of non-desirable features. Foremost is phase error – where a wave packet will travel at an incorrect speed. This is particularly concerning if the simulation is being carried out to determine the arrival time of a wave front– if the wave is travelling at the wrong speed then the method is dubious at best for this application. The second is the formation of spurious oscillations even from infinitely smooth initial conditions. Such "wiggles" are generally very obvious when simulating a non-dispersive system so they can perhaps be reasonably ignored as long as the model of interest is not physically dispersive. However, in a dispersive media when such wiggles may actually be physical, the ability to differentiate between physical and numerical dispersion by eye cannot be trusted. Therefore the quantification and reduction of numerical dispersion is an important step in the validation and verification of numerical algorithms for wave problems.

The curl-conforming finite element (FE) discretizations (edge elements), first devel-

oped by Nédélec and Whitney [44, 45], are very popular for the spatial discretization of the first order Maxwell equations or the second order vector wave equation. The popularity of edge discretizations is due to their ability to preserve the Exterior Calculus in contrast to nodal discretizations of the vector wave equation based on nodal finite elements [26, 41, 42, 43, 57]. Edge discretizations also allow for easy implementation of boundary and material interface conditions by automatically ensuring the continuity of the tangential and normal components of the vector fields [29, 38, 59]. The application of edge discretizations is a standard technique in more complicated material models, see for example [22, 32, 58] and references therein for discretization for polarization and metamaterial models.

One of the issues with FE discretizations for wave equations in general, and Maxwell's Equations equation in particular, is that a non-diagonal mass matrix has to be inverted at each time step of the solution of the resulting discrete system. This is highly inefficient for a problem where the number of time steps is typically on the order of the number of spatial steps (due to a Courant-type stability condition). A popular remedy has been an approximation of the mass matrix M with a diagonal matrix D obtained by lumping all entries of the mass matrix to the diagonal. Hence, the name for the procedure – *mass lumping*. Mass-lumped methods maintain the same order of the dispersion error as their non-lumped counterparts, however they often suffer from larger constants in their dispersion errors [40].

One of the most popular finite difference (FD) methods for the numerical discretization of Maxwell's equations is the Yee scheme [62] which has been shown to be equivalent to a mass-lumped version of the lowest order Nédélec FE method on a uniform cubic mesh [37]. An extensive overview of numerical methods for wave equations in the time domain can be found in [11]. This includes high order finite difference, high order finite element methods, and numerical dispersion analysis for the acoustics, linear elasticity, and

Maxwell's equations.

The Mimetic Finite Difference (MFD) method is a discretization technique for a large class of partial differential equations. The essential philosophy of the MFD is a *mimicry* of continuum vector Calculus in a discrete setting. A history of the method can be found in the review by Lipnikov, Manzini, and Shashkov in [34]. The history they describe is, in essence, first the development of discretizations on rectangular meshes and then proving the resulting schemes obey discrete analogues of continuum properties. For example, the Yee Scheme or Finite Difference Time Domain Method (FDTD), first developed by Kane Yee at Lawrence Livermore National Lab, c.f. [63], fits solidly into this framework. The method was developed to be second order accurate and then it was proven that it preserved a discrete analogue of the divergence for electric displacements and magnetic induction. Also fitting in this framework are staggered finite volume methods in which discrete operators are defined exactly by the divergence theorem – mimicking conservation and other desirable properties.

There is then a transition to a development focused first on discrete mimicry and then proving approximation properties of the resulting schemes by way of polynomial consistency conditions, roughly analogous to a patch test. This approach allows for the development of schemes on non-orthogonal meshes. See, for example, the work of Shashkov and Hyman for Maxwell's equations on logically rectangular meshes, c.f. [24].

In order to expand the method to more general types of polygonal and polyhedral meshes, a more rigorous approach to defining inner products and polynomial consistency was necessary. Results from this can be seen, for example, in the discretization methods of Lipnikov, Manzini, Brezzi, and Buffa for 3D magnetostatics on polyhedral meshes, c.f. [33]. A very complete description of lowest order MFD methods using this approach can be found in the book [2] as well as a review paper [34]. This deeper understanding of necessary polynomial consistency has led to arbitrary order formulations [20]. This approach has also

led to a purely variational formulation of MFD called the Virtual Element Method (VEM). Here the elements are virtual in that shape functions are not defined explicitly. Rather they are assumed satisfy a particular PDE, one which a particular class of polynomials, and some unknown other functions, will also satisfy. An early exploration of this approach can be found in [3]. The literature for VEM is still developing but there have been recent efforts in extending the approach to the DeRham Complex, [4].

The MFD method is a hybrid method adopting ideas and techniques from staggered finite differences, finite volumes, and mixed finite elements. In the MFD method we solve for degrees of freedom of a solution to a PDE rather than finding an approximating function, making it in some sense analogous to a finite difference scheme. The MFD defines discrete primal differential operators by the Stokes's theorem analogously to the finite volume method. The MFD also develops a discrete analogue of the inner product allowing for the discretization of weak formulations of PDE similar to fixed finite elements. In the MFD a well defined mapping exists between grid functions and an approximation space in the traditional finite element sense. Instead of considering control volumes around each of the variables and applying Stokes's theorem to compute fluxes, we define discrete adjoint operators for certain operators which are discretizations of weak derivatives. Finally, MFD is well defined on a large class of polygonal and polyhedral meshes rather than only on relatively simple shapes such as triangles, squares, tetrahedra, hexahedra, or pyramids as is typical in the finite element method.

There are many ingredients in a MFD method. First one must have a mesh of a domain which is nice in a topological sense. It must be a connected domain and we disallow connection between two cells to occur only at a vertex. Next we define discrete spaces of *grid functions* which are interpreted as degrees of freedom of functions sitting in appropriate Sobolev spaces. Next we define discrete analogues of differential operators on these discrete spaces – however, the operators constructed will not be sufficient on their

own to define a mixed space discretization. For example, we will construct only the gradient operator but will require a divergence operator as well. These operators are defined to preserve commutativity properties – namely that one can apply a discrete operator to the interpolant of a function or apply a continuum operator and then interpolate, and recover an identical result. Once spaces and operators are defined we construct a linear isomorphism between discrete spaces and a finite dimensional approximation space. We define this map as the *reconstruction operator* and we develop this mapping so that the reconstructed space is a virtual element space – that is it contains piecewise polynomials of a particular order and other shape functions which are of minimal norm and have a specified set of degrees of freedom. Once the accuracy of discrete spaces is established we construct polynomially consistent *inner product matrices* with in order to discretize weak formulations. The construction of inner product matrices is non-unique. A closed form exists for a stable choice of this matrix. However, there is no guarantee that this matrix will be optimal. The selection of an optimal inner product matrix for a given problem is called **M-adaptation**. We exploit this non-uniqueness by constructing parametric families of inner products. The number of parameters in these matrices grows rapidly with the dimension of the space, the number of sides on our cells, and with the order of polynomial approximation. Once we have constructed a discrete inner product we can complete the set of necessary discrete differential operators by defining *adjoint operators* which are discrete weak derivatives.

Bokil and Gibson [6] considered a number of FD discretizations of Maxwell's equations for which they demonstrated reduction of numerical dispersion when the spatial discretization order was increased from second to fourth while maintaining second order for the temporal discretization. Increasing the spatial discretization beyond fourth order did not produce any significant reduction in the dispersion error. Smith, et al. [55] were able to eliminate fourth order dispersion error by using a modified fourth-order FD

method in space and time. The modified stencil of the FD method was obtained as a weighted average of various rotated stencils.

The problem of constructing methods with optimal numerical dispersion properties has been considered in the case of acoustics, where similar results were obtained using FD and FE-type discretizations. In particular, Jo et al. [27] and Stekl and Pratt [56] derived an optimized 9-point FD method in two space dimensions for an acoustic wave equation in the frequency domain. Their idea was to consider a weighted average of the standard and "diagonal" FD methods and optimize the resulting scheme for the weights. Sescu et al. [54] extended this idea to three space dimensions.

One can approach the reduction of dispersion with time domain finite element methods (TDFEM) by employing higher order discretizations. However, as mentioned above, drawback of this approach is the necessity of inverting the mass matrix at every time step. Fisher et al. in [15] addressed this issue by employing a generalized mass lumping technique. Their approach was to increase the computational efficiency of high order Nédélec Elements by choosing Gauss-Lobatto quadrature points and using these quadratures to resolve the integrals of the mass and stiffness matrices. On orthogonal Cartesian meshes their method produces a diagonal mass matrix and on more general geometries the sparsity of the mass matrix is greatly reduced if non-diagonal. As is typical of Nédélec elements, they recover a dispersion error of order $2p$ where p is the polynomial degree. This approach is philosophically different than our approach: while they attempt to make an accurate method more efficient, we will make an efficient method more accurate. Our optimization technique produces a method which has a formal L^2 error of order two and dispersion error of order four producing higher quality solutions than those produced by the lowest order Nédélec elements. A natural extension of our work is the development of both higher order discretizations using M-adaptation and an extension to hexahedral meshes.

Another technique based on the FE framework is closer to our method, see e.g., [19, 28, 64]. Instead of using the typical lumping, i.e., by approximating the mass matrix $\mathbb{M}$ with a diagonal matrix $\mathbb{D}$, an approximation of the mass matrix $\mathbb{M} \approx \mathbb{D}\mathbb{M}^{-1}\mathbb{D}$ is used. This approach makes approximation of $\mathbb{M}^{-1} \approx \mathbb{D}^{-1}\mathbb{M}\mathbb{D}^{-1}$ simple, as it involves inverting a diagonal matrix $\mathbb{D}$. Also, in this approach the mass matrix $\mathbb{M}$ is retained in the scheme, which becomes important in the optimization step. The optimization step is similar in spirit to utilizing weighted combinations of standard and rotated stencils in the FD approach.

Our approach to the reduction of dispersion on rectangular grids is to exploit the non-uniqueness of the MFD. We begin by constructing a family of discretizations for two dimensional Maxwell's equations in free space. We discretize in time using staggered leap frog and in space using MFD. This family of schemes includes both the Nedélec method and the Yee Scheme, both of which have second order dispersion errors. By performing dispersion analysis on a parameterized family of discretizations and carefully choosing our parameters we are able to select an optimal member with order four dispersion. In this case the resulting stencil is roughly twice the size of the Yee scheme yet comparable to the Nedelec scheme. We call the resulting scheme the **M-Adapted MFD** for Maxwell's Equations.

We next extended this approach to a large class of linear polarization models, for example cold plasma, namely those models which can be modeled as linear, first order, system of ODE driven by the electric field. We first attempted to apply the standard semi-implicit time averaged schemes for these models. For this time integrator applied to these models M-adaptation to reduce dispersion fails. We then considered less typical integrators including **Exponential Time Differencing** (ETD).

The ETD method was originally introduced in computational electromagnetism as a scheme for handling stiff problems, such as computing the electric and magnetic

fields in a box surrounded by perfectly matched layers [13]. For these problems, explicit time-stepping, for example the Leapfrog time differencing method, requires an extremely small time step in order to be stable. On the other hand implicit schemes that are unconditionally stable can be costly to implement in three dimensions. ETD involves an exact integration of some of the lower order linear terms in the governing equations, and higher order accuracy can be obtained by using a higher order discretization of the resulting integral terms. However, the ETD approach has been shown to offer no major advantages over the time averaging of the lower order linear terms in the Yee scheme, for alleviating stiffness. In some cases, ETD may be less efficient by necessitating smaller step sizes [50]. We would like to emphasize that the reason for the choice of ETD in our work is not for handling stiffness, but rather that it is a good candidate for a time discretization method which allows for successful optimization in the M-adaptation technique.

In contrast to other numerical methods for the cold plasma model that use ETD discretization only for the equation of polarization current density [14], our ETMFD method is a discretization of a hybrid PDE-ODE system modeling the evolution of the polarization current density and electric field forced by spatial derivatives of field variables.

It is possible to apply the M-adaptation technique to discretization of Maxwell's Equations with a general polarization law using MFD in space and ETD in time. We call the resulting scheme the **M-Adapted ETMFD** for Maxwell's Equations in a General Polarizaiton Media. This method uses an identical choice of parameters as the free space case and still has super convergent dispersion error at order four. The equivalent properties between the two schemes can be shown as ETD is the correct generalization of the leap frog and taking limits as our polarization properties go to zero one would recover exactly the free space discretization. In addition to the superior convergence properties we also prove that the M-Adapted schemes obey a stability requirement identical to the Yee scheme. Further, both the MFD and ETMFD also preserve a discrete analogue of Gauss' Law

exactly in the absence of source currents.

1.2 Introduction to Magnetohydrodynamic Generators

Direct power extraction via magnetohydrodynamic (MHD) principles offers a potential step improvement in thermal efficiencies over energy systems utilizing traditional turbomachinery [60]. This is principally due to the lack of moving parts in an MHD generator, as the temperature limits of the moving parts tend to limit cycle temperatures in traditional combustion driven systems. A history of MHD power generation technologies can be found in [35]. It is also worth noting that the Proceedings of the Symposia on Engineering Aspects of Magnetohydrodynamic Power Generation are a primary source for the development of MHD power. Many fundamental notions and concepts on which this work rests are based on the papers published in this series. Some of these papers are now available online through the US Department of Energy OSTI website.

It was established that a major weakness toward commercialization of MHD power generation is the durability of the current collectors on the walls of the generator (electrodes). The electrodes must withstand harsh conditions, and the most damaging and perhaps most difficult to predict phenomenon experienced in the generator is arcing. Consider the example of an oxyfuel kerosene MHD Generator with a water-cooled, copper channel. The combustion product will be at approximately 2500 K while the channel will be kept at a temperature near 500 K. This large difference in temperature causes a thermal boundary layer to form in the plasma, where the bulk flow will be much hotter than a thin layer near the edge of this channel. As the plasma is thermally ionized, the conductivity will drop in this boundary layer. Large arcs of high current density will then form near the electrodes as the current which is forced through the electrodes will have to “jump the conductivity

gap." The literature on arcing in MHD generators is extensive, c.f. [36, 46, 52, 53] and references therein.

In the arc state we expect the current densities at the wall to be many orders of magnitude larger than in the diffuse state. Given these large differences in current density, the induced magnetic fields are measurably different near the arc. Therefore properties of the current density may be inferred via measurements of the induced fields. The idea of reconstructing current densities from external magnetic flux density measurements has been successfully applied to fuel cells and vacuum arc remelters [61]. The standard approach to this problem is to apply the Biot-Savart law and solve a system of *integral equations*. This formulation unfortunately requires many assumptions on the geometry and the model parameters. Instead, one can formulate the inversion by way of a simulation-based parameter estimation. This technique requires the simulation of a forward problem whose inputs are parameterized explicitly. One then matches the solution of the model to measured data by minimizing the discrepency between data and simulation using non-linear optimization techniques in the parameter space.

It is our goal here is two three two fold. First we will develop a 3D model of equilibrium MHD generators and produce simulations showing that this model is qualitatively correct. Second we will provide a proof of concept for inversion, via sensitivity analysis, that current densities inside the channel of a magnetohydrodynamic generator (MHDG) can indeed be estimated from external measurements of the induced magnetic fields. This is in comparison to using measurements of the applied field which will most often already be known. It is worth noting that the induced fields are expected to be significantly smaller than the applied field of the generator, which will be a practical issue in the design of experiments.

1.3 Outline

In Chapter 2 we present a brief introduction to electromagnetism, Maxwell's Equations, and a variety of material models.

In Chapter 3 we present a theoretical development of the Mimetic Finite Difference Method suitable for discretizations Maxwell's equations in two dimensions. This development will seek to establish similarities between the MFD and Virtual Element Methods.

In Chapter 4 we will present semi-discrete and fully discrete approximations for Maxwell's equations. In addition we will prove a number of properties of these methods including analyzing the divergence of these schemes. We will present numerical results demonstrating some of these properties.

In Chapter 5 we will introduce dispersion analysis for both continuum and discrete equations. Using these techniques we will then analyze the dispersion properties of a family of mimetic discretizations and perform M-adaptation. These results will be developed first for free space and then extended to general linear polarization laws. We present numerical results supporting our theoretical findings.

In Chapter 6 we will prove necessary conditions for stability of the M-adapted Methods constructed in Chatper 5. We will present numerical results demonstrating the sufficiency of these conditions as well as demonstrating that violating the conditions indeed leads to instability.

In Chapter 7 we will establish a model for equilibrium magnetohydrodynamic generators. We will then prove the electromagnetic fields in this model are well posed and that magnetic fields depend continuously on the electrical conductivity of the medium. We will present a numerical study of the sensitivity of magnetic fields to a heuristic model of arcing. Finally we will numerically investigate the qualitiative features of our equilibrium model.

In Chapter 8 we will present conclusions and a number of open problems.

1.4 Resulting Publications

This thesis resulted in the following works accepted or published in peer reviewed journals.

1. V. A. Bokil, N. L. Gibson, V. Gyrya, and D. A. McGregor. *Dispersion reducing methods for edge discretizations of the electric vector wave equation*, J. Comput. Phys. 287 (2015), pp. 88-109.

2. V. A. Bokil, N. L. Gibson, D. A. McGregor, and C. R. Woodside. *Toward estimating current densities in magnetohydrodynamic generator*, J. Phys. Conf. Sers. 640 (2015), p. 012032.

3. V. A. Bokil, V. Gyrya, and D. A. Mcgregor. *A dispersion minimized mimetic method for cold plasma*, ECCOMAS (2016), accepted.

1.5 Notation

TABLE 1.1: Common notation.

$\mathbf{E}$	an electric field	$\mathbf{D}$	an electric induction
$\mathbf{B}$	a magnetic flux density or induction	$\mathbf{H}$	a magnetic field
$\mathbf{J}$	current density	$\mathbf{I}$	current
$\mathbf{u}$	a velocity field	T	temperature
V	Voltage or potential difference	ρ	charge or mass density
ϵ	electrical permittivity	μ	magnetic permeability
η	electron mobility	e	electron charge
ν	fluid viscosity	c	speed of light
τ	a relaxation time	ω_I	ion collision frequency
ω_P	plasma frequency	ω_0	natural frequency
σ	electrical conductivity	ϵ_Δ	relative permittivity gap
ω	frequency	$\mathbf{k}$	wave vector
k	wave number $k = \lvert\mathbf{k}\rvert$		
∇	the gradient operator	div	the divergence operator
curl	the curl operator or vector curl in 2D	curl	the scalar curl in 2D
$\triangle$	the Laplacian	dV	infinitesimal of integration, 3D
dA	infinitesimal of integration, 2D	ds	infinitesimal of integration, 1D
$\subseteq$	the subset relation	$\leq$	when arguments are spaces, subspace relation
$\overline{A}$	the closure of A	∂A	the boundary of A
Δx	x-axis resolution	Δy	y-axis resolution
Δt	time resolution	h	spatial resolution
ν	Courant number $\nu = \frac{c\Delta t}{h}$	α	aspect ratio $\alpha = \frac{\Delta y}{\Delta x}$

2 ELECTROMAGNETIC MODELS

In this chapter we will provide a brief introduction to electromagnetics, following closely the development of [18] and [25]. We will introduce electric and magnetic fields in the stationary, or static, case and then conclude with a description of the time dependent Maxwell's equations. Our development of the time dependent case will in terms of empirical observations and then from these derive differential equations. Beginning with a static, or steady, assumption will allow for an intuitive motivation of what electric and magnetic fields are while removing much of the complexity of deriving time varying fields from fundamental principals which requires physics outside the scope of this thesis. In section 2.1 we introduce electric fields and variables associated with charge. In section 2.2 we introduce magnetism. In section 2.3 we introduce Maxwell's equations and present a number of constitutive laws. In section 2.4 we introduce function spaces suitable for the variational treatment of Maxwell's Equations.

2.1 Electricity

In this section we will investigate the physical phenomenon related to electricity and electric fields. The fundamental dimensional quantity we will discuss here is **charge**. Unlike mass, charge is a signed dimension with negative charge corresponding to electrons and positive charges corresponding to protons. Charge is measured in the unit of Coulombs (C) and the fundamental charge is that of the electron which we denote as $e \approx -1.6 \times 10^{-19}$ C. Before the development of classical electromagnetics, the forces exerted on charge were analogized to that of gravity–i.e., there is a force proportional to the distance squared between two particles. This force is described by Coulomb's law which states that the

force exerted on a particle with charge q_1 at spatial location $\mathbf{x}_1$ by a particle of charge q_2 at $\mathbf{x}_2$ is given by

$$\mathbf{F} = k_e \frac{q_1 q_2}{|\mathbf{r}|^3} \mathbf{r} \tag{2.1.1}$$

where $\mathbf{r} = \mathbf{x}_2 - \mathbf{x}_1$, and k_e is the Coulomb constant

$$k_e = 8.99 \frac{\mathrm{N\ m}^2}{\mathrm{C}^2} \tag{2.1.2}$$

where Newtons (N) is the fundamental unit of force and the meter m is measure of distance.

With the work of Faraday a radically different notion was adopted. Instead of considering forces as being driven by distinct particles we consider a globally defined vector field with units of force per unit charge $\frac{\mathrm{N}}{\mathrm{C}}$. This vector field is called *the electric field*, denoted by $\mathbf{E}$, and a particle with charge q sitting in an electric field at location $\mathbf{x}$ will have a force of $q\mathbf{E}(\mathbf{x})$ exerted upon it. To extract the value of this electric field we will define it in terms of an infinite superposition of Coulomb forces.

Let ρ be the volumetric charge density with units of $\frac{\mathrm{C}}{\mathrm{m}^3}$. The force acting on a charge q at a point $\mathbf{x}$ can then be defined by summing of all of the Coulomb forces.

$$\mathbf{F}(\mathbf{x}) = \frac{q}{4\pi} \int \frac{1}{\epsilon} \rho \frac{\mathbf{y} - \mathbf{x}}{|\mathbf{y} - \mathbf{x}|^3}\ dV. \tag{2.1.3}$$

Here ϵ is called the *electrical permittivity*. In the case of vacuum we have

$$k_e = \frac{1}{4\pi\epsilon_0} \tag{2.1.4}$$

where ϵ_0 is the electrical permittivity of vacuum. In all materials electrical permittivity determines how easily charges can reorient themselves in the presence of electric forces. We can then define $\mathbf{E}$ by the equation

$$\mathbf{F} = q\mathbf{E}. \tag{2.1.5}$$

The electric field is force per unit charge. We can define a quantity which is roughly analogous to work. We call this value the *voltage or electric potential (energy)*. Let Γ be

some path in space. We define the potential difference between the start point and end point of the path Γ to be

$$\Delta V = \int_{\Gamma} \mathbf{E} \cdot ds. \tag{2.1.6}$$

The voltage V has units of energy per unit charge defined as volts $\mathrm{V} = \frac{\mathrm{J}}{\mathrm{C}}$. In essence, moving a particle of charge q along the path requires work given by $q\Delta V$. We define the scalar voltage function $V(\mathbf{x})$ by fixing some point $\mathbf{x}_c$ and defining

$$V(\mathbf{x}) = \int_{\mathbf{x}_c}^{\mathbf{x}} \mathbf{E} \cdot ds. \tag{2.1.7}$$

From this definition we see that voltage is only well defined up to a constant as we could move the center $\mathbf{x}_c$ and change the field by a factor of ΔV, i.e.

$$\int_{\mathbf{y}_c}^{\mathbf{x}} \mathbf{E} \cdot ds = \int_{\mathbf{y}_c}^{\mathbf{x}_c} \mathbf{E} \cdot ds + \int_{\mathbf{x}_c}^{\mathbf{x}} \mathbf{E} \cdot ds = \Delta V + V(\mathbf{x}). \tag{2.1.8}$$

We will finally describe a final electric quantity which was a major contribution of Maxwell. Define the field

$$\mathbf{D}(\mathbf{x}) = \frac{1}{4\pi} \int \rho \frac{\mathbf{x} - \mathbf{y}}{|\mathbf{x} - \mathbf{y}|^3} \, d\mathbf{y}. \tag{2.1.9}$$

This field, which we will call the *electric displacement field* has units of charge per unit area $\frac{\mathrm{C}}{\mathrm{m}^2}$. A physical interpretation for this field is not straight forward. The field $\mathbf{D}$ at a point $\mathbf{x}$ is the superposition of the product of charge with displacement weighted by the displacement cubed.

We can now pose our first and simplest constitutive law for electric fields.

$$\mathbf{D} = \epsilon \mathbf{E} \tag{2.1.10}$$

This constitutive law states that $\mathbf{D}$ and $\mathbf{E}$ must be proportional for materials which possess a scalar valued permittivity ϵ or $\mathbf{D}$ and $\mathbf{E}$ must be linearly dependent pointwise when ϵ is matrix valued. There are materials for which this is not true and we can introduce

an additional field to account for the discrepancy. We call this discrepancy field field $\mathbf{P}$, the electric polarization. This field can be used to represent a preferred orientation or structure to the charges in the domain. A constitutive law including polarization is given as

$$\mathbf{D} = \epsilon\mathbf{E} + \mathbf{P}. \tag{2.1.11}$$

2.2 Magnetism

In this section we will now discuss magnetism. The magnetic effect is due to the motion of charges rather than being induced from a fundamental dimension like charge or mass. Such a quantity is hypothetically referred to as a monopole. As no such quantity is observed we call our universe *monopole free*.

So far we have assumed that charges remain fixed in space. We will now establish a notion of the flow rate of charge. We call this quantity *current*, denoted by $\mathbf{I}$, with units of charge per second $\frac{\mathrm{C}}{\mathrm{s}}$ and oriented in the direction of flow. We will denote the norm of this quantity I. As we are concerned with continuum objects we define the current density $\mathbf{J}$ through an arbitrary surface A as

$$\mathbf{I} \cdot \mathbf{n} = \int_A \mathbf{J} \cdot \mathbf{n} \, dA \tag{2.2.1}$$

A very clean theory of magnetism can be developed using the Special Theory of Relativity and in particular using Lorentz transformations. Namely that one develops electrostatics in an inertial frame of reference and then describes magnetic fields as arising when changing frame of reference. However, the elegance of this approach requires significant theory which is not directly relevant to the rest of this work. We will instead consider a less profound, but simpler development.

We consider a theoretical object referred to as a *dipole* an infinitesimal bar magnet.

In the presence of a magnetic field a dipole will orient itself with the magnetic field. The direction in which a dipole at given point in space orients in the presence of a magnetic field is in the direction of a field $\mathbf{B}$ which we call the **magnetic flux density** or **magnetic induction**. The magnitude of $\mathbf{B}$ is then given by the amount of torque exerted on the dipole

$$\boldsymbol{\tau} = \boldsymbol{\mu} \times \mathbf{B} \tag{2.2.2}$$

where $\boldsymbol{\mu}$ is called the dipole moment. Magnetic fields exert forces on *moving charges* by way of the empirical relation

$$\mathbf{F} = q\mathbf{u} \times \mathbf{B}, \tag{2.2.3}$$

where $\mathbf{u}$ is the velocity of the charged particle. This law gives us units for the field $\mathbf{B}$ in terms of force per amp per meter $\frac{\mathrm{N}}{\mathrm{Am}}$ which we define as the unit Tesla (T). This relation can be posed on an object with charge density rather than a point charge by

$$\mathbf{F} = \int \rho\mathbf{u} \times \mathbf{B}. \tag{2.2.4}$$

Since velocity times charge density is exactly the flow rate of charge per unit area, we have a continuum scale relation

$$\mathbf{f} = \mathbf{J} \times \mathbf{B}. \tag{2.2.5}$$

where $\mathbf{f}$ is the volumetric force density.

Similar to electric fields we can then define the magnetic field induced by a steady current density by the Biot-Savart law

$$\mathbf{B}(\mathbf{x}) = \int \frac{\mu}{4\pi}\mathbf{J} \times \frac{\mathbf{y} - \mathbf{x}}{|\mathbf{y} - \mathbf{x}|^3}\, dV. \tag{2.2.6}$$

Here μ is a material dependent proportionality constant called the *magnetic permeability* which the integral could change point by point in space. Also similar to the electric

variables we introduce a quantity roughly analogous to **D**, which we call the *magnetic field* denoted by **H**. It obeys a simple constitutive relation

$$\mathbf{B} = \mu\mathbf{H}. \tag{2.2.7}$$

which may not be true for all materials as it requires, as in the electric field cases, **B** and **H** to be proportional or linearly dependent. We introduce a field which would account for a non-linear discrepancy by defining the *Magnetization Field* denoted by **M**. Playing a roll similar to electrical polarization we can introduce a general constitutive law by

$$\mathbf{B} = \mu\mathbf{H} + \mathbf{M}. \tag{2.2.8}$$

2.3 Maxwell's Equations

Maxwell's equations are the synthesis of Faraday's Law and Ampére's Law. Faraday's law relates time varying magnetic fields to the curl of electric fields. It can be measured experimentally by attaching a voltmeter to a loop of wire and then moving a magnetic field in and out of the loop. The results of this experiment obey

$$\frac{\partial}{\partial t}\Phi = -\Delta V \tag{2.3.1}$$

where Φ is the total magnetic flux through the area contained in the loop. This statement can be rewritten as

$$\frac{\partial}{\partial t}\Phi = \frac{\partial}{\partial t}\int_{\Gamma} \mathbf{B}\cdot\mathbf{n}\, dA \tag{2.3.2}$$

$$-\Delta V = -\int_{\partial\Gamma} \mathbf{E}\cdot ds \tag{2.3.3}$$

which states that the total magnetic flux through the surface Γ is exactly the circulation of the electric field along the boundary.

Applying Stokes' Theorem and assuming sufficient regularity in time of $\mathbf{B}$ and in space on $\mathbf{E}$ we can pose this as the equation

$$\int_{\Gamma} \left(\frac{\partial}{\partial t}\mathbf{B} + \mathbf{curlE} \right) \cdot \mathbf{n} \; dA = 0. \tag{2.3.4}$$

By letting $|\Gamma| \to 0$ and choosing arbitrary surfaces in 3D we can deduce the differential equation

$$\frac{\partial}{\partial t}\mathbf{B} = -\mathbf{curl\ E} \qquad \text{Faraday's Law.} \tag{2.3.5}$$

An experiment to demonstrate Ampére's Law can be described as follows. Take a long wire and run a current through it. Then take a short segment of wire carrying a small current and measure the force acting on it as you move this current about the first. By carefully noting the direction and magnitude of this force, we can determine the direction and magnitude of the magnetic field about some loop around the large current.

By carefully integrating the magnetic field tangent to this loop we derive the result:

$$I = \int_{\partial\Gamma} \mathbf{H} \cdot ds \tag{2.3.6}$$

$$\int_{\Gamma} \mathbf{J} \cdot \mathbf{n} = \int_{\partial\Gamma} \mathbf{H} \cdot ds \tag{2.3.7}$$

The Maxwell correction to Ampére's Law was to decompose $\mathbf{J} = \sum_i \mathbf{J}_i$ and recognize that the time derivative of the electric displacement

$$\frac{\partial}{\partial t}\mathbf{D} \tag{2.3.8}$$

is a current. Applying this we end up with the **Maxwell-Ampére Law**, which states that

$$\frac{\partial}{\partial t}\mathbf{D} + \mathbf{J} = \mathbf{curl\ H} \qquad \text{Maxwell-Ampére Law.} \tag{2.3.9}$$

In addition to these first order time dependent equations, Maxwell's equations are bound by two divergence conditions. The first of which is the monopole free condition for magnetic fields. This condition follows from the lack of free magnetic charges and is posed

as

$$\text{div } \mathbf{B} = 0. \tag{2.3.10}$$

This condition can be derived from Faraday's law by taking the divergence of both sides.

$$\frac{\partial}{\partial t}\text{div } \mathbf{B} = -\text{div } \mathbf{curl\ E} = 0. \tag{2.3.11}$$

Then assuming that div$\mathbf{B}(0) = 0$ we have that it must remain zero for all time. **Gauss' Law**, on the other hand relates to electric charges and states that

$$\text{div } \mathbf{D} = \rho. \tag{2.3.12}$$

Combining these four equations we have a system of four partial differential equations (PDEs) referred to as **Maxwell's Equations**

$$\begin{cases} \dfrac{\partial}{\partial t}\mathbf{D} + \mathbf{J} = \mathbf{curl\ H}, & \text{Ampére-Maxwell Law} \\ \dfrac{\partial}{\partial t}\mathbf{B} = -\mathbf{curl\ E}, & \text{Faraday's Law} \\ \text{div } \mathbf{D} = \rho, & \text{Gauss' Law} \\ \text{div } \mathbf{B} = 0. & \text{Gauss' Law for Magnetism} \end{cases} \tag{2.3.13}$$

Maxwell's equations by themselves are incomplete and so we will now introduce an few constitutive laws which close the system.

2.3.1 Linear Media

Free space is the simplest constitutive Model. In particular, we assume the two constitutive relations

$$\mathbf{D} = \epsilon\mathbf{E}, \qquad \mathbf{B} = \mu\mathbf{H}. \tag{2.3.14}$$

Here the electrical permittivity ϵ and magnetic permeability μ can be functions of space and time, but they must be independent all other variables. They may be matrix or scalar

valued. In this case, the materials do not respond to the electromagnetic fields. Examples of materials which can be modeled reliably as a linear media include vacuum and air under standard conditions.

2.3.2 The Debye Model

In the Debye model is a description of the response of a relaxing dielectric to electromagnetic fields. In this model consider a material whose molecules are bound in a charge neutral configuration in the absence of and electric field. When an electric field enters the material, the charges are pushed away from the nucleus of the molecule due to the Coulomb force. After the electric field has passed, these negative charges relax into their neutral configuration with some relaxation time τ. See Figure 2.1 for illustration. The Debye model is often posed as a frequency dependent electrical permittivity

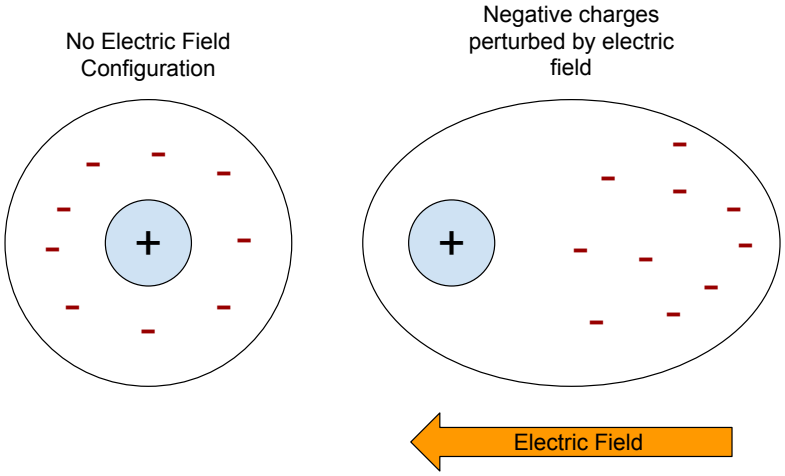

FIGURE 2.1: A simple illustration of the effects of an electric field on a Debye Material

$$\epsilon(\omega) = \epsilon_\infty + \frac{\epsilon_\Delta}{1 + \mathrm{i}\omega\tau} \tag{2.3.15}$$

Here ϵ_∞ is the permittivity of infinite frequency while ϵ_Δ is the permittivity gap of the material. We can extract an ODE model of Debye materials by taking a Fourier transform

of the Ampére-Maxwell Law and applying the Ansatz

$$\mathbf{D} = \epsilon(\omega)\mathbf{E} + \mathbf{P} \tag{2.3.16}$$

and then taking inverse transforms we recover:

$$\begin{cases} \epsilon_\infty \dfrac{\partial}{\partial t}\mathbf{E} + \dfrac{\partial}{\partial t}\mathbf{P} = \mathbf{curl\ H} \\ \tau \dfrac{\partial}{\partial t}\mathbf{P} = -\mathbf{P} + \epsilon_0 \epsilon_\Delta \mathbf{E}. \end{cases} \tag{2.3.17}$$

This equation states that $\mathbf{P}$ is a decaying exponential forced by the electric field. By eliminating the $\frac{\partial}{\partial t}\mathbf{P}$ term from the first equation we can see that the effect is that is roughly dampening:

$$\epsilon_\infty \frac{\partial}{\partial t}\mathbf{E} = -\frac{\epsilon_\Delta}{\tau}\mathbf{E} + \frac{1}{\tau}\mathbf{P} + \mathbf{curl\ H}. \tag{2.3.18}$$

The $-\frac{\epsilon_\Delta}{\tau}$ term will remove energy from $\mathbf{E}$ exponentially. While we are adding some energy to $\mathbf{E}$ through $\mathbf{P}$ we have that $\mathbf{P}$ is also relaxing towards zero.

2.3.3 Drude-Lorentz Model

The Drude-Lorentz model for electrical polarization is somewhat analogous to the Debye medium– we assume that electrons are pushed away from their positively charged nuclei by the electric field. However, instead of assuming that the when the electric field passes the electrons relax back to charge neutral we assume there behavior will be analogous to that of a spring dash-pot system.

The complex permittivity of this model is given by

$$\epsilon(\omega) = 1 + \frac{\omega_P^2}{-\omega^2 - \mathrm{i}\omega\omega_I - \omega_0^2}. \tag{2.3.19}$$

Here ω_P is the called the plasma frequency of the plasma it is essentially the frequency of oscillation induced by the Coulomb force acting on the electron shells of our molecules. The parameter ω_0 is the natural frequency and it should be interpreted as the spring

constant in the oscillation. The parameter ω_I is the ion collision frequency and it controls the rate at which energy dissipates from the media.

The polarization law which is induced by this relation is given by

$$\mathbf{D} = \epsilon\mathbf{E} + \mathbf{P}, \tag{2.3.20}$$

$$\frac{\partial^2}{\partial t^2}\mathbf{P} + \omega_I \frac{\partial}{\partial t}\mathbf{P} + \omega_0^2\mathbf{P} = \epsilon\omega_P^2\mathbf{E}. \tag{2.3.21}$$

When the natural frequency of the material is zero we have what is called the Drude model. By defining

$$\frac{\partial}{\partial t}\mathbf{P} = \mathbf{J} \tag{2.3.22}$$

we then have a first order system

$$\frac{\partial}{\partial t}\mathbf{D} = \epsilon\frac{\partial}{\partial t}\mathbf{E} + \mathbf{J} \tag{2.3.23}$$

$$\frac{\partial}{\partial t}\mathbf{J} + \omega_I\mathbf{J} = \epsilon_0\omega_P^2\mathbf{E}. \tag{2.3.24}$$

This cases has slightly different behavior as are only a single resonance frequency rather than two. In the case of $\omega_i = 0$ this plasma is called collisionless and the model is energy conservative.

2.3.4 Generalized Polarization Laws

Throughout this work we will consider a general framework which accommodates many models with similar structure to both the Debye and Drude-Lorentz Models. In particular, Polarization models which are forced by the electric field and perhaps other polarizations. These models we write in the abstract form of

$$\frac{\partial}{\partial t}\mathbf{u} = \mathbb{X}\mathbf{u} + \mathbf{F}. \tag{2.3.25}$$

where

$$\frac{\partial}{\partial t}\mathbf{u} = \begin{pmatrix} \mathbf{E} \\ \mathbf{P}_1 \\ \mathbf{P}_2 \\ \vdots \\ \mathbf{P}_M \end{pmatrix}, \qquad \mathbf{F} = \begin{pmatrix} \mathbf{curl}\ \mathbf{H} \\ 0 \\ 0 \\ \vdots \\ \mathbf{0} \end{pmatrix} \tag{2.3.26}$$

and $\mathbb{X}$ is a matrix of coefficients. For an isotropic material (i.e. one which all directions have essentially the same behavior) this matrix $\mathbb{X}$ can be written as

$$\mathbb{X} \otimes \mathbb{I}_{2\times 2}. \tag{2.3.27}$$

This is primarily the case we will consider although most of our methods will be able to handle a very mild anisotropy of form

$$\begin{pmatrix} \mathbb{X} & 0 & 0 \\ 0 & \mathbb{Y} & 0 \\ 0 & 0 & \mathbb{Z} \end{pmatrix} \tag{2.3.28}$$

where we then group the vector $\mathbf{u}$ by

$$\mathbf{u} = \begin{pmatrix} E_x & \cdots & P_{M_x,x} & E_y & \cdots & P_{M_y,y} & E_z & \cdots & P_{M_z,z} \end{pmatrix}^T \tag{2.3.29}$$

Here there is no reason for there to be an identical number of polarization fields in each direction. In addition, it is worth noting that this formulation can handle, in addition to linear combinations of polarization models, a random polarization. In this case, we would consider the macroscopic polarization to be given by

$$\mathbb{P} = \mathbb{E}[\mathbf{p}(\boldsymbol{\xi})] \tag{2.3.30}$$

where $\mathbb{E}$ is the expected value and $\mathbf{p}(\boldsymbol{\xi})$ is some ODE with random parameters $\boldsymbol{\xi}$. By discretizing the ODE of $\mathbf{p}(\boldsymbol{\xi})$ using generalized polynomial chaos methods we will end up

with an abstract evolution equation of the form (2.3.25) although our interpretation for the polarizations $\mathbf{P}_i$ will be moments of the moments of the probability distribution. See [17] for the construction development of random polarizations.

2.3.5 Generalized Ohm's Law

Ohm's law is a famous empirical law which states that

$$\Delta V = IR \tag{2.3.31}$$

where R is a material dependent proportionality constant we call *resistance*. To produce continuum fields to describe Ohm's law we make the following definitions. Define the current density $\mathbf{J}$ associated with some cross section A by

$$\int_A \mathbf{J} \cdot n \; dA = I \tag{2.3.32}$$

and define the *electrical conductivity* by

$$\int_{\mathbf{x}_c}^{\mathbf{x}} \frac{1}{\sigma} = R. \tag{2.3.33}$$

Here electrical conductivity is e linear density of the inverse of resistance which is called *conductance*. Consider a wire with area $\mathbf{A}$ then we have

$$\int_A \int_{\mathbf{x}_c}^{\mathbf{x}} \frac{\mathbf{J} \cdot n}{\sigma} \; dsdA = IR \tag{2.3.34}$$

By the definition of V as a path integral of $\mathbf{E}$ and taking the limit as $|A| \to 0$ and $|\mathbf{x} - \mathbf{x}_c| \to 0$ and by varying the orientation of of the cross section A arbitrarily we derive the relation

$$\mathbf{J} = \sigma \mathbf{E} \tag{2.3.35}$$

which is also referred to as Ohm's Law in the literature. We stress that Ohm's law is an empirical description and thus it should be considered a constitutive model rather than a universal law.

This assumes that the conductor is stationary. If the conductor moves with velocity $\mathbf{u}$ then we must account currents induced by the magnetic field

$$\mathbf{J} = \sigma(\mathbf{E} + \mathbf{u} \times \mathbf{B}). \tag{2.3.36}$$

A final additional complexity we consider is that if the currents are moving, then the Lorentz force should act upon them. However, this Lorentz force is proportional to $\mathbf{J}$ so we arrive at an implicit equation

$$\mathbf{J} = \sigma(\mathbf{E} + \mathbf{u} \times \mathbf{B}) + \eta \mathbf{J} \times \mathbf{B}. \tag{2.3.37}$$

This last term is called the Hall effect. The parameter η is called electron mobility and it accounts for how easily electrons can flow through the media. In the case of solids this value is very small but in gasses it can be significantly higher. For this reason it is a very important effect toe account for in plasma physics.

2.4 Sobolev Spaces

The fundamental object in functional analysis is the linear space.

Definition 2.4.1. A set V is a linear space over the reals, $\mathbb{R}$, if it is closed under the abstract operations of addition and scaling.

$$\forall u, v \in V : u + v \in V, \tag{2.4.1}$$

$$\forall \alpha \in \mathbb{R}, u \in V : \alpha u \in V. \tag{2.4.2}$$

If V is also a metric space, and is in particular complete, we call V a Banach Space. If V is a complete inner product space we call V a Hilbert Space.

Throughout this thesis we will make use of variational formulations of Maxwell's equations rather than strong formulations. For details on the development of weak formulations for Maxwell's equations see [5, 12, 39]. Variational formulations are developed in

special Hilbert spaces called Sobolev spaces. We define the relevant spaces here. As the curl or divergence requires significantly fewer derivatives than the gradient we will make use of a number of lower-regularity Hilbert spaces.

Definition 2.4.2. Define the following spaces.

$$L^2(\Omega) = \left\{ u : \Omega \to \mathbb{R} \text{ measurable } : \int_\Omega |u|^2 < \infty \right\}, \tag{2.4.3}$$

$$\mathbf{L}^2(\Omega) = \{\mathbf{u} : \Omega \to \mathbb{R}^d : u_i \in L^2(\Omega), 1 \leq i \leq d\}, \tag{2.4.4}$$

$$H^1(\Omega) = \{u \in L^2(\Omega) : \nabla u \in \mathbf{L}^2(\Omega)\}, \tag{2.4.5}$$

$$\mathbf{H}(\mathbf{curl}, \Omega) = \{\mathbf{u} \in \mathbf{L}^2(\Omega) : \mathbf{curl}\ \mathbf{u} \in \mathbf{L}^2(\Omega)\}, \tag{2.4.6}$$

$$\mathbf{H}(\mathrm{div}, \Omega) = \{\mathbf{u} \in \mathbf{L}^2(\Omega) : \mathrm{div}\ \mathbf{u} \in L^2(\Omega)\}. \tag{2.4.7}$$

Each of these spaces is an inner product space, complete with respect to that the norm induced by that inner product; i.e., a *Hilbert Space*. The inner product of the above spaces are written as $[\cdot, \cdot]_V$ where V is one of the above spaces.

$$[u, v]_{L^2(\Omega)} = \int_\Omega uv \ d\Omega, \tag{2.4.8}$$

$$[\mathbf{u}, \mathbf{v}]_{\mathbf{L}^2(\Omega)} = \int_\Omega \mathbf{u} \cdot \mathbf{v} \ d\Omega = \sum_i [u_i, v_i]_{L^2(\Omega)}, \tag{2.4.9}$$

$$[u, v]_{H^1(\Omega)} = [u, v]_{L^2(\Omega)} + [\nabla u, \nabla v]_{\mathbf{L}^2(\Omega)}, \tag{2.4.10}$$

$$[\mathbf{u}, \mathbf{v}]_{\mathbf{H}(\mathbf{curl},\Omega)} = [\mathbf{u}, \mathbf{v}]_{\mathbf{L}^2(\Omega)} + [\mathbf{curl}\ \mathbf{u}, \mathbf{curl}\ \mathbf{v}]_{\mathbf{L}^2(\Omega)}, \tag{2.4.11}$$

$$[\mathbf{u}, \mathbf{v}]_{\mathbf{H}(\mathrm{div},\Omega)} = [\mathbf{u}, \mathbf{v}]_{\mathbf{L}^2(\Omega)} + [\mathrm{div}\ \mathbf{u}, \mathrm{div}\ \mathbf{v}]_{L^2(\Omega)}. \tag{2.4.12}$$

The norm on an inner product space V induced by the inner product is given by

$$\|u\|_V = \sqrt{[u, u]_V}. \tag{2.4.13}$$

Definition 2.4.3. If V and W are linear spaces such that W is a linear subspace, i.e. a subset closed under addition and scaling, we denote this by

$$W \leq V. \tag{2.4.14}$$

Definition 2.4.4. If V is a linear space. Define *dual space of* V by

$$V' = \{F : V \to \mathbb{R}, F \text{ a linear functional}\}. \tag{2.4.15}$$

Definition 2.4.5. Let B be a linear space with dual space B'. Define the duality pairing by

$$\langle \cdot, \cdot \rangle_B : B' \times B \to \mathbb{R} \tag{2.4.16}$$

$$\langle F, u \rangle_B = F(u), \forall F \in B', u \in B. \tag{2.4.17}$$

We will now present traces, i.e. restrictions to the boudary. A thorough development, beyond definitions, can be found in [39].

Definition 2.4.6. Define the trace on H^1 by

$$\gamma : H^1(\Omega) \to \mathbf{H}(\text{div}, \Omega)', \tag{2.4.18}$$

$$\langle \gamma u, \mathbf{v} \rangle_{\mathbf{H}(\text{div},\Omega)} = \int_\Omega \nabla u \cdot \mathbf{v} + \int_\Omega u \text{ div } \mathbf{v} \, d\Omega, \quad \forall u \in H^1(\Omega), \mathbf{v} \in \mathbf{H}(\text{div}, \Omega). \tag{2.4.19}$$

When γu can be identified as an object in $L^2(\partial\Omega)$ we state $\gamma u = u|_{\partial\Omega}$.

Definition 2.4.7. Define the trace on $\mathbf{H}(\text{div})$ by

$$\gamma^{\mathbf{n}} : \mathbf{H}(\text{div}, \Omega) \to (H^1(\Omega))', \tag{2.4.20}$$

$$\langle \gamma^{\mathbf{n}} \mathbf{v}, u \rangle_{H^1(\Omega)} = \int_\Omega \nabla u \cdot \mathbf{v} + \int_\Omega u \text{ div } \mathbf{v} \, d\Omega, \quad \forall u \in H^1(\Omega), \mathbf{v} \in \mathbf{H}(\text{div}, \Omega). \tag{2.4.21}$$

When $\gamma^{\mathbf{n}} \mathbf{v}$ can be identified as function in $L^2(\partial\Omega)$ we state $\gamma^{\mathbf{n}} \mathbf{v} = \mathbf{n} \cdot \mathbf{v}|_{\partial\Omega}$.

Remark. The trace and on H^1 and the trace on $\mathbf{H}(\text{div})$ are related by the following adjoint property

$$\langle \gamma^{\mathbf{n}} \mathbf{v}, u \rangle_{H^1(\Omega)} = \langle \gamma u, \mathbf{v} \rangle_{\mathbf{H}(\text{div},\Omega)}. \tag{2.4.22}$$

Definition 2.4.8. We will now define the trace on $\mathbf{H}(\mathbf{curl})$. There are two cases.

- Let $\Omega \subset \mathbb{R}^3$. We define the trace on $\mathbf{H}(\mathbf{curl})$ by

$$\gamma^{\boldsymbol{\tau}} : \mathbf{H}(\mathbf{curl}, \Omega) \to \mathbf{H}(\mathbf{curl}, \Omega)', \tag{2.4.23}$$

$$\langle \gamma^{\boldsymbol{\tau}} \mathbf{u}, \mathbf{v} \rangle_{\mathbf{H}(\mathbf{curl},\Omega)} = \int_\Omega \mathbf{curl}\ \mathbf{u} \cdot \mathbf{v}\ d\Omega - \int_\Omega \mathbf{u} \cdot \mathbf{curl}\ \mathbf{v}\ d\Omega. \tag{2.4.24}$$

  If $\gamma^{\boldsymbol{\tau}} \mathbf{u}$ can be identified with an object in $\mathbf{L}^2(\partial\Omega)$ then we say $\gamma^{\boldsymbol{\tau}} \mathbf{u} = \mathbf{n} \times \mathbf{u}|_{\partial\Omega}$.

- Let $\Omega \subset \mathbb{R}^2$. We define the trace on $\mathbf{H}(\mathrm{curl})$ by

$$\gamma^{\boldsymbol{\tau}} : \mathbf{H}(\mathrm{curl}, \Omega) \to (H^1(\Omega))', \tag{2.4.25}$$

$$\langle \gamma^{\boldsymbol{\tau}} \mathbf{u}, v \rangle_{H^1(\Omega)} = \int_\Omega \mathbf{u} \cdot \mathbf{curl}\ v\ d\Omega - \int_\Omega v \mathrm{curl}\ \mathbf{u}\ d\Omega. \tag{2.4.26}$$

  $\gamma^{\boldsymbol{\tau}} \mathbf{u}$ can be identified with an object in $L^2(\partial\Omega)$ then we say $\gamma^{\boldsymbol{\tau}} \mathbf{u} = \boldsymbol{\tau} \cdot \mathbf{u}|_{\partial\Omega}$.

  We will present a number of standard estimates on these spaces.

Theorem 2.4.1. *Let for $V \leq H^1(\Omega)$ and $W \leq H^1(\Omega)$ such that for Γ is an open subset of $\partial\Omega$*

$$V = \left\{ v \in H^1(\Omega) : v|_\Gamma = 0 \right\}, \tag{2.4.27}$$

$$W = \left\{ v \in H^1(\Omega) : \int_\Omega v\ d\Omega = 0 \right\}. \tag{2.4.28}$$

Then the following estimate holds

$$\|v\|_{L^2(\Omega)} \leq C_{p.f.} \|\nabla v\|_{\mathbf{L}^2(\Omega)} \tag{2.4.29}$$

for all $v \in V$ or $v \in W$.

Proof. See [5]. **Q.E.D.**

Theorem 2.4.2. *Define the spaces*

$$\mathbf{V} = \{ \mathbf{A} \in \mathbf{H}(\mathbf{curl}, \Omega) \cap \mathbf{H}(div, \Omega) : \mathbf{A} \times \mathbf{n}|_{\partial\Omega} \in \mathbf{L}^2(\partial\Omega) \}, \tag{2.4.30}$$

$$\mathbf{W} = \{ \mathbf{A} \in \mathbf{H}(\mathbf{curl}, \Omega) \cap \mathbf{H}(div, \Omega) : \mathbf{A} \cdot \mathbf{n}|_{\partial\Omega} \in L^2(\partial\Omega) \}. \tag{2.4.31}$$

Then the following estimate holds:

$$\|div\ \mathbf{A}\|_{L^2(\Omega)} + \|\mathbf{curl}\ \mathbf{A}\|_{\mathbf{L}^2(\Omega)} + \|\mathbf{n} \times \mathbf{A}\|_{\mathbf{L}^2(\partial\Omega)} \geq C\|\mathbf{A}\|_{\mathbf{L}^2(\Omega)}, \forall \mathbf{A} \in \mathbf{V}, \tag{2.4.32}$$

$$\|div\ \mathbf{A}\|_{L^2(\Omega)} + \|\mathbf{curl}\ \mathbf{A}\|_{\mathbf{L}^2(\Omega)} + \|\mathbf{n} \cdot \mathbf{A}\|_{L^2(\partial\Omega)} \geq C\|\mathbf{A}\|_{\mathbf{L}^2(\Omega)}, \forall \mathbf{A} \in \mathbf{W}. \tag{2.4.33}$$

Proof. See [39]. **Q.E.D.**

A similar estimate holds in 2D relying upon the scalar curl and divergence.

In addition to these continuum spaces we also make use of polynomial spaces.

Definition 2.4.9. Let $\Omega \subset \mathbb{R}^d$. We define the space

$$\mathbb{P}_k(\Omega) = \{p : \Omega \to \mathbb{R}, p \text{ a polynomial of degree } \leq k\}. \tag{2.4.34}$$

3 MIMETIC FINITE DIFFERENCES IN TWO DIMENSIONS

In this chapter we present a theoretical development of a lowest order MFD in two dimensions suitable for discretizing Maxwell's equations. This theoretical development follows closely the work of [2] and [34]. However, we deviate from those works in that we present our proofs to be more consistent with the VEM. In section 3.1 we will introduce the DeRham and Hilbert Complex. In section 3.2 we will describe hypotheses on meshes for the MFD. In section 3.3 we will present discrete spaces and discrete differential operators which commute with the DeRham complex. In section 3.4 we will present reconstruction proceedures with which a MFD discretiztion can be interpreted as a lowest order virtual element method. In section 3.5 we will construct polynomially consistent inner products for the MFD. In section 3.6 we will present the local matrices of a MFD discretization on a rectangle. In section 3.7 we will define adjoint or weak differential operators for the MFD. In section 3.8 we will prove that our MFD discretization preserves the kernel and image properties of the gradient, divergence, and curl.

3.1 2D DeRham Complices

A *DeRham Complex* is an object introduced in Differential Geometry to relate function spaces of scalars and vector fields through differential mappings, c. f. [30]. The differential mapping is referred to as the *exterior derivative*, often simply called d. The exterior derivative has the property that $d^2 = 0$, a result which proves that div $\mathbf{curl} = 0$ and curl $\nabla = 0$ respectively.

In the classical case the functions spaces are always infinitely smooth. This allows for

no loss of regularity when the exterior derivative is applied. However, in the development of weak formulations of partial differential equations we make use of Hilbert spaces. For this reason we consider a DeRham Complex of Hilbert Spaces, often called a *Hilbert Complex*, c.f. [1].

Consider the first order derivatives in two dimensions. Let $f = f(x, y)$ and let $\mathbf{f} = (f_1(x, y), f_2(x, y))^T$ defined on $\Omega \subset \mathbb{R}^2$,

$$\nabla f = (\partial_x f, \partial_y f), \quad \mathbf{curl}\ f = (\partial_y f, -\partial x f)^T, \tag{3.1.1}$$

$$\text{curl}\ \mathbf{f} = \partial_x f_2 - \partial_y f_1, \quad \text{div}\ \mathbf{f} = \partial_x f_1 + \partial_y f_2. \tag{3.1.2}$$

In two dimensions there are two non-equivalent Hilbert Complices,

$$H^1 \xrightarrow{\quad\nabla\quad} \mathbf{H}(\text{curl}) \xrightarrow{\quad\text{curl}\quad} L^2 \tag{3.1.3}$$

$$H^1 \xrightarrow{\quad\mathbf{curl}\quad} \mathbf{H}(\text{div}) \xrightarrow{\quad\text{div}\quad} L^2\ . \tag{3.1.4}$$

Choosing the appropriate complex for a given MFD discretization is determined by the weak form of the partial differential equation to discretize. The Hilbert Complex (3.1.3) is required for weak formulations of Maxwell's Equations of the form

$$\begin{cases} \dfrac{\partial}{\partial t}\displaystyle\int \mathbf{D}\cdot\mathbf{\Phi}\ dA = \int H\text{curl}\ \mathbf{\Phi}\ dA, & \forall \mathbf{\Phi} \in \mathbf{H}(\text{curl}), \\ \dfrac{\partial}{\partial t}\displaystyle\int B\psi\ dA = -\int \text{curl}\ \mathbf{E}\psi\ dA, & \forall \psi \in L^2. \end{cases} \tag{3.1.5}$$

While the Hilbert Complex (3.1.4) is required for weak formulations of the form

$$\begin{cases} \dfrac{\partial}{\partial t}\displaystyle\int \mathbf{D}\cdot\mathbf{\Phi}\ dA = \int \mathbf{curl}\ H\cdot\mathbf{\Phi}\ dA, & \forall \mathbf{\Phi} \in \mathbf{L}^2, \\ \dfrac{\partial}{\partial t}\displaystyle\int B\psi\ dA = -\int \mathbf{E}\cdot\mathbf{curl}\ \psi\ dA, & \forall \psi \in H^1. \end{cases} \tag{3.1.6}$$

While this formulation is often of interest, discretizations of this system have a character very similar to those seen in acoustics which have been thoroughly analyzed in [21]. For this reason we will focus on the development of a MFD discretization of the Complex (3.1.3).

3.2 Preliminaries for Meshes

The MFD is defined on polyhedral meshes in 3D and polygonal meshes in 2D. There is a very strong connection between mesh topology and our discretization.

Consider some simply connected domain $\Omega \subset \mathbb{R}^2$ with a polygonal mesh $\mathscr{T}$. We call the set of all polygons in the mesh $\mathscr{F}$, the set of all edges $\mathscr{E}$, and the set of all vertices $\mathscr{V}$. We will refer to the polygons in $\mathscr{F}$ as faces. In general we refer to elements of $\mathscr{F}$ by the variable f, $\mathscr{E}$ by e, and $\mathscr{V}$ by $\mathbf{v}$.

The mesh $\mathscr{T}$ has the following properties:

1. The mesh is conformal to Ω, i.e.

$$\Omega = \bigcup_{f \in \mathscr{F}} f. \tag{3.2.1}$$

2. The mesh $\mathscr{T}$ is path connected. That is between every vertex $\mathbf{v}, \mathbf{w} \in \mathscr{V}$ we can construct a path from edges $e \in \mathscr{E}$ which connects $\mathbf{v}$ to $\mathbf{w}$. Further we require for any two faces $f_1, f_2 \in \mathscr{F}$ with $f_1 \cap f_2 \neq \emptyset$ that $f_1 \cap f_2 = e$ some edge in $\mathscr{E}$.

3. Every face has a *global numbering* from 1 to $N_{\mathscr{F}}$.

4. Every edge has a *global numbering* from 1 to $N_{\mathscr{E}}$.

5. Every vertex has a *global numbering* from 1 to $N_{\mathscr{V}}$.

6. Every edge has a global orientation pointing in the direction $\boldsymbol{\tau}_e$ the unit tangent vector to e. We choose $\boldsymbol{\tau}_e$'s orientation so that it forms an angle with the x axis in $[0, \pi)$.

7. For every face $f \in \mathscr{F}$ there is a *local numbering* of edges $e \in \mathscr{E}$ which form the boundary of f. This numbering is from 1 to $n_{\mathscr{E}}^f$, where we will use the convention that the local edges are numbered counter-clockwise around f.

8. For every face $f \in \mathscr{F}$ there is a *local numbering* of vertices which are exactly end points of edges which form the boundary of f. This numbering is also counter-clockwise and ranges from 1 to $n^f_{\mathscr{V}}$.

9. For every edge $e \in \mathscr{F}$ there exists two local vertices $\mathbf{v}_1, \mathbf{v}_2$ which form the endpoints e. This numbering respects the orientation of e.

3.3 Discrete Spaces and Primal Operators

In this section we will introduce the degrees of freedom and primal, discrete differential operators of the lowest order Mimetic Finite Difference method.

In the lowest order there is a very natural connection between mesh topological structures and discrete spaces. We will now present properties which we require of our interpolation operators.

Definition 3.3.1. Let V and W be linear spaces. We say an operator $L : V \to W$ is *linear* if

$$L(u + \alpha v) = L(u) + \alpha L(v) \tag{3.3.1}$$

for every $\alpha \in \mathbb{R}$ and $u, v \in V$.

Definition 3.3.2. We define the following *grid function spaces* which are represented by standard vectors in $\mathbb{R}^n$:

$$\mathscr{V}_h = \mathbb{R}^{N_{\mathscr{V}}}, \quad \mathscr{E}_h = \mathbb{R}^{N_{\mathscr{E}}}, \quad \mathscr{F}_h = \mathbb{R}^{N_{\mathscr{F}}}. \tag{3.3.2}$$

We say that the *natural topology* of $\mathscr{V}_h$ is $\mathscr{V}$ the set of vertices, $\mathscr{E}_h$ is $\mathscr{E}$ the set of edges, and $\mathscr{F}_h$ is $\mathscr{F}$ the set of faces. Grid function spaces are indexed by the numbering of the corresponding natural topology.

Definition 3.3.3. We define *discrete primal differential operators* as linear operators between grid function spaces:

$$\nabla_h : \mathscr{V}_h \to \mathscr{E}_h, \quad \operatorname{curl}_h : \mathscr{E}_h \to \mathscr{F}_h, \tag{3.3.3}$$

which are referred to as the *discrete primal gradient* and *discrete primal curl* respectively.

Definition 3.3.4. We define *interpolation operators* as linear operators

$$\mathcal{I}^{\mathscr{V}_h} : H^1(\Omega) \cap C^0(\overline{\Omega}) \to \mathscr{V}_h, \tag{3.3.4}$$

$$\mathcal{I}^{\mathscr{E}_h} : \mathbf{H}(\operatorname{curl}, \Omega) \to \mathscr{E}_h, \tag{3.3.5}$$

$$\mathcal{I}^{\mathscr{F}_h} : L^2(\Omega) \to \mathscr{F}_h. \tag{3.3.6}$$

These operators obey the following Hilbert Complex preserving properties:

$$\nabla_h \circ \mathcal{I}^{\mathscr{V}_h} = \mathcal{I}^{\mathscr{E}_h} \circ \nabla, \qquad \operatorname{curl}_h \circ \mathcal{I}^{\mathscr{E}_h} = \mathcal{I}^{\mathscr{F}_h} \circ \operatorname{curl}. \tag{3.3.7}$$

This property is illustrated in Figure 3.1.

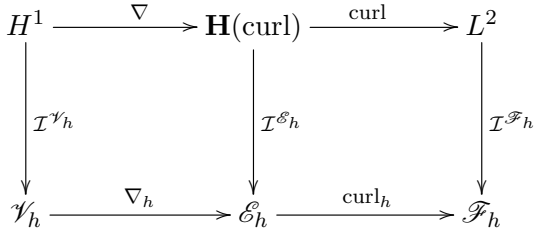

FIGURE 3.1: Hilbert complex for discrete spaces.

We also make use of the following restriction notation.

Definition 3.3.5. *The restriction of the interpolant of a grid function space $\mathscr{S}_h$ to the natural topology of $\mathscr{S}_h$* is defined by

$$\mathcal{I}_s^{\mathscr{S}_h}(u_h) = u_s \in \mathbb{R}. \tag{3.3.8}$$

This is to say that $\mathcal{I}_s^{\mathscr{S}_h}$ is exactly the degree of freedom associated with $s \in \mathscr{S}$.

Definition 3.3.6. For a grid function space $\mathscr{S}_h$ with natural topology $\mathscr{S}$ and some other topology $\mathscr{W}$ such that for $w \in \mathscr{W}$ and $s \in \mathscr{S}$, $s \in \partial w$. Then we define the restriction of $u \in \mathscr{S}_h$ to w by

$$\mathcal{I}_w^{\mathscr{S}_h}(u_h) = u_w := (u_s : s \in \partial w). \tag{3.3.9}$$

This notation will allow us to define, for example, the space of all edge degrees of freedom tangent to a face. We refer to the image space $\mathcal{I}_w^{\mathscr{S}}$ as $\mathscr{S}_w$ which is isomorphic to an appropriately sized copy of $\mathbb{R}^n$.

$\mathcal{I}_{\mathbf{v}}^{\mathscr{V}_h} : H^1 \to \mathscr{V}_{\mathbf{v}} = \mathbb{R}$		
$\mathcal{I}_e^{\mathscr{V}_h} : H^1 \to \mathscr{V}_e = \mathbb{R}^2$	$\mathcal{I}_e^{\mathscr{E}_h} : \mathbf{H}(\text{curl}) \to \mathscr{E}_e = \mathbb{R}$	
$\mathcal{I}_f^{\mathscr{V}_h} : H^1 \to \mathscr{V}_f = \mathbb{R}^{n_{\mathscr{V}}^f}$	$\mathcal{I}_f^{\mathscr{E}_h} : \mathbf{H}(\text{curl}) \to \mathscr{E}_f = \mathbb{R}^{n_{\mathscr{E}}^f}$	$\mathcal{I}_f^{\mathscr{F}_h} : L^2 \to \mathscr{F}_f = \mathbb{R}$

(3.3.10)

In order to construct a collection of discrete spaces which obey these properties we begin at the left most end of the complex with the continuum space L^2. As this space has no continuity and no trace we will discretize it with averages over every cell in $\mathscr{F}$.

Definition 3.3.7. We define the face based interpolant $\mathcal{I}^{\mathscr{F}_h}$ as follows. Assume $H \in L^2(\Omega)$,

$$\mathcal{I}_f^{\mathscr{F}_h}(H) = \frac{1}{|f|}\int_f H \; dA, f \in \mathscr{F}, \qquad \mathcal{I}^{\mathscr{F}_h}(H) = \Big(H_f : \forall f \in \mathscr{F}\Big). \tag{3.3.11}$$

Further, for an arbitrary grid function $H_h \in \mathscr{F}_h$ we define H_f to be the restriction to face f.

In order to determine the space $\mathscr{E}_h$ we consider the relevant commutativity condition. Consider it on just one cell $f \in \mathscr{F}$

$$\mathcal{I}_f^{\mathscr{F}_h} \circ \text{curl}\mathbf{E} = \frac{1}{|f|}\int_f \text{curl } \mathbf{E} \; dA, \tag{3.3.12}$$

$$= \frac{1}{|f|}\sum_{e \in \partial f}\int_e \boldsymbol{\tau} \cdot \mathbf{E} \; ds. \tag{3.3.13}$$

Given this calculation it appears that if we choose the degrees of freedom on $\mathscr{E}_h$ as proportional to the integral of tangential components on cell edges we can define curl_h to preserve the commuting property.

Definition 3.3.8. We define the interpolant on $\mathscr{E}_h$ as follows. Choose $\mathbf{E} \in \mathbf{H}(\text{curl}, \Omega)$.

$$\mathcal{I}_e^{\mathscr{E}_h}(\mathbf{E}) = \frac{1}{|e|}\int_e \boldsymbol{\tau}_e \cdot \mathbf{E}\, ds, e \in \mathscr{E}, \tag{3.3.14}$$

$$\mathcal{I}^{\mathscr{E}_h}(\mathbf{E}) = \Big(\mathbf{E}_e : \forall e \in \mathscr{E}\Big). \tag{3.3.15}$$

Definition 3.3.9. We define the discrete primal curl operator, curl_h, as follows. Let $\mathbf{E}_h \in \mathscr{E}_h$,

$$\text{curl}_h : \mathscr{E}_h \to \mathscr{F}_h \tag{3.3.16}$$

$$\text{curl}_{h,f}\mathbf{E}_f = \frac{1}{|f|}\Big(|e_1|\sigma_{f,e_1}, \cdots |e_{n_{\mathscr{E}}^f}|\sigma_{f,e_{n_{\mathscr{E}}^f}}\Big)\mathbf{E}_f. \tag{3.3.17}$$

Here $\sigma_{f,e} = \pm 1$ corrects for a counter clockwise orientation of tangent vectors to compute the curl, which in general does not agree with the global orientation of every edge. The global matrix curl_h is then assembled from local contributions on every face $f \in \mathscr{F}$:

$$\text{curl}_h\mathbf{E}_h = \Big(\text{curl}_{h,f}\mathbf{E}_f : f \in \mathscr{F}\Big). \tag{3.3.18}$$

Lemma 3.3.1. *The discrete primal curl operator, $curl_h$, as defined in Definition 3.3.8 obeys the commutativity condition*

$$curl_h \circ \mathcal{I}^{\mathscr{E}_h} = \mathcal{I}^{\mathscr{F}_h} \circ curl. \tag{3.3.19}$$

Proof. Without loss of generality we need only prove the identity for an arbitrary face

$f \in \mathscr{F}$. We then have

$$\operatorname{curl}_{h,f}\mathcal{I}_f^{\mathscr{E}_h}(\mathbf{E}) = \frac{1}{|f|}\Big(|e_1|\sigma_{f,e_1}, \cdots |e_{n_{\mathscr{E}}^f}|\sigma_{f,e_{n_{\mathscr{E}}^f}}\Big)\begin{pmatrix} \frac{1}{|e_1|}\int_{e_1}\mathbf{E}\cdot\boldsymbol{\tau}_{e_1}\,ds \\ \vdots \\ \frac{1}{|e_{n_{\mathscr{E}}^f}|}\int_{e_{n_{\mathscr{E}}^f}}\mathbf{E}\cdot\boldsymbol{\tau}_{e_{n_{\mathscr{E}}^f}}\,ds \end{pmatrix}, \tag{3.3.20}$$

$$= \frac{1}{|f|}\sum_{e\in\partial f}\int_e \mathbf{E}\cdot\boldsymbol{\tau}_e\,ds, \tag{3.3.21}$$

$$= \frac{1}{|f|}\int_f \operatorname{curl}\,\mathbf{E}\,dA, \tag{3.3.22}$$

$$= \mathcal{I}_f^{\mathscr{F}}(\operatorname{curl}\,\mathbf{E}). \tag{3.3.23}$$

Which completes the proof. **Q.E.D.**

We must now determine the space $\mathscr{V}_h$ and the discrete primal gradient. Consider the commutativity condition

$$\nabla_h \circ \mathcal{I}^{\mathscr{V}_h} = \mathcal{I}^{\mathscr{E}_h} \circ \nabla. \tag{3.3.24}$$

We will perform a calculation of the right hand side. Fix arbitrary $e \in \mathscr{E}$ with boundary vertices $\mathbf{v}_1, \mathbf{v}_2$.

$$\frac{1}{|e|}\int_e \nabla u\cdot\boldsymbol{\tau}_e = \frac{u(\mathbf{v}_2)-u(\mathbf{v}_1)}{|e|} \tag{3.3.25}$$

A natural choice of the $\mathscr{V}_h$'s degrees of freedom is therefore evaluation at vertices.

Definition 3.3.10. We define the interpolant on $\mathscr{V}_h$ as follows. Choose $u \in H^1(\Omega)\cap C^0(\Omega)$,

$$\mathcal{I}_{\mathbf{v}}^{\mathscr{V}_h}(u) = u(\mathbf{v}), \mathbf{v}\in\mathscr{V}, \qquad \mathcal{I}^{\mathscr{V}_h}(u) = \Big(u_{\mathbf{v}} : \mathbf{v}\in\mathscr{V}\Big). \tag{3.3.26}$$

Definition 3.3.11. We define the discrete primal gradient, ∇_h as follows

$$\nabla_h : \mathscr{V}_h \to \mathscr{E}_h \tag{3.3.27}$$

$$\nabla_{h,e}u_e = \frac{1}{|e|}\Big(-1, \quad 1\Big)u_e \tag{3.3.28}$$

The global matrix ∇_h is then assembled from local contributions on every edge $e \in \mathscr{E}$:

$$\nabla_h u_h = \Big(\nabla_{h,e} u_e : e \in \mathscr{E} \Big). \tag{3.3.29}$$

Lemma 3.3.2. *The discrete primal gradient, ∇_h as defined above obeys the commutativity condition*

$$\nabla_h \circ \mathcal{I}^{\mathscr{V}_h} = \mathcal{I}^{\mathscr{V}_h} \circ \nabla. \tag{3.3.30}$$

Proof. Without loss of generality we consider a single edge $e \in \mathscr{E}$.

$$\nabla_{h,e} u_e = \frac{1}{|e|} \begin{pmatrix} -1 & 1 \end{pmatrix} \begin{pmatrix} u(\mathbf{v}_1) \\ u(\mathbf{v}_2) \end{pmatrix} \tag{3.3.31}$$

$$= \frac{u(\mathbf{v}_2) - u(\mathbf{v}_1)}{|e|} \tag{3.3.32}$$

$$= \frac{1}{|e|} \int_e \nabla u \cdot \boldsymbol{\tau}_e \, ds \tag{3.3.33}$$

$$= \mathcal{I}_e^{\mathscr{E}_h}(\nabla u). \tag{3.3.34}$$

This completes the proof. **Q.E.D.**

3.4 Reconstruction and Accuracy

With our discrete operators and spaces in place there is now a question of how accurately these degrees of freedom approximate a given function. One approach for this quantification is to apply *local truncation analysis*. This approach is relatively simple on rectangular meshes. However we wish to utilize finite element theory as we are attempted to discretize weak forms. To do so we must introduce the concept of *reconstruction*.

A reconstruction problem is one in which we seek a continuum functions with prescribed of degrees of freedom. The goal is to create an isomorphism between discrete spaces and an approximation space. If the approximation space contains all polynomials

of a certain degree we can then use those functions to prove the accuracy of the method. We begin by considering *global reconstruction* and use a formulation equivalent to [2].

Definition 3.4.1. We define the following finite dimensional *Reconstructed Spaces*:

$$V_h \leq H^1(\Omega) \cap C^0(\overline{\Omega}), \qquad \mathrm{Dim} V_h = N_{\mathscr{V}}, \tag{3.4.1}$$

$$E_h \leq \mathbf{H}(\mathrm{curl}, \Omega) \qquad \mathrm{Dim} E_h = N_{\mathscr{E}}, \tag{3.4.2}$$

$$F_h \leq L^2(\Omega), \qquad \mathrm{Dim} F_h = N_{\mathscr{F}}. \tag{3.4.3}$$

We call the subspace embedding the *Conformal Approximation Property*. Further we say that V_h corresponds to $\mathscr{V}_h$, E_h corresponds to $\mathscr{E}_h$, and F_h corresponds to $\mathscr{F}_h$.

Definition 3.4.2. For a function F we say G is *right inverse of* F if

$$F \circ G = I \tag{3.4.4}$$

where I is the identity map.

Definition 3.4.3. We define *Global Reconstruction Operators* on a grid function space $\mathscr{S}_h$ as a linear mapping from $\mathscr{S}_h$ to the corresponding reconstructed space S_h

$$\mathcal{R}^{\mathscr{S}_h} : \mathscr{S}_h \to S_h. \tag{3.4.5}$$

We require the following properties.

- If S is the domain of $\mathcal{I}^{\mathscr{S}_h}$ define the inclusion map $i_S : S_h \to S$. We require $i_S \circ \mathcal{R}^{\mathscr{S}_h}$ is the right inverse of $\mathcal{I}^{\mathscr{S}_h}$.

- We additionally require the following Hilbert Complex preserving property:

$$\nabla \circ \mathcal{R}^{\mathscr{V}_h} = \mathcal{R}^{\mathscr{E}_h} \circ \nabla_h, \quad \mathrm{curl} \circ \mathcal{R}^{\mathscr{E}_h} = \mathcal{R}^{\mathscr{F}_h} \circ \mathrm{curl}_h. \tag{3.4.6}$$

It is worth noting that the Right Inverse Property and Linearity imply that $\mathcal{R}^{\mathscr{S}_h}$ is a *linear isomorphism*. Figure 3.2 illustrates many of these properties.

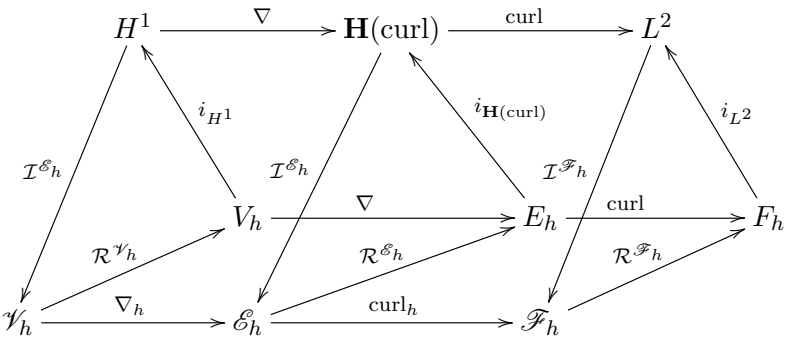

FIGURE 3.2: A commuting diagram relating discrete spaces and their reconstructions.

We will construct our global reconstructions using local reconstruction mappings. At this stage we will diverge from the formulation of [2] and instead pursue an approach closer to the Virtual Element Method as described in [3].

Definition 3.4.4. Define *Local Reconstructed Spaces* on arbitrary $\mathbf{v} \in \mathscr{V}, e \in \mathscr{E}, f \in \mathscr{F}$ as follows.

$V_{\mathbf{v}} = \mathbb{P}_0(\mathbf{v})$		
$V_e \leq H^1(e)$	$E_e = \mathbb{P}_0(e)$	
$V_f \leq H^1(f)$	$E_f \leq \mathbf{H}(\mathrm{curl}, f)$	$F_f = \mathbb{P}_0(f)$

(3.4.7)

We require these spaces have the following dimensions.

$\mathrm{Dim} V_{\mathbf{v}} = 1$		
$\mathrm{Dim} V_e = 2$	$\mathrm{Dim} E_e = 1$	
$\mathrm{Dim} V_f = n^f_{\mathscr{V}}$	$\mathrm{Dim} E_f = n^f_{\mathscr{E}}$	$\mathrm{Dim} F_f = 1$

(3.4.8)

Definition 3.4.5. We say a mapping from to a local reconstruction space S_w, where $w \in \mathscr{W}$ is some topology, has the *Data Locality Property* if domain of that mapping is is the corresponding local grid function space $\mathscr{S}_w$.

Definition 3.4.6. Let $\mathscr{W}, \mathscr{L}$ be two topologies such that for $w \in \mathscr{W}$ there is some $\ell \in \mathscr{L}$. Let $\mathscr{S}_h$ be a grid function space with reasonable restriction to ℓ and w. Let f_ℓ, f_w be two

mappings

$$f_\ell : \mathscr{S}_\ell \to S_\ell, \quad f_w : \mathscr{S}_w \to S_w \tag{3.4.9}$$

we say that f_w is *consistent* with f_ℓ if

$$f_w(u_w)|_\ell = f_\ell(u_\ell) \tag{3.4.10}$$

where u_w, u_ℓ are usual restrictions form $u_h \in \mathscr{S}_h$.

Definition 3.4.7. Let $\mathscr{W}$ be some topology on which a grid function space $\mathscr{S}_h$ has a restriction. Call the domain of $\mathcal{I}^{\mathscr{S}_h}$ the space S and let $V \leq S$ be a subspace. We say that mappings $f_w : \mathscr{S}_w \to S_w$ for every $w \in \mathscr{W}$ are V *Accurate* if for every $v \in V$

$$f_w \circ \mathcal{I}_w^{\mathscr{S}_h}(v) = v. \tag{3.4.11}$$

Definition 3.4.8. We define *Local Reconstruction Operators* as linear mappings on arbitrary $\mathbf{v} \in \mathscr{V}, e \in \mathscr{E}, f \in \mathscr{F}$ as follows.

$\mathcal{R}_{\mathbf{v}}^{\mathscr{V}_h} : \mathscr{V}_{\mathbf{v}} \to V_{\mathbf{v}}$		
$\mathcal{R}_e^{\mathscr{V}_h} : \mathscr{V}_e \to V_e$	$\mathcal{R}_e^{\mathscr{E}_h} : \mathscr{E}_e \to E_e$	
$\mathcal{R}_f^{\mathscr{V}_h} : \mathscr{V}_f \to V_f$	$\mathcal{R}_f^{\mathscr{E}_h} : \mathscr{E}_f \to E_f$	$\mathcal{R}_f^{\mathscr{F}_h} : \mathscr{F}_f \to F_f$

(3.4.12)

We require the following properties of local reconstruction operators.

- Reconstruction is data local,
- We require the following consistency conditions:
  - $\mathcal{R}_e^{\mathscr{V}_h}$ consistent with $\mathcal{R}_{\mathbf{v}}^{\mathscr{V}_h}$ and $\mathcal{R}_f^{\mathscr{V}_h}$ consistent with $\mathcal{R}_e^{\mathscr{V}_h}$,
  - $\mathcal{R}_f^{\mathscr{E}_h}$ consistent with $\mathcal{R}_e^{\mathscr{E}_h}$.
- We require the following polynomial accuracy:
  - $\mathcal{R}_w^{\mathscr{V}_h}$ must be $\mathbb{P}_1(w)$ accurate for $w \in \{\mathbf{v}, e, f\}$,

  - $\mathcal{R}_e^{\mathscr{E}_h}$ must be $\mathbb{P}_0(e)$ accurate and $\mathcal{R}_f^{\mathscr{E}_h}$ must be $\mathbb{P}_0(f)^2$ accurate,
  - $\mathcal{R}_f^{\mathscr{F}_h}$ must be $\mathbb{P}_0(f)$ accurate.

- We require the following Hilbert Complex preserving properties:

$$\operatorname{curl} \circ \mathcal{R}_f^{\mathscr{E}_h} = \mathcal{R}_f^{\mathscr{F}_h} \circ \operatorname{curl}_{h,f}, \tag{3.4.13}$$

$$\nabla \circ \mathcal{R}_w^{\mathscr{V}_h} = \mathcal{R}_w^{\mathscr{E}_h} \circ \nabla_h,\ w \in \{e, f\}. \tag{3.4.14}$$

We will now seek to realize local reconstruction operators with the above properties. The MFD construction presented in [2] relies on ill-posed PDE and then makes the reconstruction unique by adding, for example, orthogonality conditions for certain polynomials. In contrast our development will pose reconstruction as solution to well-posed PDE and then prove that the unique solutions obey the reconstruction properties more similar to Virtual Elements.

It is our goal to construct the face based reconstructions $\mathcal{R}_f^{\mathscr{S}_h}$. However, these operators natural require the reconstruction on every finer mesh structure . We will begin with the simplest reconstructions, namely those on the topology natural to each grid function space.

Definition 3.4.9. Define the reconstruction operators $\mathcal{R}_{\mathbf{v}}^{\mathscr{V}_h}, \mathcal{R}_e^{\mathscr{E}_h}, \mathcal{R}_f^{\mathscr{F}_h}$ for $\mathbf{v} \in \mathscr{V}, e \in \mathscr{E}$, and $f \in \mathscr{F}$ as

$$\mathcal{R}_{\mathbf{v}}^{\mathscr{V}_h}(u_h) = u_{\mathbf{v}} \forall u_h \in \mathscr{V}_h \tag{3.4.15}$$

$$\mathcal{R}_e^{\mathscr{E}_h}(\mathbf{E}_h) = \mathbf{E}_e, \forall \mathbf{E}_h \in \mathscr{E}_h \tag{3.4.16}$$

$$\mathcal{R}_f^{\mathscr{F}_h}(g_h) = g_f, \forall g_h \in \mathscr{F}_h. \tag{3.4.17}$$

That is we assume that our reconstructed functions will be piecewise constant on their natural topology.

Reconstruction operators as defined in 3.4.9 satisfy, trivially, all of the local reconstruction operator properties. We will now define the reconstruction of an edge function on a face.

Definition 3.4.10. Fix arbitrary $f \in \mathscr{F}$ and $\mathbf{E}_h \in \mathscr{E}_h$. We define $\mathbf{E} = \mathcal{R}_f^{\mathscr{E}_h}(\mathbf{E}_h)$ as the solution of the following variational problem: $\mathbf{E} \in \mathbf{H}_g(\mathrm{curl}, f)$ such that

$$\begin{cases} \displaystyle\int_f \mathrm{curl}\ \mathbf{E}\ \mathrm{curl}\ \boldsymbol{\Phi}\ dA + \int_f \nabla\lambda \cdot \boldsymbol{\Phi}\ dA = \int_f \mathbf{curl}(\mathcal{R}_f^{\mathscr{F}_h}(\mathrm{curl}_h \mathbf{E}_h)) \cdot \boldsymbol{\Phi}\ dA & \forall, \boldsymbol{\Phi} \in \mathbf{H}_g(\mathrm{curl}, f) \\ \displaystyle\int_f \mathbf{E} \cdot \nabla\psi = 0, & \forall \psi \in H_0^1(f). \end{cases} \tag{3.4.18}$$

Where

$$\mathbf{H}_g(\mathrm{curl}, f) = \{\boldsymbol{\Phi} \in \mathbf{H}(\mathrm{curl}, f) : \boldsymbol{\Phi} \cdot \boldsymbol{\tau}_e = \mathcal{R}_e^{\mathscr{E}_h}(\mathbf{E}_h), e \in \partial f\} \tag{3.4.19}$$

Theorem 3.4.1. *The local reconstruction operator $\mathcal{R}_f^{\mathscr{E}_h}$ satisfies the following properties:*

1. *it is a right inverse,*
2. *it is Hilbert complex preserving,*
3. *it satisfies the data locality condition,*
4. *it is consistent with $\mathcal{R}_e^{\mathscr{E}_h}$,*
5. *the map is linear,*
6. *the map is $\mathbb{P}_0(f)^2$ accurate.*

Proof. The variational problem (3.4.18) is well posed, therefore $\mathbf{E} = \mathcal{R}_f^{\mathscr{E}_h}(\mathbf{E}_h)$ is well defined and unique for every $\mathbf{E}_h \in \mathscr{E}_h$.

1. Note that $\mathbf{E} \in \mathbf{H}_g(\mathrm{curl}, f)$. Therefore $\mathbf{E}|_e \cdot \boldsymbol{\tau}_e = \mathcal{R}_e^{\mathscr{E}_h}(\mathbf{E}_h)$ for every $e \in \partial f$. As the reconstruction operator $\mathcal{R}_e^{\mathscr{E}_h}$ has the right inverse property, the operator $\mathcal{R}_f^{\mathscr{E}_h}$ has been constructed to obey it as well.

2. The function $\mathcal{R}^{\mathscr{F}_h}(\text{curl}_h \mathbf{E}_h)$ is a constant function on f. Therefore, $\mathbf{curl}\mathcal{R}^{\mathscr{F}_h}(\text{curl}_h \mathbf{E}_h) = 0$. Therefore,

$$\int_f \mathbf{curl}\mathcal{R}_f^{\mathscr{F}_h}(\text{curl}_h E_h) \cdot \nabla\psi = 0. \tag{3.4.20}$$

Therefore, $\mathbf{curl}\mathcal{R}^{\mathscr{F}_h}(\text{curl}_h \mathbf{E}_h)$ is in the kernel of our constraint operator

$$\mathcal{B}(\mathbf{E}, \psi) = \int_f \mathbf{E} \cdot \nabla\psi. \tag{3.4.21}$$

We therefore have $\lambda = 0$ as the function $\mathbf{E}$ is in the kernel of the constraint. The variational problem therefore reduces as to,

$$\int_f \text{curl } \mathbf{E} \text{ curl } \mathbf{\Phi} \; dA = \int_f \mathbf{curl} \; \mathcal{R}_f^{\mathscr{F}_h}(\text{curl}_h E_h) \cdot \mathbf{\Phi} \; dA \tag{3.4.22}$$

The operator **curl** has a kernel consisting exactly of constant functions. $\mathcal{R}^{\mathscr{F}_h}(\text{curl}_h E_h)$ is a constant function thus $\mathbf{curl}\text{curl}\mathbf{E} = 0$ in the sense of L^2. As the kernel of **curl** is exactly constants we have curl$\mathbf{E}$ a constant.

$$|f|\text{curl}\mathbf{E} = \int_f \text{curl}\mathbf{E} = \sum_{e\in\partial f} \int_e \mathbf{E} \cdot \boldsymbol{\tau}_e \; ds \qquad \text{Stokes' Theorem,} \tag{3.4.23}$$

$$= \sum_{e\in\partial f} \int_e \mathcal{R}_e^{\mathscr{E}_h}(\mathbf{E}_h) \cdot \boldsymbol{\tau}_e \qquad \mathbf{E} \in \mathbf{H}_g(\text{curl}, f), \tag{3.4.24}$$

$$= \sum_{e\in\partial f} \sigma_{f,e}|e|E_e \qquad \text{Definition of } \mathcal{R}_e^{\mathscr{E}_h}, \tag{3.4.25}$$

$$= |f|\text{curl}_{h,f}\mathbf{E}_f \qquad \text{Definition of curl}_{h,f}, \tag{3.4.26}$$

$$= |f|\mathcal{R}_f^{\mathscr{F}_h}(\text{curl}_h \mathbf{E}_h) \qquad \text{Definition of } \mathcal{R}_f^{\mathscr{F}_h}. \tag{3.4.27}$$

Thus, $\text{curl}\mathcal{R}_f^{\mathscr{E}_h}(\mathbf{E}_h) = \mathcal{R}_f^{\mathscr{F}_h}(\text{curl}_h \mathbf{E}_h)$ and we have demonstrated Hilbert complex preservation.

3. The definition of $\mathcal{R}_f^{\mathscr{E}_h}$ requires only edge data from the boundary of f therefore we satisfy data locality.

4. As $\mathbf{E} \in \mathbf{H}_g(\text{curl}, f)$, $\mathbf{E}|_e \cdot \boldsymbol{\tau}_e = \mathcal{R}_e^{\mathscr{E}_h}(\mathbf{E}_h)$. Therefore the operator is consistent.

5. Linearity is inherited from the linearity of (3.4.18) and the linearity of $\mathcal{R}_e^{\mathscr{E}_h}$.

6. Without loss of generality assume $\mathbf{E} = \mathbf{e}_i$ a standard basis vector of $\mathbb{R}^2$. Let $\mathbf{E}_h = \mathcal{I}^{\mathscr{E}_h}(\mathbf{E})$. As $\mathbf{E}$ is constant we know curl $\mathbf{E} \equiv 0$ and $\text{curl}_{h,f}\mathbf{E}_h = 0$. Therefore $\mathcal{R}_f^{\mathscr{E}_h}(\mathbf{E})$ is the unique solution to the following strong equations in the sense of L^2:

$$\begin{cases} \mathbf{curl}\text{curl}\mathcal{R}_f^{\mathscr{E}_h}(\mathbf{E}_h) = 0 & \in L^2(f) \\ \text{div}\mathcal{R}_f^{\mathscr{E}_h}(\mathbf{E}_h) = 0 & \in L^2(f) \\ \boldsymbol{\tau} \cdot \mathcal{R}_f^{\mathscr{E}_h}(\mathbf{E}_h)|_e = \mathbf{e}_1 \cdot \boldsymbol{\tau} & \in L^2(e), e \in \partial f \end{cases} \tag{3.4.28}$$

This equation is satisfied by the function $\mathbf{e}_i$ therefore by uniqueness we have

$$\mathcal{R}_f^{\mathscr{E}_h} \circ \mathcal{I}_f^{\mathscr{E}_h}(\mathbf{e}_i) = \mathbf{e}_i. \tag{3.4.29}$$

As every constant function $\mathbf{c} = c_1\mathbf{e}_1 + c_2\mathbf{e}_2$ we have demonstrated the accuracy property for $\mathbb{P}_0(f)^2$.

Q.E.D.

Next we will discuss vertex function reconstruction.

Definition 3.4.11. Fix arbitrary $e \in \mathscr{E}$ and $u_h \in \mathscr{V}_h$. Let the boundary vertices of e be $\mathbf{v}_1, \mathbf{v}_2$. We define $u = \mathcal{R}_e^{\mathscr{V}_h}(u_h)$ as the solution to the initial value problem

$$\begin{cases} \frac{\partial}{\partial \tau} u = \mathcal{R}_e^{\mathscr{E}_h}(\nabla_h u_h) \\ u(\mathbf{v}_1) = u_{\mathbf{v}_1} \end{cases} \tag{3.4.30}$$

Theorem 3.4.2. *Local edge reconstruction of vertex functions $\mathcal{R}_e^{\mathscr{V}_h}$ has the following properties:*

1. *it is a right inverse,*

2. *it is Hilbert complex preserving,*

3. *it satisfies the data locality property,*

4. *it is consistent with consistency* $\mathcal{R}_{\mathbf{v}}^{\mathscr{V}_h}$,

5. *the map is linear,*

6. *the map is* $\mathbb{P}_1$ *accurate.*

Proof. Note that $\mathcal{R}_e^{\mathscr{E}_h}(\nabla_h u_h) = \frac{u_{\mathbf{v}_2} - u_{\mathbf{v}_1}}{|e|}$ a constant function. This is sufficient to show the ODE has a unique solution, namely a linear function.

1. Our definition of u guarantees $u(\mathbf{v}_1) = u_{\mathbf{v}_1}$. We must show that $u(\mathbf{v}_2) = u_{\mathbf{v}_2}$. Solve for $\mathcal{R}_e^{\mathscr{V}_h}(u_h)$ exactly, we have

$$\mathcal{R}_e^{\mathscr{V}_h}(u_h)(s) = \frac{u_{\mathbf{v}_2} - u_{\mathbf{v}_1}}{|e|} s + u_{\mathbf{v}_1}, \quad s \in [0, |e|]. \tag{3.4.31}$$

   Evaluating at $s = |e|$ we have $\mathcal{R}_e^{\mathscr{V}_h}(u_h) = u_{\mathbf{v}_2}$ which completes the proof.

2. Apply our exact solution from the previous problem we have

$$\begin{aligned} \frac{1}{|e|} \int_e \boldsymbol{\tau} \cdot \nabla u \, ds &= \int_e \frac{\partial}{\partial \tau} u \, ds && (3.4.32) \\ &= \frac{1}{|e|} \int_0^{|e|} \frac{\partial}{\partial s} \left(\frac{u_{\mathbf{v}_2} - u_{\mathbf{v}_1}}{|e|} s + u_{\mathbf{v}_1} \right) ds && (3.4.33) \\ &= \frac{u_{\mathbf{v}_2} - u_{\mathbf{v}_1}}{|e|} && (3.4.34) \\ &= \nabla_{h,e} u_h. && (3.4.35) \end{aligned}$$

   We therefore have the Hilbert complex preserving property.

3. As $\mathcal{R}_e^{\mathscr{V}_h}$ depends only on the vertices which make up the end points of e we have data locality.

4. As the ODE governing reconstruction is linear the operator therefore is as well.

5. Suppose $u|_e(s) = as + b$ some linear polynomial in the local coordinates of e, $s \in [0, |e|]$. Let $u_h = \mathcal{I}^{\mathscr{E}_h}(u)$. We therefore have $u_e = (b, a|e| + b)^T$ and $\nabla_{h,e} u_h = a$. The exact solution of the reconstruction is given by (3.4.31) which implies

$$\mathcal{R}_e^{\mathscr{V}_h}(u_h) = as + b = u|_e. \tag{3.4.36}$$

Q.E.D.

Definition 3.4.12. Fix arbitrary $f \in \mathscr{F}$ with boundary vertices $\mathbf{v}_1, \cdots, \mathbf{v}_{n^f_{\mathscr{V}}}$ and fix arbitrary $u_h \in \mathscr{V}_h$. We define the face reconstruction of a grid function $u_h \in \mathscr{V}_h$ as $u = \mathscr{R}_f^{\mathscr{V}_h}(u_h)$ such that u is a solution to the variational problem : $u \in H^1_g(f)$ such that

$$\int_f \nabla u \cdot \nabla \varphi \, dA = -\int_f \text{div } \mathcal{R}_f^{\mathscr{E}_h}(\nabla_h u_h)\varphi \, dA, \quad \forall \varphi \in H^1_g(f). \tag{3.4.37}$$

$$H^1_g(f) = \{\varphi \in H^1(f) : \varphi|_e = \mathcal{R}_e^{\mathscr{V}_h}(u_h), e \in \partial f\}. \tag{3.4.38}$$

Theorem 3.4.3. *The local face reconstruction of vertex functions $\mathcal{R}_f^{\mathscr{V}_h}$ has the following properties:*

1. *it is right inverse,*
2. *it is Hilbert complex preserving,*
3. *it satisfies data locality conditions,*
4. *it is consistent with $\mathcal{R}_e^{\mathscr{V}_h}$,*
5. *the map is linear,*
6. *the map is $\mathbb{P}_1$ accurate.*

Proof. As the variational problem (3.4.37) is well posed and $\mathcal{R}_f^{\mathscr{V}_h}$ is well-defined and thus the map is well defined and unique for every $u_h \in \mathscr{V}_h$.

1. Let $e_i, e_j \in \partial f$, then either $e_i \cap e_j = \mathbf{v}_k$ some vertex in the boundary of f or the intersection is empty. If the intersection is non empty then $\mathcal{R}_{e_i}^{\mathscr{V}_h}$ and $\mathcal{R}_{e_j}^{\mathscr{V}_h}$ both preserve the value $u_{\mathbf{v}_k}$. We therefore have the right inverse property.

2. Similar to the other arguments we have the property

$$\Delta u = \text{div}\mathcal{R}_f^{\mathscr{V}_h}(\nabla_h u_h) \text{ in the sense of } L^2. \tag{3.4.39}$$

As the kernel of the divergence operator is exactly curls we have

$$\nabla u = \mathcal{R}_f^{\mathscr{V}_h}(\nabla_h u_h) + \mathbf{curl}\ \psi. \tag{3.4.40}$$

We must now show that $\mathbf{curl}\psi = 0$.

$$\int_f \nabla u \cdot \nabla\varphi\ dA = -\int_f \mathrm{div}\mathcal{R}_f^{\mathscr{E}_h}(\nabla_h u_h)\varphi\ dA \tag{3.4.41}$$

$$= \int_f \mathcal{R}_f^{\mathscr{E}_h}(\nabla_h u_h) \cdot \nabla\varphi\ dA \tag{3.4.42}$$

by an affine lift of H_0^1

$$\int_f (\mathcal{R}_f^{\mathscr{E}_h}(\nabla_h u_h) + \mathbf{curl}\ \psi) \cdot \nabla\varphi\ dA = \int_f \mathcal{R}_f^{\mathscr{E}_h}(\nabla_h u_h) \cdot \nabla \cdot \varphi \quad \text{by (3.4.40).} \tag{3.4.43}$$

$$\int_f \mathbf{curl}\ \psi \cdot \nabla\varphi\ dA = 0 \tag{3.4.44}$$

We will now perform integration by parts on the left hand side.

$$0 = \int_f \mathbf{curl}\ \psi \cdot \nabla\varphi\ dA \tag{3.4.45}$$

$$= \int_f \psi \mathrm{curl}\nabla\varphi\ dA - \int_{\partial f} \psi \frac{\partial}{\partial\tau}\varphi\ ds \tag{3.4.46}$$

$$= \int_{\partial f} \psi \frac{\partial}{\partial\tau}\varphi\ ds. \tag{3.4.47}$$

Applying an affine lifting argument we have the trace of ψ is zero in the sense of L^2. As $\nabla u = \mathcal{R}_e^{\mathscr{E}_h}(\nabla_h u_h) + \mathbf{curl}\psi$ on the boundary this implies that $\mathbf{curl}\psi \cdot \boldsymbol{\tau} = 0$. Further $\mathbf{curl}\psi \cdot \boldsymbol{\tau} = \nabla\psi \cdot \boldsymbol{n} = 0$. Taking the scalar curl of equation (3.4.40) we have the following PDE

$$\mathrm{curl}\ \mathbf{curl}\ \psi = -\mathrm{curl}\mathcal{R}_f^{\mathscr{V}_h}(\nabla_h u_h) \tag{3.4.48}$$

$$\Delta\psi = \mathrm{curl}\mathcal{R}_f^{\mathscr{V}_h}(\nabla_h u_h). \tag{3.4.49}$$

From Theorem 3.4.1 we know that $\text{curl}\mathcal{R}_f^{\mathscr{E}_h}(\nabla_h u_h)$ is a constant function.

$$|f|\text{curl}\mathcal{R}_f^{\mathscr{E}_h}(\nabla_h u_h) = \int_f \text{curl}\mathcal{R}_f^{\mathscr{E}_h}(\nabla_h u_h) \tag{3.4.50}$$

$$= \sum_{e\in\partial f} |e|\mathcal{R}_e^{\mathscr{E}_h}(\nabla_h u_h)\cdot\boldsymbol{\tau} \tag{3.4.51}$$

$$= (u_{\mathbf{v}_2} - u_{\mathbf{v}_1}) + (u_{\mathbf{v}_3} - u_{\mathbf{v}_1}) + \cdots + (u_{\mathbf{v}_1} - u_{\mathbf{v}_{n_f^{\mathscr{V}}}}) \tag{3.4.52}$$

$$= 0. \tag{3.4.53}$$

We therefore know that ψ satisfies the following strong equations in the sense of L^2

$$\begin{cases} \triangle\psi = 0 & \in L^2(f) \\ \psi = 0 & \in L^2(\partial f) \end{cases} \tag{3.4.54}$$

Which implies that ψ must be zero. We have therefore shown that

$$\nabla\mathcal{R}_f^{\mathscr{V}_h}(u_h) = \mathcal{R}_f^{\mathscr{E}_h}(\nabla_h u_h). \tag{3.4.55}$$

3. We have data locality as reconstruction depends only on the vertices in the boundary of f.

4. We have consistency as $\mathcal{R}_f^{\mathscr{V}_h}(u_h)|_e = \mathcal{R}_e^{\mathscr{E}_h}(u_h)$.

5. Linearity is inherited from the linearity of the PDE which defines $\mathcal{R}_f^{\mathscr{V}_h}$.

6. Let u be some function satisfying $u|_f = ax + by + c$. Let $u_h = \mathcal{I}^{\mathscr{V}_h}(u)$. Note that $\nabla u = (a, b)^T$ and by commutativity of interpolation we have

$$\nabla_h u_h = \mathcal{I}_f^{\mathscr{E}_h}(\nabla u). \tag{3.4.56}$$

However we know that $\mathcal{R}_f^{\mathscr{E}_h}$ is a right inverse on constant functions therefore

$$\nabla u = \mathcal{R}_f^{\mathscr{E}_h}(\nabla_h u_h). \tag{3.4.57}$$

Further, by $\mathbb{P}_1$ accuracy of $\mathcal{R}_e^{\mathscr{V}_h}$ we know that $\mathcal{R}_e^{\mathscr{E}_h}(u_h) = u|_e$ for every edge $e \in \partial f$. The reconstruction $\mathcal{R}^{\mathscr{V}_h}(u_h)$ satisfies the PDE

$$\begin{cases} \triangle \mathcal{R}^{\mathscr{V}_h}(u_h) = 0 & \in f \\ \mathcal{R}_f^{\mathscr{V}_h}(u_h)|_e = u|_e & e \in \partial f \end{cases} \tag{3.4.58}$$

Q.E.D.

With local reconstructions now well defined we will define the global reconstruction operators.

Definition 3.4.13. Let χ_A be the indicator function for the set A. We define the global reconstruction operator by

$$\mathcal{R}^{\mathscr{S}_h}(u_h) = \sum_{f \in \mathscr{F}} \mathcal{R}_f^{\mathscr{S}_h}(u_h)\chi_f. \tag{3.4.59}$$

Theorem 3.4.4. *The global face reconstruction operator $\mathcal{R}^{\mathscr{F}_h}$ has the following three properties:*

1. *it is a right inverse,*
2. *the mapping is linear,*
3. *the mapping has the conformal approximation property.*

Proof. 1. Fix $H_h \in \mathscr{F}_h$.

$$\begin{aligned} \mathcal{I}^{\mathscr{F}_h} \circ \mathcal{R}^{\mathscr{F}_h}(H_h) &= \left(\frac{1}{|f|} \int_f \mathcal{R}^{\mathscr{F}_h}(H_h)\ dA : f \in \mathscr{F} \right), && \text{by definition,} \\ &= \left(\frac{1}{|f|} \int_f \sum_{f \in \mathscr{F}_h} \mathcal{R}_f^{\mathscr{F}_h}(H_h)\chi_f\ dA : f \in \mathscr{F} \right), && \text{by definition,} \\ &= \left(\frac{1}{|f|} \int_f \mathcal{R}_f^{\mathscr{F}_h}(H_h)\ dA : f \in \mathscr{F} \right), && \text{integrating over } f, \\ &= \left(\mathcal{I}_f^{\mathscr{F}_h} \circ \mathcal{R}_f^{\mathscr{F}_h}(H_h)\ dA : f \in \mathscr{F} \right), && \text{by definition,} \\ &= (H_f : f \in \mathscr{F}_h) && \text{local right inverse property} \end{aligned} \tag{3.4.60}$$

2. Linearity is inherited directly from local linearity.

$$\mathcal{R}^{\mathscr{F}_h}(H_h + \alpha B_h) = \sum_{f \in \mathscr{F}_h} \mathcal{R}_f^{\mathscr{F}_h}(H_h + \alpha B_h) \tag{3.4.61}$$

$$= \sum_{f \in \mathscr{F}_h} \mathcal{R}_f^{\mathscr{F}_h}(H_h) + \alpha \mathcal{R}_f^{\mathscr{F}_h}(B_h) \tag{3.4.62}$$

$$= \sum_{f \in \mathscr{F}_h} \mathcal{R}_f^{\mathscr{F}_h}(H_h) + \alpha \sum_{f \in \mathscr{F}_h} \mathcal{R}_f^{\mathscr{F}_h}(B_h) \tag{3.4.63}$$

$$= \mathcal{R}^{\mathscr{F}_h}(H_h) + \alpha \mathcal{R}^{\mathscr{F}_h}(B_h). \tag{3.4.64}$$

3. The local reconstruction $\mathcal{R}_f^{\mathscr{F}_h}$ is constant on every $f \in \mathscr{F}_h$. Therefore we have that $F_h = \{H : H|_f \in \mathbb{P}_0\}$ a strict subspace of $L^2(\Omega)$ as Ω is compact.

Q.E.D.

Theorem 3.4.5. *The global edge reconstruction operator $\mathcal{R}^{\mathscr{E}_h}$ has the following three properties:*

1. *it is a right inverse,*
2. *the mapping is linear,*
3. *the mapping has the conformal approximation property.*

Proof. The proof of properties 1 and 2 follows exactly as in 3.4.4.

3. By construction of the reconstruction $\mathcal{R}_f^{\mathscr{E}_h}(\mathbf{E}_h)$ is in the space $\mathbf{H}(\text{curl}, f)$ for every $\mathbf{E}_h \in \mathscr{E}_h$ and $f \in \mathscr{F}$. Linearity of the map $\mathcal{R}_f^{\mathscr{E}_h}$ and the fact that $\mathscr{E}_f$ is a linear space implies closure of the space $\mathcal{R}_f^{\mathscr{E}_h}(\mathscr{E}_f)$. For any $f_1, f_2 \in \mathscr{F}$ whose boundary shares an edge e, the consistency of $\mathcal{R}_f^{\mathscr{E}_h}$ with $\mathcal{R}_e^{\mathscr{E}_h}$ guarantees that we have that

$$\mathcal{R}_{f_1}^{\mathscr{E}_h}(\mathbf{E}_h)|_e = \mathcal{R}_e^{\mathscr{E}_h}(\mathbf{E}_h) = \mathcal{R}_{f_2}^{\mathscr{E}_h}(\mathbf{E}_h)|_e. \tag{3.4.65}$$

Therefore the global function $\mathcal{R}^{\mathscr{E}_h}(\mathbf{E}_h)$ has tangential continuity across every edge $e \in \mathscr{E}$. This combined with $\mathcal{R}_f^{\mathscr{E}_h}(\mathcal{E}_f) = E_f \leq \mathbf{H}(\text{curl}, f)$ is sufficient to show $\mathcal{R}^{\mathscr{E}_h}(\mathscr{E}_h) = E_h \leq \mathbf{H}(\text{curl}, \Omega)$. **Q.E.D.**

Theorem 3.4.6. *The global vertex reconstruction operator $\mathcal{R}^{\mathscr{V}_h}$ has the following three properties:*

1. *right inverse,*
2. *linearity,*
3. *conformal approximation.*

Proof. The proof of properties 1 and 2 follows exactly as in 3.4.4.

3. By construction the reconstruction $\mathcal{R}_f^{\mathscr{V}_h}(u_h)$ is in $H^1(f)$ for every $u_h \in \mathscr{E}_h, f \in \mathscr{F}$. As before, linearity of $\mathcal{R}_f^{\mathscr{V}_h}$ implies that $V_f \leq H^1(f)$. The consistency of $\mathcal{R}_f^{\mathscr{V}_h}$ with $\mathcal{R}_e^{\mathscr{V}_h}$ and $\mathcal{R}_{\mathbf{v}}^{\mathscr{V}_h}$ guarantees that for any two faces f_1, f_2 sharing a vertex $\mathbf{v}$ and faces f_3, f_4 sharing some edge e we have

$$\mathcal{R}_{f_1}^{\mathscr{V}_h}(u_h)|_{\mathbf{v}} = \mathcal{R}_{\mathbf{v}}^{\mathscr{V}_h}(u_h) = \mathcal{R}_{f_2}^{\mathscr{V}_h}(u_h)|_{\mathbf{v}}, \tag{3.4.66}$$

$$\mathcal{R}_{f_3}^{\mathscr{V}_h}(u_h)|_e = \mathcal{R}_e^{\mathscr{V}_h}(u_h) = \mathcal{R}_{f_4}^{\mathscr{V}_h}(u_h)|_e. \tag{3.4.67}$$

Therefore every function $\mathcal{R}^{\mathscr{V}_h}(u_h)$ is globally continuous. This with local conformality property $V_f \leq H^1(f)$ guarantees that $\mathcal{R}^{\mathscr{V}_h}(\mathscr{V}_h) = V_h \leq H^1(\Omega)$. **Q.E.D.**

Theorem 3.4.7. *Global reconstruction preserves the Hilbert Complex:*

$$\nabla \circ \mathcal{R}^{\mathscr{V}_h} = \mathcal{R}^{\mathscr{E}_h} \circ \nabla_h, \qquad curl \circ \mathcal{R}^{\mathscr{E}_h} = \mathcal{R}^{\mathscr{F}_h} \circ curl_h. \tag{3.4.68}$$

Proof. We must show this property in the sense of weak derivatives. Fix arbitrary $\mathbf{\Phi} \in C_0^\infty(\Omega)^2$ and $\psi \in C_0^\infty(\Omega)$. Fix arbitrary $u_h \in \mathscr{V}_h$. In the sense of distributions $\nabla\mathcal{R}^{\mathscr{V}_h}(u_h)$ is defined to be

$$-\int_\Omega \mathcal{R}^{\mathscr{V}_h}(u_h)\mathrm{div}\mathbf{\Phi}\ dA. \tag{3.4.69}$$

We compute

$$-\int_\Omega \mathcal{R}^{\mathscr{V}_h}(u_h)\text{div}\mathbf{\Phi}\ dA = -\int_\Omega \sum_{f\in\mathscr{F}} \mathcal{R}_f^{\mathscr{V}_h}(u_h)\chi_f \text{div}\mathbf{\Phi}\ dA, \tag{3.4.70}$$

$$= -\sum_{f\in\mathscr{F}_h}\int_f \mathcal{R}_f^{\mathscr{V}_h}(u_h)\text{div}\mathbf{\Phi}\ dA, \tag{3.4.71}$$

$$= \sum_{f\in\mathscr{F}_h}\int_f \nabla\mathcal{R}_f^{\mathscr{V}_h}(u_h)\cdot\mathbf{\Phi}\ dA, \qquad \mathcal{R}_f^{\mathscr{V}_h}(u_h)\in H^1(f), \tag{3.4.72}$$

$$= \sum_{f\in\mathscr{F}_h}\int_f \mathcal{R}_f^{\mathscr{E}_h}(\nabla_h u_h)\cdot\mathbf{\Phi}\ dA, \qquad \text{local commutativity}, \tag{3.4.73}$$

$$= \int_\Omega \sum_{f\in\mathscr{F}} \mathcal{R}_f^{\mathscr{E}_h}(\nabla_h u_h)\chi_f\cdot\mathbf{\Phi}\ dA, \tag{3.4.74}$$

$$= \int_\Omega \mathcal{R}^{\mathscr{E}_h}(\nabla_h u_h)\cdot\mathbf{\Phi}\ dA. \tag{3.4.75}$$

As $\mathbf{\Phi}$ and u_h were chosen arbitrarily we have $\nabla\circ\mathcal{R}^{\mathscr{V}_h} = \mathcal{R}^{\mathscr{E}_h}\circ\nabla_h$ in the sense of distributions. Given that $\mathcal{R}^{\mathscr{V}_h}(u_h)\in H^1(\Omega)$ and that $\mathcal{R}^{\mathscr{E}_h}(\nabla_h u_h)\in L^2(\Omega)$ we have this identity in the sense of H^1 as well.

Fix arbitrary $\mathbf{E}_h\in\mathscr{E}_h$. Similarly curl $\mathcal{R}^{\mathscr{E}_h}(\mathbf{E}_h)$ in the sense of distributions is given as

$$\int_\Omega \mathcal{R}^{\mathscr{E}_h}(\mathbf{E}_h)\cdot\mathbf{curl}\psi\ dA = \sum_{f\in\mathscr{F}}\int_f \mathcal{R}_f^{\mathscr{E}_h}(\mathbf{E}_h)\cdot\mathbf{curl}\ \psi\ dA, \tag{3.4.76}$$

$$= \sum_{f\in\mathscr{F}}\int_f \text{curl}\ \mathcal{R}_f^{\mathscr{E}_h}(\mathbf{E}_h)\psi\ dA, \qquad \mathcal{R}_f^{\mathscr{E}_h}(\mathbf{E}_h)\in\mathbf{H}(\text{curl},f), \tag{3.4.77}$$

$$= \sum_{f\in\mathscr{F}}\int_f \mathcal{R}_f^{\mathscr{F}_h}(\text{curl}_h\mathbf{E}_h)\psi\ dA, \qquad \text{local commutativity}, \tag{3.4.78}$$

$$= \int_\Omega \mathcal{R}^{\mathscr{F}_h}(\text{curl}_h\mathbf{E}_h)\psi\ dA. \tag{3.4.79}$$

Similarly we have shown that curl $\mathcal{R}^{\mathscr{E}_h}(\mathbf{E}_h) = \mathcal{R}^{\mathscr{F}_h}(\text{curl}_h\mathbf{E}_h)$ in the sense of distributions and $\mathbf{H}(\text{curl},\Omega)$. **Q.E.D.**

Having now developed the theory of reconstruction we can make two qualitative observations about our Mimetic Finite Difference Method. The first observation is that

having constructed a linear isomorphism to the reconstructed spaces V_h, E_h, F_h, and given that these spaces are a conformal subspaces containing polynomials of the continuum spaces, we can argue that reconstructed spaces are in fact finite element approximation spaces. These reconstruction spaces are exactly the approximation spaces developed in the *virtual element method*. We can interpret the MFD as a discretization of the *dual space* of a given virtual element space. This is recognizable as the space $\mathscr{S}_h$ is exactly the degrees of freedom of the reconstructed space. In this sense then we have $\mathscr{S}_h = S_h'$ in the traditional Hilbert space sense.

Secondly, while we developed a class of reconstructed spaces from which we can make approximation space arguments, the MFD has no preferred approximation space. By choosing a different reconstruction procedure which guarantees equivalent approximability, the MFD would then also be a dual space representation of any such reconstructed space. From this perspective then the MFD is a discretization of the dual space of all possible virtual element spaces for a given mesh.

3.5 Inner Products

Having developed in the previous section that our MFD spaces are linearly isomorphic to their reconstructed spaces, spaces which contain piecewise polynomials and are conformal subspaces of our continuum spaces, we are very close to inheriting *a-priori* estimates from lowest order mixed finite element methods. However, we are missing a crucial component of such discretizations– namely a discrete notion of the inner product. These discrete inner products will have to respect integration against polynomials. For the other functions in our reconstructed spaces we will make errors, but these will be in essence the same as of selecting a quadrature to evaluate the integrals in a finite element method.

We will make repeated throughout the section of polynomial projections.

Definition 3.5.1. Let $A \subset \Omega$ have non-zero measure. Let u be some $L^2(\Omega)$ function. We call the $\mathbb{P}_k$ *projection of* u *on* A the function $\Pi_k^A(u)$ defined by

$$\int_A \Pi_k^A(f)p \; dA = \int_A fp \; dA, \quad \forall p \in \mathbb{P}_k(A). \tag{3.5.1}$$

We will now define our inner products.

Definition 3.5.2. We define the *global global inner* products as follows:

$$[u_h, v_h]_{\mathscr{V}} = u_h^T \mathbb{M}_{\mathscr{V}} v_h, \quad [\mathbf{E}_h, \mathbf{D}_h]_{\mathscr{E}} = \mathbf{E}_h^T \mathbb{M}_{\mathscr{E}} \mathbf{D}_h, \quad [F_h, H_h]_{\mathscr{F}} = F_h^T \mathbb{M}_{\mathscr{F}} H_h. \tag{3.5.2}$$

Where each matrix will be symmetric positive definite approximation of the L^2 inner product on Ω. Global inner products will be assembled from *local inner products* on every face $f \in \mathscr{F}$.

$$[u_f, v_f]_{\mathscr{V},f} = u_f^T \mathbb{M}_{\mathscr{V},f} v_f, \quad [\mathbf{E}_f, \mathbf{D}_f]_{\mathscr{E},f} = \mathbf{E}_f^T \mathbb{M}_{\mathscr{E},f} \mathbf{D}_f, \tag{3.5.3}$$

$$[F_f, H_f]_{\mathscr{F},f} = F_h^T \mathbb{M}_{\mathscr{F},f} H_f. \tag{3.5.4}$$

Our local inner products must satisfy the following hypotheses.

Symmetric Positive Definite: $\mathbb{M}_{\mathscr{S},f}$ must satisfy

$$u_h^T \mathbb{M}_{\mathscr{S},f} u_h \geq 0, \quad u_h^T \mathbb{M}_{\mathscr{S},f} u_h = 0 \implies u_h = \mathbf{0} \tag{3.5.5}$$

and $\mathbb{M}_{\mathscr{S},f} = \mathbb{M}_{\mathscr{S},f}^T$.

Polynomial Exactness: Our integration must be exact for polynomials. Let $\{p_i\}$ be a basis for the polynomial space $\mathbb{P}_k(f)^d$. We will have $k = 0$ for $\mathscr{E}_h, \mathscr{F}_h$ and $k = 1$ for $\mathscr{V}_h$. Further $d = 0$ for $\mathscr{V}_h, \mathscr{F}_h$ and $d = 2$ for $\mathscr{E}_h$. Let K be an appropriate inner product weight on L^2.

$$[u_h, \mathcal{I}^{\mathscr{S}_h}(p_i)]_{\mathscr{S},f} \approx \int_f K \mathcal{R}_f^{\mathscr{S}_h}(u_h) p_i \; dA. \tag{3.5.6}$$

and further if $\mathcal{R}_h^{\mathscr{S}_h}(u_h) \in \mathbb{P}_k(f)^d$ then it most hold exactly.

If we have n distinct weights $K_1, K_2, \cdots, K_n$ we will denote each inner product by

$$[\cdot,\cdot]^{K_i}_{\mathscr{S}_h} \text{ with corresponding matrix } \mathbb{M}^{K_i}_{\mathscr{S}}. \tag{3.5.7}$$

If one the weights K_j is the identity we would leave that matrix with no special marking.

Remark. When we defined our reconstructions we were able to show that every local approximation space S_f can be decomposed into $\mathbb{P}_k(f)^d \oplus \tilde{S}_f$ where $\tilde{S}_f$ could contain non-polynomial functions. This gives us $\mathcal{R}_f^{\mathscr{S}_h}(u_h) = q_k + v$ where $q_k \in \mathbb{P}_k(f)^d$ and $v \in \tilde{S}_f$. Our definition of polynomial exactness states that

$$[u_h, \mathcal{I}^{S_h}(p)]_{\mathscr{S},f} = \int_f K q_k p \; dA. \tag{3.5.8}$$

which is in essence assuming that $\tilde{S}_f$ is $L^2(K,f)$ orthogonal to $\mathbb{P}_k(f)^d$. However, $\tilde{S}_f$ is only provably L^2 orthogonal to $\mathbb{P}_k$.

While never explicitly stated this way, the literature is full of examples of this sort of approximation. For example, assuming $K\Pi_k(K^{-1}p) \approx p$ for every $p \in \mathscr{P}_k$.

In order to construct local inner product matrices we make use of the following construction.

Theorem 3.5.1. *Fix arbitrary $f \in \mathscr{F}$. Let $\{p_i\}, \{\tilde{p}_i\}$ be bases for $\mathbb{P}_k(f)^d$ satisfying:*

$$\int_f K\tilde{p}_i p \; dA = \int_f p_i p \; dA, \quad \forall p \in \mathbb{P}_k(f)^d, \tag{3.5.9}$$

where $k = 0$ for $\mathscr{E}_h, \mathscr{F}_h$ and $k = 1$ for $\mathscr{V}_h$ and $d = 1$ for $\mathscr{V}_h, \mathscr{F}_h$ and $d = 2$ for $\mathscr{E}_h$. We define the matrix $\mathbb{N}$ by its columns (called $\mathbb{N}_i$) by

$$\mathbb{N}_i = \mathcal{I}_f^{\mathscr{S}_h}(\tilde{p}_i). \tag{3.5.10}$$

We define the matrix $\mathbb{R}$ by its columns so that

$$u_h^T \mathbb{R}_i \approx \int_f K\mathcal{R}_f^{\mathscr{S}_h}(u_h)\tilde{p}_i \; dA, \quad \forall u_h \in \mathscr{S}_h \tag{3.5.11}$$

$$= \int_f \mathcal{R}^{\mathscr{S}_h}(u_h) p_i \; dA, \quad \forall u_h \text{ such that } \mathcal{R}_f^{\mathscr{S}_h}(u_h) \in \mathbb{P}_k(f)^d. \tag{3.5.12}$$

We then have the identity

$$\mathbb{M}_{\mathscr{S},f}\mathbb{N} = \mathbb{R}. \tag{3.5.13}$$

The local matrix $\mathbb{M}_{\mathscr{S}_h}$ *can be expressed in the form*

$$\mathbb{M}_{\mathscr{S}_h,f} = \mathbb{M}_1 + \mathbb{M}_2, \mathbb{M}_1 \qquad = \mathbb{R}(\mathbb{N}^T\mathbb{R})^{-1}\mathbb{R}^T \tag{3.5.14}$$

$$\mathbb{M}_2 = |f|\mathbb{Q}\mathbb{C}\mathbb{Q}^T. \tag{3.5.15}$$

Here the columns of $\mathbb{Q}$ *are a basis for the null space of* $\mathbb{N}^T$ *and* $\mathbb{C}$ *is an SPD matrix. Such an* $\mathbb{M}_{\mathscr{S}_h,f}$ *has the following four properties:*

1. *polynomial exactness,*
2. $\mathbb{N}^T\mathbb{R}$ *is SPD,*
3. $\mathbb{M}_{\mathscr{S}_h,f}$ *is SPD.*

Proof. 1. Polynomial exactness follows from the definition of the matrices $\mathbb{N}$ and $\mathbb{R}$. Consider $p_h = \mathcal{I}_f^{\mathscr{S}_h}(\tilde{p}_i)$. Then p_h is in the span $\mathbb{N}$, i.e. $\tilde{p}_h = \mathbb{N}c$ where $c_j = \delta_{ij}$.

$$[u_h, p_h]_{\mathscr{S},f} = u_h^T\mathbb{M}_{\mathscr{S},f}p_h = u_h^T\mathbb{M}_{\mathscr{S}_h,f}\mathbb{N}c, \tag{3.5.16}$$

$$= u_h^T\mathbb{R}c, \tag{3.5.17}$$

$$= \int_f \mathcal{R}_f^{\mathscr{S}_h}(u_h)p_i \; dA, \tag{3.5.18}$$

$$= \int_f \mathcal{R}_f^{\mathscr{S}_h}(u_h)p_i \; dA. \tag{3.5.19}$$

This is exactly polynomial consistency.

2. Consider the product $\mathbb{N}^T\mathbb{R}$.

$$[\mathbb{N}^T\mathbb{R}]_{i,j} = \int_f K\mathcal{R}_f^{\mathscr{S}_h} \circ \mathcal{I}_f^{\mathscr{S}_h}(\tilde{p}_i)\tilde{p}_j \tag{3.5.20}$$

$$= \int_f K\tilde{p}_i\tilde{p}_j. \qquad \mathcal{R}_f^{\mathscr{S}_h} \circ \mathcal{I}_f^{\mathscr{S}_h} \text{exact on } \mathbb{P}_k. \tag{3.5.21}$$

This is exactly the $L^2(K, f)$ Gram matrix of $\mathbb{P}_k$ which is SPD.

3. Symmetry of $\mathbb{M}_{\mathscr{S},f}$ is immediate. Consider $u_h = \mathbb{N}x + \mathbb{Q}y$.

$$u_h^T \mathbb{M}_{\mathscr{S},f} u_h = (\mathbb{N}x)^T \mathbb{M}_1 (\mathbb{N}x) + (\mathbb{Q}y)^T \mathbb{M}_2 \mathbb{Q}_y. \tag{3.5.22}$$

We will now consider each component.

$$(\mathbb{N}x)^T \mathbb{M}_1 \mathbb{N}x = (\mathbb{N}x)^T \mathbb{R}(\mathbb{N}^T\mathbb{R})^{-1}\mathbb{R}^T\mathbb{N}x \qquad \text{by definition} \tag{3.5.23}$$

$$= x^T \mathbb{N}^T \mathbb{R} x. \tag{3.5.24}$$

We have previously demonstrated $\mathbb{N}^T\mathbb{R}$ is SPD so we have positivity and definiteness. For the other component we have

$$(\mathbb{Q}y)^T \mathbb{M}_2 \mathbb{Q}y = y^T(\mathbb{Q}^T\mathbb{Q})\mathbb{C}(\mathbb{Q}^T\mathbb{Q})y. \tag{3.5.25}$$

That matrix $\mathbb{Q}^T\mathbb{Q}$ is full rank as the columns of $\mathbb{Q}$ are linearly independent. AS $\mathbb{C}$ is SPD we have positivity and definiteness.

Q.E.D.

We next construct our inner product matrices.

Construction 3.1 ($\mathbb{M}_{\mathscr{F},f}$)**.** This construction is simple enough that it does not rely upon Theorem 3.5.1, but rather is produced directly from the polynomial exactness property. Fix $H_h \in \mathscr{F}_h$. Let $p = 1$.

$$[H_h, \mathcal{I}_f^{\mathscr{F}_h}(p)]_{\mathscr{F},f} = \int_f \mu \mathcal{R}_f^{\mathscr{F}_h}(H_h) p \, dA \tag{3.5.26}$$

$$= \mathcal{R}_f^{\mathscr{F}_h}(H_h) \int_f \mu \, dA \qquad p, \mathcal{R}_f^{\mathscr{F}_h}(H_h) \text{ constant}, \tag{3.5.27}$$

$$= \mathcal{R}_f^{\mathscr{F}_h}(H_h) |f| \Pi_0^f(\mu). \tag{3.5.28}$$

Choosing $\mathbb{M}_{\mathscr{F}_h,f} = |f|\Pi_0^f(\mu)$ we then must have the polynomial exactness condition. As μ is positive and bounded we know that the resulting matrix is SPD. After assembling local matrices into the global matrix $\mathbb{M}_{\mathscr{F}}$ we will maintain this property and, in addition, have a diagonal matrix $\mathbb{M}_{\mathscr{F}}$.

Construction 3.2 ($\mathbb{M}_{\mathscr{E},f}$)**.** We will now construct the matrices $\mathbb{N}$ and $\mathbb{R}$ for the space $\mathscr{E}_h$. First we will define two polynomials.

$$p_1(x,y) = (y - y_c) - \frac{1}{|f|}\int_f (y - y_c), \quad p_2 = -(x - x_c) + \frac{1}{|f|}\int_f (x - x_c). \tag{3.5.29}$$

Here (x_c, y_c) is the barycenter of f. We have $\mathbf{curl}\ p_1 = \mathbf{e}_1$ and $\mathbf{curl}\ p_2 = \mathbf{e}_2$ where $\mathbf{e}_1, \mathbf{e}_2$ are the standard basis functions. Further the p_i's are L^2 orthogonal to constant functions by construction. Let $\tilde{\mathbf{e}}_i$ be a solution to the following projection problem on $\mathbb{P}_0(f)^2$.

$$\int_f \tilde{\mathbf{e}}_i{}^T K \mathbf{e}_j \ dA = \int_f \mathbf{e}_i^T \mathbf{e}_j \ dA \tag{3.5.30}$$

We then define the columns of the matrix $\mathbb{N}$ (referred to as $\mathbb{N}_i$) as

$$\mathbb{N}_i = \mathcal{I}_f^{\mathscr{E}_h}(\tilde{\mathbf{e}}_i). \tag{3.5.31}$$

This then gives us the identity

$$\mathbf{E}_h^T \mathbb{M}_{\mathscr{E},f} \mathbb{N} = \left(\int_f \mathcal{R}_f^{\mathscr{E}_h}(\mathbf{E}_h)^T K \tilde{e}_1 \ dA, \int_f \mathcal{R}_f^{\mathscr{E}_h}(\mathbf{E}_h)^T K \tilde{\mathbf{e}}_2 \ dA \right). \tag{3.5.32}$$

We then define the columns of $\mathbb{R}$ such that

$$\mathbf{E}_h^T \mathbb{R}_i = \int_f \mathcal{R}_f^{\mathscr{E}_h}(\mathbf{E}_h)^T K \tilde{\mathbf{e}}_i \ dA \tag{3.5.33}$$

$$= \int_f \mathcal{R}_f^{\mathscr{E}_h}(\mathbf{E}_h)^T \mathbf{e}_i \ dA. \tag{3.5.34}$$

We will now show the integral is computable.

$$\mathbf{E}_h^T \mathbb{R}_i = \int_f \mathcal{R}^{\mathscr{E}_h}(\mathbf{E}_h) \cdot \mathbf{e}_i \ dA \tag{3.5.35}$$

$$= \int_f \mathrm{curl} \mathcal{R}^{\mathscr{E}_h}(\mathbf{E}_h) p_i \ dA - \sum_{e \in \partial f} \int_e \boldsymbol{\tau}_e \mathcal{R}^{\mathscr{E}_h}(\mathbf{E}_h) p_i \ ds \qquad \text{Stokes' Theorem} \tag{3.5.36}$$

$$= \int_f \mathcal{R}^{\mathscr{F}_h}(\mathrm{curl}_h \mathbf{E}_h) p_i \ dA - \sum_{e \in \partial f} \int_e \boldsymbol{\tau}_e \mathcal{R}^{\mathscr{E}_h}(\mathbf{E}_h) p_i \ ds \qquad \text{commutativity} \tag{3.5.37}$$

$$= \int_f \mathcal{R}^{\mathscr{F}_h}(\mathrm{curl}_h \mathbf{E}_h) p_i \ dA - \sum_{e \in \partial f} \sigma_{f,e} \mathcal{R}_e^{\mathscr{E}_h}(\mathbf{E}_h) \int_e p_i \ ds \qquad \mathcal{R}_e^{\mathscr{E}_h}(\mathbf{E}_h) \text{ is constant} \tag{3.5.38}$$

Thus,

$$\mathbf{E}_h^T\mathbb{R}_i = \mathcal{R}^{\mathscr{F}_h}(\mathrm{curl}_h\mathbf{E}_h)\int_f p_i\ dA - \sum_{e\in\partial f}\sigma_{f,e}\mathcal{R}_e^{\mathscr{E}_h}(\mathbf{E}_h)\int_e p_i\ ds \qquad \mathcal{R}_f^{\mathscr{F}_h}(H_h) \text{ is constant} \tag{3.5.39}$$

$$= -\sum_{e\in\partial f}\sigma_{f,e}\mathcal{R}_e^{\mathscr{E}_h}(\mathbf{E}_h)\int_e p_i\ ds \qquad \int_f p_i = 0 \tag{3.5.40}$$

$$= -\sum_{e\in\partial f}\sigma_{f,e}\mathbf{E}_e\int_e p_i\ ds \qquad \text{right inverse property} \tag{3.5.41}$$

The integral $\int_e p_i\ ds$ is computable, for example, with the midpoint quadrature

$$\int_e p_i = |e|p_i(s_e)\ ds, \quad s_e \text{ the midpoint of } e. \tag{3.5.42}$$

We therefore have that

$$\mathbb{R}_{i,j} = -\sigma_{f,e_j}|e_j|p_i(s_{e_j}) \tag{3.5.43}$$

Using Theorem 3.5.1 and this construction we can compute the inner product matrix $\mathbb{M}_{\mathscr{E}_h,f}$.

Construction 3.3 ($\mathbb{M}_{\mathscr{V},f}$)**.** We will now construct the matrices $\mathbb{N}$ and $\mathbb{R}$ for the inner product $\mathbb{M}_{\mathscr{V},f}$. Assume our inner product has a weight σ. We consider the following basis of $\mathbb{P}_1$

$$p_1 = 1, \quad p_2 = x - x_f, \quad p_3 = y - y_f \tag{3.5.44}$$

where (x_f, y_f) is the barycenter of f. We will write $p_i = \mathrm{div}\mathbf{p}_i$ and further write $\mathbf{p}_i = \nabla q_i$ where q_i is mean zero, i.e. $\int_f q_i\ dA = 0$.

$$\mathbf{q}_1 = \frac{1}{2}\begin{pmatrix} x - x_f \\ y - y_f \end{pmatrix}, \quad \mathbf{q}_2 = \frac{1}{2}\begin{pmatrix} (x - x_f)^2 \\ 0 \end{pmatrix}, \quad \mathbf{q}_3 = \frac{1}{2}\begin{pmatrix} 0 \\ (y - y_f)^2 \end{pmatrix}, \tag{3.5.45}$$

$$\mathbf{p}_i = \mathbf{q}_i - \Pi_0^f(\mathbf{q}_i). \tag{3.5.46}$$

To define the matrix $\mathbb{N}$ we use a similar technique to the previous construction. Define the polynomial $\tilde{p}_i$ by the projection problem

$$\int_f K\tilde{p}_i p_j\ dA = \int_f p_i p_j\ dA. \tag{3.5.47}$$

We then define the columns of the matrix $\mathbb{N}$ by

$$\mathbb{N}_i = \mathcal{I}_f^{\mathscr{V}_h}(\tilde{p}_i). \tag{3.5.48}$$

Using integration by parts we will now define integration of p_i against $\mathcal{R}_f^{\mathscr{V}_h}(u_h)$ for arbitrary $u_h \in \mathscr{V}_h$.

$$u_h^T \mathbb{R}_i = \int_f K \mathcal{R}_f^{\mathscr{V}_h}(u_h)\tilde{p}_i \tag{3.5.49}$$

$$\approx \int_f \mathcal{R}_f^{\mathscr{V}_h}(u_h)p_i. \tag{3.5.50}$$

This step is justified as we are neglecting the integral against the non-polynomial part of $\mathcal{R}_f^{\mathscr{V}_h}(u_h)$.

$$u_h^T \mathbb{R}_i = \int_f \mathcal{R}_f^{\mathscr{V}_h}(u_h)\text{div}\mathbf{p}_i \, dA \tag{3.5.51}$$

$$= -\int_f \nabla \mathcal{R}_f^{\mathscr{V}_h}(u_h) \cdot \mathbf{p}_i \, dA + \sum_{e \in \partial f} \int_e \mathcal{R}_f^{\mathscr{V}_h}(u_h)\mathbf{n} \cdot \mathbf{p}_i \, ds \qquad \text{integration by parts} \tag{3.5.52}$$

$$= -\int_f \mathcal{R}_f^{\mathscr{E}_h}(\nabla_h u_h) \cdot \mathbf{p}_i \, dA + \sum_{e \in \partial f} \int_e \mathcal{R}_f^{\mathscr{V}_h}(u_h)\mathbf{n} \cdot \mathbf{p}_i \, ds \qquad \text{commutativity} \tag{3.5.53}$$

$$-\int_f \mathcal{R}_f^{\mathscr{E}_h}(\nabla_h u_h) \cdot \mathbf{p}_i \, dA + \sum_{e \in \partial f} \int_e \mathcal{R}_e^{\mathscr{V}_h}(u_h)\mathbf{n} \cdot \mathbf{p}_i \, ds \qquad \text{consistency.} \tag{3.5.54}$$

We will neglect the interior integral of $\mathcal{R}_f^{\mathscr{E}_h}(\nabla_h u_h)$ against $\mathbf{p}_i$ as $\mathbf{p}_i$ is mean zero and the gradient of the polynomial part of $\mathcal{R}_f^{\mathscr{E}_h}(\nabla_h u_h)$ is constant. We therefore have th formula

$$u_h^T \mathbb{R}_i = \sum_{e \in \partial f} \int_e \mathcal{R}_e^{\mathscr{V}_h}(u_h)\mathbf{n} \cdot \mathbf{p}_i. \tag{3.5.55}$$

This is computable as $\mathcal{R}_e^{\mathscr{V}_h}$ has a closed form and as $\mathbf{n} \cdot \mathbf{p}_i$ is a polynomial. The maximum order of the product $\mathcal{R}_e^{\mathscr{V}_h}(u_h)\mathbf{n} \cdot \mathbf{p}_i$ is 3 so it is exactly computable with a two point Gaussian quadrature on each edge.

With the following three constructions in place we now have defined classes of inner product matrices which are exact on either $\mathbb{P}_0$ or $\mathbb{P}_1$ in the case of $\mathbb{M}_{\mathscr{V}}$. The inner product matrices $\mathbb{M}_{\mathscr{E}}, \mathbb{M}_{\mathscr{V}}$ are not completely defined as they depend on choosing selecting the matrix $\mathbb{C}$.

A simple choice of $\mathbb{C}$ is given a:

$$\mathbb{C} = |f|(\mathbb{Q}^T\mathbb{Q})^{-1}. \tag{3.5.56}$$

Then the resulting $\mathbb{M}_2$ is the default choice for the MFD.

$$\mathbb{M}_2 = |f|\mathbb{Q}(\mathbb{Q}^T\mathbb{Q})^{-1}\mathbb{Q}^T = |f|(\mathbb{I} - \mathbb{N}(\mathbb{N}^T\mathbb{N})^{-1}\mathbb{N}^T). \tag{3.5.57}$$

This last equality is true as $\mathrm{Im}\mathbb{Q} \perp \mathrm{Im}\mathbb{N}$ and $\mathbb{M}_2$ is the projection onto the orthogonal complement of $\mathbb{N}$. That is to say that we integrate any function which is orthogonal to the polynomial space $\mathbb{P}_k$ by using the value $|f|$. A significant portion of the MFD literature is devoted to proving that MFD discretizations using this choice of stabilization matrix result in convergent, i.e. consistent and stable, dicretizations of PDEs.

The existence of a stable $\mathbb{M}_2$ is useful in that it does not require the selection of tuning parameters. However, the Mimetic Finite Difference does allow for tuning parameters. The selection of an optimal matrix $\mathbb{C}$ is generally referred to as **M-adaptation** or Mimetic-adaptation.

3.6 MFD Construction on Rectangular Meshes

The previous theoretical development has been rather abstract. In this section we will present local MFD constructions on a rectangular cell to make this construction concrete. We will assume no weighting functions, K, for simplicity.

We consider a cell $f = [-\frac{\Delta x}{2}, \frac{\Delta x}{2}] \times [-\frac{\Delta y}{2}, \frac{\Delta y}{2}]$ with edges e_1, e_2, e_3, e_4 and vertices $\mathbf{v}_1, \mathbf{v}_2, \mathbf{v}_3\mathbf{v}_4$ as pictured in Figure 3.3. In this context the local face function inner product

is given by

$$\mathbb{M}_{\mathscr{F},f} = \Delta x \Delta y. \tag{3.6.1}$$

Our local degrees of freedom for the spaces $\mathscr{V}_f, \mathscr{E}_f, \mathscr{F}_f$ are identical to the general con-

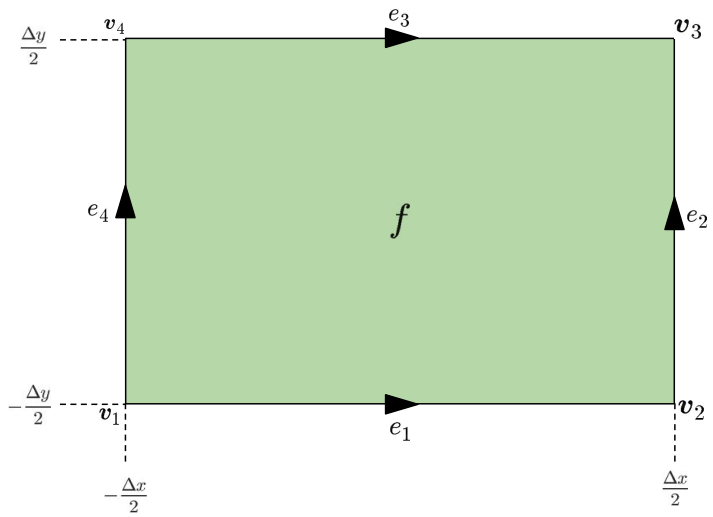

FIGURE 3.3: Local degrees of freedom for the cell f. Arrows on edges represent the orientation of our edges.

struction.

Construction 3.4. We will first compute the discrete curl operator $\text{curl}_{h,f}$. As defined before we have

$$\text{curl}_{h,f}\mathbf{E}_f = \frac{1}{|f|}\sum_{e\in\partial f}\sigma_{f,e}|e|\mathbf{E}_e = \frac{1}{|f|}\int_{\partial f}\boldsymbol{\tau}\cdot\mathbf{E}\ ds. \tag{3.6.2}$$

Where the orientation constant in (3.6.2) $\sigma_{f,e}$ guarantees that boundary path runs counter-clockwise. Given that all of our edges are oriented with the principal axes we therefore have

$$\sigma_{f,e_1} = \sigma_{f,e_2} = 1, \qquad \sigma_{f,e_3} = \sigma_{f,e_4} = -1. \tag{3.6.3}$$

Our odd numbered edges have length Δx while our even numbered edges have length Δy and $|f| = \Delta x \Delta y$. We therefore have $\text{curl}_{h,f}$ given as

$$\text{curl}_{h,f} = \frac{1}{\Delta x \Delta y}\begin{pmatrix}\Delta x & \Delta y & -\Delta x & -\Delta y\end{pmatrix}. \tag{3.6.4}$$

Construction 3.5. We will now compute the discrete graidnt on some edge e_i, ∇_{h,e_i}. The boundary vertices of edge e_i are given by i and $j = \mathrm{mod}(i,4)+1$. Our definition of ∇_h uses the fundamental theorem of line integrals applied to the direction derivative $\frac{\partial}{\partial \tau}$ and along each edge. The formulas for each edge are given by

$$\nabla_{h,e_1} = \frac{1}{\Delta x}\begin{pmatrix} -1 & 1 & 0 & 0 \end{pmatrix}, \tag{3.6.5}$$

$$\nabla_{h,e_2} = \frac{1}{\Delta y}\begin{pmatrix} 0 & -1 & 1 & 0 \end{pmatrix}, \tag{3.6.6}$$

$$\nabla_{h,e_3} = \frac{1}{\Delta x}\begin{pmatrix} 0 & 0 & -1 & 1 \end{pmatrix}, \tag{3.6.7}$$

$$\nabla_{h,e_4} = \frac{1}{\Delta x}\begin{pmatrix} -1 & 0 & 0 & 1 \end{pmatrix}. \tag{3.6.8}$$

Construction 3.6. We will now construct the matrix $\mathbb{M}_{\mathscr{E},f}$. Our two basis vectors are $\mathbf{e}_1, \mathbf{e}_2$ and their corresponding polynomials are

$$p_1 = y, \quad p_2 = -x, \text{ where } \mathbf{curl}\ p_i = \mathbf{e}_i. \tag{3.6.9}$$

Note that p_1, p_2 have zero mean. Our matrix $\mathbb{N}$ is given by the degrees of freedom of $\mathbf{e}_i$, i.e.

$$\mathbb{N} = \begin{pmatrix} 1 & 0 \\ 0 & 1 \\ 1 & 0 \\ 0 & 1 \end{pmatrix}. \tag{3.6.10}$$

To construct the matrix $\mathbb{R}$ recall our identity from Construction 3.2 that

$$\mathbb{R}_{ij} = -\sigma_{f,e_j}|e_j|p_i(s_{e_j}) \tag{3.6.11}$$

where s_{e_j} is the midpoint of e_j. This formula produces

$$\mathbb{R} = \frac{\Delta x \Delta y}{2}\mathbb{N}. \tag{3.6.12}$$

We also have $\mathbb{N}^T\mathbb{R} = \Delta x \Delta y \mathbb{I}_{2\times 2}$ which gives us

$$\mathbb{M}_1 = \mathbb{R}(\mathbb{N}^T\mathbb{R})^{-1}\mathbb{R}^T = \frac{\Delta x \Delta y}{4}\mathbb{N}\mathbb{N}^T = \frac{\Delta x \Delta y}{4}\begin{pmatrix} 1 & 0 & 1 & 0 \\ 0 & 1 & 0 & 1 \\ 1 & 0 & 1 & 0 \\ 0 & 1 & 0 & 1 \end{pmatrix}. \tag{3.6.13}$$

The columns of matrix $\mathbb{Q}$ are the orthogonal complement of the image of $\mathbb{N}$ in $\mathbb{R}^4$. We choose $\mathbb{Q}$ as

$$\mathbb{Q} = \begin{pmatrix} -1 & 0 \\ 0 & -1 \\ 1 & 0 \\ 0 & 1 \end{pmatrix}. \tag{3.6.14}$$

Under the standard choice of the matrix $\mathbb{M}_2$ we would have

$$\mathbb{Q} = 2\Delta x \Delta y \mathbb{Q}(\mathbb{Q}^T\mathbb{Q})^{-1}\mathbb{Q}^T = \Delta x \Delta y \begin{pmatrix} 1 & 0 & -1 & 0 \\ 0 & 1 & 0 & -1 \\ -1 & 0 & 1 & 0 \\ 0 & -1 & 0 & 1 \end{pmatrix}. \tag{3.6.15}$$

For a parameterized choice of $\mathbb{M}_2$ we define

$$\mathbb{C} = \begin{pmatrix} w_1 & w_2 \\ w_2 & w_3 \end{pmatrix}. \tag{3.6.16}$$

Thus,

$$\mathbb{M}_2 = 2\Delta x \Delta y \mathbb{Q}\mathbb{C}\mathbb{Q}^T = \Delta x \Delta y \begin{pmatrix} w_1 & w_2 & -w_1 & -w_2 \\ w_2 & w_3 & -w_2 & -w_3 \\ -w_1 & -w_2 & w_1 & w_2 \\ -w_2 & -w_3 & w_2 & w_3 \end{pmatrix} \tag{3.6.17}$$

when we allow our parameters to absorb the constant 2.

Construction 3.7. We will now construct the local matrix $\mathbb{M}_{\mathscr{V},f}$. Our basis for $\mathbb{P}_1(f)$ and their corresponding vectors in $\mathbb{P}_2(f)^2$ are given by

$$p_1 = 1, \quad p_2 = \frac{x}{\Delta x}, \quad p_3 = \frac{y}{\Delta y}, \tag{3.6.18}$$

$$\mathbf{p}_1 = \frac{1}{2}\begin{pmatrix} x \\ y \end{pmatrix}, \quad \mathbf{p}_2 = \frac{1}{2\Delta x}\begin{pmatrix} x^2 - \frac{\Delta x^2}{12} \\ 0 \end{pmatrix}, \quad \mathbf{p}_2 = \frac{1}{2\Delta y}\begin{pmatrix} 0 \\ y^2 - \frac{\Delta y^2}{12} \end{pmatrix}. \tag{3.6.19}$$

Note that we have div $\mathbf{p}_i = p_i$. The matrix $\mathbb{N}$ is given by

$$\mathbb{N} = \begin{pmatrix} 1 & -\frac{1}{2} & -\frac{1}{2} \\ 1 & \frac{1}{2} & -\frac{1}{2} \\ 1 & \frac{1}{2} & \frac{1}{2} \\ 1 & -\frac{1}{2} & \frac{1}{2} \end{pmatrix}. \tag{3.6.20}$$

As per construction 3.3 we have the definition of $u_h^T\mathbb{R}_i$ as

$$u_h^T\mathbb{R}_i = \sum_{\mathrm{e}\in\partial f}\int_e \mathcal{R}_e^{\mathscr{V}_h}(u_h)\mathbf{n}\cdot\mathbf{p}_i \, ds. \tag{3.6.21}$$

We will now apply the formula for each i and extract a corresponding column vector.

$$u_h^T\mathbb{R}_1 = \int_{e_1}\left(\frac{u_{\mathbf{v}_2} - u_{\mathbf{v}_1}}{\Delta x}x + \frac{u_{\mathbf{v}_2} + u_{\mathbf{v}_1}}{2}\right)\left(-\frac{\Delta y}{4}\right)\, dx \tag{3.6.22}$$

$$+ \int_{e_2}\left(\frac{u_{\mathbf{v}_3} - u_{\mathbf{v}_2}}{\Delta y}y + \frac{u_{\mathbf{v}_3} + u_{\mathbf{v}_2}}{2}\right)\left(\frac{\Delta x}{4}\right)\, dy \tag{3.6.23}$$

$$+ \int_{e_3}\left(\frac{u_{\mathbf{v}_3} - u_{\mathbf{v}_4}}{\Delta x}x + \frac{u_{\mathbf{v}_3} + u_{\mathbf{v}_4}}{2}\right)\left(\frac{\Delta y}{4}\right)\, dx \tag{3.6.24}$$

$$+ \int_{e_4}\left(\frac{u_{\mathbf{v}_4} - u_{\mathbf{v}_1}}{\Delta y}y + \frac{u_{\mathbf{v}_4} + u_{\mathbf{v}_1}}{2}\right)\left(-\frac{\Delta x}{4}\right)\, dy, \tag{3.6.25}$$

$$= \frac{\Delta x\Delta y}{4}\Big(u_{\mathbf{v}_1} + u_{\mathbf{v}_2} + u_{\mathbf{v}_3} + u_{\mathbf{v}_4}\Big). \tag{3.6.26}$$

We therefore have

$$\mathbb{R}_1 = \frac{\Delta x\Delta y}{4}\begin{pmatrix} 1 & 1 & 1 & 1 \end{pmatrix}^T. \tag{3.6.27}$$

For the second column we have

$$u_h^T \mathbb{R}_2 = \int_{e_2} \left(\frac{u_{\mathbf{v}_3} - u_{\mathbf{v}_2}}{\Delta y} y + \frac{u_{\mathbf{v}_3} + u_{\mathbf{v}_2}}{2} \right) \left(\frac{\Delta x}{12} \right) \, dy \tag{3.6.28}$$

$$+ \int_{e_4} \left(\frac{u_{\mathbf{v}_4} - u_{\mathbf{v}_1}}{\Delta y} y + \frac{u_{\mathbf{v}_4} + u_{\mathbf{v}_1}}{2} \right) \left(-\frac{\Delta x}{12} \right) \, dy, \tag{3.6.29}$$

$$= \frac{\Delta x \Delta y}{24} \Big(- u_{\mathbf{v}_1} + u_{\mathbf{v}_2} + u_{\mathbf{v}_3} - u_{\mathbf{v}_4} \Big). \tag{3.6.30}$$

From this equality we can infer that

$$\mathbb{R}_2 = \frac{\Delta x \Delta y}{24} \begin{pmatrix} -1 & 1 & 1 & -1 \end{pmatrix}^T. \tag{3.6.31}$$

For the third column we have

$$u_h^T \mathbb{R}_3 = \int_{e_1} \left(\frac{u_{\mathbf{v}_2} - u_{\mathbf{v}_1}}{\Delta x} x + \frac{u_{\mathbf{v}_2} + u_{\mathbf{v}_1}}{2} \right) \left(-\frac{\Delta y}{12} \right) \, dx \tag{3.6.32}$$

$$+ \int_{e_3} \left(\frac{u_{\mathbf{v}_3} - u_{\mathbf{v}_4}}{\Delta x} x + \frac{u_{\mathbf{v}_3} + u_{\mathbf{v}_4}}{2} \right) \left(\frac{\Delta y}{12} \right) \, dx, \tag{3.6.33}$$

$$= \frac{\Delta x \Delta y}{24} \Big(- u_{\mathbf{v}_1} - u_{\mathbf{v}_2} + u_{\mathbf{v}_3} + u_{\mathbf{v}_4} \Big). \tag{3.6.34}$$

We can now determine the final column of $\mathbb{R}$.

$$\mathbb{R}_3 = \frac{\Delta x \Delta y}{24} \begin{pmatrix} -1 & -1 & 1 & 1 \end{pmatrix}^T. \tag{3.6.35}$$

The full matrix $\mathbb{R}$ is then given by

$$\mathbb{R} = \frac{\Delta x \Delta y}{4} \begin{pmatrix} 1 & -\frac{1}{6} & -\frac{1}{6} \\ 1 & \frac{1}{6} & -\frac{1}{6} \\ 1 & \frac{1}{6} & \frac{1}{6} \\ 1 & -\frac{1}{6} & \frac{1}{6} \end{pmatrix}. \tag{3.6.36}$$

The product $\mathbb{N}^T \mathbb{R}$ agrees exactly with the L^2 Gram matrix of our basis $\{p_1, p_2, p_3\}$,

$$\mathbb{N}^T \mathbb{R} = \Delta x \Delta y \begin{pmatrix} 1 & & \\ & \frac{1}{12} & \\ & & \frac{1}{12} \end{pmatrix}. \tag{3.6.37}$$

The inner product matrix for the polynomials is then given by

$$\mathbb{M}_1 = \frac{\Delta x \Delta y}{48} \begin{pmatrix} 5 & 3 & 1 & 3 \\ 3 & 5 & 3 & 1 \\ 1 & 3 & 5 & 3 \\ 3 & 1 & 3 & 5 \end{pmatrix}. \tag{3.6.38}$$

The matrix $\mathbb{Q}$ is the orthogonal compliment of the columns of $\mathbb{N}$ given by

$$\mathbb{Q} = \begin{pmatrix} -1 & 1 & -1 & 1 \end{pmatrix}^T. \tag{3.6.39}$$

The standard choice of $\mathbb{M}_2$ is given by

$$\mathbb{M}_2 = \mathrm{Tr}(\mathbb{M}_1)\mathbb{Q}(\mathbb{Q}^T\mathbb{Q})^{-1}\mathbb{Q} = \frac{5\Delta x \Delta y}{48} \begin{pmatrix} 1 & -1 & 1 & -1 \\ -1 & 1 & -1 & 1 \\ 1 & -1 & 1 & -1 \\ -1 & 1 & -1 & 1 \end{pmatrix}. \tag{3.6.40}$$

The matrix $\mathbb{M}_2$ is rank 1 our parameterized choice replaces the constant $\frac{5}{48}$ by some parameter w_1.

3.7 Adjoint Operators

With inner product matrices defined we will now introduce the concept of *adjoint differential operators*. Adjoint operators appear when the continuum variational formulation has moved differentiation from a variable of interest onto a test function. For example in the Ampere-Maxwell Law:

$$\int_\Omega \left(\frac{\partial}{\partial t}\mathbf{D} + \mathbf{J} \right) \cdot \mathbf{\Phi} \; dA = \int_\Omega H(\mathrm{curl}\mathbf{\Phi}) \; dA. \tag{3.7.1}$$

In the standard sense we are using the adjoint of the continuum **curl** operator applied to H rather than the primal **curl**. We would then discretize this variational formulation as

$$\left[\mathbf{\Phi}_h, \frac{\partial}{\partial t}\mathbf{D}_h + \mathbf{J}_h\right]_{\mathscr{V}_h} = \left[\mathrm{curl}_h \mathbf{\Phi}_h, H_h\right]_{\mathscr{F}_h} \tag{3.7.2}$$

Definition 3.7.1. Let H_1, H_2 be Hilbert spaces with corresponding inner products $[\cdot,\cdot]_{H_1}$ and $[\cdot,\cdot]_{H_2}$, and $\mathcal{A} : H_1 \to H_2$ be a bounded linear operator. We define $\mathcal{A}'$, *the adjoint of* $\mathcal{A}$, by the identity

$$[\mathcal{A}u, v]_{H_2} = [u, \mathcal{A}'v]_{H_1}, \quad \forall u \in H_1, v \in H_2. \tag{3.7.3}$$

Definition 3.7.2. Rather than writing all discretizations variationally we will instead define equivalent *adjoint differential operators.*

$$\widetilde{\mathrm{curl}}_h : \mathscr{F}_h \to \mathscr{E}_h, \tag{3.7.4}$$

$$[\mathbf{\Phi}_h, \widetilde{\mathrm{curl}}_h H_h]_{\mathscr{E}_h} = [\mathrm{curl}_h \mathbf{\Phi}_h, H_h]_{\mathscr{F}_h}, \quad \forall \mathbf{\Phi} \in \mathscr{E}_h, H_h \in \mathscr{F}_h, \tag{3.7.5}$$

$$\widetilde{\mathrm{div}}_h : \mathscr{E}_h \to \mathscr{V}_h, \tag{3.7.6}$$

$$[\psi_h, \widetilde{\mathrm{div}}_h \mathbf{E}_h]_{\mathscr{V}_h} = -[\nabla_h \psi_h, \mathbf{E}_h]_{\mathscr{E}_h}, \quad \forall \psi_h \in \mathscr{V}_h, \mathbf{E}_h \in \mathscr{E}_h. \tag{3.7.7}$$

These definitions naturally assume a homogeneous Dirichlet type boundary conditions. If you were interested in more sophisticated boundary conditions, we would build them into the adjoint operator. We define two adjoint operators for our 2D complex. A closed form of the adjoint operator can be computed as follows. Let $\mathbf{\Phi}_h \in \mathscr{E}_h$ and $H_h \in \mathscr{F}_h$.

$$[\mathbf{\Phi}_h, \widetilde{\mathrm{curl}}_h H_h]_{\mathscr{E}_h} = [\mathrm{curl}_h \mathbf{\Phi}_h, H_h]_{\mathscr{F}_h}, \tag{3.7.8}$$

$$\mathbf{\Phi}_h^T \mathbb{M}_{\mathscr{E}_h} \widetilde{\mathrm{curl}}_h H_h = \mathbf{\Phi}_h^T \mathrm{curl}_h^T \mathbb{M}_{\mathscr{F}_h} H_h, \tag{3.7.9}$$

$$\widetilde{\mathrm{curl}}_h = \mathbb{M}_{\mathscr{E}_h}^{-1} \mathrm{curl}_h^T \mathbb{M}_{\mathscr{F}_h}. \tag{3.7.10}$$

A closed form $\widetilde{\text{div}}_h$ can be computed as follows. Let $\mathbf{E}_h \in \mathscr{E}_h$ and $\psi_h \in \mathscr{V}_h$.

$$[\psi_h, \widetilde{\text{div}}_h \mathbf{E}_h]_{\mathscr{V}_h} = -[\nabla_h \psi_h, \mathbf{E}_h]_{\mathscr{E}_h}, \tag{3.7.11}$$

$$\psi_h^T \mathbb{M}_{\mathscr{V}_h} \widetilde{\text{div}}_h \mathbf{E}_h = -\psi_h^T \nabla_h^T \mathbb{M}_{\mathscr{E}_h} \mathbf{E}_h, \tag{3.7.12}$$

$$\widetilde{\text{div}}_h \mathbf{E}_h = -\mathbb{M}_{\mathscr{V}_h}^{-1} \nabla_h^T \mathbb{M}_{\mathscr{E}_h}. \tag{3.7.13}$$

3.8 Exact Sequence Property

The exact sequence property states in essence states that our discrete representation preserve the exterior calculus.

Definition 3.8.1. Consider an abstract Hilbert Complex with a corresponding discretization

$$\begin{array}{ccccccc} S_1 & \xrightarrow{d^1} & S_2 & \xrightarrow{d^2} & \cdots & \xrightarrow{d^{n-1}} & S_n \\ \downarrow{\scriptstyle \mathcal{I}^{\mathscr{S}_1}} & & \downarrow{\scriptstyle \mathcal{I}^{\mathscr{S}_2}} & & & & \downarrow{\scriptstyle \mathcal{I}^{\mathscr{S}_n}} \\ \mathscr{S}_1 & \xrightarrow{d_h^1} & \mathscr{S}_2 & \xrightarrow{d_h^2} & \cdots & \xrightarrow{d_h^{n-1}} & \mathscr{S}_n \end{array} \tag{3.8.1}$$

We say the discrete complex has the *exact sequence property* if

$$\text{Im}(d_h^{i-1}) = \text{Ker}(d_h^i), \quad 2 \leq i \leq n-1. \tag{3.8.2}$$

Theorem 3.8.1. *The 2D mimetic discretization of a* $(\nabla, curl)$ *Hilbert complex has the exact sequence property:*

$$Im(\nabla_h) = Ker(curl_h). \tag{3.8.3}$$

Proof. $\subseteq$**:** We will first show that $\text{curl}_h \nabla_h u_h = \mathbf{0}_{N_{\mathscr{F}}}$. Fix arbitrary $u_h \in \mathscr{V}_h$. Let $u =$

$\mathcal{R}^{\mathscr{V}_h}(u_h)$. Note that $\mathcal{I}^{\mathscr{V}_h}(u) = u_h$ by the right inverse property.

$$\begin{aligned}
\mathrm{curl}_h \circ \nabla_h \circ \mathcal{I}^{\mathscr{V}_h}(u) &= \mathrm{curl}_h \circ \mathcal{I}^{\mathscr{E}_h}(\nabla u) && \text{commutativity property,} && (3.8.4)\\
&= \mathcal{I}^{\mathscr{F}_h} \circ (\mathrm{curl}\nabla u) && \text{commutativity property,} && (3.8.5)\\
&= \mathcal{I}^{\mathscr{F}_h}(0) && \mathrm{curl}\nabla = 0 \text{ in the continuum,} && (3.8.6)\\
&= \mathbf{0}_{N_{\mathscr{F}}} && \text{interpolation is linear.} && (3.8.7)
\end{aligned}$$

This implies that $\mathrm{curl}_h \nabla_h u_h = \mathbf{0}_{N_{\mathscr{F}}}$.

$\supseteq$**:** Fix $\mathbf{E}_h \in \mathscr{E}_h$ such that $\mathrm{curl}_h \mathbf{E}_h = 0$. We will now show that $\mathbf{E}_h = \nabla_h u_h$ for some $u \in \mathscr{V}_h$. We will rely on commutativity properties of reconstruction operators.

$$\begin{aligned}
0 &= \mathcal{R}^{\mathscr{F}_h}(\mathrm{curl}_h \mathbf{E}_h), && \text{reconstruction is linear,} && (3.8.8)\\
&= \mathrm{curl} \circ \mathcal{R}^{\mathscr{E}_h}(\mathbf{E}_h), && \text{commutativity property.} && (3.8.9)
\end{aligned}$$

The space $E_h = \mathcal{R}^{\mathscr{E}_h}(\mathscr{E}_h)$ is embedded continuously in $\mathbf{H}(\mathrm{curl}, \Omega)$. Therefore $\mathcal{R}^{\mathscr{E}_h}(\mathbf{E}_h) \in \mathbf{H}(\mathrm{curl})$. As $\mathbf{H}(\mathrm{curl})$ has the Helmholtz decomposition property we know that $\mathcal{R}^{\mathscr{E}_h}(\mathbf{E}_h) = \nabla u$ for some $u \in H^1$.

$$\begin{aligned}
\mathbf{E}_h &= \mathcal{I}^{\mathscr{E}_h} \circ \mathcal{R}^{\mathscr{E}_h}(\mathbf{E}_h) && \text{right inverse property,} && (3.8.10)\\
&= \mathcal{I}^{\mathscr{E}_h}(\nabla u) && \text{Helmholtz decomposition on } \mathbf{H}(\mathrm{curl}), && (3.8.11)\\
&= \nabla_h \circ \mathcal{I}^{\mathscr{V}_h}(u) && \text{commutativity property.} && (3.8.12)
\end{aligned}$$

We have therefore shown that $\mathrm{curl}_h \mathbf{E}_h = 0$ implies $\mathbf{E}_h = \nabla_h u_h$ for some $u_h \in \mathscr{V}_h$.

Q.E.D.

Corollary 3.8.2. *Adjoint operators obey the exact sequence property:*

$$Im(\widetilde{curl}_h) = Ker(\widetilde{div}_h) \tag{3.8.13}$$

Proof. We have the following two adjoint properties:

$$[\mathbf{\Phi}, \widetilde{\text{curl}}_h H_h]_{\mathscr{E}_h} = [\text{curl}_h \mathbf{\Phi}, H_h]_{\mathscr{F}_h}, \tag{3.8.14}$$

$$[\psi, \widetilde{\text{div}}_h \mathbf{E}_h]_{\mathscr{V}_h} = -[\nabla_h \psi, \mathbf{E}_h]_{\mathscr{E}_h}. \tag{3.8.15}$$

Therefore, $\widetilde{\text{curl}}_h$ is adjoint to curl_h and $\widetilde{\text{curl}}_h$ and $-\widetilde{\text{div}}_h$ is adjoint to ∇_h in the traditional Hilbert space sense. We apply the fundamental theorem of linear algebra which states that if A is an operator and A' is its adjoint then $\text{Im}(A)^\perp = \text{Ker}(A')$ and equivalently $\text{Ker}(A) = \text{Im}(A')^\perp$ by way of the fact that $A'' = A$.

$$\begin{aligned}
\text{Ker}(\widetilde{\text{div}}_h) &= \text{Im}(-\nabla_h)^\perp && \text{Fundamental Theorem of Linear Algebra,} && (3.8.16)\\
&= \text{Im}(\nabla_h)^\perp && \text{linear closure,} && (3.8.17)\\
&= \text{Ker}(\text{curl}_h)^\perp && \text{Theorem 3.8.1,} && (3.8.18)\\
&= (\text{Im}(\widetilde{\text{curl}}_h)^\perp)^\perp && \text{Fundamental Theorem of Linear Algebra,} && (3.8.19)\\
&= \text{Im}(\widetilde{\text{curl}}_h). && && (3.8.20)
\end{aligned}$$

This last result follows from the following argument. If W is a linear subspace of a Hilbert space V, then $(W^\perp)^\perp = W$ if and only if W is closed in V. All linear subspaces are closed in finite dimensions therefore the result applies.

Q.E.D.

We will have the following result regarding the dimensions of our given subspaces.

Theorem 3.8.3. *The following subspaces have the given dimensions*

$$Dim(Im(\nabla_h)) = N_{\mathscr{E}} - N_{\mathscr{F}}, \tag{3.8.21}$$

$$Dim(Im(curl_h)) = N_{\mathscr{F}}, \tag{3.8.22}$$

$$Dim(Ker(\nabla_h)) = 1, \tag{3.8.23}$$

$$Dim(Ker(curl_h)) = N_{\mathscr{E}} - N_{\mathscr{F}}. \tag{3.8.24}$$

Proof. **Dim(Im(curl$_h$)):** We prove that the operator curl$_h$ is onto $\mathscr{F}_h$. We will primarily utilize reconstruction. Fix arbitrary $H_h \in \mathscr{F}_h$. Define $H = \mathcal{R}^{\mathscr{F}_h}(H_h)$. The operator curl : $\mathbf{H}(\text{curl}) \to L^2$ is onto therefore $H = \text{curl } \mathbf{E}$ for some $\mathbf{E} \in \mathbf{H}(\text{curl})$.

$$H_h = \mathcal{I}^{\mathscr{F}_h} \circ \mathcal{R}^{\mathscr{E}_h}(H_h) \qquad \text{right inverse property,} \tag{3.8.25}$$

$$= \mathcal{I}^{\mathscr{F}_h}(\text{curl}\mathbf{E}) \qquad \text{curl is onto } L^2, \tag{3.8.26}$$

$$= \text{curl}_h \circ \mathcal{I}^{\mathscr{F}_h}(\mathbf{E}) \qquad \text{commutativity property.} \tag{3.8.27}$$

Therefore every $H_h = \text{curl}_h \mathbf{E}_h$. We have shown that $\text{Im}(\text{curl}_h) = \mathscr{F}_h$, therefore

$$\text{Dim}(\text{Im}(\text{curl}_h)) = \text{Dim}(\mathscr{F}_h) = N_{\mathscr{F}}. \tag{3.8.28}$$

Dim(Ker(∇_h)): We have assumed that $\mathscr{T}$ is path connected. That is between any two vertices $\mathbf{v}, \mathbf{w} \in \mathscr{V}$ there exists a collection of edges $\{e_j\}_{j=1}^M \subset \mathscr{E}$ which forms a path between $\mathbf{v}$ and $\mathbf{w}$. Constant functions are in the kernel of ∇_h as we calculate our gradients by

$$\nabla_{h,e} u_e = \frac{u_{\mathbf{v}_2} - u_{\mathbf{v}_2}}{|e|} \tag{3.8.29}$$

with $u_{\mathbf{v}_2} = u_{\mathbf{v}_1}$ if and only if $\nabla_{h,e} u_e = 0$. Assume $\nabla_h u_h = \mathbf{0}_{\mathscr{E}_h}$.

Fix some vertex $\mathbf{v}_0 \in \mathscr{V}$. Now consider an arbitrary vertex $\mathbf{v}_{N+1} \in \mathscr{V}$. Path connected, gives us a sequence of intermediary vertices $\{\mathbf{v}_i\}_{i=1}^N$ such that $\mathbf{v}_i$ and $\mathbf{v}_{i-1}$ share an edge. By induction you can then show at every vertex we have

$$u_{\mathbf{v}_i} = u_{\mathbf{v}_{i+1}}, \tag{3.8.30}$$

which implies that $u_{\mathbf{v}_0} = u_{\mathbf{v}_{N+1}}$. As the choice of $\mathbf{v}_{N+1}$ was arbitrary we have this property for every vertex. Therefore

$$\text{Ker}(\nabla_h) = \{\mathcal{I}^{\mathscr{V}_h}(c) : c \in \mathbb{R}\} \implies \text{Dim}(\text{Ker}(\nabla_h))) = 1. \tag{3.8.31}$$

It is worth noting that if $\mathscr{T}$ is not path connected then the dimension of the kernel of ∇_h is the number of path connected components in $\mathscr{T}$.

Dim(Ker($\mathbf{curl}_h$)): In order to prove this result we will utilize the famous Rank-Nullity theorem.

$$\mathrm{Dim}(\mathscr{E}_h) = \mathrm{Dim}(\mathrm{Im}(\mathrm{curl}_h)) + \mathrm{Dim}(\mathrm{Ker}(\mathrm{curl}_h)). \tag{3.8.32}$$

We know that the dimensions of $\mathscr{E}_h$ is the number of edges in $\mathscr{T}$ therefore $\mathrm{Dim}\mathscr{E}_h = N_{\mathscr{E}}$. We have previously shown that the $\mathrm{Dim}(\mathrm{Im}(\mathrm{curl}_h)) = N_{\mathscr{F}}$. Therefore,

$$\mathrm{Dim}(\mathrm{Im}(\mathrm{curl}_h)) = N_{\mathscr{E}} - N_{\mathscr{F}}. \tag{3.8.33}$$

Dim(Im(∇_h)) : This is proven by utilizing $\mathrm{Dim}(\mathrm{Ker}(\mathrm{curl}_h)) = N_{\mathscr{E}} - N_{\mathscr{F}}$ and applying Theorem 3.8.1.

Q.E.D.

4 MFD DISCRETIZATIONS FOR MAXWELL'S EQUATIONS

In this chapter we present the construction and analysis of discrete approximations to a number of electromagnetic models using the mimetic finite difference (MFD) method in space.

In Section 4.1 we present semi-discretizations in space of Maxwell's equations with various constitutive laws using the MFD tecnique. In Section 4.2 we present time integration schemes which are appropriate for discretizating the transient Maxwell's equations. In Section 4.3 we present fully discrete formulations of Maxwell's equations using MFD discretizations in space and time staggering methods. In Section 4.4 we provide some numerical demonstrations of the discrete divergence preservering properties of MFD discretizations of Maxwell's equations.

4.1 Semi Discrete MFD Formulations of Maxwell's Equations

We start with the 2D transverse electric mode of Maxwell's Equations in free space and describe the construction of MFD discretizations in space. We next consider Maxwell's equations in linear dispersive materials in which the constitutive law for the electric displace ment $\mathbf{D}$ can be decomposed into an electric field $\mathbf{E}$ and a macroscopic field called the polarization $\mathbf{P}$. A system of ODEs describes the dynamic evolution of $\mathbf{P}$ forced by the electric field. We discuss the construction of MFD discretizations in space for these models. Many of the discretizations discussed in this section, particularly in space, are very similar to those found in [2, 10].

4.1.1 Transverse Electric Maxwell's Equations in Free Space

Recall Maxwell's equations in free space:

$$\frac{\partial}{\partial t}(\epsilon \mathbf{E}) = \mathbf{curl} H - \mathbf{J} \qquad \frac{\partial}{\partial t}(\mu H) = -\text{curl}\mathbf{E} \tag{4.1.1}$$

subject to the constraints

$$\text{div}\epsilon\mathbf{E} = \rho, \qquad \frac{\partial}{\partial t}\rho = -\text{div}\mathbf{J}. \tag{4.1.2}$$

We will consider the variational formulation of problem (4.1.1)-(4.1.2) given by

$$\begin{array}{l} \text{find } (\mathbf{E}, \mathbf{H}) \in C^1([0,T], \mathbf{H}_0(\text{curl}, \Omega)) \times C^1([0,T], L^2(\Omega) \text{ satisfying :} \\ \left\{ \begin{array}{ll} \displaystyle\int_\Omega \frac{\partial}{\partial t}(\epsilon \mathbf{E}) \cdot \mathbf{\Phi}\ dA = \int_\Omega H \text{curl}\mathbf{\Phi}\ dA - \int_\Omega \mathbf{J} \cdot \mathbf{\Phi}\ dA, & \forall \mathbf{\Phi} \in \mathbf{H}_0(\text{curl}, \Omega), \\ \displaystyle\int_\Omega \frac{\partial}{\partial t}(\mu H)\psi\ dA = -\int_\Omega \text{curl}\mathbf{E}\psi\ dA, & \forall \psi \in L^2(\Omega). \\ \mathbf{E}(0) = \mathbf{E}_0 \in \mathbf{H}(\text{curl}, \Omega), \quad H(0) = H_0 \in L^2(\Omega). & \end{array} \right. \end{array} \tag{4.1.3}$$

Assuming ϵ, μ are constant in time the semi-discrete formulation of this problem using an MFD discretization is

$$\begin{array}{l} \text{find } \mathbf{E}_h \in C^1([0,T], \mathscr{E}_h), H_h \in C^1([0,T], \mathscr{F}_h) \text{ satisfying} \\ \left\{ \begin{array}{ll} \left[\frac{\partial}{\partial t}\mathbf{E}_h, \mathbf{\Phi}_h\right]^\epsilon_{\mathscr{E}_h} = \left[H_h, \text{curl}_h \mathbf{\Phi}_h\right]_{\mathscr{F}_h} - \left[\mathbf{F}_h, \mathbf{\Phi}_h\right]^\epsilon_{\mathscr{E}_h}, & \forall \mathbf{\Phi}_h \in \mathscr{E}_h, \\ \left[\frac{\partial}{\partial t}H_h, \psi_h\right]^\mu_{\mathscr{F}_h} = \left[\text{curl}_h \mathbf{E}_h, \psi_h\right]_{\mathscr{F}_h}, & \forall \psi_h \in \mathscr{F}_h. \\ \mathbf{E}_h(0) = \mathcal{I}^{\mathscr{E}_h}(\mathbf{E}_0), \quad H_h(0) = \mathcal{I}^{\mathscr{F}_h}(H_0), \quad \mathbf{F}_h = \mathcal{I}^{\mathscr{E}_h}(\epsilon^{-1}\mathbf{J}). & \end{array} \right. \end{array} \tag{4.1.4}$$

By choosing $\mathbf{\Phi}_h$ and ψ_h as standard basis vectors we can extract from this discrete variational statement a matrix evolution equation

$$\begin{array}{l} \text{find } \mathbf{E}_h \in C^1([0,T], \mathscr{E}_h), H_h \in C^1([0,T], \mathscr{F}_h) \text{ satisfying} \\ \left\{ \begin{array}{l} \mathbb{M}^\epsilon_{\mathscr{E}} \left(\frac{\partial}{\partial t}\mathbf{E}_h\right) = \text{curl}^T_h \mathbb{M}_{\mathscr{F}} H_h - \mathbb{M}^\epsilon_{\mathscr{E}} \mathbf{F}_h, \\ \mathbb{M}^\mu_{\mathscr{F}} \left(\frac{\partial}{\partial t}H_h\right) = -\mathbb{M}_{\mathscr{F}} \text{curl}_h \mathbf{E}_h, \\ \mathbf{E}_h(0) = \mathcal{I}^{\mathscr{E}}(\mathbf{E}_0), \quad H_h(0) = \mathcal{I}^{\mathscr{F}_h}(H_0), \quad \mathbf{F}_h = \mathcal{I}^{\mathscr{E}_h}(\epsilon^{-1}\mathbf{J}). \end{array} \right. \end{array} \tag{4.1.5}$$

We will now present a series of theorems introduced in [2]. The proofs of these results follow a standard format specific to the MFD literature and illustrates one of the fudnamental advantages of the approach. We present them in their entirety here in order to illustrate how MFD discretiztions mimic continuum properties.

Theorem 4.1.1. *An MFD semi-discrete formulation of Maxwell's equations obeys a discrete analogue of the continuity equation given in* (4.1.2).

Proof. We will consider the adjoint divergence $\widetilde{\mathrm{div}}_h$ induced by the inner product $[\cdot,\cdot]^{\epsilon}_{\mathscr{E}_h}$ as defined in (3.7.7)

$$\widetilde{\mathrm{div}}_h = -\mathbb{M}^{-1}_{\mathscr{V}} \nabla_h^T (\mathbb{M}^{\epsilon}_{\mathscr{E}})^{-1}. \tag{4.1.6}$$

Appling the inverse matrix $(\mathbb{M}^{\epsilon}_{\mathscr{E}})^{-1}$ to both sides of the semi-discrete Ampere-Maxwell Law, given in (4.1.4) and we derive

$$\frac{\partial}{\partial t}\mathbf{E}_h = \widetilde{\mathrm{curl}}_h H_h - \mathbf{F}_h. \tag{4.1.7}$$

Here the adjoint curl, $\widetilde{\mathrm{curl}}_h$ is defined per equation (3.7.6). Now apply the operator $\widetilde{\mathrm{div}}_h$.

$$\frac{\partial}{\partial t}\widetilde{\mathrm{div}}_h \mathbf{E}_h = \widetilde{\mathrm{div}}_h \widetilde{\mathrm{curl}}_h H_h - \widetilde{\mathrm{div}}_h \mathbf{F}_h, \tag{4.1.8}$$

$$= -\widetilde{\mathrm{div}}_h \mathbf{F}_h. \tag{4.1.9}$$

This last identity is true by Corollary 3.8.2. We define the grid function $\rho_h = \widetilde{\mathrm{div}}_h \mathbf{E}_h$. Then ρ_h must then satisfy the inital value problem

$$\begin{cases} \dfrac{\partial}{\partial t}\rho_h = -\widetilde{\mathrm{div}}_h \mathbf{F}_h(0), \\ \rho_h(0) = \widetilde{\mathrm{div}}_h \mathbf{E}_h(0). \end{cases} \tag{4.1.10}$$

This initial value problem is a discrete approximation of the IVP for the continuum Gauss' law. This can be shown as follows. Testing (4.1.10) against arbitrary $\varphi_h \in \mathscr{V}_h$ and rewriting the discrete statement variationally, we have

$$\Big[\frac{\partial}{\partial t}\mathbf{E}_h, \nabla_h \varphi_h\Big]^{\epsilon}_{\mathscr{E}} = -\Big[\mathbf{F}_h, \nabla_h \varphi_h\Big]^{\epsilon}_{\mathscr{E}} = -\Big[\mathcal{I}^{\mathscr{F}_h}(\epsilon^{-1}\mathbf{J}), \nabla_h \varphi_h\Big]^{\epsilon}_{\mathscr{E}}. \tag{4.1.11}$$

This is an MFD approximation of the continuum variational statement

$$\int_\Omega \frac{\partial}{\partial t}(\epsilon \mathbf{E}) \cdot \nabla \varphi \; dA = -\int_\Omega \mathbf{J} \cdot \nabla \varphi \; dA, \; \forall \psi \in H_0^1(\Omega). \tag{4.1.12}$$

This is a weak formulation of the continuity equation. **Q.E.D.**

Theorem 4.1.2. *A spatial MFD discretization of Maxwell's equations in free space is energy conservative, for the discrete energy*

$$\mathcal{E}_h = \left((\|\mathbf{E}_h\|^\epsilon_{\mathscr{E}_h})^2 + (\|H_h\|^\mu_{\mathscr{F}_h})^2 \right)^{1/2}. \tag{4.1.13}$$

Proof. We begin with the discrete variational formulation but choose our test functions carefully.

$$\left[\frac{\partial}{\partial t}\mathbf{E}_h, \mathbf{E}_h\right]^\epsilon = \left[H_h, \mathrm{curl}_h \mathbf{E}_h\right]_{\mathscr{F}_h}, \tag{4.1.14}$$

$$\left[\frac{\partial}{\partial t}H_h, H_h\right]^\mu = -\left[\mathrm{curl}\mathbf{E}_h, H_h\right]_{\mathscr{F}_h}. \tag{4.1.15}$$

Adding the two equations together we rewrite as

$$\left[\frac{\partial}{\partial t}\mathbf{E}_h, \mathbf{E}_h\right]^\epsilon_{\mathscr{E}_h} + \left[\frac{\partial}{\partial t}H_h, H_h\right]^\mu_{\mathscr{F}_h} = 0. \tag{4.1.16}$$

Applying the product rule in time we have

$$\frac{\partial}{\partial t}\frac{1}{2}((\|\mathbf{E}_h\|^\epsilon_{\mathscr{E}_h})^2 + (\|H_h\|^\mu_{\mathscr{F}_h})^2) = \frac{\partial}{\partial t}\frac{1}{2}\mathcal{E}_h^2 = 0. \tag{4.1.17}$$

Therefore $\mathcal{E}_h^2$ is constant for all time. Note that $\mathcal{E}_h$ is the Euclidean norm of a vector $(\|\mathbf{E}_h\|^\epsilon_{\mathscr{E}_h}, \|H_h\|^\mu_{\mathscr{F}_h})^T$ and is therefore non-negative. We therefore know that $\mathcal{E}_h$ is constant for all time. **Q.E.D.**

This discrete energy conservation is an analogue of the continuum energy conservation

$$\frac{\partial}{\partial t}\frac{1}{2}\int_\Omega \left(\epsilon|\mathbf{E}|^2 + \mu|H|^2\right) = 0 \tag{4.1.18}$$

4.1.2 Transient Maxwell's Equations in a Linear Polarization Media

Consider a general polarization law with $1 \leq m \leq M$ polarization fields is modelled by the following system of equations:

$$\frac{\partial}{\partial t}\begin{pmatrix}\epsilon\mathbf{E}\\ \mathbf{P}_m\end{pmatrix} = \mathbb{X}\begin{pmatrix}\mathbf{E}\\ \mathbf{P}_m\end{pmatrix} + \begin{pmatrix}\mathbf{curl}H\\ 0\end{pmatrix}, \qquad \frac{\partial}{\partial \mu}H = -\text{curl}\mathbf{E}. \tag{4.1.19}$$

Let $\mathbf{x}_j$, $1 \leq j \leq M+1$ be the rows of $\mathbb{X}$, i.e

$$\mathbb{X} = \begin{pmatrix}\mathbf{x}_1\\ \mathbf{x}_2\\ \vdots\\ \mathbf{x}_{M+1}\end{pmatrix}. \tag{4.1.20}$$

The variational formulation of (4.1.19) is written as follows:

find $(\mathbf{E}, \mathbf{P}_m, H) \in C^1([0,T], \mathbf{H}_0(\text{curl}, \Omega)) \times [C^1([0,T], \mathbf{L}^2(\Omega))]^M \times C^1([0,T], L^2(\Omega))$ satisfying

$$\begin{cases} \displaystyle\int_\Omega \frac{\partial}{\partial t}\epsilon\mathbf{E}\cdot\mathbf{\Phi}\ dA = \int_\Omega \mathbf{x}_1\begin{pmatrix}\mathbf{E}\\ \mathbf{P}_m\end{pmatrix}\cdot\mathbf{\Phi} + \int_\Omega H\text{curl}\mathbf{\Phi}\ dA, & \forall\mathbf{\Phi}\in\mathbf{H}_0(\text{curl},\Omega),\\ \displaystyle\int_\Omega \frac{\partial}{\partial t}\mathbf{P}_j\cdot\mathbf{\Theta}_j\ dA = \int_\Omega \mathbf{x}_{j+1}\begin{pmatrix}\mathbf{E}\\ \mathbf{P}_m\end{pmatrix}\cdot\mathbf{\Theta}_j\ dA, & \mathbf{\Theta}_j\in\mathbf{L}^2T(\Omega),\\ \displaystyle\int_\Omega \frac{\partial}{\partial t}\mu H\psi\ dA = -\int_\Omega \text{curl}\mathbf{E}\ \psi\ dA, & \forall\psi\in L^2(\Omega).\\ \mathbf{E}(0) = \mathbf{E}_0\in\mathbf{H}_0(\text{curl},\Omega), \quad \mathbf{P}_m(0) = \mathbf{P}_{m,0}\in\mathbf{H}(\text{curl}),\\ H(0) = H_0\in L^2(\Omega) \end{cases} \tag{4.1.21}$$

The semi discrete mimetic variational formulation of (4.1.21) is posed as follows:

$$\text{find } (\mathbf{E}_h, \mathbf{P}_{m,h}, H_h) \in [C^1([0,T], \mathscr{E}_h)]^{M+1} \times C^1([0,T], \mathscr{F}_h) \text{ such that}$$
$$\begin{cases} \Big[\dfrac{\partial}{\partial t}\mathbf{E}_h, \mathbf{\Phi}_h\Big]_{\mathscr{E}_h}^{\epsilon} = \Big[\mathbf{E}_h, \mathbf{\Phi}_h\Big]_{\mathscr{E}_h}^{x_{1,1}} + \displaystyle\sum_{j=1}^{M} [\mathbf{P}_j, \mathbf{\Phi}_h]_{\mathscr{E}_h}^{x_{1,j+1}} + [H_h, \mathrm{curl}\mathbf{\Phi}_h]_{\mathscr{F}_h}, & \forall \mathbf{\Phi}_h \in \mathscr{E}_h, \\ \Big[\dfrac{\partial}{\partial t}\mathbf{P}_{j,h}, \mathbf{\Theta}_h\Big]_{\mathscr{E}_h} = \Big[\mathbf{E}_h, \mathbf{\Theta}_h\Big]_{\mathscr{E}_h}^{x_{j+1,1}} + \displaystyle\sum_{i=1}^{M} [\mathbf{P}_i, \mathbf{\Theta}_h]_{\mathscr{E}_h}^{x_{j+1,i+1}}, & \forall \mathbf{\Theta}_h \in \mathscr{E}_h, \\ \Big[\dfrac{\partial}{\partial t}H_h, \psi_h\Big]_{\mathscr{F}_h}^{\mu} = -\Big[\mathrm{curl}\mathbf{E}_h, \psi_h\Big]_{\mathscr{F}_h} & \forall \psi_h \in \mathscr{F}_h, \\ \mathbf{E}_h(0) = \mathcal{I}^{\mathscr{E}_h}(\mathbf{E}_0), \quad \mathbf{P}_{m,h}(0) = \mathcal{I}^{\mathscr{E}_h}(\mathbf{P}_{m,0}), \quad \mathbf{H}_h(0) = \mathcal{I}^{\mathscr{F}_h}(H_0). \end{cases} \tag{4.1.22}$$

While the case of $\mathbb{X}$ depending on space is very realistic, we will primarily analyze the case where $\mathbb{X}, \epsilon, \mu$ are constant in space and time. In this case the MFD can be written relatively compactly in the following matrix equation.

$$\frac{\partial}{\partial t}\begin{pmatrix} \mathbb{M}_{\mathscr{E}}\mathbf{E}_h \\ \mathbb{M}_{\mathscr{E}}\mathbf{P}_{m,h} \end{pmatrix} = \frac{1}{\epsilon}\mathbb{X} \otimes \mathbb{I} \begin{pmatrix} \mathbb{M}_{\mathscr{E}}\mathbf{E}_h \\ \mathbb{M}_{\mathscr{E}}\mathbf{P}_h \end{pmatrix} + \frac{1}{\epsilon}\begin{pmatrix} \mathrm{curl}_h^T \mathbb{M}_{\mathscr{F}} H_h \\ 0 \end{pmatrix} \tag{4.1.23}$$

$$\frac{\partial}{\partial t}H_h = -\mathrm{curl}_h \mathbb{E}_h \tag{4.1.24}$$

Here $\otimes$ is the Kronecker product and $\mathbb{I}$ is a $(M+1)N_{\mathscr{E}} \times (M+1)N_{\mathscr{E}}$ identity matrix. This can be expressed in terms of adjoint operators as follows:

$$\frac{\partial}{\partial t}\begin{pmatrix} \mathbf{E}_h \\ \mathbf{P}_{m,h} \end{pmatrix} = \frac{1}{\epsilon}\mathbb{X} \otimes \mathbb{I} \begin{pmatrix} \mathbf{E}_h \\ \mathbf{P}_h \end{pmatrix} + \frac{1}{\epsilon}\begin{pmatrix} \widetilde{\mathrm{curl}}_h H_h \\ 0 \end{pmatrix} \tag{4.1.25}$$

$$\frac{\partial}{\partial t}H_h = -\mathrm{curl}_h \mathbb{E}_h \tag{4.1.26}$$

Where $\widetilde{\mathrm{curl}}_h$ is defined in (3.7.6). We will now prove energy decay a simple example media. This result, while relying on the underlying techniques of the MFD technology is original to this work and does not appear in [2].

Theorem 4.1.3. *A MFD discretization of a Cold Isotropic Plasma with constant coeffi-*

cients (a Drude Polarization Law) has energy decay. Namely the energy of the system

$$\mathcal{E}_h = \left(\frac{1}{2}\left(\epsilon\|\mathbf{E}_h\|^2_{\mathscr{E}_h} + \mu\|H\|^2_{\mathscr{F}_h} + \frac{1}{\epsilon\omega_P^2}\|\mathbf{J}_h\|^2_{\mathscr{E}_h}\right)\right)^{1/2} \tag{4.1.27}$$

obeys the differential equation

$$\frac{\partial}{\partial t}\mathcal{E}_h^2 = -\frac{\omega_I}{\epsilon\omega_P^2}\|\mathbf{J}\|^2_{\mathscr{E}}. \tag{4.1.28}$$

Proof. The Cold Isotropic plasma model has the matrix $\mathbb{X}$ given as

$$\mathbb{X} = \begin{pmatrix} 0 & -1 \\ \epsilon\omega_P^2 & -\omega_I \end{pmatrix}. \tag{4.1.29}$$

The mimetic variational form is then given as:

$$\begin{cases} \text{find } \mathbf{E}_h, \mathbf{J}_h \in C^1([0,T], \mathscr{E}_h), H_h \in C^1([0,T], \mathscr{F}_h) \text{ such that} \\ \epsilon\left[\frac{\partial}{\partial t}\mathbf{E}_h, \mathbf{\Phi}_h\right]_{\mathscr{E}_h} + \left[\mathbf{J}_h, \mathbf{\Phi}_h\right]_{\mathscr{E}_h} = \left[H, \operatorname{curl}_h \mathbf{\Phi}_h\right]_{\mathscr{F}_h}, & \forall \mathbf{\Phi}_h \in \mathscr{E}_h, \\ \left[\frac{\partial}{\partial t}\mathbf{J}, \mathbf{\Theta}_h\right]_{\mathscr{E}_h} = -\omega_I\left[\mathbf{J}_h, \mathbf{\Theta}_h\right]_{\mathscr{E}_h} + \epsilon\omega_P^2\left[\mathbf{E}_h, \mathbf{\Theta}_h\right]_{\mathscr{E}_h}, & \forall \mathbf{\Theta}_h \in \mathscr{E}_h, \\ \mu\left[\frac{\partial}{\partial t}H_h, \psi_h\right]_{\mathscr{F}_h} = -\left[\operatorname{curl}_h \mathbf{E}_h, \psi_h\right]_{\mathscr{F}_h}, & \forall \psi_h \in \mathscr{F}_h. \end{cases} \tag{4.1.30}$$

As in free space we test the discrete Ampere-Maxwell Law against $\mathbf{E}_h$ and the discrete Faraday's Law against H_h and add the results to arrive at

$$\epsilon\left[\frac{\partial}{\partial t}\mathbf{E}_h, \mathbf{E}_h\right]_{\mathscr{E}} + \mu\left[\frac{\partial}{\partial t}H_h, H_h\right]_{\mathscr{F}} + \left[\mathbf{J}_h, \mathbf{E}_h\right]_{\mathscr{E}} = 0 \tag{4.1.31}$$

By testing the Drude Law against $\mathbf{J}_h$ we can solve for $[\mathbf{E}_h, \mathbf{J}]_{\mathscr{E}}$.

$$\frac{1}{\epsilon\omega_P^2}\left[\frac{\partial}{\partial t}\mathbf{J}_h, \mathbf{J}_h\right]_{\mathscr{E}_h} + \frac{\omega_I}{\epsilon\omega_P^2}\left[\mathbf{J}_h, \mathbf{J}_h\right]_{\mathscr{E}_h} = \left[\mathbf{E}_h, \mathbf{J}_h\right]_{\mathscr{E}_h}. \tag{4.1.32}$$

Substituting this into the Equation (4.1.31) we have

$$\frac{\partial}{\partial t}\frac{1}{2}\left(\epsilon\|\mathbf{E}_h\|^2_{\mathscr{E}_h} + \frac{1}{\epsilon\omega_P^2}\|\mathbf{J}_h\|^2_{\mathscr{E}_h} + \|H_h\|^2_{\mathscr{F}_h}\right) = -\frac{\omega_I}{\epsilon\omega_P^2}\|\mathbf{J}\|^2_{\mathscr{E}_h}. \tag{4.1.33}$$

Which implies that

$$\frac{\partial}{\partial t}\mathcal{E}_h^2 < 0. \tag{4.1.34}$$

Assuming $\mathcal{E}_h$ non-zero we then have $\frac{\partial}{\partial t}\mathcal{E}_h < 0$. **Q.E.D.**

4.2 Time Integration

Having developed semi-discrete approximations of Maxwell's equations, we will now consider the time discretizations that will be employed to build fully discrete methods. Maxwell's equations can be written in the framework of the abstract, first order wave equation. We will develop time discretizations for this abstract equation to suggest the usefullness of our discretizations in more general wave problem applications. Let U, V be Hilbert spaces. Let $D : V \to U'$ be a bounded linear operator and D' be its adjoint where DD' and $D'D$ are elliptic. Let $\mathbf{f} \in U'$, $\mathbf{g} \in V'$.

$$\begin{aligned} &\text{find } \mathbf{u} \in C^1([0,T],\mathbf{U}), \mathbf{v} \in C^1([0,T],\mathbf{V}) \text{ such that} \\ &\begin{cases} \dfrac{\partial}{\partial t}\mathbf{u} = D\mathbf{v} + \mathbf{f} \\ \dfrac{\partial}{\partial t}\mathbf{v} = D'\mathbf{u} + \mathbf{g} \end{cases} . \end{aligned} \tag{4.2.1}$$

Where $\mathbf{u}$ and $\mathbf{v}$ are vectors in two distinct spaces (for example the discrete spaces $\mathscr{E}_h$ and $\mathscr{F}_h$). Assuming that $\mathbf{f}$ and $\mathbf{g}$ are independent of $\mathbf{u}, \mathbf{v}$ we can apply the following staggering in time.

Let $\Delta t > 0$ and define $\mathbf{u}^n$ and $\mathbf{v}^{n+1/2}$ as

$$\mathbf{u}^n \approx \mathbf{u}(t_n), \qquad t_n = n\Delta t, \tag{4.2.2a}$$

$$\mathbf{v}^{n+1/2} \approx \mathbf{v}(t_{n+1/2}), \qquad t_{n+1/2} = (n+1/2)\Delta t. \tag{4.2.2b}$$

For an abstract wave equation of the form (4.2.1) we define the **staggered leap frog** method as follows:

$$\begin{cases} \mathbf{u}^{n+1} = \mathbf{u}^n + \Delta t D\mathbf{v}^{n+1/2} + \Delta t \mathbf{f}^{n+1/2}, \\ \mathbf{v}^{n+1/2} = \mathbf{v}^{n-1/2} + \Delta t D\mathbf{u}^n + \Delta t \mathbf{g}^n. \end{cases} . \tag{4.2.3}$$

Lemma 4.2.1. *Staggered leap frog is $\mathcal{O}(\Delta t^2)$ accurate.*

Proof. We need only consider one equation to prove accuracy.

$$\int_{t_n}^{t_{n+1}} \frac{\partial}{\partial t}\mathbf{u}\ dt = \int_{t_n}^{t_{n+1}} D\mathbf{v} + \mathbf{f}\ dt \tag{4.2.4}$$

$$\mathbf{u}(t_{n+1}) - \mathbf{u}(t_n) = \int_{t_n}^{t_{n+1}} D\mathbf{v} + \mathbf{f}\ dt \qquad \text{Fundamental Theorem,} \tag{4.2.5}$$

$$\mathbf{u}(t_{n+1}) - \mathbf{u}(t_n) = \Delta t(D\mathbf{v} + \mathbf{f})|_{t_{n+1/2}} + \mathcal{O}(\Delta t^3) \qquad \text{midpoint quadrature} \tag{4.2.6}$$

Dividing both sides by Δt yields the following local truncation estimate

$$\frac{\mathbf{u}(t_{n+1}) - \mathbf{u}(t_n)}{\Delta t} - D\mathbf{v}t(t_{n+1/2}) - \mathbf{f}(t_{n+1/2}) = (\frac{\partial}{\partial t}\mathbf{u} - D\mathbf{v} - \mathbf{f})(t_{n+1/2}) + \mathcal{O}(\Delta t^2). \tag{4.2.7}$$

Q.E.D.

We will utilize this time integrator for Maxwell's equations in free space. Now consider a more complex abstract dispersive wave equation

$$\begin{cases} \dfrac{\partial}{\partial t}\mathbf{u} - \mathbb{X}\mathbf{u} = D\mathbf{v} + \mathbf{g} \\ \dfrac{\partial}{\partial t}\mathbf{v} - \mathbb{Y}\mathbf{v} = D'\mathbf{u} + \mathbf{f} \end{cases} . \tag{4.2.8}$$

Here $\mathbf{u} \in U^M$ and $\mathbf{v} \in V^N$ for U and V Hilbert Spaces. The operators $D : V^N \to (U^M)'$ and D' the adjoint. The forcing terms $\mathbf{g} \in (U^M)'$ and $\mathbf{f} \in (V^N)'$. Here $\mathbb{X}, \mathbb{Y}$ are $M \times M$ and $N \times N$ matrices respectively representing lower order terms. In general this abstract equation could be dispersive or dissipative or both. For example Maxwell's equations in conductive media or general polarization media fall into this category as do damped acoustic waves. We will present two possible time integrators for this system.

Consider $\mathbf{u}^n, \mathbf{v}^{n+1/2}$ as in Definition (4.2). We define **Time Averaged Differencing** by

$$\begin{cases} \dfrac{\mathbf{u}^{n+1} - \mathbf{u}^n}{\Delta t} - \mathbb{X}\dfrac{\mathbf{u}^{n+1} + \mathbf{u}^n}{2} = D\mathbf{v}^{n+1/2} + \mathbf{f}^{n+1/2}, \\ \dfrac{\mathbf{v}^{n+1/2} - \mathbf{v}^{n-1/2}}{\Delta t} - \mathbb{Y}\dfrac{\mathbf{v}^{n+1/2} - \mathbf{v}^{n-1/2}}{2} = D'\mathbf{u}^n + \mathbf{g}^n, \end{cases} \tag{4.2.9}$$

Lemma 4.2.2. *Time averaged differencing is $\mathcal{O}(\Delta t^2)$ accurate.*

Proof. As before we consider only a single equation without loss of generality.

$$\int_{t_n}^{t_{n+1}} \frac{\partial}{\partial t}\mathbf{u}\ dt = \int_{t_n}^{t_{n+1}} \mathbb{X}\mathbf{u} + D\mathbf{v} + \mathbf{f}\ dt \tag{4.2.10}$$

$$\mathbf{u}(t_{n+1}) - \mathbf{u}(t_n) = \int_{t_n}^{t_{n+1}} \mathbb{X}\mathbf{u} + D\mathbf{v} + \mathbf{f} \qquad \text{Fundamental Theorem} \tag{4.2.11}$$

To resolve the $D\mathbf{v} + \mathbf{g}$ term we apply the midpoint rule as in time staggering. For the term $\mathbb{X}\mathbf{u}$ we use the trapezoid rule, both of which are order Δt^2 accurate.

$$\int_{t_n}^{t_{n+1}} \mathbb{X}\mathbf{u}\ dt = \Delta t \mathbb{X}\frac{\mathbf{u}(t_{n+1}) + \mathbf{u}(t_n)}{2} + \mathcal{O}(\Delta t^3), \tag{4.2.12}$$

$$\int_{t_n}^{t_{n+1}} D\mathbf{v} + \mathbf{f}\ dt = \Delta t(D\mathbf{v}(t_{n+1/2}) + \mathbf{f}(t_{n+1/2})) + \mathcal{O}(\Delta t^3). \tag{4.2.13}$$

Dividing both sides by Δt we recover an order Δt^2 local truncation error.

$$\frac{\mathbf{u}(t_{n+1}) - \mathbf{u}(t_n)}{\Delta t} - \mathbb{X}\frac{\mathbf{u}(t_{n+1}) + \mathbf{u}(t_n)}{2} - D\mathbf{v}(t_{n+1/2}) - \mathbf{f}(t_{n+1/2}) \tag{4.2.14}$$

$$= \left(\frac{\partial}{\partial t}\mathbf{u} - \mathbb{X}\mathbf{u} + D\mathbf{v} + \mathbf{f}\right)(t_{n+1/2}) + \mathcal{O}(\Delta t^2). \tag{4.2.15}$$

Q.E.D.

We also consider time integrator which relies upon the method of integrating factors.

Definition 4.2.1. Consider a matrix $\mathbb{A} \in \mathbb{R}^{N\times N}$. We define the **Matrix Exponential** of $\mathbb{A}$ by the formal power series:

$$\mathrm{e}^{\mathbb{A}t} = \sum_{n=0}^{\infty} \mathbb{A}^n \frac{t^n}{n!}. \tag{4.2.16}$$

This series converges uniformly on every compact subset of $\mathbb{R}^{N\times N}$ similar to the case of the series for the scalar exponential case.

We rely upon the following property of the matrix exponential.

Lemma 4.2.3. *For a matrix $\mathbb{A} \in \mathbb{R}^{N\times N}$, the matrix exponential $\mathrm{e}^{\mathbb{A}t}$ has the following properties:*

1. $(\mathrm{e}^{\mathbb{A}t})^{-1} = \mathrm{e}^{-\mathbb{A}t}$.

2. $\frac{\partial}{\partial t}\mathrm{e}^{\mathbb{A}t} = \mathbb{A}\mathrm{e}^{\mathbb{A}t}$.

Proof. See [31]. **Q.E.D.**

We will now briefly reproduce the method of integrating factors.

Construction 4.1. Consider the semi-linear system of ODE

$$\dot{\mathbf{u}} - \mathbb{A}\mathbf{u} = \mathbf{F}, \tag{4.2.17}$$

where $\mathbf{u}, \mathbf{F}(\mathbf{u}, t) \in \mathbb{R}^N$ and $\mathbb{A} \in \mathbb{R}^{N\times N}$. We have

$$\int_{t_n}^{t_{n+1}} \frac{\partial}{\partial t}\mathrm{e}^{-\mathbb{A}t}\mathbf{u}\ dt = \int_{t_n}^{t_{n+1}} \mathrm{e}^{-\mathbb{A}t}\left(\frac{\partial}{\partial t}\mathbf{u} - \mathbb{A}\mathbf{u}\right)\ dt \tag{4.2.18}$$

$$= \int_{t_n}^{t_{n+1}} \mathrm{e}^{-\mathbb{A}t}\mathbf{F}(\mathbf{u}(t), t)\ dt. \tag{4.2.19}$$

We can apply the fundamental theorem of Calculus to the left hand side of (4.2.18) and arrive at

$$\mathrm{e}^{-\mathbb{A}t_{n+1}}\mathbf{u}(t_{n+1}) - \mathrm{e}^{-\mathbb{A}t_n}\mathbf{u}(t_n) = \int_{t_n}^{t_{n+1}} \mathrm{e}^{-\mathbb{A}t}\mathbf{F}(\mathbf{u}(t), t)\ dt. \tag{4.2.20}$$

As $t_{n+1} - t_n = \Delta t$ and apply the exponential $\mathrm{e}^{\mathbb{A}t_{n+1}}$ to both sides and compute

$$\mathbf{u}(t_{n+1}) - \mathrm{e}^{\mathbb{A}\Delta t}u(t_n) = \int_{t_n}^{t_{n+1}} \mathrm{e}^{\mathbb{A}(t_{n+1}-t)}\mathbf{F}(\mathbf{u}(t), t)\ dt \tag{4.2.21}$$

$$= \int_0^{\Delta t} \mathrm{e}^{\mathbb{A}s}\mathbf{F}(\mathbf{u}(s + t_n), s + t_n)\ ds. \tag{4.2.22}$$

This now creates a formula which relates the solution at a later time to values at a previous time and response to the function $\mathbf{F}$.

Using Construction 4.1 we now introduce the **Exponential Time Differencing** technique. This time integrator is well known to the FDTD literature. Originally applied to reduce stiffness in Perfectly Matched Layers it has been shown in [50] to offer no major

advantages in this regard over time staggered differences. We will show that it does provide advantages as a "mimetic" time integrator. Higher order ETD discretizations can be found in [13] which are more successful at reducing stiffness in systems of ODE. The following general formulation of ETD for an abstract dispersive wave generalizes the approach laid out in [50].

Assume $\mathbf{u}^n, \mathbf{v}^{n+1/2}$ are staggered per (4.2). We define **Exponential Time Differencing** for the abstract dispersive wave problem (4.2.8) by

$$\begin{cases} \mathbf{u}^{n+1} = \mathrm{e}^{\mathbb{X}\Delta t}\mathbf{u}^n + \left(\int_0^{\Delta t} \mathrm{e}^{\mathbb{X}s}\ ds\right)\left(D\mathbf{v}^{n+1/2} + \mathbf{f}^{n+1/2}\right) \\ \mathbf{v}^{n+1/2} = \mathrm{e}^{\mathbb{Y}\Delta t}\mathbf{v}^{n-1/2} + \left(\int_0^{\Delta t} \mathrm{e}^{\mathbb{Y}s}\ ds\right)\left(D'\mathbf{u}^n + \mathbf{g}^n\right) \end{cases} . \tag{4.2.23}$$

Lemma 4.2.4. *Exponential Time Differencing is $\mathcal{O}(\Delta t^2)$ accurate.*

Proof. Given that our terms not multiplied by the integral in (4.2.23) are exact we need only show that

$$f(t_{n+1/2})\int_0^{\Delta t} g(s)\ ds = \int_0^{\Delta t} f(s+t_n)g(s)\ ds + \mathcal{O}(\Delta t^3) \tag{4.2.24}$$

for arbitrarily smooth f, g. Expand the integral in a Taylor series in Δt about $t_{n+1/2}$

$$\int_0^{\Delta t} g(s)\cdot f(s+t_{n+1/2})\ ds = \Delta t g(t_{n+1/2})f(t_{n+1/2}) \tag{4.2.25}$$

$$+\frac{\Delta t^3}{24}\Big(2\dot{g}(t_0)\dot{f}(t_{n+1/2}) + \ddot{g}(t_{n+1/2})f(t_{n+1/2}) + g(t_{n+1/2})\ddot{f}(t_{n+1/2})\Big) + \mathcal{O}(\Delta t^4). \tag{4.2.26}$$

Now we will compute the Taylor series for our approximation about $t_{n+1/2}$ in Δt.

$$f(t_0)\int_0^{\Delta t} g(s)\ ds = \Delta t g(t_{n+1/2})f(t_{n+1/2}) + \frac{\Delta t^3}{24}\ddot{g}(t_{n+1/2})f(t_{n+1/2}) + \mathcal{O}(\Delta t^4). \tag{4.2.27}$$

As both integrals scale like Δt and differ at the $\mathcal{O}(\Delta t^3)$ the two are within $\mathcal{O}(\Delta t^3)$. **Q.E.D.**

Remark. It is worth noting of that leap frog defined in (4.2.3) is directly generalized by exponential time differencing, defined in (4.2.23), by assuming $\mathbb{X} = \mathbb{Y} = 0$. Further,

the exponential time differencing is exact for homogeneous problems by construction. In addition when $\mathbb{A}$ is invertible the integral

$$\int_0^{\Delta t} \mathrm{e}^{\mathbb{A}s}\, ds = \mathbb{A}^{-1}\Big(\mathrm{e}^{\mathbb{A}\Delta t} - \mathbb{I}\Big). \tag{4.2.28}$$

4.3 Fully Discrete Approximations for Transient Maxwell's Equations

Having developed second order time integrators for Maxwell's equations, we will now consider fully discrete mimetic discretizations for transient Maxwell's equations.

Definition 4.3.1. We present a fully discrete mimetic method for Maxwell's equations with variable coefficients ϵ, μ in space. We discretize in space with MFD in space and leap frog in time. Let $\widetilde{\mathrm{curl}}_h = (\mathbb{M}^{\epsilon}_{\mathscr{E}})^{-1}\mathrm{curl}_h^T\mathbb{M}_{\mathscr{F}}$ as in (3.7.6),

$$\begin{cases} \dfrac{\mathbf{E}_h^{n+1} - \mathbf{E}_h^n}{\Delta t} = \widetilde{\mathrm{curl}}_h H^{n+1/2} + \mathbf{F}^{n+1/2} \\ \mathbb{M}^{\mu}_{\mathscr{F}} \dfrac{H_h^{n+1} - H_h^{n-1/2}}{\Delta t} = -\mathbb{M}_{\mathscr{F}}\mathrm{curl}_h \mathbf{E}_h^n \\ \mathbf{E}_h^0 = \mathcal{I}^{\mathscr{E}_h}(\mathbf{E}(0)), \quad \mathbf{F}^{n+1/2} = \mathcal{I}^{\mathscr{E}_h}(\epsilon^{-1}\mathbf{J}(t_{n+1/2})) \\ H^{-1/2} = \mathcal{I}^{\mathscr{F}_h}(H(t_{-1/2})) \end{cases} \tag{4.3.1}$$

In the case of ϵ, μ constants this reduces to the following:

$$\begin{cases} \dfrac{\mathbf{E}_h^{n+1} - \mathbf{E}_h^n}{\Delta t} = \dfrac{1}{\epsilon}\widetilde{\mathrm{curl}}_h H^{n+1/2} + \dfrac{1}{\epsilon}\mathbf{J}^{n+1/2} \\ \dfrac{H_h^{n+1} - H_h^{n-1/2}}{\Delta t} = -\dfrac{1}{\mu}\mathrm{curl}_h \mathbf{E}_h^n \\ \mathbf{E}_h^0 = \mathcal{I}^{\mathscr{E}_h}(\mathbf{E}(0)), \quad \mathbf{J}^{n+1/2} = \mathcal{I}^{\mathscr{E}_h}(\mathbf{J}(t_{n+1/2})) \\ H^{-1/2} = \mathcal{I}^{\mathscr{F}_h}(H(t_{-1/2})) \end{cases} \tag{4.3.2}$$

where $\widetilde{\mathrm{curl}}_h = \mathbb{M}_{\mathscr{E}}^{-1}\mathrm{curl}_h^T\mathbb{M}_{\mathscr{F}}$ in (4.3.2).

For a general polarization law with variable or constant coefficients we can formulate Maxwell's equations with time averaged differencing.

Definition 4.3.2. Consider a linear polarization law with M polarization fields and $\mathbb{X}_{i,j} = x_{i,j}$. Define the matrix $\mathbb{M}^{\mathbb{X}}_{\mathscr{E}}$ by

$$\mathbb{M}^{\mathbb{X}}_{\mathscr{E}} = \begin{pmatrix} \mathbb{M}^{x_{1,1}}_{\mathscr{E}} & \cdots & \mathbb{M}^{x_{1,M}}_{\mathscr{E}} \\ \vdots & & \vdots \\ \mathbb{M}^{x_{M,1}}_{\mathscr{E}} & \cdots & \mathbb{M}^{x_{M,M}}_{\mathscr{E}} \end{pmatrix}. \tag{4.3.3}$$

The **Time Averaged Mimetic Finite Differnce Method (TAMFD)** for a linear polarization law is posed then as

$$\begin{cases} \dfrac{1}{\Delta t}\begin{pmatrix} \mathbb{M}^{\epsilon}_{\mathscr{E}}(\mathbf{E}^{n+1}_h - \mathbf{E}^n_h) \\ \mathbb{M}_{\mathscr{E}}(\mathbf{P}^{n+1}_{m,h} - \mathbf{P}^n_{m,h}) \end{pmatrix} = \dfrac{1}{2}\mathbb{M}^{\mathbb{X}}_{\mathscr{E}}\begin{pmatrix} \mathbf{E}^{n+1}_h + \mathbf{E}^n_h \\ \mathbf{P}^{n+1}_{m,h} + \mathbf{P}^n_{m,h} \end{pmatrix} + \begin{pmatrix} \mathrm{curl}^T_h \mathbb{M}_{\mathscr{F}} H^{n+1/2} \\ 0 \end{pmatrix}, \\ \mathbb{M}^{\mu}_{\mathscr{F}} \dfrac{H^{n+1}_h - H^{n-1/2}_h}{\Delta t} = -\mathbb{M}_{\mathscr{F}} \mathrm{curl}_h \mathbf{E}^n_h, \\ \mathbf{E}^0_h = \mathcal{I}^{\mathscr{E}_h}(\mathbf{E}(0)), \quad \mathbf{P}^0_{m,h} = \mathcal{I}^{\mathscr{E}_h}(\mathbf{P}_m(0)), \\ H^{-1/2} = \mathcal{I}^{\mathscr{F}_h}(H(t_{-1/2})). \end{cases} \tag{4.3.4}$$

In the case of constant coefficients this formulation is then posed as

$$\begin{cases} \dfrac{1}{\Delta t}\begin{pmatrix} \mathbf{E}^{n+1}_h - \mathbf{E}^n_h \\ \mathbf{P}^{n+1}_{m,h} - \mathbf{P}^n_{m,h} \end{pmatrix} = \dfrac{1}{2}\mathbb{X} \otimes \mathbb{I}\begin{pmatrix} \mathbf{E}^{n+1}_h + \mathbf{E}^n_h \\ \mathbf{P}^{n+1}_{m,h} + \mathbf{P}^n_{m,h} \end{pmatrix} + \begin{pmatrix} \epsilon^{-1}\widetilde{\mathrm{curl}}_h H^{n+1/2} \\ 0 \end{pmatrix}, \\ \dfrac{H^{n+1}_h - H^{n-1/2}_h}{\Delta t} = -\mu^{-1}\mathrm{curl}_h \mathbf{E}^n_h, \\ \mathbf{E}^0_h = \mathcal{I}^{\mathscr{E}_h}(\mathbf{E}(0)), \quad \mathbf{P}^0_{m,h} = \mathcal{I}^{\mathscr{E}_h}(\mathbf{P}_m(0)), \\ H^{-1/2} = \mathcal{I}^{\mathscr{F}_h}(H(t_{-1/2})). \end{cases} \tag{4.3.5}$$

Where $\widetilde{\mathrm{curl}}_h = \mathbb{M}^{-1}_{\mathscr{V}} \mathrm{curl}^T_h \mathbb{M}_{\mathscr{E}}$. Finally we will present a fully discrete formulation of a linear polarization law using exponential time differencing. In this approach we assume constant coefficients to obtain a computationally feasible discretization. This is due to do the fact computation of $\mathrm{e}^{\mathbb{M}^{x_{1,1}}_{\mathscr{E}}\Delta t}$ may be infeasible.

Definition 4.3.3. Consider a general polarization law having M polarization fields with matrix $\mathbb{X}$. The **Exponential Time Mimetic Finite Difference Method (ETMFD)** for a linear polarization law is posed as

$$\begin{cases} \begin{pmatrix} \mathbf{E}_h^{n+1} \\ \\ \mathbf{P}_{m,h}^{n+1} \end{pmatrix} = \mathrm{e}^{\mathbb{X}\Delta t} \otimes \mathbb{I} \begin{pmatrix} \mathbf{E}^n \\ \\ \mathbf{P}_{m,h}^n \end{pmatrix} + \frac{1}{\epsilon} \left(\int_0^{\Delta t} \mathrm{e}^{\mathbb{X}s}\, ds \right) \otimes \mathbb{I} \begin{pmatrix} \widetilde{\mathrm{curl}}_h H_h^{n+1/2} \\ \\ 0 \end{pmatrix}, \\ H_h^{n+1/2} = H_h^{n-1/2} - \dfrac{\Delta t}{\mu} \mathrm{curl}_h \mathbf{E}_h^n \\ \mathbf{E}_h^0 = \mathcal{I}^{\mathscr{E}_h}(\mathbf{E}(0)), \quad \mathbf{P}_{m,h}^0 = \mathcal{I}^{\mathscr{E}_h}(\mathbf{P}_m(0)), \\ H^{-1/2} = \mathcal{I}^{\mathscr{F}_h}(H(t_{-1/2})). \end{cases} \tag{4.3.6}$$

4.3.1 Efficient Treatment of Inner Product Matrices

In the discretization of the MFD we will necessarily solve a linear system of equations at every time step: for example,

$$\mathbf{E}_h^{n+1} = \mathbf{E}_h^n + \frac{\Delta t}{\epsilon} \mathbb{M}_{\mathscr{E}}^{-1} \mathrm{curl}_h^T \mathbb{M}_{\mathscr{F}}. \tag{4.3.7}$$

Given that $\mathbb{M}_{\mathscr{E}}$ is symmetric positive definite and scales like $|f|$ this system can be approximately solved with a few steps of the conjugate gradient method. However, on rectangles we have access to a procedure analogous to **mass lumping**. Recall that on a rectangle we have a parameterized choice of edge based inner product matrix is given by

$$\mathbb{M}_{\mathscr{E},f}(w_1, w_2, w_3) = \frac{\Delta x \Delta y}{4} \begin{pmatrix} 1+4w_1 & 4w_2 & -4w_1 & 1-4w_2 \\ 4w_2 & 1+4w_3 & -4w_2 & 1-4w_3 \\ 1-4w_1 & -4w_2 & 1+4w_1 & 4w_2 \\ -4w_2 & 1-4w_3 & 4w_2 & 1+4w_3 \end{pmatrix}. \tag{4.3.8}$$

By choosing our parameters $w_1 = w_3 = \frac{1}{4}$ and $w_2 = 0$ we produce a diagonal matrix

$$\mathbb{M}_{\mathscr{E},f}\left(\frac{1}{4}, 0, \frac{1}{4}\right) = \frac{\Delta x \Delta y}{2} \mathbb{I}_{4\times 4} := \mathbb{D}_{\mathscr{E},f}. \tag{4.3.9}$$

Therefore on rectangular meshes it is possible to perform mass lumping using M-adaptation. Mass lumping is a finite element technique where one selects a quadrature to increase the sparsity of an inner product (or mass) matrix, c.f. [12]. Once the mass lumped matrix has been produced we could then formulate a completely explicit scheme as

$$\mathbf{E}_h^{n+1} = \mathbf{E}_h^n + \frac{\Delta t}{\epsilon}\widetilde{\text{curl}}_h H_h^{n+1/2}, \quad \widetilde{\text{curl}}_h = \mathbb{D}_{\mathscr{E}}^{-1}\text{curl}_h^T \mathbb{M}_{\mathscr{F}}. \tag{4.3.10}$$

However, in this approach we loose all of our available parameters to make our inner product matrix diagonal. In order to still have parameters available for optimization we note that as all choices of parameters w_i result in a matrix which is exact on polynomials it is reasonable to assume that

$$\mathbb{D}_{\mathscr{E}} \approx \mathbb{M}_{\mathscr{E}} \implies \mathbb{D}_{\mathscr{E}}^{-1} \approx \mathbb{M}_{\mathscr{E}}^{-1} \tag{4.3.11}$$

where $\mathbb{M}_{\mathscr{E}}$ is any possible edge inner product matrix. Using this approximation we can introduce an approximate inverse inner product matrix

$$\mathbb{W}_{\mathscr{E}} := \mathbb{D}_{\mathscr{E}}^{-1}\mathbb{M}_{\mathscr{E}}\mathbb{D}_{\mathscr{E}}^{-1} \approx \mathbb{M}_{\mathscr{E}}^{-1}. \tag{4.3.12}$$

On rectangles we have $\mathbb{D}_{\mathscr{E},f} = \frac{\Delta x \Delta y}{2}\mathbb{I}$ we have $\mathbb{D}_{\mathscr{E}} = \Delta x \Delta y \mathbb{I}_{N_{\mathscr{E}} \times N_{\mathscr{E}}}$. This gives us

$$\mathbb{W}_{\mathscr{E}} = \frac{1}{\Delta x^2 \Delta y^2}\mathbb{M}_{\mathscr{E}}, \quad \mathbb{W}_{\mathscr{E},f} = \frac{1}{\Delta x^2 \Delta y^2}\mathbb{M}_{\mathscr{E},f}. \tag{4.3.13}$$

This then allows us to formulate truly explicit schemes which still retain a family of free parameters in the form

$$\mathbf{E}_h^{n+1} = \mathbf{E}_h^n + \frac{\Delta t}{\epsilon}\widetilde{\text{curl}}_h H_h^{n+1/2}, \quad \widetilde{\text{curl}}_h = \mathbb{W}_{\mathscr{E}}\text{curl}_h^T \mathbb{M}_{\mathscr{F}}. \tag{4.3.14}$$

This explicit mass lumping leads to the following system of evolution equation for Maxwell's in free space.

Find $\mathbf{E}_h^n \in \mathscr{E}_h, H_h \in \mathscr{F}_h$ such that

$$\begin{cases} \mathbf{E}_h^{n+1} = \mathbf{E}_h^n + \Delta t \widetilde{\text{curl}}_h H_h^{n+1/2} + \mathbf{F}_h^{n+1/2} \\ \mathbb{M}_{\mathscr{F}}^{\mu} \mathbf{H}_h^{n+1/2} = H_h^{n-1/2} - \Delta t \mathbb{M}_{\mathscr{F}} \text{curl} \mathbf{E}_h^n \\ \mathbf{E}^0 = \mathcal{I}^{\mathscr{E}_h}(\mathbf{E}(0)), \quad H_h^{-1/2} = \mathcal{I}^{\mathscr{F}_h}(H(t_{-1/2})) \\ \mathbf{F}_h^{n+1/2} = \mathcal{I}^{\mathscr{E}_h}(\epsilon^{-1}\mathbf{J}(t_{n+1/2})) \end{cases}, \tag{4.3.15}$$

$$\widetilde{\text{curl}}_h = \mathbb{W}_{\mathscr{E}}^{\epsilon^{-1}} \text{curl}_h^T \mathbb{M}_{\mathscr{F}}. \tag{4.3.16}$$

This formulation does not appear to be truly explicit; however, $\mathbb{M}_{\mathscr{F}}^K$ is always diagonal therefore the product

$$[(\mathbb{M}_{\mathscr{F}}^{\mu})^{-1} \mathbb{M}_{\mathscr{F}}]_{f,f} = \frac{|f|}{\int_f \mu}. \tag{4.3.17}$$

In the case of constant coefficients this reduces to

$$\begin{cases} \mathbf{E}_h^{n+1} = \mathbf{E}_h^n + \frac{\Delta t}{\epsilon} \widetilde{\text{curl}}_h H_h^{n+1/2} + \mathbf{J}_h^{n+1/2} \\ \mathbf{H}_h^{n+1/2} = H_h^{n-1/2} - \frac{\Delta t}{\mu} \text{curl} \mathbf{E}_h^n \\ \mathbf{E}^0 = \mathcal{I}^{\mathscr{E}_h}(\mathbf{E}(0)), \quad H_h^{-1/2} = \mathcal{I}^{\mathscr{F}_h}(H(t_{-1/2})) \\ \mathbf{J}_h^{n+1/2} = \mathcal{I}^{\mathscr{E}_h}(\mathbf{J}(t_{n+1/2})) \end{cases}, \tag{4.3.18}$$

$$\text{where } \widetilde{\text{curl}}_h = \mathbb{W}_{\mathscr{E}} \text{curl}_h^T \mathbb{M}_{\mathscr{F}}. \tag{4.3.19}$$

This technique can also be applied to linear polarization laws although we will only present the case of constant coefficients. The time averaged formulation in this case is

given by

$$\text{find } \mathbf{E}_h, \mathbf{P}_{m,h} \in \mathscr{E}_h, H_h \in \mathscr{F}_h \text{ such that}$$
$$\begin{cases} \dfrac{1}{\Delta t}\begin{pmatrix} \mathbf{E}_h^{n+1} - \mathbf{E}_h^n \\ \\ \mathbf{P}_{m,h}^{n+1} - \mathbf{P}_{m,h}^n \end{pmatrix} + \dfrac{1}{2\epsilon}\mathbb{X}\otimes\mathbb{I}\begin{pmatrix} \mathbf{E}_h^{n+1} + \mathbf{E}_h^n \\ \\ \mathbf{P}_{m,h}^{n+1} + \mathbf{P}_{m,h}^n \end{pmatrix} = \dfrac{1}{\epsilon}\begin{pmatrix} \widetilde{\text{curl}}_h H_h^{n+1/2} \\ \\ 0 \end{pmatrix} \\ \dfrac{H_h^{n+1/2} - H_h^{n-1/2}}{\Delta t} = -\dfrac{1}{\mu}\text{curl}_h \mathbf{E}_h^n \\ \mathbf{E}_h^0 = \mathcal{I}^{\mathscr{E}_h}(\mathbf{E}(0)), \quad \mathbf{P}_{m,h}^0 = \mathcal{I}^{\mathscr{E}_h}(\mathbf{P}_m(0)), \\ H^{-1/2} = \mathcal{I}^{\mathscr{F}_h}(H(t_{-1/2})). \end{cases} \tag{4.3.20}$$

$$\text{where } \widetilde{\text{curl}}_h = \mathbb{W}_{\mathscr{E}}\text{curl}_h^T\mathbb{M}_{\mathscr{F}}. \tag{4.3.21}$$

The ETMFD for linear polarization laws with mass lumping is given by

$$\text{find } \mathbf{E}_h, \mathbf{P}_{h,m} \in \mathscr{E}_h, H_h \in \mathscr{F}_h$$
$$\begin{cases} \begin{pmatrix} \mathbf{E}_h^{n+1} \\ \\ \mathbf{P}_{m,h}^{n+1} \end{pmatrix} = \mathrm{e}^{\mathbb{X}\Delta t}\otimes\mathbb{I}\begin{pmatrix} \mathbf{E}_h^{n+1} \\ \\ \mathbf{P}_{m,h}^{n+1} \end{pmatrix} + \dfrac{1}{\epsilon}\left(\displaystyle\int_0^{\Delta t}\mathrm{e}^{\mathbb{X}s}\,ds\right)\otimes\mathbb{I}\begin{pmatrix} \widetilde{\text{curl}}_h H_h^{n+1/2} \\ \\ 0 \end{pmatrix}, \\ H^{n+1/2} = H^{n-1/2} - \dfrac{1}{\mu}\text{curl}_h \mathbf{E}_h^n, \\ \mathbf{E}_h^0 = \mathcal{I}^{\mathscr{E}_h}(\mathbf{E}(0)), \quad \mathbf{P}_{m,h}^0 = \mathcal{I}^{\mathscr{E}_h}(\mathbf{P}_m(0)), \\ H^{-1/2} = \mathcal{I}^{\mathscr{F}_h}(H(t_{-1/2})). \end{cases} \tag{4.3.22}$$

4.3.2 Discrete Gauss' Law and Continuity Equation

Theorem 4.3.1. *Let $n \geq 1$ and $\mathbf{E}_h^n$ satisfying the discrete evolution equation*

$$\begin{cases} \mathbf{E}_h^{n+1} = \mathbf{E}_h^n + \Delta t c_0^2 \widetilde{curl}_h B^{n+1/2}, & n \geq 0, \\ B_h^{n+1/2} = B_h^{n-1/2} - \Delta t\, curl_h E_h^n, & n \geq 1 \end{cases} \tag{4.3.23}$$

and given initial conditions

$$\mathbf{E}_h^0 = \mathcal{I}^{\mathscr{E}_h}(\mathbf{E}(0)), \qquad B_h^{1/2} = \mathcal{I}^{\mathscr{F}_h}(B(\Delta t/2)). \tag{4.3.24}$$

Then

$$\widetilde{div}_h \mathbf{E}_h^n = \widetilde{div}_h \mathbf{E}_h^0. \tag{4.3.25}$$

Proof. We calculate the discrete divergence of the discrete Ampére-Maxwell Law (4.3.23)

$$\frac{\widetilde{\mathrm{div}}_h \mathbf{E}_h^{n+1} - \widetilde{\mathrm{div}}_h \mathbf{E}_h^n}{\Delta t} = c_0^2 \widetilde{\mathrm{div}}_h \widetilde{\mathrm{curl}}_h B_h^{n+1/2} = 0. \tag{4.3.26}$$

This gives us the identity

$$\widetilde{\mathrm{div}}_h \mathbf{E}_h^{n+1} = \widetilde{\mathrm{div}}_h \mathbf{E}_h^n, \quad n \geq 0. \tag{4.3.27}$$

Applying the identity recursively yields

$$\widetilde{\mathrm{div}}_h \mathbf{E}^n = \widetilde{\mathrm{div}}_h \mathcal{I}^{\mathscr{E}_h}(\mathbf{E}(0)). \tag{4.3.28}$$

Q.E.D.

This is a discrete analogue of Gauss' Law (4.1.2)

$$\mathrm{div}(\epsilon \mathbf{E}) = \rho. \tag{4.3.29}$$

Here we have that the initial divergence is preserved for all discrete time points which is the discrete analogue of for free space in the continuum. In particular if we introduce the discrete charge density

$$\rho_h^n = \widetilde{\mathrm{div}}_h \mathbf{E}_h^n \tag{4.3.30}$$

then we have that

$$\rho_h^n = \rho_h^0, \forall n \geq 0. \tag{4.3.31}$$

We will now extend this approach to show discrete continuity equation is not preserved exactly for a time averaged discretization of a simple conductive media. First note that

for a conductive medium, combining the Guass' law with the continuity equation we and assuming uniform σ and ϵ we have the identity

$$\mathrm{div}\epsilon\mathbf{E} = \rho, \quad \frac{\partial}{\partial t}\rho = -\mathrm{div}\sigma\mathbf{E} \implies \frac{\partial}{\partial t}\rho = -\frac{\sigma}{\epsilon}\rho. \tag{4.3.32}$$

Time averaging will only approximate this property in time.

Theorem 4.3.2. *Let $n \geq 1$ and $\mathbf{E}_h^n \in \mathscr{E}_h, B_h^{n+1/2} \in \mathscr{F}_h$ satisfying*

$$\begin{cases} \dfrac{\mathbf{E}_h^{n+1} - \mathbf{E}_h^n}{\Delta t} + \dfrac{\sigma}{\epsilon}\dfrac{\mathbf{E}_h^{n+1} + \mathbf{E}_h^n}{2} = c^2\widetilde{curl}_h B_h^{n+1/2} \\ \dfrac{B_h^{n+1/2} - B_h^{n-1/2}}{\Delta t} = -curl_h E_h^n \end{cases} \tag{4.3.33}$$

and given initial data

$$\mathbf{E}_h^0 = \mathcal{I}^{\mathscr{E}_h}(\mathbf{E}(0)), \qquad B_h^{1/2} = \mathcal{I}^{\mathscr{F}_h}(B(\Delta t/2)). \tag{4.3.34}$$

Then we have

$$\widetilde{div}_h\mathbf{E}_h^{n+1} = \left(\frac{1 - \frac{\sigma\Delta t}{2\epsilon}}{1 + \frac{\sigma\Delta t}{2\epsilon}}\right)^{n+1} \widetilde{div}_h\mathbf{E}_h^0. \tag{4.3.35}$$

Proof. The proof here follows much like the free space case– we apply the adjoint divergence, $\widetilde{\mathrm{div}}_h$ to our discrete Ampére-Maxwell Law and then compute.

$$\widetilde{\mathrm{div}}_h\frac{\mathbf{E}_h^{n+1} - \mathbf{E}_h^n}{\Delta t} + \frac{\sigma}{\epsilon}\widetilde{\mathrm{div}}_h\frac{\mathbf{E}_h^{n+1} + \mathbf{E}_h^n}{2} = c^2\widetilde{\mathrm{div}}_h\widetilde{\mathrm{curl}}_h B_h^{n+1/2} \tag{4.3.36}$$

$$= 0 \qquad \text{by Corollary 3.8.2} \tag{4.3.37}$$

$$\widetilde{\mathrm{div}}_h\mathbf{E}_h^{n+1} = \frac{1 - \frac{\sigma\Delta t}{2\epsilon}}{1 + \frac{\sigma\Delta t}{2\epsilon}}\widetilde{\mathrm{div}}_h\mathbf{E}_h^n. \tag{4.3.38}$$

Applying this identity recursively yields the result. **Q.E.D.**

Note that in the case of $\widetilde{\mathrm{div}}_h\mathbf{E}_h^0 = 0$ we have the exactness property again, that the divergence free condition is conserved for all time steps. However, if $\mathbf{E}_h^{n+1}$ is not divergence free, then time averaging will not capture the decay of the divergence exactly. This is due to the fact that the exact solution to

$$\dot{\rho} = -\frac{\sigma}{\epsilon}\rho \tag{4.3.39}$$

is given by

$$\rho(t) = \mathrm{e}^{-\frac{\sigma}{\epsilon}t}\rho(0). \tag{4.3.40}$$

However, expanding in Taylor series about the point $n\Delta t$ we have

$$\left(\frac{1-\frac{\sigma\Delta t}{2\epsilon}}{1+\frac{\sigma\Delta t}{2\epsilon}}\right)^{n+1} = \mathrm{e}^{\frac{\sigma}{\epsilon}n\Delta t} + \mathcal{O}(\Delta t^2). \tag{4.3.41}$$

This is in contrast to the ETMFD for which we will have exact agreement in the discrete sense.

Theorem 4.3.3. *Let $n \geq 0$ and consider $\mathbf{E}_h^n, \mathbf{P}_{m,h}^n \in \mathscr{E}_h$ and $B_h^{n+1/2} \in \mathscr{F}_h$ a solution to the ETMFD for a general polarization law*

$$\begin{cases} \begin{pmatrix} \mathbf{E}_h^{n+1} \\ \\ \mathbf{P}_{m,h}^{n+1} \end{pmatrix} = \mathrm{e}^{\mathbb{X}\Delta t} \begin{pmatrix} \mathbf{E}_h^{n} \\ \\ \mathbf{P}_{m,h}^{n} \end{pmatrix} + c^2 \left(\int_0^{\Delta t} \mathrm{e}^{\mathbb{X}s}\ ds \right) \begin{pmatrix} \widetilde{curl}_h B_h^{n+1/2} \\ \\ 0 \end{pmatrix}, \\ B_h^{n+1/2} = B_h^{n-1/2} - curl_h \mathbf{E}_h^n. \end{cases} \tag{4.3.42}$$

subject to appropriate initial conditions

$$\mathbf{E}_h^0 = \mathcal{I}^{\mathscr{E}_h}(\mathbf{E}(0)), \quad \mathbf{P}_{m,h}^0 = \mathcal{I}^{\mathscr{E}_h}(\mathbf{P}_m(0)), \quad B_h^{1/2} = \mathcal{I}^{\mathscr{F}_h}(B(\Delta t/2)). \tag{4.3.43}$$

We then have that

$$\begin{pmatrix} \widetilde{div}_h \mathbf{E}_h^{n+1} \\ \widetilde{div}_h \mathbf{P}_{m,h}^{n+1} \end{pmatrix} = \mathrm{e}^{\mathbb{X}(n+1)\Delta t} \begin{pmatrix} \widetilde{div}_h \mathbf{E}_h^{0} \\ \widetilde{div}_h \mathbf{P}_{m,h}^{0} \end{pmatrix}. \tag{4.3.44}$$

Proof. Let $\mathbb{Y} = c_0^2 \left(\int_0^{\Delta t} \mathrm{e}^{\mathbb{X}s}\ ds \right)$. Let the i,j entry of $\mathbb{Y}$ be given by $y_{i,j}$. We have the identity

$$\left(\int_0^{\Delta t} \mathrm{e}^{\mathbb{X}s}\ ds \right) \begin{pmatrix} \widetilde{\mathrm{curl}}_h B_h^{n+1/2} \\ 0 \end{pmatrix} = \begin{pmatrix} y_{1,1}\widetilde{\mathrm{curl}}_h B_h^{n+1/2} \\ \vdots \\ y_{1,M+1}\widetilde{\mathrm{curl}}_h B_h^{n+1/2} \end{pmatrix} \tag{4.3.45}$$

We will now take the discrete adjoint divergence of every row of our Ampére-Maxwell-Polarization Law equation.

$$\begin{pmatrix} \widetilde{\mathrm{div}}_h \mathbf{E}_h^{n+1} \\ \widetilde{\mathrm{div}}_h \mathbf{P}_{m,h}^{n+1} \end{pmatrix} = \mathrm{e}^{\mathbb{X}\Delta t} \begin{pmatrix} \widetilde{\mathrm{div}}_h \mathbf{E}_h^{n} \\ \widetilde{\mathrm{div}}_h \mathbf{P}_{m,h}^{n} \end{pmatrix} + \begin{pmatrix} y_{1,1} \widetilde{\mathrm{div}}_h \widetilde{\mathrm{curl}}_h B_h^{n+1/2} \\ \vdots \\ y_{1,M+1} \widetilde{\mathrm{div}}_h \widetilde{\mathrm{curl}}_h B_h^{n+1/2} \end{pmatrix} \tag{4.3.46}$$

$$= \mathrm{e}^{\mathbb{X}\Delta t} \begin{pmatrix} \widetilde{\mathrm{div}}_h \mathbf{E}_h^{n} \\ \widetilde{\mathrm{div}}_h \mathbf{P}_{m,h}^{n} \end{pmatrix}. \tag{4.3.47}$$

Applying the above identity recursively yeilds the result. **Q.E.D.**

Note that the first row of $\mathbb{X}$ decribes the consitutive law

$$\mathbf{D} = \epsilon \mathbf{E} + \sum_{m=1}^{M} x_{1,m} \mathbf{P}_m. \tag{4.3.48}$$

Thus the above result is a discrete analogue of the continuity equation for the polarization media.

4.4 Numerical Demonstration of Continuity Equation

In this section we will demonstrate the discrete divergence results as developed in Theorem 4.3.1. Throughout the section we will consider a media where $\epsilon = \mu = \eqsim 1$ for simplicity.

Given that the discrete weak divergence is defined as

$$\widetilde{\mathrm{div}}_h = \mathbb{M}_{\mathscr{V}}^{-1} \nabla_h^T \mathbb{W}_{\mathscr{E}}^{-1}, \tag{4.4.1}$$

we must solve a linear systems in order to compute the weak divergence. For efficiency we choose $\mathbb{M}_{\mathscr{V},f} = \Delta x \Delta y \mathbb{I}_{4\times 4}$ using M-adaptation to perform mass lumping. In order to

solve the problem

$$\mathbb{W}_{\mathscr{E}}\mathbf{F}_h = \mathbf{E}_h, \tag{4.4.2}$$

for the vector $\mathbf{F}_h$ we use the conjugate gradient method in order to avoid assembling the global matrix. In order to guarantee accuracy we choose a relative residual tolerance of 10^{-15} which is attained in approximately 10 iterations for our problem. The accuracy of this linear solve does seem to influence the exactness of the method so high precision appears necessary.

Further, the construction of the weak divergence developed in this work requires $\mathscr{V}_h$ to have discrete homogeneous Dirichlet boundary conditions. This is then built into the inner product matrix $\mathbb{M}_{\mathscr{V}}$.

Experiment 1. In our first experiment we will demonstrate that $\mathrm{Im}(\widetilde{\mathrm{curl}}_h) \subset \mathrm{Ker}(\widetilde{div}_h)$ and that for divergence free initial data the fully discrete Maxwell's Equations with MFD in space and leap frog in time has a discrete weak divergence within machine precision. Consider the initial value problem in free space

$$\begin{cases} \frac{\partial}{\partial t}\mathbf{E} = \mathbf{curl}B, & \in [0,6]^2 \\ \frac{\partial}{\partial t}H = -\mathrm{curl}\mathbf{E}, & \in [0,6]^2 \\ \mathbf{E}\times\mathbf{n} = 0, & \in \partial[0,6]^2 \\ \mathbf{E}(0) = \mathbf{0}, & \\ H(0) = \mathrm{e}^{-100((x-3)^2+(y-3)^2)}. & \end{cases} \tag{4.4.3}$$

Given that the initial conditions are divergence free the continuum setting $\mathrm{div}\mathbf{E} = 0$ for all time.

See Figure 4.1 for results. We find that the discrete charge density $\rho_h^n = \widetilde{\mathrm{div}}_h\mathbf{E}$ stays at or below machine precision for all time and the L^2 norm of this field is computed at approximately 10^{-32}.

This experiment provides numerical evidence that $\widetilde{\mathrm{div}}_h\widetilde{\mathrm{curl}}_h = \mathbf{0}$.

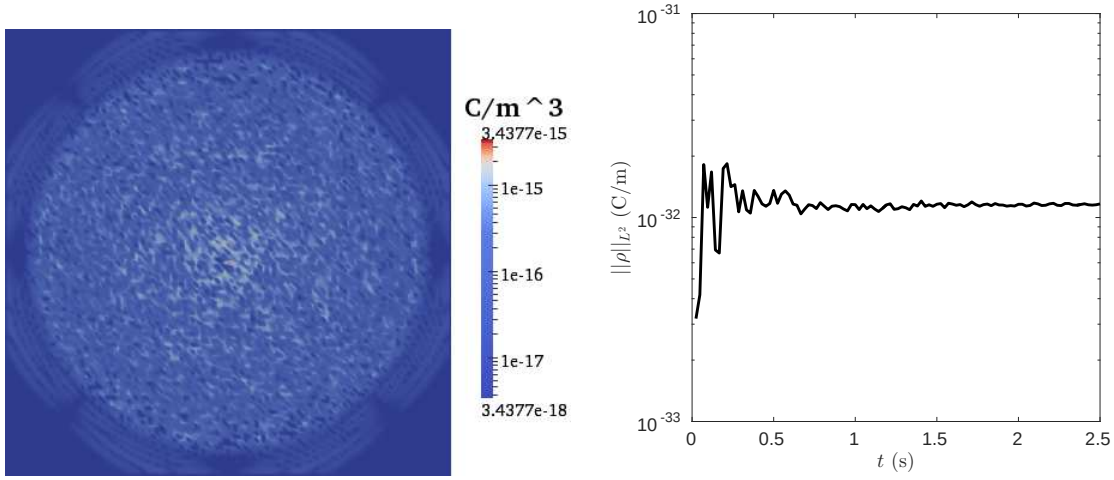

(a) (b)

FIGURE 4.1: By resolving $\mathbb{W}_{\mathscr{E}}^{-1}$ using conjugate gradients to a tolerance of 10^{-15} we produce a discrete charge density $\rho_h^n = \widetilde{\text{div}}_h \mathbf{E}_h^n$ which is pointwise on the order of 10^{-15} for divergence free initial conditions. Over time L^2 norm of ρ_h^n stays bellow 10^{-30} for divergence free initial data. Subfigure (a) shows the charge density $|\rho_h^n|$ at time 2.5 with log scale coloring while subfigure (b) shows the L^2 norm of the field.

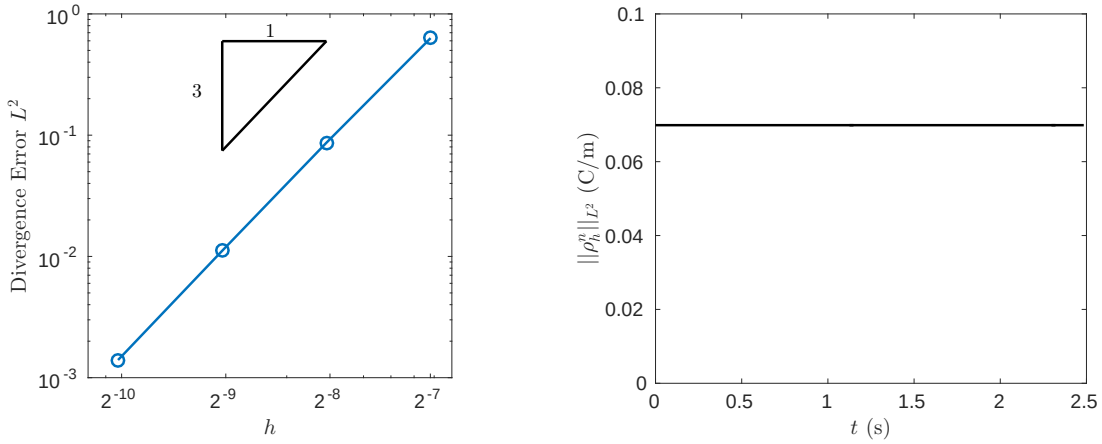

FIGURE 4.2: (a) We present the difference L^2 divergence error for initial conditions which are not divergence free. (b) we show the quantity $\|\rho_h^n\|_{L^2}$ at our lowest resolution $h = 2^{-7}$. Charge appears to be conserved throughout computation

Experiment 2. In this second experiment we consider initial data which is not divergence

free.

$$\begin{cases} \frac{\partial}{\partial t}\mathbf{E} = \mathbf{curl}B & \in [0,6]^2, \\ \frac{\partial}{\partial t}H = -\text{curl}\mathbf{E} & \in [0,6]^2, \\ \mathbf{E}\times\mathbf{n} = 0 & \in \partial[0,6]^2, \\ \mathbf{E}(0) = (\mathrm{e}^{-100((x-3)^2+(y-3)^2)}, 0)^T, & \\ H(0) = 0. & \end{cases} \tag{4.4.4}$$

A continuum calculation gives us that

$$\rho = \text{div}\mathbf{E}(0) = -200(x-3)\mathrm{e}^{-100((x-3)^2+(y-3)^2)} \tag{4.4.5}$$

for all time. For this experiment we advance the approximation to time 2.5 and then compute

$$\rho_h^n = \widetilde{\text{div}}_h\mathbf{E}_h^n \tag{4.4.6}$$

the discrete charge density. We will compute the L^2 error of this discrete representation and the interpolant of the exact solution

$$\mathcal{E}_{\text{div}} = \sqrt{(\rho_h^n - \mathcal{I}^{\mathscr{V}_h}(\rho))^T\mathbb{M}_{\mathscr{V}}(\rho_h^n - \mathcal{I}^{\mathscr{V}_h}(\rho))}. \tag{4.4.7}$$

Here we find an unexpected super convergence result, namely that ρ_h appears to converge at order three, i.e. $\mathcal{E}_{\text{div}} = \mathcal{O}(h^3)$. Further we provide the quantity $\|\rho_h^n\|_{L^2}$ as function of time for our lowest resolution case. We find that this quantity is approximately constant during the calculation suggesting conservation of charge. See Table 4.1 and Figure 4.2 for results.

These experiments provide evidence that the method also preserves non-divergence free solutions with high accuracy.

These two experiments show that MFD preserves Gauss' Law and the continuity equation well. We find that when using iterative solvers to compute the adjoint divergence high accuracy is especially important. We do not recommend converging a $\mathbb{M}_{\mathscr{E}}^{-1}$ to only

discretiztion error levels as this will violate the adjoint properties which guarentee our mimetic properties. However, when $\mathbb{M}_{\mathscr{E}}^{-1}$ is computed accurately we see that divergence free soutions appear to remain divergence free for all time and solutions with non-zero divergence exhibit super convergence of dispersion error.

TABLE 4.1: Divergence errors for a free space problem with non-zero divergence initial data. Errors appear to converge at order h^3.

$\log_2(h)$	$\mathcal{E}_{\text{div}}$	rate
-7	0.6313	–
-8	0.0866	2.86
-9	0.0111	2.95
-10	0.0014	2.99

5 DISPERSION ANALYSIS AND M-ADAPTATION

5.1 Introduction to Dispersion Analysis

In this chapter we will focus in more depth on mimetic methods for transient wave problems arising from Maxwell's equations. One of the major challenges of numerical approximation of wave propagation is that discretization errors result in waves travelling at non-physical speeds.

In order to quantify dispersion error the **Fourier Transform** is employed. The Fourier transform is an isomorphism on L^2 which carries functions which depend on time t and space $\mathbf{x}$ to functions which depend on frequencies ω and wave vectors $\mathbf{k}$. Both frequency and wave vectors are inversely proportional to the period (in time) and wave length (in space) of a given plane wave. Intuitively, the Fourier Transform produces the parameters which decompose a function into a continuous superposition of plane waves. A major feature of the Fourier Transform is that it transforms differential equations in physical space into algebraic equations in frequency-wave vector space. An equality of this algebraic equation is called the **dispersion relation** for a PDE and it relates the wave vectors and frequencies of a given solution. Using this technique one can infer the wave speed and dispersive characteristics of a given PDE. The Fourier transform can also be employed in the analysis of numerical methods, however the dispersion relations become trigonometric rather than algebraic equations but they are amenable to Taylor series analysis.

In this section we will perform dispersion analysis for a number of transient models for Maxwell's equations as well as MFD discretizations. Once we have performed this analysis we will select optimal parameters in the MFD which reduces the dispersion error

of the method using an method optimization technique called **M-adaptation**. Section 5.2 we introduce continuum dispersion analysis. In Section 5.4 we perform a dispersion analysis of the MFD and perform M-adaptation. In Section 5.5 we present numerical results which support our theoretical findings.

5.2 Continuum Fourier Analysis

In its classical application, dispersion analysis is performed by transforming a (partial) differential equation from physical space-time to frequency domain. This is accomplished by way of the Fourier transform. We will use the following Fourier transform convention. Note that it will have different signs depending on whether we are transforming in space or time. We will follow the notational conventions similar to those laid out in [12].

Definition 5.2.1. Consider a function of space $u : \mathbb{R}^d \to \mathbb{R}$ with $d = 1, 2, 3$. We define its spatial Fourier transform as

$$\mathcal{F}(u)(\mathbf{k}) = \frac{1}{(2\pi)^{d/2}} \int_{\mathbb{R}^d} u(\mathbf{x}) \mathrm{e}^{-\mathrm{i}\mathbf{k}\cdot\mathbf{x}} \, d\mathbf{x}. \tag{5.2.1}$$

Where, $\mathcal{F}(u) : \mathbb{R}^d \to \mathbb{R}$.

We call the domain of this transformed function the *wave vector space* with variable wave vector $\mathbf{k}$. We use the convention that a wave vector $\mathbf{k}$ has an associated wave number $k = |\mathbf{k}|$. The Fourier transform is invertible.

Let $f : \mathbb{R} \to \mathbb{R}$ be a function of time. We define its Fourier transform as

$$\mathcal{G}(f)(\omega) = \frac{1}{\sqrt{2\pi}} \int_{\mathbb{R}} f(t) \mathrm{e}^{\mathrm{i}\omega t} \, dt. \tag{5.2.2}$$

This transform $\mathcal{G}(f)$ is also a function now mapping $\mathbb{R} \to \mathbb{R}$. We call its domain *frequency space* denoted by the frequency ω. The inverse Fourier transform in time is given as follows.

We will also consider transforms on (time dependent) vector fields $\mathbf{u} : \mathbb{R}^d \to \mathbb{R}^n$ where $n \geq 2$ and $\mathbf{u} = (u_1, u_2, \cdots, u_n)$. In this case Fourier transforms in time and space are defnied component wise by $\mathcal{F}(\mathbf{u}) = (\mathcal{F}(u_1), \mathcal{F}(u_2), \cdots \mathcal{F}(u_n))$ and $\mathcal{G}(\mathbf{u}) = (\mathcal{G}(u_1), \mathcal{G}(u_2), \cdots, \mathcal{G}(u_n))$ respectively.

Before developing Fourier Analysis on vector valued equations we will start with the scalar case.

Theorem 5.2.1. *The Fourier transforms $\mathcal{F}$ and $\mathcal{G}$ are invertible with inverses given as follows. Let $\hat{u} = \mathcal{F}(u)$ and $\tilde{f} = \mathcal{G}(f)$*

$$u(x) = \frac{1}{(2\pi)^{d/2}} \int_{\mathbb{R}^d} \hat{u}(\mathbf{k}) \mathrm{e}^{\mathrm{i}\mathbf{k}\cdot\mathbf{x}} \, d\mathbf{k} \tag{5.2.3}$$

$$f(t) = \frac{1}{\sqrt{2\pi}} \int_{\mathbb{R}} \tilde{f}(\omega) \mathrm{e}^{-\mathrm{i}\omega t} \, d\omega \tag{5.2.4}$$

We will now introduce the concepts of symbols and dispersion relations. To do so we must first establish some notation.

Definition 5.2.2. We define a multi-index notation for differential operators as follows. Consider an array of integers $\mathbf{a} = (a_1, a_2, \ldots, a_n, a_{n+1})$. We define

$$D^{\mathbf{a}} = \frac{\partial^{|\mathbf{a}|}}{\partial_{x_1}^{a_1} \partial_{x_2}^{a_2} \cdots \partial_{x_n}^{a_n} \partial_t^{a_{n+1}}} \tag{5.2.5}$$

Where $|\mathbf{a}|$ is the usual taxicab norm of $\mathbf{a}$

$$|\mathbf{a}| = \sum_{i=1}^{n} |a_i|. \tag{5.2.6}$$

Assume that $\tilde{\mathbf{a}} = (a_1, \cdots, a_d, a_t)$. We define the multi-index polynomial

$$(\mathbf{k}, \omega)^{\tilde{\mathbf{a}}} = \omega^{a_t} \prod_{i=1}^{d} k_i^{a_i} \tag{5.2.7}$$

where $\mathbf{k} = (k_1, \cdots, k_d)$.

With the multi-index in place we can now define the symbol and dispersion relation of a PDE.

Definition 5.2.3. Consider a linear n^{th} order differential operator (in time and space) defined by

$$Lu = \sum_{|\mathbf{a}|\leq n} c_{\mathbf{a}} D^{\mathbf{a}} u, \tag{5.2.8}$$

where the constants $c_{\mathbf{a}}$ are real numbers associated to each component of the operator $D^{\mathbf{a}}$. We define the **Symbol of** L to be

$$\mathcal{F}[L] = \sum_{|\mathbf{a}|\leq n} c_{\mathbf{a}} (\mathrm{i}\mathbf{k}, -\mathrm{i}\omega)^{\mathbf{a}} \tag{5.2.9}$$

This definition is typical to the Fourier Analysis found in [12]

Lemma 5.2.2. *Assume that L is an n^{th} order differential operator in time and space*

$$Lu = \sum_{|\mathbf{a}|\leq n} c_{\mathbf{a}} D^{\mathbf{a}} u. \tag{5.2.10}$$

Let $\hat{u}$ be the Fourier transform in time and space of u

$$Lu = \mathcal{F}^{-1} \circ \mathcal{G}^{-1}(\mathcal{F}[L]\hat{u}) \tag{5.2.11}$$

Proof. Let $\hat{u}$ be the Fourier transform in time and space of $u(\mathbf{x}, t)$.

$$Lu = \sum_{|\mathbf{a}|\leq n} c_{\mathbf{a}} D^{\mathbf{a}} \frac{1}{(2\pi)^{\frac{d+1}{2}}} \int_{\mathbb{R}^d} \int_{\mathbb{R}} \hat{u}(\mathbf{k}, \omega) \mathrm{e}^{\mathrm{i}\mathbf{k}\cdot\mathbf{x} - \mathrm{i}\omega t} \, d\omega \, d\mathbf{k} \tag{5.2.12}$$

Assuming sufficient regularity we commute the sum over $c_{\mathbf{a}} D^{\mathbf{a}}$ with the integrals.

$$Lu = \frac{1}{(2\pi)^{\frac{d+1}{2}}} \int_{\mathbb{R}^d} \int_{\mathbb{R}} \hat{u}(\mathbf{k}, \omega) \sum_{|\mathbf{a}|\leq n} c_{\mathbf{a}} D^{\mathbf{a}} \mathrm{e}^{\mathrm{i}\mathbf{k}\cdot\mathbf{x} - \mathrm{i}\omega t} \, d\omega \, d\mathbf{k}. \tag{5.2.13}$$

Consider $\mathbf{a} = (a_1, \cdots, a_d, a_t)$. Then we have

$$c_{\mathbf{a}} D^{\mathbf{a}} \mathrm{e}^{\mathrm{i}(\mathbf{k}\cdot\mathbf{x} - \omega t)} = c_{\mathbf{a}} (\mathrm{i}\mathbf{k}, -\mathrm{i}\omega)^{\mathbf{a}} \mathrm{e}^{\mathrm{i}(\mathbf{k}\cdot\mathbf{x} - \omega t)}. \tag{5.2.14}$$

Therefore

$$Lu = \frac{1}{(2\pi)^{\frac{d+1}{2}}} \int_{\mathbb{R}^d} \int_{\mathbb{R}} \hat{u}(\mathbf{k}, \omega) \sum_{|\mathbf{a}|\leq n} c_{\mathbf{a}} (\mathrm{i}\mathbf{k}, -\mathrm{i}\omega)^{\mathbf{a}} \, d\omega \, d\mathbf{k}. \tag{5.2.15}$$

$$= \mathcal{F}^{-1} \circ \mathcal{G}^{-1}(\mathcal{F}[L]\hat{u}) \tag{5.2.16}$$

Q.E.D.

The previous result relates to us the symbol of $\mathcal{F}[L]$ and $\mathcal{G}[L]$ to L in terms of the Fourier transform. Note that we can compute the symbol rather quickly by the following lemma.

Lemma 5.2.3. *The symbol of an operator L is determined by its action on plane waves, i.e., functions of the form $\mathrm{e}^{\mathrm{i}(\mathbf{k}\cdot\mathbf{x}-\omega t)}$ by*

$$\mathcal{F}[L] = \frac{L\mathrm{e}^{\mathrm{i}(\mathbf{k}\cdot\mathbf{x}-\omega t)}}{\mathrm{e}^{\mathrm{i}(\mathbf{k}\cdot\mathbf{x}-\omega t)}} \tag{5.2.17}$$

Proof. This is immediate using the definitions of Fourier Transform, its inverse, and Lemma 5.2.3. **Q.E.D.**

So far we have considered only scalar valued differential operators. As this work mostly concerns electromagnetism we must provide an interpretation for higher dimensional derivatives. There are roughly three classes of these operators: operators which take vectors to scalars (such as the divergence or scalar curl in 2D), operators which take scalars to vectors (such as the gradient or vector curl in 2D), and operators which take vectors to vectors (such as the curl in 3D).

We prefer to interpret such operators as matrices of scalar equations.

$$\text{for } d = 3 \qquad\qquad \text{for } d = 2 \tag{5.2.18}$$

$$\mathrm{div} = \left(\frac{\partial}{\partial x}, \frac{\partial}{\partial y}, \frac{\partial}{\partial z}\right) \qquad\qquad \mathrm{curl} = \left(-\frac{\partial}{\partial y}, \frac{\partial}{\partial x}\right) \tag{5.2.19}$$

$$\nabla = \begin{pmatrix} \frac{\partial}{\partial x} \\ \frac{\partial}{\partial y} \\ \frac{\partial}{\partial z} \end{pmatrix} \qquad\qquad \mathbf{curl} = \begin{pmatrix} \frac{\partial}{\partial y} \\ -\frac{\partial}{\partial x} \end{pmatrix} \tag{5.2.20}$$

$$\mathbf{curl} = \begin{pmatrix} 0 & -\frac{\partial}{\partial z} & \frac{\partial}{\partial y} \\ \frac{\partial}{\partial z} & 0 & -\frac{\partial}{\partial x} \\ -\frac{\partial}{\partial y} & \frac{\partial}{\partial x} & 0 \end{pmatrix} \tag{5.2.21}$$

In the scalar case action by plane waves do not depend upon initial amplitudes. However, for operators which take vectors for inputs we must include the possibility of different amplitudes in different components. For this reason we introduce the following formalism when computing the symbol of a higher dimensional derivative.

Definition 5.2.4. Consider $\mathbf{u}$ an m vector valued function and $\mathbb{L}$ an $n \times m$ linear operator. Defined as

$$\mathbb{L} = \begin{pmatrix} L_{1,1} & \cdots & L_{1,m} \\ \vdots & & \vdots \\ L_{n,1} & \cdots & L_{n,m} \end{pmatrix} \tag{5.2.22}$$

where $L_{i,j}$ are abstract, linear, differential operators in space and time. We define its symbol as

$$\mathcal{F}[\mathbb{L}] = \begin{pmatrix} \mathcal{F}[L_{1,1}] & \cdots & \mathcal{F}[L_{1,m}] \\ \vdots & & \vdots \\ \mathcal{F}[L_{n,1}] & \cdots & \mathcal{F}[L_{n,m}] \end{pmatrix}. \tag{5.2.23}$$

This definition is similar to one found in [12].

Similar to Lemma 5.2.3 we have that high dimension linear differential operators have symbols determined by their action on plane waves of the form $\mathbf{E}_0 \mathrm{e}^{\mathrm{i}(\mathbf{k}\cdot\mathbf{x}-\omega t)}$ where $\mathbf{E}_0$ is a constant unit vector. We have the following lemma.

Lemma 5.2.4. *If $\mathbb{L}_1$ is a $m \times n$ linear differential operator and $\mathbb{L}_2$ is a $r \times m$ linear operator then we have*

$$\mathcal{F}[\mathbb{L}_2\mathbb{L}_1] = \mathcal{F}[\mathbb{L}_2]\mathcal{F}[\mathbb{L}_1]. \tag{5.2.24}$$

Proof. This follows immediately from linearity of the Fourier symbol and the definition of matrix multiplication. **Q.E.D.**

We will now provide several simple examples, c.f. [12].

Example 5.2.1. Consider the gradient operator ∇ defined by

$$\nabla = (\frac{\partial}{\partial x_1}, \cdots, \frac{\partial}{\partial x_d})^T \tag{5.2.25}$$

Calculating its action on a plane wave we have

$$\nabla \mathrm{e}^{\mathrm{i}\mathbf{k}\cdot\mathbf{x}} = (\mathrm{i}k_1, \cdots, \mathrm{i}k_d)^T \mathrm{e}^{\mathrm{i}\mathbf{k}\cdot\mathbf{x}} \tag{5.2.26}$$

Therefore the symbol of $\mathcal{F}[\nabla] = \mathrm{i}\mathbf{k}$.

Example 5.2.2. Consider the divergence operator div. We calculate its action on a plane wave of the form $\mathbf{E}_0 \mathrm{e}^{\mathrm{i}\mathbf{k}\cdot\mathbf{x}}$.

$$\mathrm{div}\mathbf{E}_0 \mathrm{e}^{\mathrm{i}\mathbf{k}\cdot\mathbf{x}} = \sum_{i=1}^{d} (ik_i) E_i = \mathrm{i}\mathbf{k}^T \mathbf{E}_0. \tag{5.2.27}$$

Therefore the symbol $\mathcal{F}[\mathrm{div}] = \mathrm{i}\mathbf{k}^T$.

Example 5.2.3. Consider the curl operator **curl** acting on $\mathbf{E}_0 \mathrm{e}^{\mathrm{i}\mathbf{k}\cdot\mathbf{x}}$.

$$\mathbf{curl}\mathbf{E}_0 \mathrm{e}^{\mathrm{i}\mathbf{k}\cdot\mathbf{x}} = \begin{pmatrix} \mathrm{i}k_y E_z - \mathrm{i}k_z E_y \\ \mathrm{i}k_z E_x - \mathrm{i}k_x E_z \\ \mathrm{i}k_x E_y - \mathrm{i}k_y E_x \end{pmatrix} = \mathrm{i}\mathbf{k} \times \mathbf{E}_0 \tag{5.2.28}$$

Therefore $\mathcal{F}[\nabla\times] = \mathrm{i}[\mathbf{k}]_\times$ where this notation describes a cross product $[\mathbf{a}]_\times \mathbf{b} = \mathbf{a} \times \mathbf{b}$.

Example 5.2.4. We will now calculate the symbol of the Laplace operator $\triangle = \mathrm{div}\nabla$.

$$\mathcal{F}[\triangle] = \mathcal{F}[\mathrm{div}]\mathcal{F}[\nabla] = (\mathrm{i}\mathbf{k})^T(\mathrm{i}\mathbf{k}) = -k^2. \tag{5.2.29}$$

5.3 Continuum dispersion relations

Having developed some well known theory to describe the linear differential operators in frequency domain we use this to solve differential equations.

Lemma 5.3.1. *Consider the linear differential equation*

$$\mathbb{L}\mathbf{u} = \mathbf{0} \tag{5.3.1}$$

where $\mathbb{L}$ *is a* $m \times n$ *linear differential operator and* $\mathbf{u} : \mathbb{R}^d \to \mathbb{R}^n$. *If* $\mathbf{u} = \mathbf{E}_0 \mathrm{e}^{\mathrm{i}(\mathbf{k}\cdot\mathbf{x}-\omega t)}$ *is a plane wave whose wave vector* $\mathbf{k}$ *and frequency* ω *satisfy*

$$\mathcal{F}[\mathbb{L}]\mathbf{E}_0 \mathrm{e}^{\mathrm{i}(\mathbf{k}\cdot\mathbf{x}-\omega t)} = \mathbf{0} \tag{5.3.2}$$

then

$$\mathbb{L}\mathbf{E}_0 \mathrm{e}^{\mathrm{i}(\mathbf{k}\cdot\mathbf{x}-\omega t)} = \mathbf{0} \tag{5.3.3}$$

Proof. This follows immediately as the action of $\mathbb{L}$ on plane waves is its symbol $\mathcal{F}[\mathbb{L}]$. **Q.E.D.**

We can also use this theory to generate solutions to equations of the form

$$\mathbb{L}\mathbf{u} = \mathbf{F}. \tag{5.3.4}$$

Definition 5.3.1. Consider a linear differential equation

$$\mathbb{L}\mathbf{u} = \mathbf{F}. \tag{5.3.5}$$

Then the dispersion relation is given by

$$\mathcal{F}[\mathbb{L}]\hat{\mathbf{u}}(\mathbf{k}, \omega) = \hat{\mathbf{F}}(\mathbf{k}, \omega). \tag{5.3.6}$$

Note that for many problems we are interested in the case $\mathbf{F} = \mathbf{0}$.

In this respect a symbol is the action of a linear operator on plane waves while dispersion relations are equations relating symbols of operators for plane wave solutions of differential equation.

5.3.1 Dispersion Relation for Scalar Wave Equation

We will now present several examples of dispersion relations. For our first example we consider the scalar wave equation

$$\frac{\partial^2}{\partial t^2}u = c^2 \triangle u. \tag{5.3.7}$$

We will first calculate the symbol of the operator $\partial_{tt} - c^2\triangle$.

$$\left(\frac{\partial^2}{\partial t^2} - c^2\triangle\right) \mathrm{e}^{\mathrm{i}(\mathbf{k}\cdot\mathbf{x}-\omega t)} = -\omega^2 + c^2k^2. \tag{5.3.8}$$

The dispersion relation is then posed by setting the symbol equal to zero

$$-\omega^2 = -c^2k^2 \tag{5.3.9}$$

which has two solutions, namely $\omega = \pm ck$.

5.3.2 Dispersion Relation for Maxwell's Equations in Vacuum

Next we will present the dispersion relation for Maxwell's equations in vacuum in the absence of source currents. That is, consider the curl equations

$$\begin{cases} \dfrac{\partial}{\partial t}\mathbf{E} = \dfrac{1}{\epsilon}\mathbf{curl}\mathbf{H}, \\ \dfrac{\partial}{\partial t}\mathbf{H} = -\dfrac{1}{\mu}\mathbf{curl}\mathbf{E}. \end{cases} \tag{5.3.10}$$

To calculate the dispersion relation we will rewrite the operator in the form of a matrix equation

$$\begin{pmatrix} \dfrac{\partial}{\partial t}\mathbb{I}_{3\times 3} & -\dfrac{1}{\epsilon}\mathbf{curl} \\ \dfrac{1}{\mu}\mathbf{curl} & \dfrac{\partial}{\partial t}\mathbb{I}_{3\times 3} \end{pmatrix} \begin{pmatrix} \mathbf{E} \\ \mathbf{H} \end{pmatrix} = \begin{pmatrix} \mathbf{0} \\ \mathbf{0} \end{pmatrix} \tag{5.3.11}$$

To calculate the symbol with constant ϵ, μ we assume $\mathbf{E} = \mathbf{E}_0\mathrm{e}^{\mathrm{i}(\mathbf{k}\cdot\mathbf{x}-\omega t)}$ and $\mathbf{H} = \mathbf{H}_0\mathrm{e}^{\mathrm{i}(\mathbf{k}\cdot\mathbf{x}-\omega t)}$ where $\mathbf{E}_0, \mathbf{H}_0$ are unit vectors in $\mathbb{R}^3$. Thus we have,

$$\begin{pmatrix} -\mathrm{i}\omega\mathbb{I}_{3\times 3} & -\mathrm{i}\epsilon^{-1}[\mathbf{k}]_\times \\ \mathrm{i}\mu^{-1}[\mathbf{k}]_\times & -\mathrm{i}\omega\mathbb{I}_{3\times 3} \end{pmatrix} \begin{pmatrix} \mathbf{E}_0 \\ \mathbf{H}_0 \end{pmatrix} = \begin{pmatrix} \mathbf{0} \\ \mathbf{0} \end{pmatrix} \tag{5.3.12}$$

The dispersion relation is now posed as a zero eigenvalue problem. In particular we need both the eigenvalues and eigenvectors. First we will find the eigenvalues first. To this end we compute

$$\det \begin{pmatrix} -\mathrm{i}\omega\mathbb{I}_{3\times 3} & -\mathrm{i}\epsilon^{-1}[\mathbf{k}]_\times \\ \mathrm{i}\mu^{-1}[\mathbf{k}]_\times & -\mathrm{i}\omega\mathbb{I}_{3\times 3} \end{pmatrix} = 0. \tag{5.3.13}$$

We will begin by eliminating the variable $\mathbf{H}$ in (5.3.13). This choice is arbitrary and we could as easily eliminate $\mathbf{E}$ and recover identical solutions. This produces an equivalent dispersion relation as can be seen by the final calculation. To do so we note that the lower left hand block commutes with both $[\mathbf{k}]_\times$ blocks therefore we can apply the block determinate formula.

$$\det \begin{pmatrix} -\mathrm{i}\omega\mathbb{I}_{3\times 3} & -\mathrm{i}\epsilon^{-1}[\mathbf{k}]_\times \\ \mathrm{i}\mu^{-1}[\mathbf{k}]_\times & -\mathrm{i}\omega\mathbb{I}_{3\times 3} \end{pmatrix} = \det\Big((-\mathrm{i}\omega)^2\mathbb{I}_{3\times 3} - (\epsilon\mu)^{-1}[\mathbf{k}]_\times^2\Big). \tag{5.3.14}$$

Since $c^2 = (\epsilon\mu)^{-1}$, we have the following eigenvalue problem.

$$\Big(-\omega^2\mathbb{I}_{3\times 3} - c_0^2[\mathbf{k}]_\times^2\Big)\mathbf{E}_0 = \mathbf{0}. \tag{5.3.15}$$

The matrix $[\mathbf{k}]_\times^2 = \mathbf{k}\mathbf{k}^T - k^2\mathbb{I}_{3\times 3}$ has three eigenvectors. The vector $\mathbf{k}$ is asscoiated a zero eigenvalue and $\mathbf{k}_1^\perp$ and $\mathbf{k}_2^\perp$ which are orthogonal to $\mathbf{k}$ and are $-k^2$. By choosing $\mathbf{E}_0$ in the span of $\mathbf{k}$ we have

$$-\omega^2\mathbf{E}_0 = \mathbf{0}. \tag{5.3.16}$$

The solution is $\omega = 0$. As $\mathbf{E}_0||\mathbf{k}$ we have that div$\mathbf{E}_0$ is non-zero as the symbol of div is $\mathrm{i}\mathbf{k}^T$. This tells us that divergent components of $\mathbf{E}$ are *evanescent*, that is they do not propagate. If we choose $\mathbf{E}_0 \in \langle \mathbf{k}_1^\perp, \mathbf{k}_2^\perp\rangle$ the dispersion relation is given by

$$(-\omega^2 + c_0^2k^2)\mathbf{E}_0 = \mathbf{0}. \tag{5.3.17}$$

In this case we have $\omega = \pm c_0 k$. To find the solution for $\mathbf{H}_0$ we consider the equation

$$(-\mathrm{i}\omega)\mathbf{B} = -\mathrm{i}\mu^{-1}\mathbf{k} \times \mathbf{E} \tag{5.3.18}$$

$$\mathbf{B} = \frac{1}{\mu\omega}\mathbf{k} \times \mathbf{E}. \tag{5.3.19}$$

This tells us that if $\mathbf{E}||\mathbf{k}$ then $\mathbf{B} = 0$. If $\mathbf{E}_0 \in \langle \mathbf{k}_1^{\perp}, \mathbf{k}_2^{\perp} \rangle$ then $\mathbf{B}_0$ will be orthogonal to $\mathbf{E}_0$ but also in the plane $\langle \mathbf{k}_1^{\perp}, \mathbf{k}_2^{\perp} \rangle$.

5.3.3 Dispersion Relation for Maxwell's Equations in Conductive Media

Maxwell's equations in a conductive media are governed by the following system of equations.

$$\begin{cases} \dfrac{\partial}{\partial t}\mathbf{E} + \dfrac{\sigma}{\epsilon}\mathbf{E} = \dfrac{1}{\epsilon}\mathbf{curlH} \\ \dfrac{\partial}{\partial t}\mathbf{H} = -\dfrac{1}{\mu}\mathbf{curlE} \end{cases} \tag{5.3.20}$$

Define the relaxation frequency $\gamma = \frac{\sigma}{\epsilon}$. We rewrite the system as a matrix equation we eliminate the variable $\mathbf{H}$ to the second order equation

$$\frac{\partial^2}{\partial t^2}\mathbf{E} + \gamma\frac{\partial}{\partial t}\mathbf{E} = -c^2\mathbf{curlcurlE}. \tag{5.3.21}$$

We calculate the dispersion relation by consider the plane wave Ansatz $\mathbf{E} = \mathbf{E}_0 \mathrm{e}^{\mathrm{i}(\mathbf{k}\cdot\mathbf{x} - \omega t)}$.

$$(-\omega^2 - \mathrm{i}\gamma\omega)\mathbf{E}_0 = c^2\mathbf{k} \times \mathbf{k} \times \mathbf{E}_0. \tag{5.3.22}$$

As before we have two classes of eigenvalues. For $\mathbf{E}_0||\mathbf{k}$ we have the dispersion relation

$$\omega^2 + \mathrm{i}\gamma\omega = 0. \tag{5.3.23}$$

Which is solved by $\omega = 0$ and $\omega = -\mathrm{i}\gamma$ which gives us two evanescent modes. One which does not propagate and one which decays exponentially with rate $\mathrm{e}^{-\gamma t}$. These solutions state that divergent electric waves are decaying and evanescent. In the case of $\mathbf{E}_0 \in \langle \mathbf{k}_1^{\perp}, \mathbf{k}_2^{\perp} \rangle$ we have the dispersion relation for transient modes

$$\omega^2 + \mathrm{i}\gamma\omega - c_0^2 k^2 = 0. \tag{5.3.24}$$

This relation implies that the transient waves are also decaying.

5.3.4 Dispersion Relation for Maxwell's Equations in Debye Media

In a Polarization Medium, a polarization field is introduced to account for the discrepancy between electric fields and electric induction. For the Debye Model of Polarization, one assumes that atoms in the material are deformed by the presence of the electric field and then relax back to an equilibrium configuration after some time. For this reason Debye Media are also referred to as relaxing dielectrics. The Debye model is given by appending **Auxilary Differential Equations** to Maxwell's equations to account for the polarization field. The model is given as follows:

$$\begin{cases} \frac{\partial}{\partial t}\mathbf{E} + \frac{1}{\epsilon}\frac{\partial}{\partial t}\mathbf{P} = \frac{1}{\epsilon_0}\nabla \times \mathbf{H} \\ \frac{\partial}{\partial t}\mathbf{P} = -\frac{1}{\tau} + \epsilon_0\frac{\epsilon_\Delta}{\tau}\mathbf{E} \\ \frac{\partial}{\partial t}\mathbf{H} = -\frac{1}{\mu_0}\nabla \times \mathbf{E} \end{cases} \tag{5.3.25}$$

Here the parameter τ is the relaxation time of the medium and ϵ_Δ is the band gap– namely the relative difference in electrical permittivity for infinite frequency signals and zero frequency signals. Many materials can be modeled as Debye materials – biological tissues and water being common examples. For water $\tau = \mathcal{O}(10^{-12})$ and $\epsilon_\Delta \approx 80$. Typically one eliminates the variable $\frac{\partial}{\partial t}\mathbf{P}$ from the Maxwell-Ampére law.

$$\frac{\partial}{\partial t}\mathbf{E} = -\frac{\epsilon_\Delta}{\tau}\mathbf{E} + \frac{1}{\epsilon_0\tau}\mathbf{P} + \frac{1}{\epsilon_0}\nabla \times \mathbf{H} \tag{5.3.26}$$

We will now compute the dispersion relation assuming all fields are plane waves initial orientations $\mathbf{E}_0, \mathbf{P}_0, \mathbf{H}_0$.

$$\begin{pmatrix} -\mathrm{i}\omega + \frac{\epsilon_\Delta}{\tau} & -\frac{1}{\epsilon_0\tau} & 0 \\ -\epsilon_0\frac{\epsilon_\Delta}{\tau} & -\mathrm{i}\omega + \frac{1}{\tau} & 0 \\ 0 & 0 & -\mathrm{i}\omega \end{pmatrix} \begin{pmatrix} \mathbf{E}_0 \\ \mathbf{P}_0 \\ \mathbf{H}_0 \end{pmatrix} = \begin{pmatrix} 0 & 0 & \frac{\mathrm{i}}{\epsilon}[\mathbf{k}]_\times \\ 0 & 0 & 0 \\ -\frac{\mathrm{i}}{\mu}[\mathbf{k}]_\times & 0 & 0 \end{pmatrix} \tag{5.3.27}$$

Eliminating the variables $\mathbf{P}_0$ and $\mathbf{H}_0$ gives us the following. We begin with some geometric analysis. The dispersion equation governing $\mathbf{P}$ guarantees that $\mathbf{P}$ and $\mathbf{E}$ should be colinear

$$\mathbf{P}_0 = \frac{\epsilon_0 \epsilon_\Delta}{1 - \mathrm{i}\omega\tau}\mathbf{E}_0. \tag{5.3.28}$$

We know that $\mathbf{E}_0, \mathbf{H}_0$ must be eigenvectors of $[\mathbf{k}]_\times$. Further, we know that $\mathbf{H}_0 \perp \mathbf{E}_0$ by the third equation. The matrix $\mathrm{i}/\epsilon[\mathbf{k}]_\times$ has three eigenvectors, $\mathbf{k}, \mathbf{k}_1^\perp, \mathbf{k}_2^\perp$. There are two cases.

1. $\mathbf{E}_0 = \mathbf{k}$. To be an eigenvector of the RHS we must have $\mathbf{H}_0 = \mathbf{k}$. This reduces the right hand side to zero. We are left to solve the eigenvalue problem

$$\begin{pmatrix} -\mathrm{i}\omega + \frac{\epsilon_\Delta}{\tau} & -\frac{1}{\epsilon_0\tau} & 0 \\ -\epsilon_0\frac{\epsilon_\Delta}{\tau} & -\mathrm{i}\omega + \frac{1}{\tau} & 0 \\ 0 & 0 & -\mathrm{i}\omega \end{pmatrix} \begin{pmatrix} \mathbf{E}_0 \\ \mathbf{P}_0 \\ \mathbf{H}_0 \end{pmatrix} = \begin{pmatrix} 0 \\ 0 \\ 0 \end{pmatrix} \tag{5.3.29}$$

   This is done in the standard way where we take the determinate of the matrix, resulting in a characteristic polynomial in ω and search for roots.

$$0 = \mathrm{Det}\begin{pmatrix} -\mathrm{i}\omega + \frac{\epsilon_\Delta}{\tau} & -\frac{1}{\epsilon_0\tau} & 0 \\ -\epsilon_0\frac{\epsilon_\Delta}{\tau} & -\mathrm{i}\omega + \frac{1}{\tau} & 0 \\ 0 & 0 & -\mathrm{i}\omega \end{pmatrix} = \mathrm{i}\tau\omega^2(\epsilon_0\tau\omega + \mathrm{i}\epsilon_0(1+\epsilon_\Delta)) \tag{5.3.30}$$

   Solving this equation for ω we are left with two distinct solutions

$$\omega = 0, \qquad \omega = -\mathrm{i}\frac{1+\epsilon_\Delta}{\tau}. \tag{5.3.31}$$

2. Let $\mathbf{E}_0 \in \langle \mathbf{k}_1^\perp, \mathbf{k}_2^\perp \rangle$. We have a dispersion relation given by

$$0 = \mathrm{Det}\begin{pmatrix} -\mathrm{i}\omega + \frac{\epsilon_\Delta}{\tau} & -\frac{1}{\epsilon_0\tau} & -\frac{\mathrm{i}}{\epsilon}k \\ -\epsilon_0\frac{\epsilon_\Delta}{\tau} & -\mathrm{i}\omega + \frac{1}{\tau} & 0 \\ \frac{\mathrm{i}}{\mu}k & 0 & -\mathrm{i}\omega \end{pmatrix} = \omega^2(\mathrm{i}\tau\omega - (1+\epsilon_\Delta)) + ck^2(\mathrm{i}\tau\omega - 1). \tag{5.3.32}$$

5.3.5 Dispersion Relation for Maxwell's Equation in Cold Isotropic Plasma

Consider a cold isotropic plasma model with constant coefficients:

$$\begin{cases} \dfrac{\partial}{\partial t}\mathbf{E} + \dfrac{1}{\epsilon}\mathbf{J} = \mathbf{curl}\mathbf{H} \\ \dfrac{\partial}{\partial t}\mathbf{J} = -\omega_I \mathbf{J} + \epsilon\omega_P^2 \mathbf{E} \\ \dfrac{\partial}{\partial t}\mathbf{H} = -\dfrac{1}{\mu}\mathbf{curl}\mathbf{E} \end{cases} \tag{5.3.33}$$

Assuming the plane wave Ansatz this system of equations reduces to the following generalized eigenvalue problem

$$\begin{pmatrix} -\mathrm{i}\omega & \frac{1}{\epsilon} & 0 \\ -\epsilon\omega_P^2 & -\mathrm{i}\omega + \omega_I & 0 \\ 0 & 0 & -\mathrm{i}\omega \end{pmatrix} \begin{pmatrix} \mathbf{E}_0 \\ \mathbf{J}_0 \\ \mathbf{H}_0 \end{pmatrix} = \begin{pmatrix} 0 & 0 & \frac{\mathrm{i}}{\epsilon}[\mathbf{k}]_\times \\ 0 & 0 & 0 \\ -\frac{\mathrm{i}}{\mu}[\mathbf{k}]_\times & 0 & 0 \end{pmatrix} \begin{pmatrix} \mathbf{E}_0 \\ \mathbf{J}_0 \\ \mathbf{H}_0 \end{pmatrix} \tag{5.3.34}$$

We eliminate the variable $\mathbf{H}$ by the identity

$$-\mathrm{i}\omega\mathbf{H} = -\frac{\mathrm{i}}{\mu}\mathbf{k} \times \mathbf{E}_0 \tag{5.3.35}$$

This reduces the system as follows:

$$\begin{pmatrix} -\omega^2 & -\mathrm{i}\omega\frac{1}{\epsilon} \\ -\epsilon\omega_P^2 & -\mathrm{i}\omega + \omega_I \end{pmatrix} \begin{pmatrix} \mathbf{E}_0 \\ \mathbf{J}_0 \end{pmatrix} = \begin{pmatrix} -c^2[\mathbf{k}]_\times^2 & 0 \\ 0 & 0 \end{pmatrix} \begin{pmatrix} \mathbf{E}_0 \\ \mathbf{J}_0 \end{pmatrix}. \tag{5.3.36}$$

It is now clear that we must consider eigenvectors of the matrix $[\mathbf{k}]_\times^2$, i.e. $\mathbf{E} \propto \mathbf{k}$ or $\mathbf{E} \propto \mathbf{k}^\perp$.

$\mathbf{k}^\perp$: In case of $\mathbf{E} \propto \mathbf{k}^\perp$ the system reduces as follows:

$$\begin{pmatrix} -\omega^2 + c^2k^2 & -\mathrm{i}\omega\frac{1}{\epsilon} \\ \epsilon\omega_P^2 & -\mathrm{i}\omega + \omega_I \end{pmatrix} \begin{pmatrix} \mathbf{E}_0 \\ \mathbf{J}_0 \end{pmatrix} = \begin{pmatrix} 0 \\ 0 \end{pmatrix} \tag{5.3.37}$$

Calculating the determinate of this system we arrive at the dispersion relation

$$\mathrm{i}\omega^3 - \omega^2\omega_I + \mathrm{i}\omega(\omega_P^2 - c^2k^2) + c^2\omega_I k^2 = 0 \tag{5.3.38}$$

k: Choosing $\mathbf{E}_0 \propto \mathbf{k}$ there is no $\mathbf{k}$ dependence.

$$\begin{pmatrix} -\omega^2 & -\mathrm{i}\omega\frac{1}{\epsilon} \\ -\epsilon\omega_P^2 & -\mathrm{i}\omega + \omega_I \end{pmatrix} \begin{pmatrix} \mathbf{E}_0 \\ \mathbf{J}_0 \end{pmatrix} = \begin{pmatrix} 0 \\ 0 \end{pmatrix} \tag{5.3.39}$$

Calculating the determinant of this matrix we arrive at the dispersion relation

$$\mathrm{i}\omega(\omega^2 + \mathrm{i}\omega\omega_I + \omega_P^2) = 0. \tag{5.3.40}$$

5.4 Discrete Fourier Analysis

In this section we will extend dispersion analysis from the continuum setting to discrete approximations. This sort of analysis is simplest when applied to discretizations with uniform grids.

To begin with we will shift our interpretation of symbols slightly. In the continuum setting we focused on symbols as objects arising from Fourier transforms of the continuum PDE and then proved equivalence with the action of the operators on plane waves.

In the discrete setting we will not attempt to create a discrete representation of the Fourier Transform but instead jump immediately to action on plane waves. To do so we must consider discretizations of plane waves. In the case of finite difference methods discrete plane waves are exactly the degrees of freedom of a plane wave. For finite element interpretations we may consider the interpolant the plane wave's degrees of freedom in the appropriate polynomial space. For our purposes we will focus primarily on finite difference interpretation.

Example 5.4.1. Consider degrees of freedom for the Yee scheme or lowest order edge-based mimetic discretizations:

$$\mathbf{E}_e = \frac{1}{|e|}\int_e \mathbf{E}\cdot\boldsymbol{\tau}_e \, de \tag{5.4.1}$$

where e are the edges of the mesh and $\boldsymbol{\tau}_e$ is the unit tangent vector to that edge. Assume a rectangular discretization oriented with the x and y axes where the midpoints of horizontal edges lie at points $(i\Delta x, (j+1/2)\Delta y)$ and the midpoints of vertical edges lie at $((i+1/2)\Delta x, j\Delta y)$. Call horizontal edges $e_{i,j+1/2}$ and vertical edges $e_{i+1/2,j}$

The degrees of freedom of the plane wave $\mathbf{E} = \mathbf{E}_0 \mathrm{e}^{\mathrm{i}\mathbf{k}\cdot\mathbf{x}}$ are then given by as follows.

$$\mathbf{E}_{e_{i,j+1/2}} = E_x \mathrm{e}^{\mathrm{i}\mathbf{k}\cdot(i\Delta x,(j+1/2)\Delta y)} \frac{2\sin\frac{k_x\Delta x}{2}}{k_x}, \tag{5.4.2}$$

$$\mathbf{E}_{e_{i+1/2,j}} = E_y \mathrm{e}^{\mathrm{i}\mathbf{k}\cdot((i+1/2)\Delta x,j\Delta y)} \frac{2\sin\frac{k_y\Delta y}{2}}{k_y}. \tag{5.4.3}$$

This immediately implies the relation

$$\mathbf{E}_{e_{i,j+1/2}} = \mathrm{e}^{\mathrm{i}\mathbf{k}\cdot(i\Delta x,j\Delta y)} \mathbf{E}_{e_{0,1/2}}, \tag{5.4.4}$$

$$\mathbf{E}_{e_{i+1/2,j}} = \mathrm{e}^{\mathrm{i}\mathbf{k}\cdot(i\Delta x,j\Delta y)} \mathbf{E}_{e_{1/2,0}}. \tag{5.4.5}$$

This shows the discrete plane wave is controlled by two degrees of freedom – analogous to free space where we needed consider only each component of the wave.

Once we have established our discrete plane waves we apply the discretization of PDE to these waves to compute symbols. This is generally done by reducing to a minimal number of degrees of freedom and considering the action of the discretization on the discrete plane waves. In general the resulting generalized eigenvalues are trigonometric functions of discretization parameters and $(\omega, \mathbf{k})$ rather than polynomials as was the case in the continuum setting.

For the schemes to be consistent discrete symbols must approximate continuum symbols in the limit of high grid resolution. However, any discrepancy will cause what is referred to as *Dispersion Error*. Dispersion error is typically observed as non-physical oscillations or phase errors in discrete solutions. The source of these numerical artifacts can be attributed to a difference in the frequency-wave number pairs which solve the continuum dispersion relation and the discrete dispersion relation.

We will illustrate this now by way of an example.

Example 5.4.2. Consider the one dimensional transport equation

$$\frac{\partial}{\partial t}u = -c\frac{\partial}{\partial x}u. \tag{5.4.6}$$

If we try to solve this equation for some data $f(x)$ we have the exact solution given by $u(x,t) = f(x-ct)$. The dispersion relationship for this PDE is given by

$$-\mathrm{i}\omega = -\mathrm{i}ck \implies \omega = ck. \tag{5.4.7}$$

The dispersion relation implies the identity

$$c = \frac{\omega}{k} \tag{5.4.8}$$

which says that the wave speed should be given by the ratio of frequency to wave number. Consider the classical Leap-frog discretization of the transport equation

$$\frac{u_j^{n+1} - u_j^{n-1}}{2\Delta t} = -c\frac{u_{j+1}^n - u_{j-1}^n}{2\Delta x}, \qquad u_j^n \approx u(j\Delta x, n\Delta t). \tag{5.4.9}$$

Assuming the discrete plane wave Ansatz we have

$$u_j^n = u_0 \mathrm{e}^{\mathrm{i}kj\Delta x - \mathrm{i}\omega n\Delta t}. \tag{5.4.10}$$

Applying the stencil to this Ansatz we are left with the following discrete dispersion relation

$$-\mathrm{i}\frac{\sin\omega\Delta t}{\Delta t}u_0^0 = -\mathrm{i}c\frac{\sin k\Delta x}{\Delta x}u_0^0. \tag{5.4.11}$$

Define the variable

$$c_n = \frac{\Delta x}{\Delta t}\frac{\sin\omega\Delta t}{\sin k\Delta x} = \frac{\omega}{k} + \Delta x^2\frac{c^2k^2\omega - \nu^2\omega^3}{6c^2k} + \mathcal{O}(\Delta x^4), \quad \nu = \frac{c\Delta t}{\Delta x}. \tag{5.4.12}$$

Assuming a true root of the dispersion relation $\omega = ck$ we can then simplify this expression

$$c_n = c + \frac{\Delta x^2}{6c}(1-\nu^2)\omega + \mathcal{O}(\Delta x^4). \tag{5.4.13}$$

This suggests that discrete waves will propagate at non-physical speeds.

We will now define our preferred quantification of dispersion error.

Definition 5.4.1. Consider a linear partial differential equation defined as

$$L_t \mathbf{u} = L_x \mathbf{u}. \tag{5.4.14}$$

Here L_t is a linear differential with only temporal operators and L_x is a differential with only spatial operators. We use the following notation for the symbols

$$\mathcal{T}(\omega) := \mathcal{F}[L_t] \qquad \mathcal{S}(\mathbf{k}) := \mathcal{F}[L_x]. \tag{5.4.15}$$

Consider a discretization of this differential equation. Say the method has a discrete temporal symbol $\mathcal{T}_{\Delta t}(\omega)$ and discrete spatial symbol $\mathcal{S}_h(\mathbf{k})$.

Let $(\mathbf{k}, \omega)$ be a solution to the continuum dispersion relation

$$\mathcal{T}(\omega)\mathbf{u}_0 = \mathcal{S}(\mathbf{k})\mathbf{u}_0. \tag{5.4.16}$$

Assume that Δt is proportional to h. We say the numerical method has r^{th} order dispersion error if

$$\Big(\mathcal{T}_{\Delta t}(\omega) - \mathcal{S}_h(\mathbf{k})\Big)\mathbf{u}_0 = \mathcal{O}(h^r). \tag{5.4.17}$$

This definition is exactly the *local truncation error* assuming that the exact solution is a plane wave. Another potential approach to the quantification is to find solutions to both discrete and continuum dispersion relations

$$\mathcal{T}_{\Delta t}(\omega_{\Delta t})\mathbf{u}_h = \mathcal{S}_h(\mathbf{k}_h)\mathbf{u}_h \qquad \mathcal{T}(\omega)\mathbf{u}_0 = \mathcal{S}(\mathbf{k})\mathbf{u}_0 \tag{5.4.18}$$

and then calculate the norm of the difference between $(\omega, \mathbf{k})$ and $(\omega_{\Delta t}, \mathbf{k}_h)$ in an appropriate vector norm. However, for most systems solutions for $\omega_{\Delta t}$ and $\mathbf{k}_h$ are very difficult to work with. For this reason we prefer the presented definition.

5.4.1 Dispersion Analysis for MFD Discretizations of Maxwell's Equations

Our primary analytical tool for M-adaptation will be discrete dispersion analysis. In order to infer properties of the method we will consider the action of the numerical discretization on numerical representations of plane waves. This approach seems unlikely to be much use on bounded domains at first inspection. However, for many geometries (for example squares) the Fourier modes of the geometry are in fact finite superpositions of plane waves. In general one can prove that plane waves are dense in the solution space. This allows for optimization for plane waves to have far reaching consequences.

We will work primarily with two discrete plane waves.

$$\mathbf{E}_h^n = \mathcal{I}^{\mathscr{E}_h}(\mathbf{E}_0 \exp \mathrm{i}(\mathbf{k}\cdot\mathbf{x} - \omega n \Delta t)) \tag{5.4.19}$$

$$\mathbf{B}_h^{n+1/2} = \mathcal{I}^{\mathscr{F}_h}(B_0 \exp \mathrm{i}(\mathbf{k}\cdot\mathbf{x} - \omega (n+1/2) \Delta t)) \tag{5.4.20}$$

Further we will consider the case in the absence of external currents, namely $\mathbf{J} = 0$ for all time.

Here one can think of $\mathbf{E}_0$ and B_0 as encoding the initial orientation and intensity of the electric and magnetic fields respectively. In particular, each plane wave is determined by only a few degrees of freedom (2 in the case of $\mathbf{E}_h^n$ and one in the case of $B_h^{n+1/2}$). This allows one to describe the effect of a global discrete operator acting on either grid function in terms of local contributions. We will present three lemmata which illustrate this fact.

Definition 5.4.2. We define the restriction of a grid function $u_h \in \mathscr{S}$ to a collection of

objects $s_1, s_2, \cdots, s_n$ as follows

$$u_{(s_1,s_2,\cdots s_n)} = \begin{pmatrix} u_{s_1} \\ u_{s_2} \\ \vdots \\ u_{s_n} \end{pmatrix} \tag{5.4.21}$$

Definition 5.4.3. For a space $\mathscr{S}$ and some face f we define the matrix $\mathbb{T}_{\mathscr{S},f}$ by

$$[\mathbb{T}_{\mathscr{S},f}]_{i,j} = \begin{cases} 1 & \text{local number } j \text{ has global number } i \\ 0 & \text{otherwise} \end{cases}. \tag{5.4.22}$$

We call the matrix $\mathbb{T}_{\mathscr{S},f}$ a restriction matrix.

Definition 5.4.4. Let $\mathbb{X} \in \mathcal{L}(\mathscr{S}_h, \mathscr{W}_h)$. We call $\mathbb{X}$ **uniform** if there exists a matrix $\mathbb{X}_\ell$ such that

$$\mathbb{X} = \sum_{f \in \mathscr{F}_h} \mathbb{T}^T_{\mathscr{W},f} \mathbb{X}_\ell \mathbb{T}_{\mathscr{E},f}. \tag{5.4.23}$$

Further if $\mathbb{X}$ is uniform call the matrix $\mathbb{X}_\ell$ **the local matrix of** $\mathbb{X}$

Lemma 5.4.1. *Let $\mathscr{T}$ be a uniform rectangular mesh, $\mathbb{X} \in \mathcal{L}(\mathscr{E}_h, \mathscr{E}_h)$ be uniform with local matrix $\mathbb{X}_\ell$, and let (e_1, e_2) be the first and second local edges for some face f (i.e. e_1 is the bottom edge and e_2 is the right edge as described in Figure 3.3) then*

$$\big(\mathbb{X}\mathbf{E}^n_h\big)|_{(e_1,e_2)} = \mathbb{S}^\star \mathbb{X}_\ell \mathbb{S}\big(\mathbf{E}_h|_{(e_1,e_2)}\big) \tag{5.4.24}$$

where $\mathbb{S}$ is defined as

$$\mathbb{S} = \begin{pmatrix} 1 & 0 \\ 0 & 1 \\ \mathrm{e}^{\mathrm{i}k_y\Delta y} & 0 \\ 0 & e^{-\mathrm{i}k_x\Delta x} \end{pmatrix} \tag{5.4.25}$$

and $\star$ is the complex conjugate.

Proof. Let

$$\mathbf{E}^n_{(e_1,e_2)} = \begin{pmatrix} u_1 \\ u_2 \end{pmatrix} \qquad \text{and} \qquad \mathbb{X}\mathbf{E}^n_{(e_1,e_2)} = \begin{pmatrix} v_1 \\ v_2 \end{pmatrix}. \tag{5.4.26}$$

If e_1, e_2 are the bottom and right edges of f then let e_3 and e_4 be the top and left edges respectively. Without loss of generality we will assume that the barycenter of f is (0,0). First note that if $\mathbf{E}$ is a plane wave then we have the following two identities

$$\frac{1}{\Delta x}\int_{e_3}(1,0)\mathbf{E}_0 \mathrm{e}^{\mathrm{i}(k_x x + k_y \frac{\Delta y}{2} - \omega t)} dx = \frac{\mathrm{e}^{\mathrm{i}k_y \Delta y}}{\Delta x}\int_{e_1}(1,0)\mathbf{E}_0 \mathrm{e}^{\mathrm{i}(k_x x - k_y \frac{\Delta y}{2} - \omega t)} dx, \tag{5.4.27}$$

$$\frac{1}{\Delta y}\int_{e_4}(0,1)\mathbf{E}_0 \mathrm{e}^{\mathrm{i}(-k_x \frac{\Delta x}{2} + k_y y - \omega t)} dy = \frac{\mathrm{e}^{-\mathrm{i}k_x \Delta x}}{\Delta y}\int_{e_2}(0,1)\mathbf{E}_0 \mathrm{e}^{\mathrm{i}(k_x \frac{\Delta x}{2} + k_y y - \omega t)} dy. \tag{5.4.28}$$

Therefore as $\mathbf{E}^n_f$ is the interpolant of a plane wave on the face f we have

$$\mathcal{I}^{\mathscr{C}_h}_f(\mathbf{E}) = \begin{pmatrix} u_1 \\ u_2 \\ \mathrm{e}^{\mathrm{i}k_y \Delta y} u_1 \\ \mathrm{e}^{-\mathrm{i}k_x \Delta x} u_2 \end{pmatrix} = \mathbb{S}\mathbf{E}^n_{(e_1,e_2)}. \tag{5.4.29}$$

The matrix product given by

$$\mathbb{X}_\ell \mathbb{S}(\mathbf{E}^n_{(e_1,e_2)}) \tag{5.4.30}$$

is the local contribution of $\mathbb{X}$ from the cell f. We introduce two additional cells, f_E which is one cell to the right ($+x$ direction) of f and f_S which is one cell bellow f ($-y$ direction), see Figure 5.1. In order to calculate the total contribution of $\mathbb{X}$ the edges e_1 and e_2 we must account for contributions from the cells f_S and f_E. To do so we note that u_1 lies on edge 3 in cell f_S and u_2 lies on edge 4 in cell f_E. The global contribution on these edges is then given by

$$v_1 = (1,0,0,0)\mathbb{X}_\ell \mathbb{S} \begin{pmatrix} u_1 \\ 0 \end{pmatrix} + \mathrm{e}^{-\mathrm{i}k_y \Delta y}(0,0,1,0)\mathbb{X}_\ell \mathbb{S} \begin{pmatrix} u_1 \\ 0 \end{pmatrix} \tag{5.4.31}$$

$$v_2 = (0,1,0,0)\mathbb{X}_\ell \mathbb{S} \begin{pmatrix} 0 \\ u_2 \end{pmatrix} + \mathrm{e}^{\mathrm{i}k_x \Delta x}(0,0,0,1)\mathbb{X}_\ell \mathbb{S} \begin{pmatrix} 0 \\ u_2 \end{pmatrix} \tag{5.4.32}$$

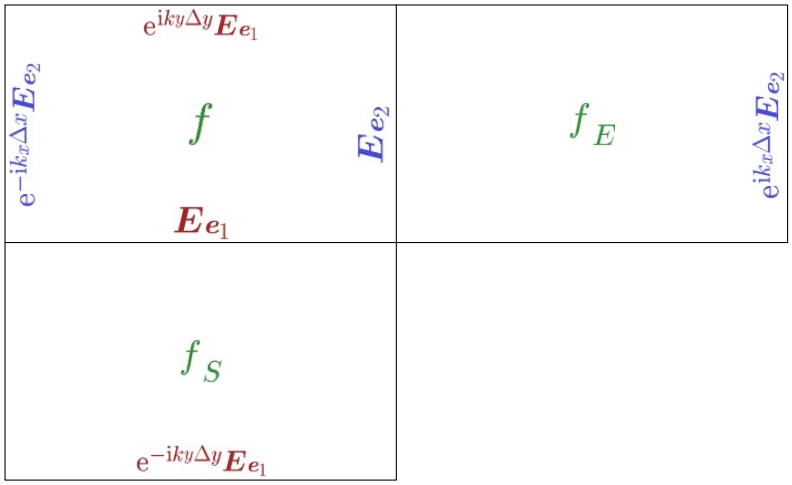

FIGURE 5.1: Three cells used to assemble the contributions after multiplication by a uniform matrix.

Collecting the above calculation as a matrix product gives us the desired identity

$$\begin{pmatrix} v_1 \\ v_2 \end{pmatrix} = \mathbb{S}^\star \mathbb{X}_\ell \mathbb{S} \begin{pmatrix} u_1 \\ u_2 \end{pmatrix}. \tag{5.4.33}$$

Q.E.D.

The next two results can be proven by using the machinery presented in the previous proof.

Corollary 5.4.2. *Let $\mathscr{T}$ be a uniform rectangular mesh, $\mathbb{X} \in \mathcal{L}(\mathscr{E}_h, \mathscr{F}_h)$ be uniform with local matrix $\mathbb{X}_\ell$, and let e_1, e_2 be the first two degrees of freedom of a cell f then*

$$\mathbb{X}\mathbf{E}_f^n = \mathbb{X}_\ell \mathbb{S}\mathbf{E}^2_{(e_1,e_2)}. \tag{5.4.34}$$

Where $\mathbb{S}$ is defined as in Lemma 5.4.1.

Proof. As in Lemma 5.4.1 we have that

$$\mathbf{E}_f^n = \mathbb{S}\mathbf{E}^n_{(e_1,e_2)}. \tag{5.4.35}$$

As the operator $\mathbb{X}$ is uniform on $\mathcal{T}$ we have that v depends only $\mathbf{E}_f^n$. Therefore

$$\mathbb{X}\mathbf{E}_f^n = \mathbf{X}_\ell \mathbb{S}\mathbf{E}_{(e_1,e_2)}^n. \tag{5.4.36}$$

Q.E.D.

Corollary 5.4.3. *Let $\mathscr{T}$ be a uniform rectangular mesh, $\mathbb{X} \in \mathcal{L}(\mathscr{F}_h, \mathscr{E}_h)$ be uniform with local mass matrix $\mathbb{X}_\ell$, and let e_1, e_2 be the first two degrees of freedom in a cell f then*

$$\mathbb{X}B_{(e_1,e_2)} = \mathbb{S}^\star \mathbb{X}_\ell B_f \tag{5.4.37}$$

where $\mathbb{S}$ is defined in 5.4.1 and $\star$ is the conjugate transpose.

Proof. As $\mathbb{X}$ is uniform we have that for $e \in \mathscr{E}$, $\mathbf{E}_e$ depends on all f such that $e \in \partial f$. Therefore $\mathbb{X}B_{e_1}^n$ has contributions from f and f_S and $\mathbb{X}B_{e_2}^n$ has contributions from f, f_E. Note that as B is a plane wave we have

$$B_{f_S} = \mathrm{e}^{-\mathrm{i}k_x\Delta x}B_f, \quad B_{f_E} = \mathrm{e}^{\mathrm{i}k_y\Delta y}B_f. \tag{5.4.38}$$

Applying the argument developed in Lemma 5.4.1 we have

$$\mathbb{X}B_{e_1} = (1,0,0,0)\mathbb{X}_\ell B_f + \mathrm{e}^{-\mathrm{i}k_y\Delta y}(0,0,1,0)\mathbb{X}_\ell B_f, \tag{5.4.39}$$

$$\mathbb{X}B_{e_2} = (0,1,0,0)\mathbb{X}_\ell B_f + \mathrm{e}^{\mathrm{i}k_x\Delta x}(0,0,0,1)\mathbb{X}_\ell B_F. \tag{5.4.40}$$

which can be rewritten as

$$\mathbb{X}B_{(e_1,e_2)} = \mathbb{S}^\star \mathbb{X}_\ell B_f. \tag{5.4.41}$$

Q.E.D.

With these results in place we will introduce simplifying notation.

Definition 5.4.5. Let $\mathscr{T}$ be a uniform rectangular mesh. Define uniform operators

$$\mathbb{X} \in \mathcal{L}(\mathscr{E}_h, \mathscr{E}_h) \quad \mathbb{Y} \in \mathcal{L}(\mathscr{E}_h, \mathscr{F}_h) \quad \mathbb{Z} \in \mathcal{L}(\mathscr{F}_h, \mathscr{E}_h) \tag{5.4.42}$$

with local matrices $\mathbb{X}_\ell, \mathbb{Y}_\ell$, and $\mathbb{Z}_\ell$ respectively. We define the action of these operators on plane waves as

$$\overline{\mathbb{X}} = \mathbb{S}^\star \mathbb{X}_\ell \mathbb{S} \tag{5.4.43}$$

$$\overline{\mathbb{Y}} = \mathbb{Y}_\ell \mathbb{S} \tag{5.4.44}$$

$$\overline{\mathbb{Z}} = \mathbb{S}^\star \mathbb{Z}_\ell \tag{5.4.45}$$

where $\mathbb{S}$ is defined as in equation (5.4.25). Note that by this definition we have

$$\mathbb{Z} = \mathbb{Y}^T \implies (\overline{\mathbb{Z}})^\star = \overline{\mathbb{Y}^T} \tag{5.4.46}$$

With these results in place we can now compute the discrete dispersion relationship.

Theorem 5.4.4. *The discrete dispersion relationship for the discrete evolution equation* (4.3.18) *neglecting source currents is given by*

$$\mathcal{T}_{\Delta t}(\omega) = \mathcal{S}_h(\mathbf{k}) \tag{5.4.47}$$

where

$$\mathcal{T}_{\Delta t}(\omega) = -4\frac{\sin^2 \frac{\omega \Delta t}{2}}{\Delta t^2}, \tag{5.4.48}$$

$$\mathcal{S}_h(\mathbf{k}) = -\frac{4c_0^2}{\Delta x^2}\sin^2\frac{k_x\Delta x}{2}\Big(1 + (1-4w_3)\sin^2\frac{k_x\Delta x}{2}\Big) \tag{5.4.49}$$

$$-\frac{32c_0^2}{\Delta x\Delta y}w_2\sin^2\frac{k_x\Delta x}{2}\sin^2\frac{k_y\Delta y}{2} \tag{5.4.50}$$

$$-\frac{4c_0^2}{\Delta y^2}\sin^2\frac{k_y\Delta y}{2}\Big(1 + (1-4w_1)\sin^2\frac{k_y\Delta y}{2}\Big). \tag{5.4.51}$$

Proof. In order to prove the result we must calculate the Fourier symbol in time and space. The temporal result is classical for staggered differences while the symbol in space will rely upon the previous assembly. To compute the result we will first eliminate the magnetic field from the evolution equation.

$$\frac{\frac{\mathbf{E}_h^{n+1}-\mathbf{E}_h^n}{\Delta t}-\frac{\mathbf{E}^n-\mathbf{E}^{n-1}}{\Delta t}}{\Delta t}=c_0^2\mathbb{W}_{\mathscr{E}}\mathrm{curl}_h^T\mathbb{M}_{\mathscr{F}}\left(\frac{B_h^{n+1/2}-B_h^{n-1/2}}{\Delta t}\right) \tag{5.4.52}$$

$$\frac{\mathbf{E}_h^{n+1}-2\mathbf{E}_h^n+\mathbf{E}_h^{n-1}}{\Delta t^2}=-c_0^2\mathbb{W}_{\mathscr{E}}\mathrm{curl}_h^T\mathbb{M}_{\mathscr{F}}\mathrm{curl}_h\mathbf{E}^n. \tag{5.4.53}$$

Given this second order equation we will now compute the Fourier Symbol in time.

$$\frac{\mathbf{E}_h^{n+1}-2\mathbf{E}_h^n+\mathbf{E}_h^{n-1}}{\Delta t^2}=\frac{\mathrm{e}^{-\mathrm{i}\omega\Delta t}-2+\mathrm{e}^{\mathrm{i}\omega\Delta t}}{\Delta t^2}\mathbf{E}_h^n \tag{5.4.54}$$

$$=\frac{2\cos(\omega\Delta t)-2}{\Delta t^2}\mathbf{E}_h^n \tag{5.4.55}$$

$$=-\frac{4\sin^2\frac{\omega\Delta t}{2}}{\Delta t^2} \tag{5.4.56}$$

$$=:\mathcal{T}_{\Delta t}(\omega) \tag{5.4.57}$$

Similarly the discrete Fourier symbol in space can be calculated using Definition 5.4.5

$$\left(\mathbb{W}_{\mathscr{E}}\mathrm{curl}_h^T\mathbb{M}_{\mathscr{F}}\mathrm{curl}_h\mathbf{E}^n_{(e_1,e_2)}\right)=\overline{\mathbb{W}}_{\mathscr{E}}\ (\overline{\mathrm{curl}_h})^\star\Delta x\Delta y(\overline{\mathrm{curl}}_h)(\mathbf{E}^n_{(e_1,e_2)}). \tag{5.4.58}$$

Define the matrix

$$\overline{\mathbb{A}}_h=\overline{\mathrm{curl}_h^\star}\Delta x\Delta y\overline{\mathrm{curl}}_h. \tag{5.4.59}$$

We then have the identities

$$\overline{\mathbb{W}}_{\mathscr{E}}=\frac{1}{\Delta x\Delta y}\begin{pmatrix}2(1-(1-4w_1)\sin^2\frac{k_y\Delta y}{2}) & (1-\mathrm{e}^{-\mathrm{i}k_x\Delta x})(1-\mathrm{e}^{-\mathrm{i}k_y\Delta y})w_2\\ (\mathrm{e}^{\mathrm{i}k_x\Delta x}-1)(\mathrm{e}^{\mathrm{i}k_y\Delta y}-1)w_2 & 2(1-(1-4w_3)\sin^2\frac{k_x\Delta x}{2})\end{pmatrix}, \tag{5.4.60}$$

$$\overline{\mathbb{A}}_h=\begin{pmatrix}4\frac{\Delta x}{\Delta y}\sin^2\frac{k_y\Delta y}{2} & (1-\mathrm{e}^{-\mathrm{i}k_x\Delta x})(1-\mathrm{e}^{-\mathrm{i}k_y\Delta y})\\ (\mathrm{e}^{\mathrm{i}k_x\Delta x}-1)(\mathrm{e}^{\mathrm{i}k_y\Delta y}-1) & 4\frac{\Delta y}{\Delta x}\sin^2\frac{k_x\Delta x}{2}\end{pmatrix}. \tag{5.4.61}$$

Combining the two statements yields a 2×2 eigenvalue problem

$$\mathcal{T}_{\Delta t}(\omega)(\mathbf{E}^n_{(e_1,e_2)})=-c_0^2\overline{\mathbb{W}}_{\mathscr{E}}\ \overline{\mathbb{A}}_h(\mathbf{E}_h^n|_{(e_1,e_2)}). \tag{5.4.62}$$

As is typical of the continuum setting solution pairs of $\omega,\mathbf{k}$ are determined by solving the eigenvalue problem. To do this we must first find the eigenvalues of the spatial symbol.

However, as $\text{curl}_h^T \text{curl}_h$ is rank 1 we have that $(\overline{\text{curl}_h})^\star(\overline{\text{curl}_h})$ is at most rank 1. Therefore the resulting spatial symbol $-c_0^2 \overline{W}_{\mathscr{E}} \overline{\mathbb{A}}_h$ is rank one. As the matrix is only 2×2 this gives us that the non-zero eigenvalue of the matrix is given by its trace. No optimization can be done for the zero eigenvalues which correspond to the divergence of the solution which is handled by the exactness property of MFD. For the divergence free, transient modes we have the discrete dispersion relation

$$-\frac{4\sin^2\left(\frac{\omega\Delta t}{2}\right)}{\Delta t^2} = -c_0^2 \text{Tr}(\overline{\mathbb{W}}_{\mathscr{E}} \overline{\mathbb{A}}_h). \tag{5.4.63}$$

Defining $\mathcal{S}_h(\mathbf{k}) = \text{Tr}(\overline{\mathbb{W}}_{\mathscr{E}} \overline{\mathbb{A}}_h)$ and carrying out a detailed but straightforward calculation we arrive at

$$\mathcal{S}_h(\mathbf{k}) = -\frac{4c_0^2}{\Delta x^2} \sin^2 \frac{k_x \Delta x}{2} \Big(1 + (1 - 4w_3) \sin^2 \frac{k_x \Delta x}{2}\Big) \tag{5.4.64a}$$

$$- \frac{32 c_0^2}{\Delta x \Delta y} w_2 \sin^2 \frac{k_x \Delta x}{2} \sin^2 \frac{k_y \Delta y}{2} \tag{5.4.64b}$$

$$- \frac{4c_0^2}{\Delta y^2} \sin^2 \frac{k_y \Delta y}{2} \Big(1 + (1 - 4w_1) \sin^2 \frac{k_y \Delta y}{2}\Big). \tag{5.4.64c}$$

This completes the proof. **Q.E.D.**

We will now justify the discrete elimination of the magnetic field $B_h^{n+1/2}$ in the previous calculation.

Lemma 5.4.5. *The MFD for Maxwell's equations in free space in first order formulation and second order formulation have an identical dispersion relation*

Proof. Note that while this analysis was performed for the second order evolution equation it also applies to the first order system. For the first order system the discrete dispersion relation is a 3×3 generalized eigenvalue problem.

$$\frac{\mathrm{e}^{-\mathrm{i}\omega\Delta t} - 1}{\Delta t} \begin{pmatrix} \mathbf{E}^n_{(e_1,e_2)} \\ \mathrm{e}^{-\mathrm{i}\omega\Delta t/2} B_f^n \end{pmatrix} = \begin{pmatrix} 0 & c^2 \mathrm{e}^{-\mathrm{i}\omega\Delta t/2} \overline{\mathbb{W}}_{\mathscr{E}} \overline{\text{curl}}_h^\star \Delta x \Delta y \\ \mathrm{e}^{-\mathrm{i}\omega\Delta t} \overline{\text{curl}}_h & 0 \end{pmatrix} \begin{pmatrix} \mathbf{E}^n_{(e_1,e_2)} \\ B_f^n \end{pmatrix} \tag{5.4.65}$$

Define the matrix $\mathcal{D}_h$ by

$$\mathcal{D}_h = \begin{pmatrix} \frac{1}{\Delta t}(\mathrm{e}^{-\mathrm{i}\omega\Delta t} - 1) & -c_0^2 \mathrm{e}^{-\mathrm{i}\omega\Delta t/2}\overline{\mathbb{W}}_{\mathscr{E}}\overline{\mathrm{curl}}_h^{\star}\Delta x\Delta y \\ \mathrm{e}^{-i\omega\Delta t}\overline{\mathrm{curl}}_h & \frac{1}{\Delta t}\mathrm{e}^{-\mathrm{i}\omega\Delta t/2}(\mathrm{e}^{-\mathrm{i}\omega\Delta t} - 1) \end{pmatrix}. \tag{5.4.66}$$

The dispersion relation can then be posed as

$$\mathcal{D}_h \begin{pmatrix} \mathbf{E}^n_{(e_1,e_2)} \\ B_f^{n+1/2} \end{pmatrix} = \mathbf{0}. \tag{5.4.67}$$

One solution to this problem is given by $\omega = 0$ which corresponds to the non-divergence free mode and can be neglected. Consider instead ω away from zero. We can then apply the Schur compliment formula for the determinant.

$$\det \mathcal{D}_h = \mathrm{e}^{-\mathrm{i}\omega\Delta t/2}\frac{\mathrm{e}^{-\mathrm{i}\omega\Delta t} - 1}{\Delta t}\det\Big(\frac{\mathrm{e}^{-\mathrm{i}\omega\Delta t} - 1}{\Delta t}\mathbb{I} \tag{5.4.68}$$

$$+ c_0^2\Delta t\mathrm{e}^{-\mathrm{i}\omega\Delta t}(\mathrm{e}^{-\mathrm{i}\omega\Delta t} - 1)^{-1}\overline{\mathbb{W}}_{\mathscr{E}}\overline{\mathrm{curl}}_h^{\star}\alpha h^2\overline{\mathrm{curl}}_h\Big) \tag{5.4.69}$$

$$= \mathrm{e}^{-\mathrm{i}\omega\Delta t/2}\frac{(\mathrm{e}^{-\mathrm{i}\omega\Delta t} - 1)(1 - \mathrm{e}^{\mathrm{i}\omega\Delta t})}{\Delta t}\det\left(\frac{(\mathrm{e}^{-\mathrm{i}\omega\Delta t} - 1)(1 - \mathrm{e}^{\mathrm{i}\omega\Delta t})}{\Delta t^2}\mathbb{I} + c_0^2\overline{\mathbb{W}}_{\mathscr{E}}\overline{\mathbb{A}}\right) \tag{5.4.70}$$

From this perspective the condition $\det \mathcal{D}_h = 0$ is equivalent to either $\omega = 0$ or

$$\det\left(\frac{(\mathrm{e}^{-\mathrm{i}\omega\Delta t} - 1)(1 - \exp^{\mathrm{i}\omega\Delta t})}{\Delta t^2}\mathbb{I} + c_0^2\overline{\mathbb{W}}_{\mathscr{E}}\overline{\mathbb{A}}\right) = 0 \tag{5.4.71}$$

Which is exactly the dispersion relationship for the second order formulation. **Q.E.D.**

5.4.2 M-Adaptation for Free Space

Having established the dispersion relation for the entire MFD family of discretizations for Maxwell's equations in free space we will now choose a member of the family which has minimal dispersion error.

Definition 5.4.6. We define the dispersion error minimization M-adaptation problem as follows. Let $\mathcal{T}_{\Delta t}(\omega), \mathcal{S}_h(\mathbf{k})$ be defined as in Theorem 5.4.4. We seek $(w_1^\star, w_2^\star, w_3^\star)$ such that

$$(w_1^\star, w_2^\star, w_3^\star) = \arg\min_{\mathbb{R}^3} |\mathcal{T}_{\Delta t}(\omega) - \mathcal{S}_h(\mathbf{k})| \tag{5.4.72}$$

for every $(\omega, \mathbf{k})$ as solution to the continuum dispersion relation

$$\omega^2 = c_0^2 k^2. \tag{5.4.73}$$

We define the MFD method whose matrix $\mathbb{W}_{\mathscr{E}}$ uses the parameters $(w_1^\star, w_2^\star, w_3^\star)$ the **M-adapted MFD for Maxwell's equations in free space** or where confusion will not arise the **M-adapted MFD**.

Remark. It is also possible to formulate M-adaptation which reduces dispersion error for a specific frequency. The resulting method may have superior dispersion properties than the frequency oblivious approach we will formulate. However, given that most time domain solvers are interested in data with very large frequency content we will not consider this approach.

We relate our three resolution parameters Δx, Δy, and Δt to a single parameter h which we arbitrarily choose as $h = \Delta x$. Namely we introduce the aspect ratio

$$\alpha = \frac{\Delta y}{\Delta x}. \tag{5.4.74}$$

Using this parameter we can relate $\Delta y = \alpha h$. Similarly for time we will use the famous Courant number

$$\nu = \frac{c_0 \Delta t}{h} \tag{5.4.75}$$

which gives us $\Delta t = \frac{\nu h}{c_0}$.

Lemma 5.4.6. *Parameterize the wave vector* $\mathbf{k} = k(\cos\theta, \sin\theta)^T$. *The discrete spatial symbol*

$$\mathcal{S}_h(\mathbf{k}) = -c_0^2 k^2 + \left(\frac{3w_3 - 1}{3} \cos^4\theta + 2\alpha w_2 \cos^2\theta \sin^2\theta \right. \tag{5.4.76}$$

$$\left. + \frac{\alpha^2(3w_1 - 1)}{3} \sin^4\theta \right) c_0^2 k^4 h^2 + \mathcal{O}(h^4). \tag{5.4.77}$$

is a second order approximation of the continuous symbol $-c_0^2k^2$ *By choosing parameters* w_1, w_3 *such that*

$$w_1 = \frac{3w_2\alpha^{-1} + 1}{3}, \qquad w_3 = \frac{3w_2\alpha + 1}{3} \tag{5.4.78}$$

the symbol $\mathcal{S}_h$ *is an isotropic order 2 approximation of the continuous symbol* $-c_0^2k^2$

$$\mathcal{S}_h(\mathbf{k}) = -c_0^2k^2 = \alpha w_2 c_0^2 k^4 h^2 + \mathcal{O}(h^4). \tag{5.4.79}$$

Proof. Assume the parameterization $\mathbf{k} = k(\cos\theta, \sin\theta)^T$. We begin by expanding $\mathcal{S}_h(\mathbf{k})$ in a Taylor series in h.

$$\mathcal{S}_h = -c_0^2k^2 + \left(\frac{3w_3 - 1}{3}\cos^4\theta + 2\alpha w_2 \cos^2\theta \sin^2\theta \right. \tag{5.4.80a}$$

$$\left. + \frac{\alpha^2(3w_1 - 1)}{3}\sin^4\theta \right) c_0^2 k^4 h^2 + \mathcal{O}(h^4). \tag{5.4.80b}$$

Making the described parameter choice implies

$$\frac{3w_3 - 1}{3} = \alpha w_2 = \frac{\alpha^2(3w_1 - 1)}{3}. \tag{5.4.81}$$

Which eliminates the dependence of the second order term on θ.

$$\mathcal{S}_h = -c_0^2k^2 + \alpha w_2(\cos^4\theta + 2\cos^2\theta\sin^2\theta + \sin^4\theta)c_0^2k^4h^2 + \mathcal{O}(h^4), \tag{5.4.82}$$

$$= -c_0^2k^2 + \alpha w_2 c_0^2 k^4 h^2 + \mathcal{O}(h^4). \tag{5.4.83}$$

Q.E.D.

Using this Lemma it appears that choosing $\omega_2 = 0$ and therefore $w_1 = w_3 = \frac{1}{3}$ would produce a spatial symbol whose dispersion error is order four.

One possible strategy for producing a fully discrete scheme with fourth order dispersion error using a lowest would be to apply a fourth order time integration scheme such as the fourth famous order Runge-Kutta method. This will produce a method with high dispersion error accuracy; however, high order integrators are sometimes avoided due to

there larger storage requirements which may not be practical for very large problems. For this reason we will try and produce a scheme with high dispersion accuracy from staggered leap frog and its generalizations.

Theorem 5.4.7. *The M-adapted MFD for free space is obtained by the choice of parameters*

$$w_1 = \frac{4 - \frac{\nu^2}{\alpha^2}}{12}, \quad w_2 = -\frac{\nu^2}{12\alpha}, \quad w_3 = \frac{4 - \nu^2}{12}, \tag{5.4.84}$$

which results in a scheme with fourth order dispersion error.

Proof. We begin by selecting w_1 and w_3 as constructed in Lemma 5.4.6 and consider the discrete dispersion relation developed in Theorem 5.4.4. Consider a root of the continuum dispersion relation

$$(\omega, \mathbf{k}) : \omega^2 = c_0^2 k^2. \tag{5.4.85}$$

Parameterize the discrete wave vector $\mathbf{k} = k(\cos\theta, \sin\theta)^T$. We can now expand the difference of the symbols in a Taylor series in h.

$$\mathcal{T}_{\Delta t}(\omega) - \mathcal{S}_h(\mathbf{k}) \tag{5.4.86}$$

$$= (-\omega^2 + c^2 k^2) + \frac{h^2}{12c_0^2}\Big(\nu^2\omega^4 + 12\alpha w_2 c_0^4 k^4\Big) + \mathcal{O}(h^4). \tag{5.4.87}$$

Given that $(\omega, \mathbf{k})$ are roots of the continuum equation we have

$$\mathcal{T}_{\Delta t}(\omega) - \mathcal{S}_h(\mathbf{k}) = \frac{h^2}{12c_0^2}\omega^4\Big(\nu^2 + 12\alpha w_2\Big) + \mathcal{O}(h^4) \tag{5.4.88}$$

$$\tag{5.4.89}$$

By choosing w_2 as

$$w_2 = -\frac{\nu^2}{12\alpha} \tag{5.4.90}$$

we can eliminate the $\mathcal{O}(h^2)$ term entirely leaving us with

$$\mathcal{T}_{\Delta t}(\omega) - \mathcal{S}_h(\mathbf{k}) = \mathcal{O}(h^4) \tag{5.4.91}$$

The choice of w_2 determines w_1 and w_3 uniquely. As the choice of $(\omega, \mathbf{k})$ is arbitrary and as our parameters were chosen independently of frequency and wave number this optimization holds for all $(\omega, \mathbf{k})$. **Q.E.D.**

With this choice of parameters the matrix $\mathbb{W}_{\mathscr{E}|f}$ is given by

$$\mathbb{W}_{\mathscr{E}|f} = \frac{1}{12\Delta x \Delta y} \begin{pmatrix} 7-\nu_y^2 & -\nu_x\nu_y & \nu_y^2-1 & \nu_x\nu_y \\ -\nu_x\nu_y & 7-\nu_x^2 & \nu_x\nu_y & \nu_x^2-1 \\ \nu_y^2-1 & \nu_x\nu_y & 7-\nu_y^2 & -\nu_x\nu_y \\ \nu_x\nu_y & \nu_x^2-1 & -\nu_x\nu_y & 7-\nu_x^2 \end{pmatrix}, \tag{5.4.92}$$

$$\nu_x = \frac{c_0\Delta t}{\Delta x}, \qquad \nu_y = \frac{c_0\Delta t}{\Delta y}. \tag{5.4.93}$$

5.4.3 Necessary and sufficient conditions for M-adaptation

The entire previous optimization procedure relies upon finding the following property of the numerical temporal symbol

$$\mathcal{T}_{\Delta t}(\omega) = -\omega^2 \left(1 - \frac{\Delta t^2}{12}\omega^2 + \mathcal{O}(\Delta t^4)\right). \tag{5.4.94}$$

This suggests that for any constitutive law for transient Maxwell's equations, if the continuum symbol in time is given by $\mathcal{T}$ then any time integrator which has a discrete symbol of the form

$$\mathcal{T}_{\Delta t}(\omega) = \mathcal{T}(\omega) + c_0\Delta t^2 \mathcal{T}(\omega)^2 + \mathcal{O}(\Delta t^4) \tag{5.4.95}$$

for some real value c which is independent of ω and Δt then we can successfully perform M-adaptation to cancel the second order dispersion error.

Definition 5.4.7. Consider Maxwell's equations with a linear constitutive law such that the dispersion relation for transient waves is given by

$$\mathcal{T}(\omega) = \mathcal{S}(\mathbf{k}). \tag{5.4.96}$$

Then the dispersion error minimization M-adaptation problem is defined as follows. Let the discrete Fourier the time integrator be $\mathcal{T}_{\Delta t}(\omega)$ and let the family of mimetic spatial discretizations have the symbol $\mathcal{S}(\mathbf{k})$. We seek $(w_1^\star, w_2^\star, w_3^\star)$ such that

$$(w_1^\star, w_2^\star, w_3^\star) = \arg\min_{\mathbb{R}^3} |\mathcal{T}_{\Delta t}(\omega) - \mathcal{S}_h(\mathbf{k})| \tag{5.4.97}$$

for every $(\omega, \mathbf{k})$ solutions to the continuum dispersion relation (5.4.96). As before we refer to a scheme which uses $\mathbb{W}_{\mathscr{E}}$ with these parameters as the **M-adapted MFD**.

Theorem 5.4.8. *The M-adaptation for MFD discretizations of TE or TM formulations of Maxwell's equations results in a method with fourth order dispersion error if and only if the temporal symbol $\mathcal{T}_{\Delta t}(\omega)$ has the property*

$$\mathcal{T}_{\Delta t}(\omega) = \mathcal{T}(\omega)(1 + C\Delta t^2 T(\omega) + \mathcal{O}(\Delta t^4)) \tag{5.4.98}$$

where $\mathcal{T}(\omega)$ is the continuum symbol in time.

Proof. Consider the formal discretization of TE or TM Maxwell's equations with MFD in space and a time discretization whose symbol is given by $\mathcal{T}_{\Delta t}(\omega)$. Assume we choose parameters w_1, w_3 as in Lemma 5.4.6 and that we have $(\omega, \mathbf{k})$ a root of the continuum dispersion relationship

$$\mathcal{T}(\omega) = \mathcal{F}(\mathbf{k}) \qquad \text{note } \mathcal{F}(\mathbf{k}) = c^2 k^2 \tag{5.4.99}$$

($\Leftarrow$) Assume we there exists a ω_2 independent of $(\omega, \mathbf{k})$ such that

$$\mathcal{T}_{\Delta t}(\omega) - \mathcal{F}_h(\mathbf{k}) = \mathcal{O}(h^4). \tag{5.4.100}$$

Assume the following formal Taylor of $\mathcal{T}_{\Delta t}(\omega)$

$$\mathcal{T}_{\Delta t}(\omega) = \mathcal{T}_0(\omega) + \mathcal{T}_1(\omega)\Delta t + \mathcal{T}_2(\omega)\Delta t^2 + \mathcal{T}_3(\omega)\Delta t^3 + \mathcal{O}(\Delta t^4). \tag{5.4.101}$$

As the spatial symbol is given by

$$\mathcal{F}_h(\mathbf{k}) = -c^2 k^2 + c^2 k^4 \alpha w_2 h^2 + \mathcal{O}(h^4) \tag{5.4.102}$$

we know that $T_0 = \mathcal{T}(\omega)$ and $\mathcal{T}_1 = \mathcal{T}_3 = 0$.

$$\mathcal{T}_{\Delta t}(\omega) - \mathcal{F}_{\Delta t}(\mathbf{k}) = \frac{h^2}{c^2}(\nu^2 \mathcal{T}_2(\omega) + \alpha w_2 c^4 k^4) + \mathcal{O}(\Delta t^4). \tag{5.4.103}$$

As the second order term is equal to zero we have the identity

$$0 = \nu^2 T_2(\omega) + \alpha w_2 c^4 k^4 \tag{5.4.104}$$

$$= \nu^2 T_2(\omega) + \alpha w_2 \mathcal{T}(\omega)^2 \qquad c^2 k^2 = \mathcal{T}(\omega) \tag{5.4.105}$$

$$\mathcal{T}_2(\omega) = -\frac{\alpha w_2}{\nu^2}\mathcal{T}(\omega)^2 \tag{5.4.106}$$

As w_2, α, ν are all real numbers independent of ω we have $\mathcal{T}_2(\omega) = C\mathcal{T}(\omega)^2$ for some real number C. We therefore have that $\mathcal{T}_{\Delta t}(\omega) = \mathcal{T}(\omega) + C\mathcal{T}(\omega)^2\Delta t^2 + \mathcal{O}(\Delta t^4)$ is a necessary condition for M-adaptation.

($\Rightarrow$) Now let

$$\mathcal{T}_{\Delta t}(\omega) = \mathcal{T}(\omega) + C\mathcal{T}(\omega)^2\Delta t^2 + \mathcal{O}(\Delta t^4). \tag{5.4.107}$$

Calculate the formal dispersion error about a true root $(\omega, \mathbf{k})$

$$\mathcal{T}_{\Delta t}(\omega) - \mathcal{F}_h(\mathbf{k}) = (\mathcal{T}(\omega) + c^2k^2) + \frac{h^2}{c^2}(\nu^2 C^2 \mathcal{T}(\omega)^2 + \alpha w_2 c^4 k^4) + \mathcal{O}(h^4) \tag{5.4.108}$$

$$= \frac{h^2}{c^2}\mathcal{T}(\omega)^2(\nu^2 C^2 + \alpha w_2) + \mathcal{O}(h^4). \tag{5.4.109}$$

Choosing $w_2 = -\frac{\nu^2 C}{\alpha}$ will eliminate the order h^2 dispersion error. Thus we have shown that the condition is sufficient for M-adaptation. **Q.E.D.**

Further if $c = \frac{1}{12}$ then resultant M-adapted method will have an identical spatial discretization to the algorithm developed in this chapter. In this chapter we will introduce just such a time integrator and apply M-adaptation to a large class of linear constitutive laws for Maxwell's equations.

5.4.4 M-adaptation fails for Time Averaged Schemes

The standard averaged differencing is the standard way of handling low order terms in the Yee scheme. Consider a conductive media

$$\frac{\partial}{\partial t}\mathbf{E} + \frac{1}{\tau}\mathbf{E} = \frac{1}{\epsilon}\mathbf{curl}H, \quad \tau = \frac{\epsilon}{\sigma} \tag{5.4.110}$$

$$\frac{\partial}{\partial t}H = -\frac{1}{\mu}\mathrm{curl}\mathbf{E}. \tag{5.4.111}$$

Calculating the symbol in time we have

$$\mathcal{T}(\omega) = -\omega^2 - \frac{\mathrm{i}}{\tau}\omega. \tag{5.4.112}$$

The standard semi-implicit leapfrog discretization in time is then given as follows

$$\frac{\mathbf{E}^{n+1} - \mathbf{E}^n}{\Delta t} + \frac{\mathbf{E}^{n+1} + \mathbf{E}^n}{2\tau} = \frac{1}{\epsilon}\mathbf{curl}H^{n+1/2} \tag{5.4.113}$$

$$\frac{H^{n+1/2} - H^{n-1/2}}{\Delta t} = -\frac{1}{\mu}\mathrm{curl}\mathbf{E}^n. \tag{5.4.114}$$

To calculate the discrete symbol we eliminate the magnetic field H and are left with the following second order stencil

$$\frac{\mathbf{E}^{n+1} - 2\mathbf{E}^n + \mathbf{E}^{n-1}}{\Delta t^2} + \frac{\mathbf{E}^{n+1} - \mathbf{E}^{n-1}}{2\tau\Delta t} = -c^2\mathbf{curl}\mathrm{curl}\mathbf{E}^n. \tag{5.4.115}$$

Substituting the plane wave Ansatz $\mathbf{E}^n = \mathrm{e}^{-\mathrm{i}\omega n\Delta t}\mathbf{E}(\mathbf{x})$ we have arrive at the following symbol

$$\mathcal{T}_{\Delta t}(\omega) = -\frac{4\sin^2\frac{\omega\Delta t}{2}}{\Delta t^2} - \frac{\mathrm{i}}{\tau}\frac{\sin\omega\Delta t}{\Delta t}. \tag{5.4.116}$$

By expanding the symbol in a Taylor series in Δt we have

$$\mathcal{T}_{\Delta t}(\omega) = \left(-\omega^2 - \frac{\mathrm{i}}{\tau}\omega\right) + \frac{\Delta t^2}{12}\left(\omega^2\left(\omega^2 + \frac{2\mathrm{i}}{\tau}\omega\right)\right) + \mathcal{O}(\Delta t^4). \tag{5.4.117}$$

However,

$$\left(\omega^2\left(\omega^2 + \frac{2\mathrm{i}}{\tau}\omega\right)\right) \neq \left(-\omega^2 - \frac{\mathrm{i}}{\tau}\omega\right)^2. \tag{5.4.118}$$

Therefore Theorem 5.4.8 implies that wideband M-adaptation is impossible for time-averaged differences applied to TE conductive media.

5.4.5 Dispersion Analysis for the ETMFD

Consider the ETMFD discretization for a general polarization law as described in (4.3.6). In order to obtain from (4.3.6) an appropriate second order formulation we will eliminate the magnetic induction $B_h^{n+1/2}$ from the discrete evolution equation. We do this by applying a leap-frog step to both sides of the first equation in (4.3.6). This yields a discretization

$$\begin{pmatrix} \mathbf{E}_h^{n+1} \\ \mathbf{P}_{m,h}^{n+1} \end{pmatrix} = (\mathbb{I} + e^{\mathbb{X}\Delta t}) \begin{pmatrix} \mathbf{E}_h^{n} \\ \mathbf{P}_{m,h}^{n} \end{pmatrix} - \mathrm{e}^{\mathbb{X}\Delta t} \begin{pmatrix} \mathbf{E}_h^{n-1} \\ \mathbf{P}_{m,h}^{n-1} \end{pmatrix} - c_0^2 \Delta t \mathbb{Y} \begin{pmatrix} \widetilde{\mathrm{curl}}_h \mathrm{curl}_h \mathbf{E}_h^n \\ 0 \end{pmatrix}. \quad (5.4.119)$$

Here $\mathbb{Y} = \int_0^{\Delta t} \mathrm{e}^{\mathbb{X}s}\, ds$.

Lemma 5.4.9. *The continuum temporal system for the general polarization law* (4.1.19) *is given as*

$$\mathcal{T}(\omega) = -\omega^2 \mathbb{I} + \mathrm{i}\omega \mathbb{X}. \quad (5.4.120)$$

Proof. This follows immediately from eliminating the variable H from the continuum equations.

$$\frac{\partial^2}{\partial t^2} \begin{pmatrix} \mathbf{E} \\ \mathbf{P}_j \end{pmatrix} - \mathbb{X} \begin{pmatrix} \mathbf{E} \\ \mathbf{P}_j \end{pmatrix} = \begin{pmatrix} -c^2 \mathbf{curl}\mathrm{curl}\mathbf{E} \\ \mathbf{0}_j \end{pmatrix} \quad (5.4.121)$$

Assuming time harmonic waves produces the desired result.

$$-\mathbb{I}\omega \begin{pmatrix} \mathbf{E} \\ \mathbf{P}_j \end{pmatrix} + \mathrm{i}\omega \mathbb{X} \begin{pmatrix} \mathbf{E} \\ \mathbf{P}_j \end{pmatrix} = \begin{pmatrix} -c^2 \mathbf{curl}\mathrm{curl}\mathbf{E} \\ \mathbf{0}_j \end{pmatrix}. \quad (5.4.122)$$

Q.E.D.

Lemma 5.4.10. *Exponential time differencing for a general polarization law* (4.1.19) *has a temporal symbol*

$$\mathcal{T}_{\Delta t}(\omega) = \mathbb{Y}^{-1} \frac{-\mathrm{e}^{-\mathrm{i}\omega\Delta t}\mathbb{I} - (\mathbb{I} + \mathrm{e}^{\mathbb{X}\Delta t}) + \mathrm{e}^{\mathbb{X}\Delta t}}{\Delta t} = \mathcal{T}(\omega) + \frac{\Delta t^2}{12}\mathcal{T}^2(\omega) + \mathcal{O}(\Delta t^4). \quad (5.4.123)$$

Proof. To obtain a discrete in time dispersion relation we divide both sides of (5.4.119) by the exponential integrator $\mathbb{Y}$ to calculate

$$\frac{1}{\Delta t}\mathbb{Y}^{-1}\left[\begin{pmatrix}\mathbf{E}_h^{n+1}\\ \mathbf{P}_{j,h}^{n+1}\end{pmatrix}-(\mathbb{I}+e^{\mathbb{X}\Delta t})\begin{pmatrix}\mathbf{E}_h^{n}\\ \mathbf{P}_{j,h}^{n}\end{pmatrix}+\mathrm{e}^{\mathbb{X}\Delta t}\begin{pmatrix}\mathbf{E}_h^{n-1}\\ \mathbf{P}_{j,h}^{n-1}\end{pmatrix}\right]=\begin{pmatrix}-c_0^2\ \widetilde{\mathrm{curl}}_h\ \mathrm{curl}_h & 0\\ 0 & 0\end{pmatrix}\begin{pmatrix}\mathbf{E}_h^{n}\\ \mathbf{P}_{j,h}^{n}\end{pmatrix}. \tag{5.4.124}$$

Assuming time-harmonic solutions in the above equation we produce the system

$$\mathbb{Y}^{-1}\frac{\mathrm{e}^{-\mathrm{i}\omega\Delta t}\mathbb{I}-(\mathbb{I}+\mathrm{e}^{\mathbb{X}\Delta t})+\mathrm{e}^{\mathrm{i}\omega\Delta t}\mathrm{e}^{\mathbb{X}\Delta t}}{\Delta t}\begin{pmatrix}\mathbf{E}_h\\ \mathbf{P}_{j,h}\end{pmatrix}=\begin{pmatrix}-c_0^2\ \widetilde{\mathrm{curl}}_h\ \mathrm{curl}_h & 0\\ 0 & 0\end{pmatrix}\cdot\begin{pmatrix}\mathbf{E}_h\\ \mathbf{P}_{j,h}\end{pmatrix} \tag{5.4.125}$$

Defining the discrete symbol in time to be

$$\mathcal{T}_{\Delta t}(\omega)=\mathbb{Y}^{-1}\frac{\mathrm{e}^{-\mathrm{i}\omega\Delta t}\mathbb{I}-(\mathbb{I}+\mathrm{e}^{\mathbb{X}\Delta t})+\mathrm{e}^{\mathrm{i}\omega\Delta t}\mathrm{e}^{\mathbb{X}\Delta t}}{\Delta t}, \tag{5.4.126}$$

and expanding $\mathcal{T}_{\Delta t}$ in a Taylor Series in the variable Δt we obtain

$$\mathcal{T}_{\Delta t}(\omega)=(-\omega^2\mathbb{I}+\mathrm{i}\omega\mathbb{X})+\frac{\Delta t^2}{12}(-\omega^2\mathbb{I}+\mathrm{i}\omega\mathbb{X})^2+\mathcal{O}(\Delta t^4). \tag{5.4.127}$$

Q.E.D.

This result will allow us to apply Theorem 5.4.8.

5.4.6 M-adaptation for the ETMFD

Consider an ETMFD discretization of a linear polarization model

Theorem 5.4.11. *There exists a choice of parameters in the mimetic discretization, w_1, w_2, w_3, such that the ETMFD for a general polarization law* (4.3.6) *has order four dispersion error.*

Proof. Intuitively the dispersion relation for (4.3.6) would be determined by equality between the space discrete symbol $\mathcal{S}_h$ defined in (5.4.64) and the time discrete symbol $\mathcal{T}_{\Delta t}$

defined in Lemma 5.4.10. However, the temporal symbol as defined is matrix valued while the spatial symbol is scalar. However, this symbol acts on values $\mathbf{E}^n_{(e_1,e_2)}$ and has no dependence on any field $\mathbf{P}^n_{j,(e_1,e_2)}$ therefore the discrete symbol in this context is given by

$$\tilde{\mathcal{S}}_h(\mathbf{k}) = \begin{pmatrix} \mathcal{S}_h(\mathbf{k}) & \mathbf{0}_{1\times J} \\ \mathbf{0}_{J\times 1} & \mathbf{0}_{J\times J} \end{pmatrix} \tag{5.4.128}$$

We begin by choosing parameters w_1, w_3 as described in Lemma 5.4.6

$$\frac{\alpha^2(3w_1-1)}{3} = \alpha w_2 = \frac{(3w_3-1)}{3}, \quad \text{i.e.} \quad \begin{matrix} w_1 = \dfrac{3w_2\alpha^{-1}+1}{3}, \\ w_3 = \dfrac{3w_2\alpha+1}{3}. \end{matrix} \tag{5.4.129}$$

This then gives us the identity

$$\tilde{\mathcal{S}}_h(\mathbf{k}) = \begin{pmatrix} \mathcal{S}(\mathbf{k}) & \mathbf{0}_{1\times J} \\ \mathbf{0}_{J\times 1} & \mathbf{0}_{J\times J} \end{pmatrix} + \alpha w_2 h^2 \begin{pmatrix} \mathcal{S}(\mathbf{k})^2 & \mathbf{0}_{1\times J} \\ \mathbf{0}_{J\times 1} & \mathbf{0}_{J\times J} \end{pmatrix} + \mathcal{O}(h^4). \tag{5.4.130}$$

Lemma 5.4.10 shows that

$$\mathcal{T}_{\Delta t}(\omega) = \mathcal{T}(\omega) + \frac{\Delta t^2}{12}\mathcal{T}(\omega)^2. \tag{5.4.131}$$

These two results are exactly the sufficient conditions of Theorem 5.4.8. Therefore the ETMFD for a general polarization law can be M-adapted by choosing

$$w_2 = -\frac{\nu^2}{12\alpha}, \nu = \frac{c\Delta t}{h}, \alpha = \frac{\Delta x}{\Delta y}, h = \Delta x. \tag{5.4.132}$$

This completes the proof. **Q.E.D.**

This theorem shows that the ETMFD can be M-adapted to produce a fourth order dispersion error method for a general polarization law. Most interestingly we have shown that the resulting method *uses an identical choice of parameters as the free space case.*

5.5 Numerical Demonstrations of Dispersion Analysis

5.5.1 L^2 and Dispersion Errors for Free Space

In this section we will present L^2 and divergence errors for the M-adapted MFD. We consider the initial value problem on the unit square with $\epsilon = \mu = c = 1$.

$$\begin{cases} \frac{\partial}{\partial t}\mathbf{E} = \mathbf{curl}B & \in [0,1]^2 \\ \frac{\partial}{\partial t}B = -\text{curl}\mathbf{E} & \in [0,1]^2 \\ \mathbf{E}\times\mathbf{n} = 0 & \in \partial[0,1]^2 \\ \mathbf{E}(0) = \Big(-k_y\cos(k_x x)\sin(k_y y), k_x \sin(k_x x)\cos(k_y y)\Big)^T & \\ B(0) = 0 & \end{cases} . \tag{5.5.1}$$

We consider $k_x, k_y \in \pi\mathbb{Z}$ for compatibility with the boundary conditions. This problem has a known exact solution given by

$$\mathbf{E} = \cos(\omega t)\begin{pmatrix} -k_y\cos(k_x x)\sin(k_y y) \\ k_x \sin(k_x x)\cos(k_y y)\end{pmatrix}, \quad \omega = \sqrt{k_x^2 + k_y^2}, \tag{5.5.2}$$

$$H = \frac{k_x^2 + k_y^2}{\omega}\sin(\omega t)\cos(k_x x)\cos(k_y y). \tag{5.5.3}$$

To calculate errors we consider relative L^2 and dispersion errors. L^2 errors are calculated using an appropriate mimetic inner product matrix $\mathbb{M}_{\mathscr{E}}$ and $\mathbb{M}_{\mathscr{F}}$ as appropriate.

$$\mathcal{E}_{L^2}(\mathbf{E}_h^n) = \frac{\Big(\mathbf{E}_h^n - \mathcal{I}^{\mathscr{E}}(\mathbf{E}(n\Delta t))\Big)^T \mathbb{M}_{\mathscr{E}}\Big(\mathbf{E}_h^n - \mathcal{I}^{\mathscr{E}}(\mathbf{E}(n\Delta t))\Big)}{\mathcal{I}^{\mathscr{E}}(\mathbf{E}(n\Delta t))^T \mathbb{M}_{\mathscr{E}}\mathcal{I}^{\mathscr{E}}(\mathbf{E}(n\Delta t))} \tag{5.5.4}$$

$$\mathcal{E}_{L^2}(B_h^{n+1/2}) = \frac{\Big(B_h^{n+1/2} - \mathcal{I}^{\mathscr{F}}(B((n+1/2)\Delta t))\Big)^T \mathbb{M}_{\mathscr{F}}\Big(B_h^{n+1/2} - \mathcal{I}^{\mathscr{F}}(B((n+1/2)\Delta t))\Big)}{\mathcal{I}^{\mathscr{F}}(B((n+1/2)\Delta t))^T \mathbb{M}_{\mathscr{F}}\mathcal{I}^{\mathscr{F}}(B((n+1/2)\Delta t))} \tag{5.5.5}$$

To compute dispersion errors we perform a parameter estimation problem problem. Namely we collect a time history of the functions $\{\mathbf{E}_e^n\}_{n=1}^N$ and $\{H_f^{n+1/2}\}_{n=1}^N$ at an edge e and face

f. We construct a model of the exact solution by

$$d_e^n = a_h \cos(\omega_h n \Delta t) \quad \text{for field } \mathbf{E}, \tag{5.5.6}$$

$$d_f^{n+1/2} = \frac{k_x^2 + k_y^2}{\omega_h} \sin(\omega_h (n+1/2)\Delta t) \quad \text{for field } B. \tag{5.5.7}$$

When find two independent (a_h, ω_h) which each minimize one of

$$\min_{a_h \in \mathbb{R}, \omega_h \geq 0} \sum_{n=1}^{N} |d_e^n - \mathbf{E}_e^n|^2, \qquad \min_{a_h, \omega_h \geq 0} \sum_{n=1}^{N} |d_f^{n+1/2} - B_f^{n+1/2}|. \tag{5.5.8}$$

To solve the problem we use Levenburg-Marquarte and enforce the constraint $\omega \geq 0$ in order to the appropriate root using a pull-back method. We use the exact solution ω as our initial guess but require a very accurate solution by selecting our relative residual tolerance as 10^{-13}. Each estimation problem is done separately and defines an error

$$\mathcal{E}_{\text{disp}}(\mathbf{U}) = \frac{|\omega_h - \omega|}{|\omega|}, \quad \mathbf{U} = \{\mathbf{E}_h^n\}_{n=1}^N, \{B_h^{n+1/2}\}_{n=1}^N. \tag{5.5.9}$$

In this section we will present two experiments. The first will show L^2 and dispersion errors for a first order formulation of the m-adapted MFD while the second experiment presents results for a second order formulation with the field B eliminated.

Our method optimization can be interpreted by way of a local truncation error analysis for a plane wave Ansatz. For this reason, dispersion error reduction should translate to reduced local truncation error for a plane waves. The Fourier mode exact solution presented in Equation (5.5.2) is exactly the super position of four plane waves with distinct directions of propagation

$$\mathbf{k}_1 = (k_x, k_y)^T, \quad \mathbf{k}_2 = (-k_x, k_y)^T, \quad \mathbf{k}_3 = (-k_x, -k_y)^T, \quad \mathbf{k}_4 = (k_x, -k_y)^T, \tag{5.5.10}$$

$$\mathbf{E} = \sum_{i=1}^{4} \frac{\mathbf{k}_i^{\perp}}{k_i} \mathrm{e}^{\mathrm{i}(\mathbf{k}_i \cdot \mathbf{x} - \omega t)}, \quad (\mathbf{k}_i^{\perp})^T \mathbf{k}_i = 0. \tag{5.5.11}$$

For this reason, we expect to recover order four L^2 errors for the M-adapted MFD for a Fourier mode.

Experiment 3. In this first experiment we consider a first order system formulation of an MFD discretization of the initial boundary value problem described in Equation (5.5.1). For convenience we include the first order formulation below:

$$\begin{cases} \mathbf{E}_h^{n+1} = \mathbf{E}_h^n + \Delta t \mathbb{W}_{\mathscr{E}} \text{curl}_h^T \mathbb{M}_{\mathscr{F}} B_h^{n+1/2} & 0 \leq n \leq N \\ B_h^{n+1/2} = B_h^{n-1/2} - \Delta t \text{curl}_h \mathbf{E}_h^n & 1 \leq n \leq N \\ \mathbf{E}_h^0 = \mathcal{I}^{\mathscr{E}_h}((-k_y \cos(k_x x)\sin(k_y y), (k_x \sin(k_x x)\cos(k_y y))^T) & \\ B_h^{1/2} = \mathcal{I}^{\mathscr{F}_h}(\frac{k_x^2+k_y^2}{\omega}\sin(\omega \Delta t/2)\cos(k_x x)\cos(k_y y)) & \end{cases} \tag{5.5.12}$$

To compute initial conditions we use exact integration for all degrees of freedom assuming $k_x = k_y = \pi$. For reference we also provide results for the Yee scheme which can be easily computed by choosing $\mathbb{W}_{\mathscr{E}} = \frac{1}{\Delta x \Delta y}\mathbb{I}$.

For results see Tables 5.1 and 5.2 as well as Figures 5.2 and 5.3. Using the first order formulation we find that while errors and rates are superior to the Yee scheme. However, we do not recover the theoretically optimal order four errors in both dispersion and L^2 errors for our Fourier mode.

It is unclear exactly the what the source of this error is. However, the improved accuracy and super-quadratic rates for MFD suggest that the method may be very close to performing optimally.

TABLE 5.1: Relative L^2 errors for a first order formulation of the MFD and Yee Schemes.

	Electric Field **E**				Magnetic Induction B			
$\log_2(h)$	Yee	rate	MFD	rate	Yee	rate	MFD	rate
-4	2.3233e+00		1.6494e-01		1.7785e+00		4.4583e-01	
-5	5.6606e-01	2.04	1.0759e-02	3.94	8.8462e-01	1.00	4.5181e-02	3.30
-6	1.3686e-01	2.05	7.3857e-04	3.86	2.2969e-01	1.95	7.6301e-03	2.57
-7	3.3865e-02	2.02	5.4404e-05	3.76	5.5913e-02	2.04	1.7050e-03	2.16
-8	8.4427e-03	2.00	4.4298e-06	3.62	1.3631e-02	2.03	4.1452e-04	2.04

TABLE 5.2: Relative dispersion errors for a first order formulation of the MFD and Yee Schemes.

	Electric Field **E**				Magnetic Induction B			
$\log_2(h)$	Yee	rate	MFD	rate	Yee	rate	MFD	rate
-4	1.3277e-02		9.9181e-04		1.3276e-02		9.9255e-04	
-5	3.2437e-03	2.03	6.6906e-05	3.89	3.2438e-03	2.03	6.6991e-05	3.89
-6	8.0570e-04	2.01	4.7613e-06	3.81	8.0571e-04	2.01	4.7722e-06	3.81
-7	2.0103e-04	2.00	3.6955e-07	3.69	2.0103e-04	2.00	3.7090e-07	3.69
-8	5.0223e-05	2.00	3.2085e-08	3.53	5.0223e-05	2.00	3.2252e-08	3.52

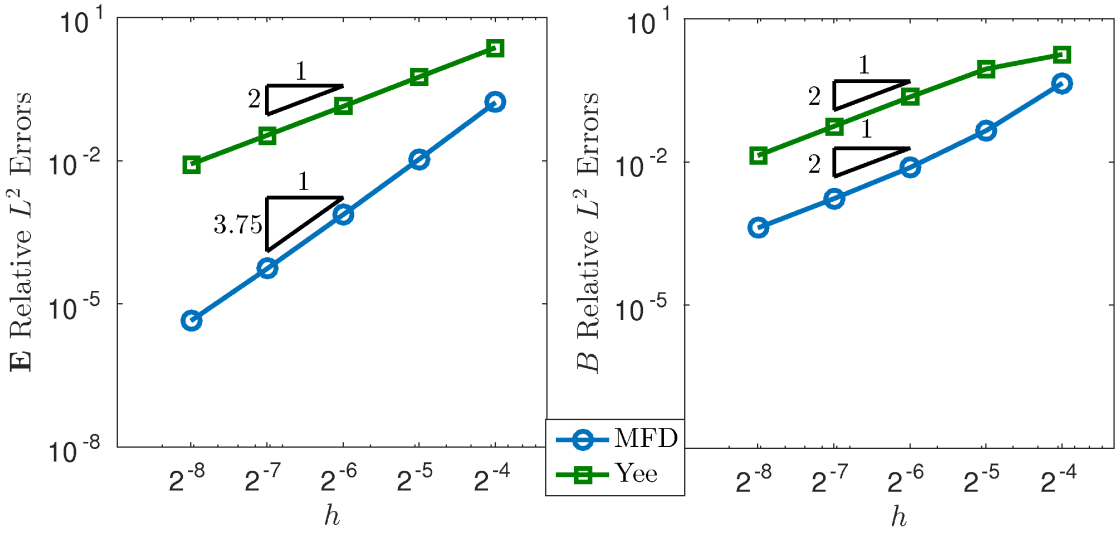

FIGURE 5.2: L^2 errors for **E** and B for a first order formulation of m-adapted MFD discretization. Errors appear super-quadratic but bellow theoretical estimates

Experiment 4. In this experiment we consider a second order or **Vector Wave** formulation of the MFD to discretize (5.5.1).

$$\begin{cases} \mathbf{E}_h^{n+1} = 2\mathbf{E}_h^n - \mathbf{E}_h^{n-1} - \Delta t^2 \mathbb{W}_{\mathscr{E}} \mathrm{curl}_h^T \mathbb{M}_{\mathscr{F}} \mathrm{curl}_h \mathbf{E}_h^n & 1 \le n \le N \\ \mathbf{E}_h^0 = \mathcal{I}^{\mathscr{E}_h}((-k_y \cos(k_x x)\sin(k_y y), (k_x \sin(k_x x)\cos(k_y y))^T) \\ \mathbf{E}_h^{-1} = \cos(-\omega\Delta t)\mathcal{I}^{\mathscr{E}_h}((-k_y \cos(k_x x)\sin(k_y y), (k_x \sin(k_x x)\cos(k_y y))^T) \end{cases} \tag{5.5.13}$$

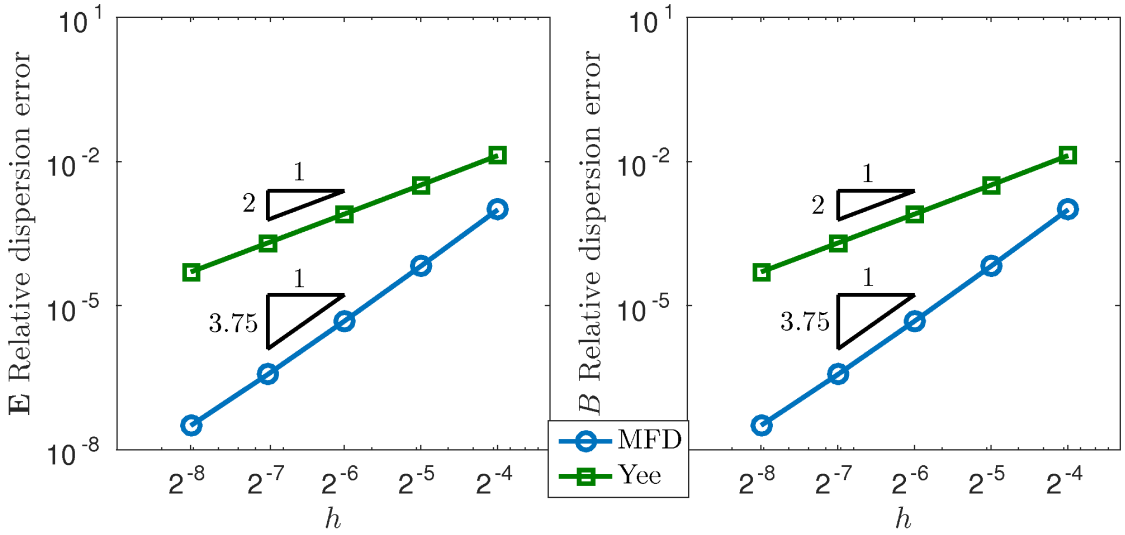

FIGURE 5.3: Dispersion errors for **E** and B for a first order formulation of m-adapted MFD discretization. Errors appear super-quadratic but bellow theoretical estimates

For this experiment we calculate our initial conditions exactly assuming $k_x = k_y = \pi$. See Table 5.3 and Figure 5.4 for results. In the second order, vector wave formulation we recover theoretically optimal dispersion error and L^2 error convergence for both the MFD and Yee formulations.

TABLE 5.3: Relative errors for a vector wave formulation of the MFD and Yee Schemes.

	Relative L^2 errors				Relative dispersion errors			
$\log_2(h)$	Yee	rate	MFD	rate	Yee	rate	MFD	rate
-4	2.3316e+00		1.5734e-01		1.3355e-02		9.2767e-04	
-5	5.6721e-01	2.04	9.7352e-03	4.01	3.2530e-03	2.04	5.8003e-05	4.00
-6	1.3699e-01	2.05	6.0779e-04	4.00	8.0685e-04	2.01	3.6209e-06	4.00
-7	3.3882e-02	2.02	3.7964e-05	4.00	2.0117e-04	2.00	2.2608e-07	4.00
-8	8.4447e-03	2.00	2.3718e-06	4.00	5.0241e-05	2.00	1.4122e-08	4.00

These experiments highlight a strong sensitivity to initial conditions– namely by the suboptimal results in the first order formulation. Future work will be devoted to finding a

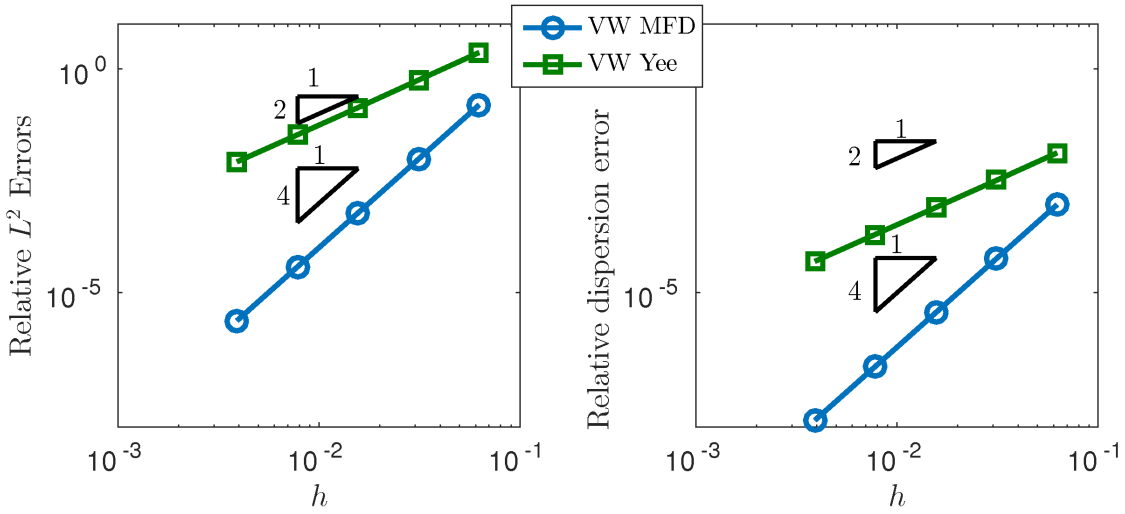

FIGURE 5.4: Using a second order formulation of MFD we recover theoretically optimal errors.

quadrature for initial conditions which provides optimal rates of convergence for the first order formulation.

5.5.2 L^2 and Dispersion errors for Cold Isotropic Plasma

For our experiments we introduce a change of variables for $\mathbb{X}$ which allows for an easier formulation of the matrix exponential.

$$\mathbb{X} = \begin{pmatrix} 0 & -\epsilon_0^{-1} \\ \epsilon_0(\alpha^2+\beta^2) & 2\alpha \end{pmatrix}, \quad \alpha = -\frac{\omega_i}{2}, \ \beta = \frac{\sqrt{4\omega_P^2 - \omega_i^2}}{2}. \tag{5.5.14}$$

The ODE system governing the cold plasma model is a classical damped, driven oscillator. For different values of the parameters the character of the system changes. We present results for the case when the system is under damped ($\omega_i^2 < 4\omega_p^2$). The matrix exponential for $\mathbb{X}\Delta t$ is given by

$$e^{\mathbb{X}\Delta t} = e^{\alpha\Delta t}\begin{pmatrix} \cos(\beta\Delta t) - \alpha\dfrac{\sin(\beta\Delta t)}{\beta} & -\dfrac{\sin(\beta\Delta t)}{\epsilon_0\beta} \\ \epsilon_0(\alpha^2+\beta^2)\dfrac{\sin(\beta\Delta t)}{\beta} & \cos(\beta\Delta t) + \alpha\dfrac{\sin(\beta\Delta t)}{\beta} \end{pmatrix} := \begin{pmatrix} \alpha_1 & \alpha_2 \\ \beta_2 & \beta_1 \end{pmatrix}. \tag{5.5.15}$$

The integral of this matrix is given by

$$\int_0^{\Delta t} \mathrm{e}^{\mathbb{X}s}\, ds = \begin{pmatrix} \alpha_3 & \alpha_4 \\ \beta_3 & \beta_4 \end{pmatrix}, \tag{5.5.16}$$

where the coefficients in the matrix above are defined as

$$\alpha_3 := \frac{1}{\beta}\left(\frac{\mathrm{e}^{\alpha\Delta t}(2\alpha\beta\cos(\beta\Delta t) + (\beta^2-\alpha^2)\sin(\beta\Delta t)) - 2\alpha\beta}{\alpha^2+\beta^2}\right), \tag{5.5.17}$$

$$\alpha_4 := \frac{1}{\beta}\left(-\frac{\beta - \mathrm{e}^{\alpha\Delta t}(\alpha\sin(\beta\Delta t) - \beta\cos(\beta\Delta t))}{\epsilon_0(\alpha^2+\beta^2)}\right), \tag{5.5.18}$$

$$\beta_3 := \frac{1}{\beta}\left(\epsilon_0(\beta + \mathrm{e}^{\alpha\Delta t}(\alpha\sin(\beta\Delta t) - \beta\cos(\beta\Delta t)))\right), \tag{5.5.19}$$

$$\beta_4 := \frac{1}{\beta}\left(\mathrm{e}^{\alpha\Delta t}\sin(\beta\Delta t)\right). \tag{5.5.20}$$

The second order formulation for the discrete electric field $\mathbf{E}$ and polarization current density $\mathbf{J}$, as introduced in Section 5.4, was a convenient formulation of the discrete ETMFD method for the analysis of numerical dispersion. However, in our numerical experiments we have found that L^2 errors in the second order system for $\mathbf{E}$ and $\mathbf{J}$ are very sensitive to the choice of initial conditions. Thus, for our numerical simulations we will use a different formulation of the discrete ETMFD method, with an equivalent numerical dispersion relation, that retains the second order discrete evolution equation for the electric field, but uses a first order discrete evolution equation for the polarization current density $\mathbf{J}$. Since the focus of this paper is on numerical dispersion optimized methods, we do not investigate the appropriate initialization of the discrete ETMFD scheme here. We defer this investigation to future work.

The hybrid second order evolution equation for the discrete electric field $\mathbf{E}$ and first order evolution equation for the polarization density $\mathbf{J}$ is given as

$$\mathbf{E}_h^{n+1} = (1+\alpha_1)\mathbf{E}_h^n + \alpha_2\mathbf{J}_h^n - \alpha_1\mathbf{E}_h^{n-1} - \alpha_2\mathbf{J}_h^{n-1} - c_0^2\Delta t\alpha_3\mathbb{W}_{\mathscr{E}}\mathbb{A}_h\mathbf{E}_h^n \quad n \geq 2, \tag{5.5.21}$$

$$\mathbf{J}_h^{n+1} = \beta_1\mathbf{J}_h^n + \beta_2\mathbf{E}_h^n + \frac{\beta_3}{\alpha_3}(\mathbf{E}_h^{n+1} - \alpha_1\mathbf{E}_h^n - \alpha_2\mathbf{J}_h^n) \quad n \geq 1. \tag{5.5.22}$$

This formulation is explicit when we compute $\mathbf{E}^{n+1}$ before $\mathbf{J}^{n+1}$. It requires three initial conditions given by

$$\mathbf{E}_h^0 = \mathcal{I}^{\mathscr{E}_h}(\mathbf{E}(0)), \qquad \mathbf{E}_h^1 = \mathcal{I}^{\mathscr{E}_h}(\mathbf{E}(\Delta t)), \qquad \mathbf{J}_h^0 = \mathcal{I}^{\mathscr{E}_h}(\mathbf{J}(0)). \tag{5.5.23}$$

In our numerical simulations we used a midpoint quadrature on every edge for $\mathbf{E}_h$ and computed $\mathbf{J}_h$ exactly; i.e.,

$$\mathbf{E}_{h|e}^j = \boldsymbol{\tau}_e \cdot \mathbf{E}(x_c, y_c, j\Delta t), \quad j = \{0, 1\}, \qquad \mathbf{J}_{h|e}^0 = \frac{1}{|e|}\int_e \mathbf{J}(x, y, 0) \cdot \boldsymbol{\tau}_e ds. \tag{5.5.24}$$

The following experiment will make use of this stencil to show the accuracy of the scheme.

Experiment 5. We will investigate the accuracy of our ETMFD method for discretizing problems with a known exact solution. For $\mathbf{k} = (k_x, k_y)^T$ with $k_x, k_y \in \pi\mathbb{Z}$, let $a + \mathrm{i}b = \omega$ be a (complex) root of the dispersion relation (5.3.38). We consider the exact solution for the Maxwell-CIP model given by

$$\mathbf{E}(x, y, t) = \mathrm{e}^{at}\cos(bt)\begin{pmatrix} -k_y \cos(k_x x)\sin(k_y y) \\ k_x \sin(k_x x)\cos(k_y y) \end{pmatrix}, \tag{5.5.25}$$

$$\mathbf{J}(x, y, t) = \epsilon_0 \omega_p^2 \mathrm{e}^{at}\frac{(a + \omega_i)\cos(bt) + b\sin(bt)}{b^2 + (a + \omega_i)^2}\begin{pmatrix} -k_y \cos(k_x x)\sin(k_y y) \\ k_x \sin(k_x x)\cos(k_y y) \end{pmatrix}. \tag{5.5.26}$$

For our experiments we consider $\omega_P = \omega_i = \epsilon_0 = c = 1$ and $k_x = k_y = \pi$. For this we have $a \approx 0.023$ and $b \approx 4.55$. We choose the final time to be $T = 4$. To calculate relative L^2 errors we use an appropriate inner product, based on our mimetic discretization, which is defined as

$$\mathcal{E}_{L^2}^h(\mathbf{F}_h^n) := \frac{\sqrt{(\mathbf{F}_h^n - \mathcal{I}^{\mathscr{E}_h}(\mathbf{F}(n\Delta t))^T \mathbb{M}_{\mathscr{E}}(\mathbf{F}_h^n - \mathcal{I}^{\mathscr{E}_h}(\mathbf{F}(n\Delta t))}}{\sqrt{\mathcal{I}^{\mathscr{E}_h}(\mathbf{F}(n\Delta t))^T \mathbb{M}_{\mathscr{E}} \mathcal{I}^{\mathscr{E}_h}(\mathbf{F}(n\Delta t))}}, \tag{5.5.27}$$

where $\mathbf{F}_h^n = (\mathbf{E}_h^n, \mathbf{J}_h^n)^T$.

To define the dispersion error we fit an appropriate temporal function, $F(t : \omega_h)$, to temporal grid data $\{\mathbf{E}_{h,e_i}^n\}_{n=0}^N$ at some edge e_i to find the best discrete frequency w_h.

To calculate the relative dispersion errors, we perform the following procedure. If (a_h, b_h) is the result of the non-linear least squares fitting of time tracking data $\{\mathbf{F}^n_{h|e}\}_{n=1}^N$ to the appropriate function $(\exp(a_h t)\cos(b_h t)$ for the electric field and $\epsilon_0\omega_p^2 \mathrm{e}^{a_h t}\frac{(a_h+\omega_i)\cos(b_h t)+b_h\sin(b_h t)}{b_h^2+(a_h+\omega_i)^2}$ for the current density) then we define the relative dispersion error by

$$\mathcal{E}_d^h(\mathbf{F}_h) := \sqrt{\frac{(a-a_h)^2+(b-b_h)^2}{a^2+b^2}} \tag{5.5.28}$$

where a, b are the true data. For comparison, we have also performed our simulations with the corresponding ET-Yee scheme (i.e., Yee spatial staggering with ETD), which is second order accurate in space and time. In Table 5.4 we present relative L^2 errors in the electric field and polarization density, while in Table 5.5 we present relative dispersion errors for the electric field and polarization density, respectively. Figures 5.5, and 5.6 plot the results of Tables 5.4-5.5. Our results indicate fourth order dispersion and L^2 error convergence for the ETMFD as compared to the corresponding (well known) second order convergence for the ET-Yee scheme.

TABLE 5.4: Relative L^2 Errors for Experiment 2.

	Electric Field, **E**				Current Density, **J**			
$\log_2(h)$	ET-Yee	rate	ETMFD	rate	ET-Yee	rate	ETMFD	rate
-4	1.1024e-02		4.8495e-05		3.0064e-02		1.3322e-04	
-5	2.7237e-03	2.0170	3.0206e-06	4.0049	7.4940e-03	2.0042	8.3901e-06	3.9890
-6	6.7826e-04	2.0057	1.8844e-07	4.0026	1.8704e-03	2.0024	5.3485e-07	3.9715
-7	1.6931e-04	2.0021	1.1767e-08	4.0013	4.6717e-04	2.0013	3.4784e-08	3.9426
-8	4.2303e-05	2.0009	7.3501e-10	4.0008	1.1674e-04	2.0007	2.3361e-09	3.8963

5.5.3 Numerical Anisotropy in Free Space

In this section we will present two experiments. The first will be a semi-analytic calculation of dispersion error for the M-adapted MFD. In the second experiment we con-

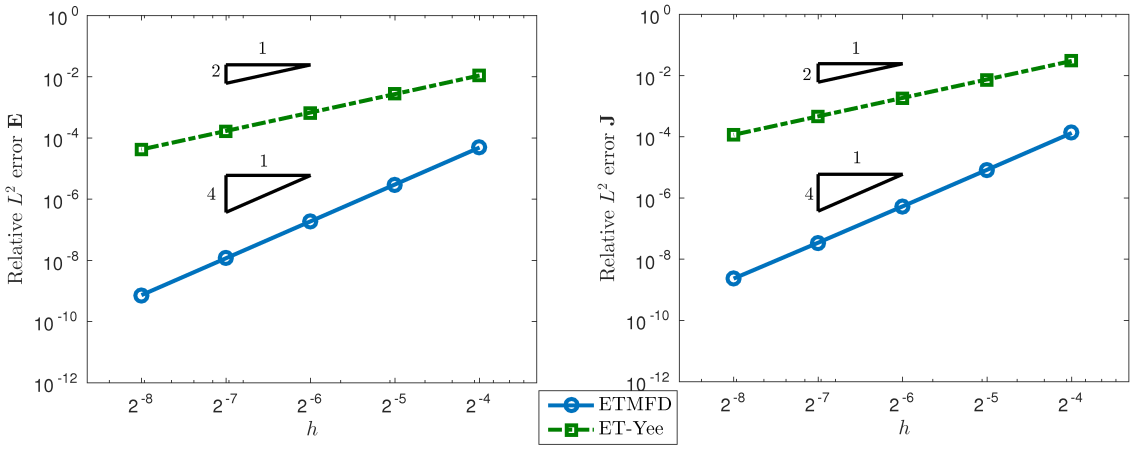

FIGURE 5.5: Relative L^2 errors for Experiment 2.

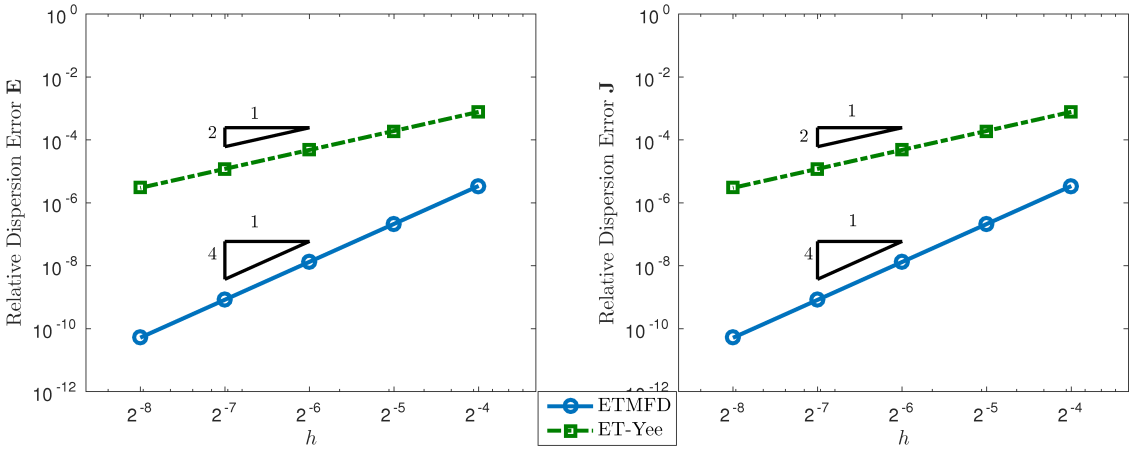

FIGURE 5.6: Relative dispersion errors for Experiment 2.

TABLE 5.5: Relative Dispersion Errors for Experiment 2.

	Electric Field, **E**				Current Density, **J**			
$\log_2(h)$	ET-Yee	rate	ETMFD	rate	ET-Yee	rate	ETMFD	rate
-4	7.7638e-04		3.4427e-06		8.7152e-04		3.4530e-06	
-5	1.9280e-04	2.0129	2.1407e-07	4.0080	2.1720e-04	2.0045	2.1487e-07	4.0063
-6	4.8070e-05	2.0066	1.3345e-08	4.0042	5.4246e-05	2.0014	1.3399e-08	4.0032
-7	1.2002e-05	2.0033	8.3287e-10	4.0021	1.3557e-05	2.0005	8.3655e-10	4.0016
-8	2.9985e-06	2.0017	5.1994e-11	3.9892	3.3886e-06	2.0003	5.2097e-11	4.0052

sider a radially symmetric pulse generated by Gaussian initial data we will then quantify the point-wise error along a circle relative to a well resolved reference solution.

Experiment 6. In this first experiment we compute the effect of angle of propagation on dispersion with the theory developed in the previous section. In particular we consider a root of the continuous dispersion relationship

$$(\omega, \mathbf{k}) : \omega = c^2 k^2 \tag{5.5.29}$$

where $\mathbf{k} = k(\cos\theta, \sin\theta)^T$. Throughout the section we consider experiment value of k, namely 4 and consider the wave speed $c = 1$. We assume the Courant number $\nu = \frac{1}{2}$. We define the dispersion error then as

$$\mathcal{E}_{\text{disp}}(\theta) = \frac{|\mathcal{T}_{\Delta t}(\omega) - \mathcal{S}_h(\mathbf{k})|}{\omega}. \tag{5.5.30}$$

Figure 5.7 shows our the results of varying θ in several cases. These plots are log-polar. Namely that the radius is determined by the log of the error. A circle on this diagram would represent an isotropic dispersion error. In subfigure (a) we have hold $\alpha = 1$ and consider the effect of refinement. Namely we choose h such that we guarantee 12 and 24 points per wavelength. We provide comparison to the Yee scheme for reference. This shows that the M-adapted MFD is anisotropic but that the magnitude of dispersion errors is significantly reduced in comparison to the Yee scheme.

In subfigure (b) we show the effect of varying the aspect ratio on the dispersion errors. Here we fix h to guarantee 48 points per wavelength. We then choose $\alpha = 4, 1, \frac{1}{4}$. This shows that dispersion error can be reduced in the direction of increased refinement at the expense of larger errors in the unrefined directions. It also appears that the dispersion minimizing angles change as function of α. For $\alpha = 1$ these angles are clearly $\theta = \pi/4 + n\pi$.

Experiment 7. In this experiment we will demonstrate qualitative agreement with the previous experiment by considering the case of $c = 1$ and an initial value problem on the

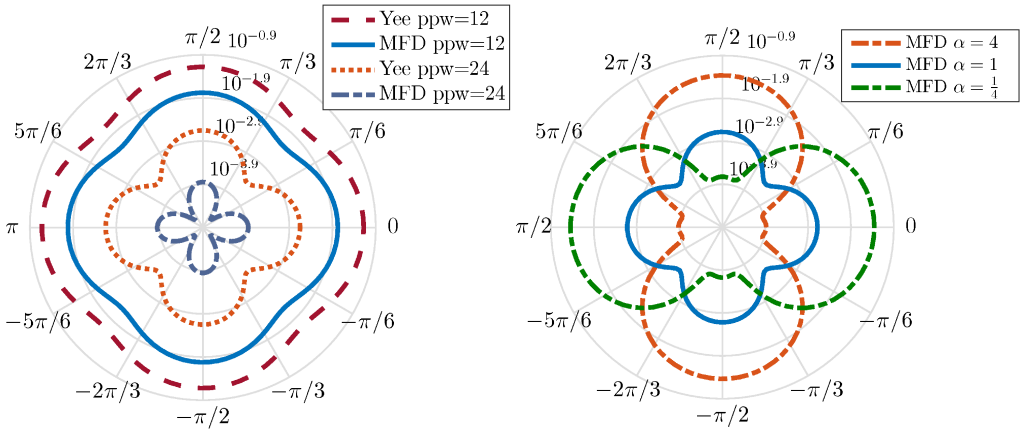

(a) (b)

FIGURE 5.7: (a) comparison of dispersion errors of the m-adapted MFD and the Yee scheme as a function of angle of propagation θ. Model parameters are $c = 1, k = 4$ solutions are calculated at 12 and 24 points per wavelength. (b) a comparison of dispersion errors for three aspect ratios. Here $c = 1, k = 4$ and we chose 48 h to such that there were 48 points per wavelength.

square $[0, 6]^2$ where

$$\frac{\partial}{\partial t}\mathbf{E} = \mathbf{curl}B \qquad \frac{\partial}{\partial t}B = -\text{curl}\mathbf{E} \tag{5.5.31}$$

$$\mathbf{E}(0) = \mathbf{0}, \qquad B(0) = 100\mathrm{e}^{-100((x-3)^2+(y-3)^2)}. \tag{5.5.32}$$

We advance the solution to a final time of $T = 2.5$ to avoid reflections off of the boundary. We will advance the solution using a second order stencil in B:

$$B_h^{n+1} = 2B_h^n - B_h^{n-1} - c^2\Delta t^2 \text{curl}_h\widetilde{\text{curl}}_h B^n. \tag{5.5.33}$$

Figures 5.8 and 5.9 show the B field at this time with different colorings, proportional to B and proportional $\log_{10}|B|$ respectively. Subfigures (a) show the Yee scheme while subfigures (b) show the m-adapted MFD. For the Yee scheme we see significant dispersion in aligned with the x and y axis as high frequency content of the pulse lags behind the front. In addition the Yee scheme also displays some of the wave dispersing ahead of the front, although this is mostly visible in the log colored plot.

M-adapted MFD also shows some spurious oscillations lagging behind the wave front

but the general effect is radially symmetric showing that reducing the order of dispersion error reduces the anisotropy.

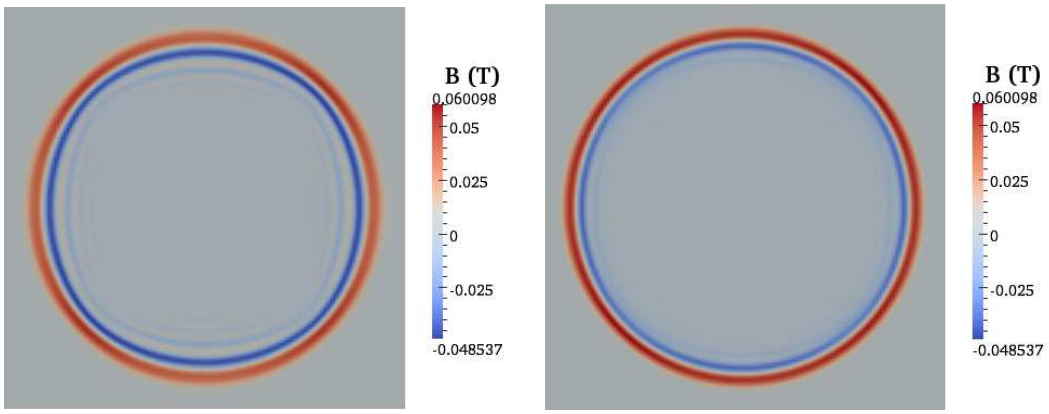

(a) (b)

FIGURE 5.8: Yee scheme and M-adapted MFD propagating a radially symmetric pulse in free space generated by initial conditions $\mathbf{E} = 0$ and $B(0) = \mathrm{e}^{-100|\mathbf{x}-(3,3)^T|^2}$ on $[0,6]^2$. We chose $c = 1$ and $\nu = \frac{1}{2}$. We performed time integration until $T = 2.5$. (a) shows the Yee Scheme and (b) shows the m-adapted MFD

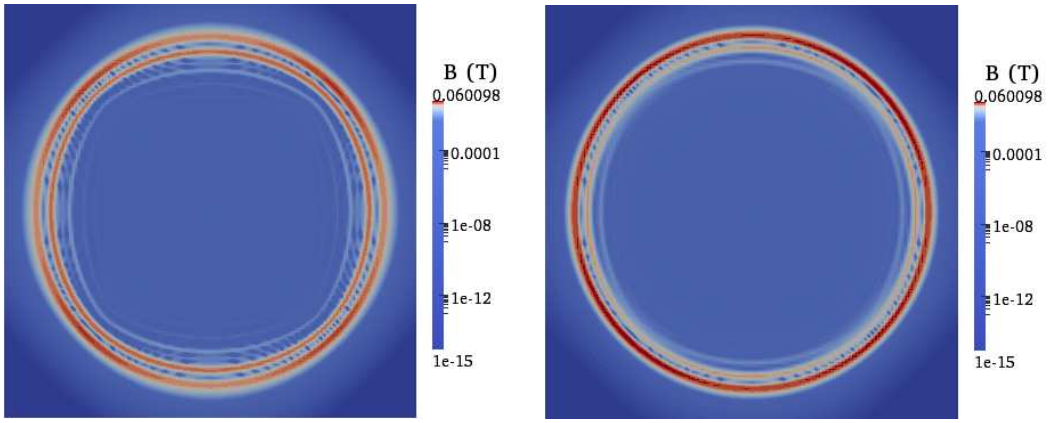

(a) (b)

FIGURE 5.9: Same experiment as Figure 5.8 but coloring by $\log_{10}|H|$.

To quantify these qualitative results we will sample the function H_h on a circle which is roughly in the center of the wave front after 2.5 seconds. We can then plot the amplitude of H_h to show the effect of numerical anisotropy. To compute errors we can

compare course grid solutions to a very well resolved numerical approximation.

Consider the circle centered at $\mathbf{x}_c = (x_c, y_c)$ of radius r, call this circle $\Gamma_r(x_c, y_c)$. Points in $\Gamma_r(x_c, y_c)$ can be parameterized uniquely by

$$\Gamma_r = \{(r\cos\theta + x_c, r\sin\theta + y_c), \theta \in [0, 2\pi)\}. \tag{5.5.34}$$

Let $\{\theta_n\}_{n=1}^N$ be a collection of angles uniformly spaced in in $[0, 2\pi)$. Define the sampled points

$$\Gamma_N = \{(r\cos\theta_n + x_c, r\sin\theta_n + y_c) : 1 \leq n \leq N\}. \tag{5.5.35}$$

Call the collection of all barycenters of faces $X_{\mathscr{F}}$. A point $\mathbf{x} \in {}_N$ lies in the face f if the barycenter of f minimizes the distance to $\mathbf{x}$ over the collection of all barycenters. As the reconstruction of B_h on every face is constant we are justified in stating that H_h's restriction to Γ_N is B_h's value at all faces in which points in Γ_N lie.

For our experiment we choose our circle as $\Gamma_{2.54}(3, 3)$ (defined as (5.5.34)) and compute a reference solution using the M-adapted MFD with $h = 2^{-11}$. The amplitudes of our computed waves for both the MFD and Yee schemes have obvious numerical anisotropy at a resolution of $h = 2^{-7}$ with the M-adapted MFD closer to reference than Yee. When we double the resolution to $h = 2^{-8}$ both schemes perform significantly better; however M-adapted MFD is still closer to reference than the Yee scheme. In order to quantify this visual improvement we consider the relative error

$$\frac{|B_{\Gamma_N} - B^\star_{\Gamma_N}|}{|B^\star_{\Gamma_N}|}, \tag{5.5.36}$$

Where $B^\star_{\Gamma_N}$ is the value of the reference solution. Here we see that the relative error of the MFD is completely contained in the error of the Yee scheme at both resolutions. The roughness of these diagrams is due to the piece-wise constant reconstruction of the field B_h. See Figures 5.10 and 5.11 for results.

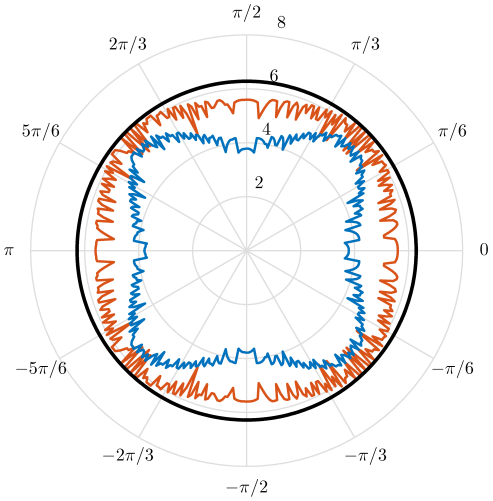

$h = 2^{-7}$

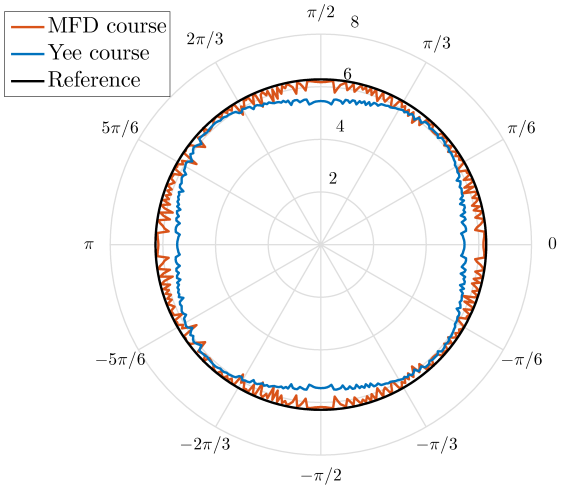

$h = 2^{-8}$

FIGURE 5.10: We present the amplitude of the discrete field B_h along the circle of radius 2.54 centered at $(3, 3)$. We compute a reference solution with $h = 2^{-11}$ using the M-adapted MFD.

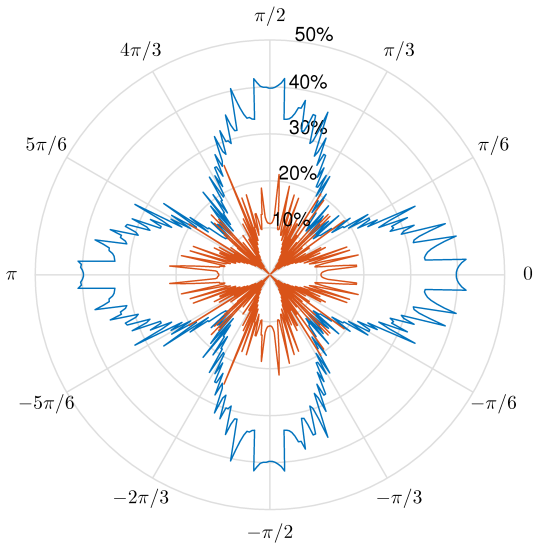

$h = 2^{-7}$

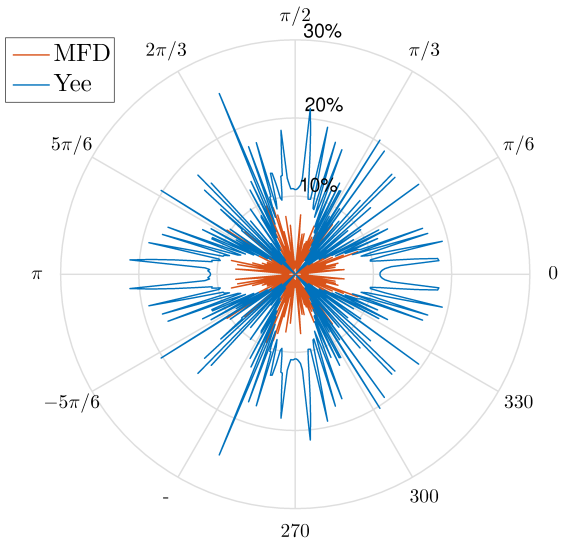

$h = 2^{-8}$

FIGURE 5.11: Point-wise relative error of the M-adapted MFD and Yee scheme along the circle of radius 2.54 centered at $(3, 3)$.

5.5.4 Numerical Anisotropy in Debye Media

Similar to the previous experiment in this section we will consider the numerical anisotropy of the ETMFD for a Debye medium.

Experiment 8. Consider a ETMFD TM formulation of Maxwell-Debye with the magnetic field eliminated.

$$\begin{cases} E_h^{n+1} = (1+a_1)E_h^n + a2P_h^n - a_1E_h^{n-1} - a_2P_h^{n-2} - c_0^2\mathrm{curl}_h\widetilde{\mathrm{curl}}_hE_h^n \\ P_h^{n+1} = b_1E_h^n + b_2P_h^n + \frac{b_3}{b_2}(E_h^{n+1} - a_1E_h^n - a_2J_h^n) \\ E_h^0 = E_h^{-1} = \mathcal{I}^{\mathscr{F}_h}(100\exp(-100((x-3)^2+(y-3)^2))) \\ P^0 = \mathcal{I}^{\mathscr{F}_h}(0) \end{cases} \tag{5.5.37}$$

where the following definitions hold

$$\widetilde{\mathrm{curl}}_h = \mathbb{W}_{\mathscr{E}}\mathrm{curl}_h^T\mathbb{M}_{\mathscr{F}}, \qquad \mathbb{X} = \frac{1}{\tau}\begin{pmatrix} -\epsilon_\Delta & 1 \\ \epsilon_0\epsilon_\Delta & -1 \end{pmatrix}, \tag{5.5.38}$$

$$\mathrm{e}^{\mathbb{X}\Delta t} = \begin{pmatrix} a_1 & a_2 \\ b_1 & b_2 \end{pmatrix}, \qquad \left(\int_0^{\Delta t}\mathrm{e}^{\mathbb{X}s}\,ds\right) = \begin{pmatrix} a_3 & a_4 \\ b_3 & b_4 \end{pmatrix}. \tag{5.5.39}$$

For this experiment we choose our model parameters $c = 1, \epsilon_\Delta = 4, \tau = \frac{1}{2}$. We will show the function E_h restricted to the circle $\Gamma_{0.8}(3,3)$. In order to quantify the numerical anisotropy of the method we consider relative point-wise errors along this curve at time $T = 3$. As we have no exact solution available we compre a course grid solution with $h = 2^{-7}$ to a reference solution computed with the ETMFD at a resolution of $h = 2^{-10}$. In this case we do not see significant difference between the EMTFD and a Yee scheme with equivalent exponential time integration. In fact, the relative point-wise error for the ET-Yee scheme seems to be outperforming the ETMFD. One possible explanation for this is the dissipative nature of the Yee Scheme.

In the limit of infinite real wave numbers, the imaginary part of ω converges to the value ϵ_Δ. Thus, high frequency content, which we constructed our initial conditions to

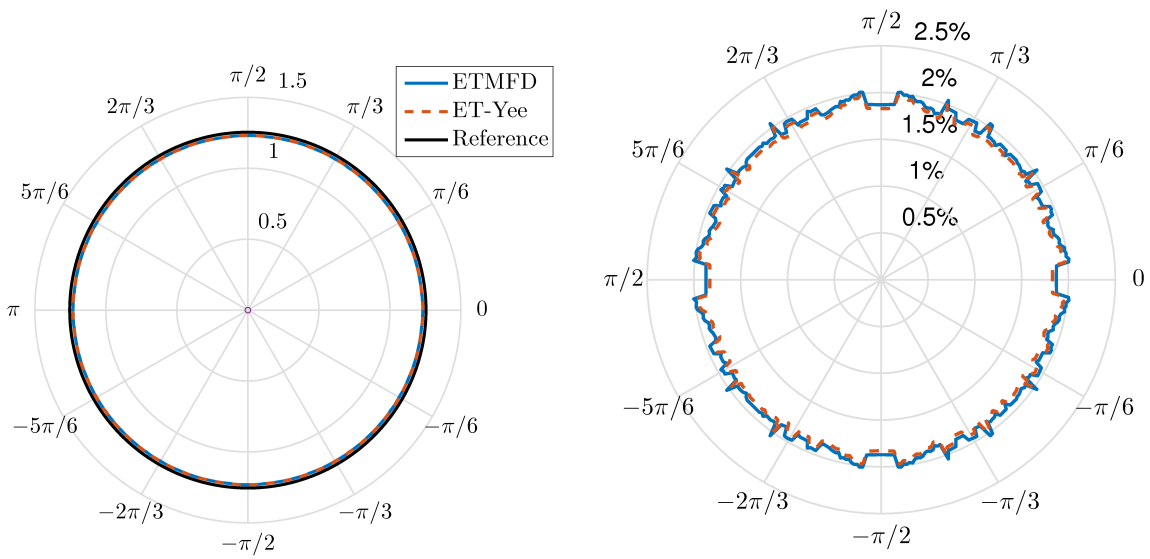

(a) (b)

FIGURE 5.12: We illustrate numerical anisotropy for a Debye medium. (a) shows the amplitude of the electric field along the circle of radius 0.8 centered at (3,3). (b) shows the relative error compared to a reference solution.

contain, are very quickly dissipated from the system. Thus, after even a short time, this high frequency content will be removed from the wave resulting in mostly well resolved frequencies and diminishing the importance of dispersion errors. See Figure 5.12 for illustration. This plot shows the amplitude of the electric field along the circle $\Gamma_{0.8}(3,3)$ and the relative error of this solution compared to reference.

5.5.5 Numerical Anisotropy in Collisionless Cold Plasma

In order to illustrate the reduction of dispersion for a dispersive media, we consider the case of cold plasma. In order to remove the smoothing provided by dissipation we consider the collisionless, or non-dissipative case.

Experiment 9. We will now conduct an experiment identical to 8 for a collisionless cold

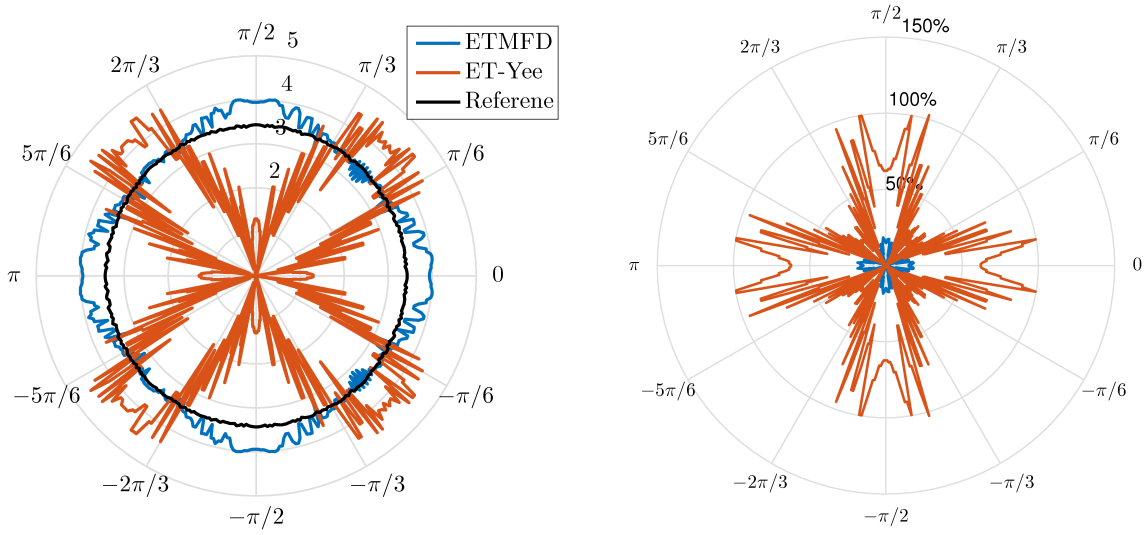

(a) (b)

FIGURE 5.13: We demonstrate levels of numerical anisotropy for a collisionless cold plasma. (a) shows the amplitude of the electric field along the circle of radius 2.01 centered at (3,3). (b) shows the relative error compared to a reference solution.

plasma. Our second order TM formulation is given by

$$\begin{cases} E_h^{n+1} = (1+a_1)E_h^n + a2J_h^n - a_1E_h^{n-1} - a_2J_h^{n-2} - c_0^2\text{curl}_h\widetilde{\text{curl}}_hE_h^n \\ J_h^{n+1} = b_1E_h^n + b_2J_h^n + \frac{b_3}{b_2}(E_h^{n+1} - a_1E_h^n - a_2J_h^n) \\ E_h^0 = E_h^{-1} = \mathcal{I}^{\mathscr{F}_h}(100\exp(-100((x-3)^2+(y-3)^2))) \\ J^0 = \mathcal{I}^{\mathscr{F}_h}(0) \end{cases} \tag{5.5.40}$$

This stencil is identical to the Maxwell-debye case although our parameters a_i, b_i wil lbe different as the matrix $\mathbb{X}$ is defined as

$$\mathbb{X} = \begin{pmatrix} 0 & -\frac{1}{\epsilon} \\ \epsilon\omega_P^2 & 0 \end{pmatrix} \tag{5.5.41}$$

For this experiment we consider $\epsilon = \mu = 1$ and $\omega_P^2 = 12$. We restrict E along the circle $\Gamma_{2.01}(3,3)$ and advance to a time $T = 2.5$. This radius was selected by looking for the midpoint of a wave crest on the reference solution and then applied to the course grid solutions. Our course grid was computed with a resolution $h = 2^{-7}$ and a reference

solution at $h = 2^{-10}$ In this case we the ETMFD significantly outperforming the ET-Yee scheme. It appears that the Yee scheme has values lagging significantly behind the reference solution, resulting in close to one hundred percent relative error. See Figure 5.13.

6 VON NEUMANN STABILITY ANALYSIS FOR M-ADAPTED MFD

In this chapter we will prove that the M-Adapted methods constructed in Chapter 5 are stable– in particular we will show necessary conditions for stability using von Neumann Analysis.

In Section 6.1 we will provide a brief introduction to von Neumann analysis. In Section 6.2 we will prove necessary conditions for stability. In Section 6.3 we will present numerical evidence of the sufficiency of our necessary conditions.

6.1 Preliminaries

Stability of a time integration method is roughly that numerical errors, both discretization and truncation, do not grow during time integration. We consider a classical approach to proving the stability of the M-adapted MFD methods. In particular, we proceed with a technique refered to as *von Neumann Analysis*. In von Neumann analysis we seek to prove that the numerical scheme does not result in an increase in the amplitude of plane waves. In general this approach results only in necessary conditions for stability – as certainly any stable method would be stable for plane waves. However, for many discretizations the bound by von Neumann analysis will be exactly the sufficient condition.

Definition 6.1.1. A polynomial p is a **simple von Neumann polynomial** if for every root of z_i of p, all of p's roots lie within the closed unit disc of the complex plane and no root on the unit circle is repeated.

Definition 6.1.2. Assume some abstract numerical method can be written in the form

$$\mathbf{u}_h^{n+1} = \mathbb{A}_h \mathbf{u}_h^n \tag{6.1.1}$$

where $\mathbb{A}$ is some linear operator. Assume bu_h^n is an interpolation of a plane wave $\mathbf{u}_0 \mathrm{e}^{\mathrm{i}(\mathbf{k}\cdot\mathbf{x})}$ and all other degrees of freedom of $\mathbf{u}_h^n$ are uniquely determined by $\mathbf{u}_{h,0}$. Let $\mathbb{G}$ be the action of the numerical method restricted to $\mathbf{u}_{h,0}$ such that

$$\mathbf{u}_{h,0}^{n+1} = \mathbb{G}\mathbf{u}_{h,0}^n. \tag{6.1.2}$$

We call the matrix $\mathbb{G}$ the **amplification matrix** of the numerical method. Further we say that the numerical method satisfies the **von Neumann stability criteria** if and only if the characteristic polynomial of $\mathbb{G}$ is a simple von Neumann polynomial.

This condition on the characteristic polynomial of $\mathbb{G}$ guarantees that the matrix $\mathbb{G}$ has eigenvalues which lie in the closed unit disc, and as the minimal polynomial divides the characteristic polynomial, that no roots of modulus one are repeated.

To illustrate why this stability condition is necessary consider an abstract amplification matrix $\mathbb{G}$. Suppose that $(\lambda, \mathbf{x})$ is an eigenvalue/vector pair such that $|\lambda| > 1$. Choose $\mathbf{u}_{0,h}^0 = \mathbf{x}$. Then we have

$$\|\mathbf{u}_{0,h}^n\| = \|\mathbb{G}^n \mathbf{u}_{0,h}^0\| = |\lambda|^n \|\mathbf{u}_{0,h}^0\|. \tag{6.1.3}$$

Taking the limit of $n \to \infty$ shows that the norm of this solution will grow exponentially. One might suggest that as long as you avoided the eigenvector $\mathbf{x}$ in initial conditions the method may be practical. However, given that numerical errors are made at every step, we will eventually add some small error $\epsilon\mathbf{x}$ to the value $\mathbf{u}_h^{n+1}$ which would later come to dominate the entire solution due to its exponential growth.

We will make use of the following lemma.

Lemma 6.1.1. *A quadratic polynomial, $z^2+\beta_1 z+\beta_0$ is a simple von Neumann polynomial if and only if*

1. $|\beta_0| = 1$, $\beta_1 = \beta_0\overline{\beta}_1$, *and* $|\beta_1| < 2$ *or*

2. $|\beta_0| < 1$ *and* $|\beta_1 - \beta_0\overline{\beta}_1| < 1 - |\beta_0|^2$.

where $\overline{z}$ *is the complex conjugate of* $z \in \mathbb{C}$.

6.2 Stability Analysis for M-adapted MFD

Having developed the minimal dispersion method from our family of MFD for free space we must now address the stability of this method. Our optimization of dispersion properties did not take into account stability, thus it is now left to us to prove that our choice of parameters is a stable one.

Theorem 6.2.1. *A necessary condition for the* ***M-Adapted MFD for Maxwell's Equations in Free Space****, is* ν_x, ν_y *satisfying the bound*

$$0 \leq \max\{\nu_x, \nu_y\} < \frac{1}{\sqrt{2}}. \tag{6.2.1}$$

Proof. We will proceed with a standard von Neumann analysis approach. That is we assume an initial condition which is a real valued plane-wave in space. We will then rewrite the discrete time evolution as a matrix acting on a few degrees of freedom in a cell f

$$\begin{pmatrix} \mathbf{E}^{n+1}_{(e_1,e_2)} \\ H^{n+3/2}_f \end{pmatrix} = \mathbb{G} \begin{pmatrix} \mathbf{E}^{n}_{(e_1,e_2)} \\ H^{n+1/2}_f \end{pmatrix} \tag{6.2.2}$$

where $\mathbb{G}$ is the amplification matrix. We will call the method stable if $\|\mathbb{G}^n\|$ is bounded in some operator norm. A necessary condition for this is that the spectral radius $\rho(\mathbb{G}) \leq 1$. We will construct a mapping from the pair $(\mathbf{E}^n_{(e_1,e_2)}, H^{n+1/2}_f)$ to the pair $(\mathbf{E}^{n+1}_{(e_1,e_2)}, H^{n+3/2}_f)$. Ampere's law is the most simple.

$$\mathbf{E}^{n+1}_h = \mathbf{E}^n_h + \frac{\Delta t}{\epsilon}\mathbb{W}_{\mathscr{E}}\mathrm{curl}_h\mathbb{M}_{\mathscr{F}}H^{n+1/2}_h \tag{6.2.3}$$

We will have to substitute this step into the equation for $H^{n+3/2}$ and derive

$$H_h^{n+3/2} = H_h^{n+1/2} - \frac{\Delta t}{\mu}\mathrm{curl}_h \mathbf{E}_h^{n+1}, \tag{6.2.4}$$

$$= H_h^{n+1/2} - \frac{\Delta t}{\mu}\mathrm{curl}_h \left(\mathbf{E}_h^n + \frac{\Delta t}{\epsilon}\mathbb{W}_{\mathscr{E}}\mathrm{curl}_h \mathbb{M}_{\mathscr{F}} H_h^{n+1/2}\right), \tag{6.2.5}$$

$$= \left(\mathbb{I} - c_0^2\Delta t^2 \mathrm{curl}_h \mathbb{W}_{\mathscr{E}}\mathrm{curl}_h^T \mathbb{M}_{\mathscr{F}}\right) H_h^{n+1/2} - \frac{\Delta t}{\mu}\mathrm{curl}_h \mathbf{E}_h^n, \tag{6.2.6}$$

By assuming a plane wave Ansatz we arrive at $\mathbb{G}$ given as follow:.

$$\mathbb{G} = \begin{pmatrix} \mathbb{I} & \frac{\Delta t}{\epsilon}\Delta x\Delta y \overline{\mathbb{W}}_{\mathscr{E}} \overline{\mathrm{curl}}_h^{\star} \\ -\frac{\Delta t}{\mu}\overline{\mathrm{curl}}_h & 1 - c_0^2\Delta t^2 \Delta x\Delta y \overline{\mathrm{curl}}_h \overline{\mathbb{W}}_{\mathscr{E}} \overline{\mathrm{curl}}_h^{\star} \end{pmatrix} \tag{6.2.7}$$

The characteristic polynomial of $\mathbb{G}$ is given as

$$p_{\mathbb{G}}(z) := (1-z)(z^2 - \left(2 - c_0^2\Delta t^2 \Delta x\Delta y \overline{\mathrm{curl}}_h \overline{\mathbb{W}}_{\mathscr{E}} \overline{\mathrm{curl}}_h^{\star}\right) z + 1). \tag{6.2.8}$$

We will now attempt to apply the Lemma 6.1.1 to prove that the quadratic has roots in the unit disc.

$$\beta_0 = 1 \qquad \text{and} \qquad \beta_1 = -\left(2 - c_0^2\Delta t^2 \alpha h^2 \overline{\mathrm{curl}}_h \overline{\mathbb{W}}_{\mathscr{E}} \overline{\mathrm{curl}}_h^{\star}\right). \tag{6.2.9}$$

We will now simplify the coefficient β_1. As $\overline{\mathrm{curl}}_h \overline{\mathbb{W}}_{\mathscr{E}} \overline{\mathrm{curl}}_h^{\star}$ is 1×1 we have

$$c_0^2\Delta t^2 \Delta x\Delta y \overline{\mathrm{curl}}_h \overline{\mathbb{W}}_{\mathscr{E}} \overline{\mathrm{curl}}_h^{\star} = c_0^2\Delta t^2 \Delta x\Delta y \mathrm{Tr}(\overline{\mathrm{curl}}_h \overline{\mathbb{W}}_{\mathscr{E}} \overline{\mathrm{curl}}_h^{\star}) \tag{6.2.10}$$

$$= \mathrm{Tr}(\mathbb{W}_{\mathscr{E}} \overline{\mathrm{curl}}_h^{\star} \overline{\mathrm{curl}}_h) \tag{6.2.11}$$

as the trace is invariant under cycle permutations. We calculated $\mathrm{Tr}(\mathbb{W}_{\mathscr{E}} \overline{\mathrm{curl}}_h^{\star} \overline{\mathrm{curl}}_h)$ in Theorem 5.4.4, c.f. Equation (5.4.51). As we are considering the M-adapted scheme we have w_1, w_2, w_3 as in Theorem 5.4.7. Carefully reducing this expression results in the following form:

$$\beta_0 = 1 \qquad \beta_1 = -\left(2 - F(\sin^2\frac{k_x\Delta x}{2}, \sin^2\frac{k_y\Delta y}{2})\right), \tag{6.2.12a}$$

$$F(x,y) = \frac{4}{3}\left(\nu_x^2 x(3 + (1-\nu_x^2)x - \nu_y^2 y) + \nu_y^2 y(3 + (1-\nu_y^2)y - \nu_x^2 x)\right), \tag{6.2.12b}$$

where we again consider

$$\nu_x = \frac{c_0 \Delta t}{\Delta x}, \quad \nu_y = \frac{c_0 \Delta t}{\Delta y}. \tag{6.2.13}$$

By assuming that $0 \leq \nu_x, \nu_y \leq 1$ we know that the function F is maximized on $[0,1]^2$ at the point $(1,1)$

$$F \leq \frac{4}{3}(4 - \nu_x^2 - \nu_y^2)(\nu_x^2 + \nu_y^2). \tag{6.2.14}$$

The condition $|\beta_1| < 2$ reduces to the bound

$$0 < (4 - \nu_x^2 - \nu_y^2)(\nu_x^2 + \nu_y^2) < 3. \tag{6.2.15}$$

The matrix $\mathbb{W}_{\mathscr{E}}$ is SPD if the matrix of parameters

$$\mathbb{C} = \begin{pmatrix} w_1 & w_2 \\ w_2 & w_3 \end{pmatrix} \tag{6.2.16}$$

is positive. If $\mathbb{W}$ is SPD then $F = c_0^2 \Delta x \Delta y \overline{\text{curl}}_h \overline{\mathbb{W}}_{\mathscr{E}} \overline{\text{curl}}_h^{\star}$ is positive. Assuming parameters per Theorem 5.4.7 we have that $\mathbb{C}$ is SPD for $\nu_x^2 \leq 4\frac{\alpha^2}{1+\alpha^2}$. Therefore $\nu_x \leq 2$ implies the bound from below.

$$(4 - \nu_x^2 - \nu_y^2)(\nu_x^2 + \nu_y^2) \leq 2(4 - 2\nu^2)\nu^2. \tag{6.2.17}$$

By choosing

$$\nu < \frac{1}{\sqrt{2}} \tag{6.2.18}$$

we then have

$$2(4 - 2\nu^2)\nu^2 < 3. \tag{6.2.19}$$

Q.E.D.

We will now extend this stability result to include the case of a linear polarization media. Instead of proving stability for a full system, we will instead prove stability for a representative problem– namely for a conductive media whose conductivity can be complex valued. This result is approximately proving stability for a diagonalizable system but neglecting the effects of coupling between the different eigenmodes of the matrix $\mathbb{X}$.

Theorem 6.2.2. *Consider Maxwell's equations with complex conductivity r, i.e a Maxwell-Ampere Law given by*

$$\frac{\partial}{\partial t}\mathbf{E} = r\mathbf{E} + \frac{1}{\epsilon}\mathbf{curl}H. \tag{6.2.20}$$

A necessary condition for stability of the M-adapted ETMFD for this scheme is

$$Re(r) \leq 0, \qquad |Im(\Delta t\beta)| \ll 1, \qquad \max\{\nu_x, \nu_y\} < \frac{1}{\sqrt{2}}. \tag{6.2.21}$$

Proof. Here we have absorbed the factor of ϵ^{-1} into the quantity r which is a complex number. We will proceed similarly to Theorem 6.2.1. Applying the ETMFD to this model we have the following amplification matrix for plane waves $\mathbf{E}$ and H.

$$\begin{pmatrix} E^{n+1}_{(e_1,e_2)} \\ H^{n+3/2}_f \end{pmatrix} = \mathbb{G} \begin{pmatrix} E^{n}_{(e_1,e_2)} \\ H^{n+1/2}_f \end{pmatrix}, \tag{6.2.22}$$

$$\mathbb{G} = \begin{pmatrix} \mathrm{e}^{r\Delta t}\mathbb{I} & \frac{1-\mathrm{e}^{r\Delta t}}{\epsilon r}\Delta x\Delta y\overline{\mathbb{W}}_{\mathscr{E}}\overline{\mathrm{curl}}^{\star}_h \\ -\frac{\Delta t}{\mu}\mathrm{e}^{r\Delta t}\overline{\mathrm{curl}}_h & 1 - c_0^2\Delta t\frac{\mathrm{e}^{-r\Delta t}-1}{r}\Delta x\Delta y\overline{\mathrm{curl}}_h\overline{\mathbb{W}}_{\mathscr{E}}\overline{\mathrm{curl}}^{\star}_h \end{pmatrix}. \tag{6.2.23}$$

As before we must show that the spectral radius of $\mathbb{G}$ is bounded by 1 and that the characteristic polynomial is a simple Von-Neumann polynomial. The characteristic polynomial of $\mathbb{G}$ is given by

$$p_{\mathbb{G}}(z) = (\mathrm{e}^{r\Delta t} - z)p_2(z), \tag{6.2.24}$$

$$p_2(z) = \Big(z^2 - \left(1 + \mathrm{e}^{r\Delta t} - c_0^2\Delta t\frac{\mathrm{e}^{r\Delta t}-1}{r}\Delta x\Delta y\overline{\mathrm{curl}}_h\overline{\mathbb{W}}_{\mathscr{E}}\overline{\mathrm{curl}}^{\star}_h\right)z + \mathrm{e}^{r\Delta t}\Big). \tag{6.2.25}$$

The characteristic polynomial has a root at $\mathrm{e}^{r\Delta t}$. Therefore the spectral radius will exceed one if $\mathrm{Re}(r) > 0$. This is our first and simplest stability constraint. We will now consider the roots of p_2. For this polynomial we have our coefficients

$$\beta_1 = \left(1 + \mathrm{e}^{r\Delta t} - c_0^2 \Delta t \frac{\mathrm{e}^{r\Delta t} - 1}{r} \Delta x \Delta y \overline{\mathrm{curl}}_h \overline{\mathbb{W}}_{\mathscr{E}} \overline{\mathrm{curl}}_h^\star\right), \quad \beta_0 = \mathrm{e}^{r\Delta t}. \tag{6.2.26}$$

To apply Lemma 6.1.1 we have two cases. The first case we is $\mathrm{Re}(r) = 0$ in which case $|\mathrm{e}^{r\Delta t}| = 1$. For $\mathrm{Re}(r) < 0$ we have $|\mathrm{e}^{r\Delta t}| < 1$.

$\mathrm{Re}(r) = 0$: In this case we seek to prove that $0 < |\beta_1| < 2$ and $\beta_0 \overline{\beta_1} = \beta_1$. Manipulating β_1 we can rewrite it similarly to Equation (6.2.12).

$$\beta_2 = 1 + \mathrm{e}^z - \frac{\mathrm{e}^z - 1}{z} F\left(\sin^2 \frac{k_x \Delta x}{2}, \sin^2 \frac{k_y \Delta y}{2}\right) \tag{6.2.27}$$

where $z = r\Delta t$ and F is defined as in (6.2.12). Further note that as F is real valued $\overline{F} = F$. We will now show $\beta_0 \overline{\beta_1} = \beta_1$. As $\mathrm{Re}(r) = 0$ we have that $\overline{z} = -z$.

$$\begin{aligned} \beta_0 \overline{\beta}_1 &= \mathrm{e}^z (1 + \mathrm{e}^{-z} - \frac{\mathrm{e}^{-z} - 1}{-z} F), & (6.2.28)\\ &= 1 + \mathrm{e}^z - \frac{1 - \mathrm{e}^z}{-z} F, & (6.2.29)\\ &= \beta_1. & (6.2.30) \end{aligned}$$

If $z = r\Delta t \ll 1$ then we have

$$\beta_2 \approx 2 - F \tag{6.2.31}$$

which is exactly the quantity manipulated in Theorem 6.2.1. We would therefore have the bound

$$0 < |\beta_1| < 2 \tag{6.2.32}$$

for $\max\{\nu_x, \nu_y\} < \frac{1}{\sqrt{2}}$.

$\mathrm{Re}(r) < 0$: As $\mathrm{Re}(r) < 0$ we have $\beta_0 < 0$. We must show that $|\beta_1 - \beta_0\overline{\beta_1}| < 1 - |\beta_0|^2$. Let $z = r\Delta t$. We have

$$1 - |\beta_0|^2 = 1 - \mathrm{e}^{2\mathrm{Re}\ z} \tag{6.2.33}$$

$$|\beta_1 - \beta_0\overline{\beta}_1| = -\left|1 - \mathrm{e}^{2\mathrm{Re}\ z} - F\left(\frac{\mathrm{e}^z - 1}{z} - \mathrm{e}^z\frac{\mathrm{e}^{\overline{z}} - 1}{\overline{z}}\right)\right|. \tag{6.2.34}$$

Note that the assumption $|\Delta t\ \mathrm{Im}(r)| \ll 1$ give us the approximate identity

$$\left|1 - \mathrm{e}^{2\mathrm{Re}\ z} - F\left(\frac{\mathrm{e}^w - 1}{z} - \mathrm{e}^z\frac{\mathrm{e}^{\overline{z}} - 1}{\overline{z}}\right)\right| \approx \left|1 - \mathrm{e}^{2\mathrm{Re}(w)} -\right| \tag{6.2.35}$$

Note that the right hand side is a real quantity so we can now work with equivalent absolute values.

$$\begin{array}{ccccc} -(1 - \mathrm{e}^{2\mathrm{Re}(z)}) & < & 1 - \mathrm{e}^{2\mathrm{Re}(z)} - F(1 - e^{\mathrm{Re}(z)})\left(\dfrac{e^{\mathrm{Re}(z)} - 1}{\mathrm{Re}(z)}\right) & < & 1 - \mathrm{e}^{2\mathrm{Re}(z)} \\ 0 & < & F(1 - e^{\mathrm{Re}(z)})\left(\dfrac{e^{\mathrm{Re}(z)} - 1}{\mathrm{Re}(z)}\right) & < & 2(1 - \mathrm{e}^{2\mathrm{Re}(z)}) \\ 0 & < & F\left(\dfrac{e^{\mathrm{Re}(z)} - 1}{\mathrm{Re}(z)}\right) & < & 2(1 + \mathrm{e}^{\mathrm{Re}(z)}) \end{array} \tag{6.2.36}$$

Note that the term $\frac{\mathrm{e}^{\mathrm{Re}(z)}-1}{\mathrm{Re}(z)}$ is positive as $\mathrm{Re}(r) < 0$. Therefore as long as F is positive we satisfy the lower bound. We also have the bound

$$F\frac{\mathrm{e}^{\mathrm{Re}(z)} - 1}{\mathrm{Re}(z)} \leq F \leq \frac{4}{3}(4 - \nu_x^2 - \nu_y^2)(\nu_x^2 + \nu_y^2). \tag{6.2.37}$$

We therefore only need show

$$(4 - \nu_x^2 - \nu_y^2)(\nu_x^2 + \nu_y^2) < 3 \tag{6.2.38}$$

which is satisfied by the condition

$$\max\{\nu_x, \nu_y\} < \frac{1}{\sqrt{2}} \tag{6.2.39}$$

as was demonstrated in Theorem 6.2.1.

Q.E.D.

6.3 Numerical Demonstration of Stability

6.3.1 Free Space

In this section we will check the sufficiency of the stability conditions developed in Section 6.2. We will present two experiments. The first experiment will compute the norm of the stability matrix $\|\mathbb{G}^n\|$ as n grows. In the second experiment we will show that for Courant numbers ν slightly larger than $\frac{1}{\sqrt{2}}$ the method exhibits exponential growth.

Experiment 10. The amplification matrix for the M-adapted MFD for free space.

$$\mathbb{G} = \begin{pmatrix} \mathbb{I} & -c_0^2 \Delta t \overline{\mathbb{W}}_{\mathscr{E}} \overline{\text{curl}}_h^{\star} \Delta x \Delta y \\ \Delta t \overline{\text{curl}}_h & 1 - c^2 \Delta t^2 \overline{\text{curl}}_h \overline{\mathbb{W}}_{\mathscr{E}} \overline{\text{curl}}_h^{\star} \Delta x \Delta y \end{pmatrix}. \tag{6.3.1}$$

The matrix $\mathbb{G}$ carries a plane wave in space from one time step to the next

$$\begin{pmatrix} \mathbf{E}_{(e_1,e_2)}^{n+1} \\ H_f^{n+3/2} \end{pmatrix} = \mathbb{G} \begin{pmatrix} \mathbf{E}_{(e_1,e_2)}^{n} \\ H_f^{n+1/2} \end{pmatrix}. \tag{6.3.2}$$

Therefore if $\|\mathbb{G}^n\|$ stays bounded as $n \to \infty$ we know that plane wave solutions will grow in time. In Figure 6.1 we compute the quantity $\|\mathbb{G}^n\|$ for the Courant number $\nu = \frac{1}{\sqrt{2}}$ when $c = 1, \alpha = 1$ and h is chosen to guarantee a certain number of points per wavelength of resolution. We consider plane waves with $k = 4$ and consider ten angles in $(0, 2\pi)$ although there is no difference in each curve to the eye.

This experiment shows that the norm of the amplification matrix stays bounded through many time steps suggesting our stability bound is sufficient. In Figure 6.1 we see that the matrix norm appears larger for lower resolution (12 ppw) rather than the higher resolution (48 ppw). Both resolutions exhibit oscillation in the matrix norm, but the reduced rate of oscillation in higher resolution case is due to smaller time steps.

Experiment 11. In this experiment we show that violating the necessary stability condition developed in Theorem 6.2.1 leads to instability. By choosing Courant numbers ν slightly

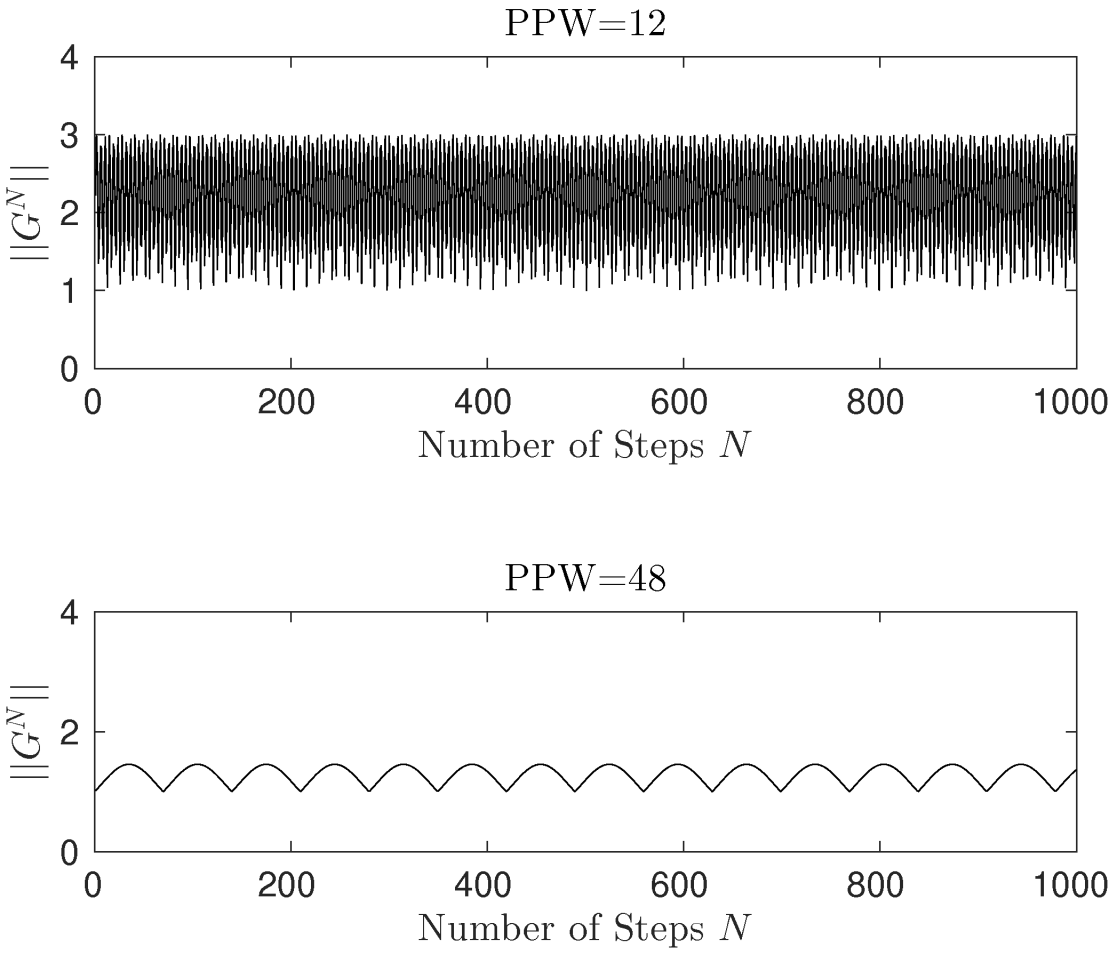

FIGURE 6.1: We show $\|\mathbb{G}^n\|$ for 10 angles of propagation in $(0, 2\pi)$ for 12 and 48 points per wavelength of resolution at $\nu = \frac{1}{2}$. In both cases the norm of the matrix is bounded. The slower rate of oscillation in the higher resolution graph is due to the smaller time steps necessitated by higher resolution.

larger than the stability bound $\frac{1}{\sqrt{2}}$ we show that an approximation of the Fourier mode exhibits exponential growth after a period of apparent stability. See Figure 6.2 for demonstration. While the Fourier mode appears stable at the value $\nu = \frac{1}{\sqrt{2}}$ we recommend a smaller time step to guarantee the method remains stable, namely $\nu = \frac{1}{2}$.

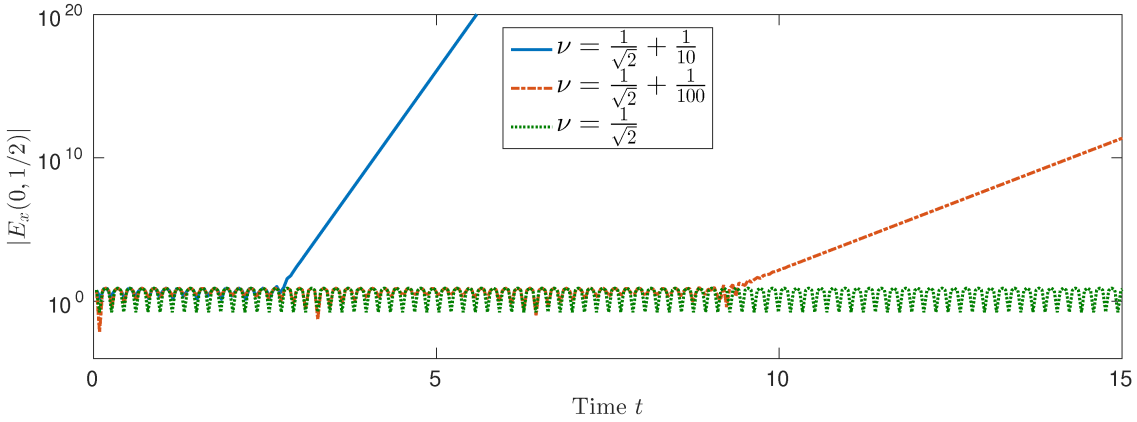

FIGURE 6.2: Here we show the magnitude of $E_x(0, 1/2)$ for a Fourier mode on $[0, 1]^2$. As we increase ν past the stability condition the method becomes unstable resulting in exponential growth in the solution after a period of seeming stability.

6.3.2 Linear Polarization Media

Experiment 12. A major question raised by this analysis is just how well the oscillations of $\mathbb{X}$ must be resolved.

In Figure 6.3 we present a numerical experiment where we calculate the maximum of $|\beta_1|$ for a mesh with $\min\{\nu_x, \nu_y\} = \frac{1}{2}$ for several aspect ratios. Note that there is a fairly large window where this value is bounded above by two, i.e. the method will be stable. This calculation suggests that $\Delta t \mathrm{Im}(r) \ll 1$ is an overly restrictive requirement and tighter bound should be possible. However, this plot also confirms that there is a resolution requirement to guarantee stability. If a medium has very fast natural oscillations, these oscillations must be resolved relatively well, for example when $\alpha = 1$ we recommend $\Delta t \mathrm{Im}(r) < 4$.

Experiment 13. We will now numerically demonstrate the sufficiency of these conditions. That is we will show $\|\mathbb{G}^n\|_2$ stays bounded for large n. We consider both a dissipative and a conservative mode and choose $\min\{\nu_x, \nu_y\} = \frac{1}{2}$ and show that $\|\mathbb{G}^n\|$ stays bounded. See Figure 6.4 for results.

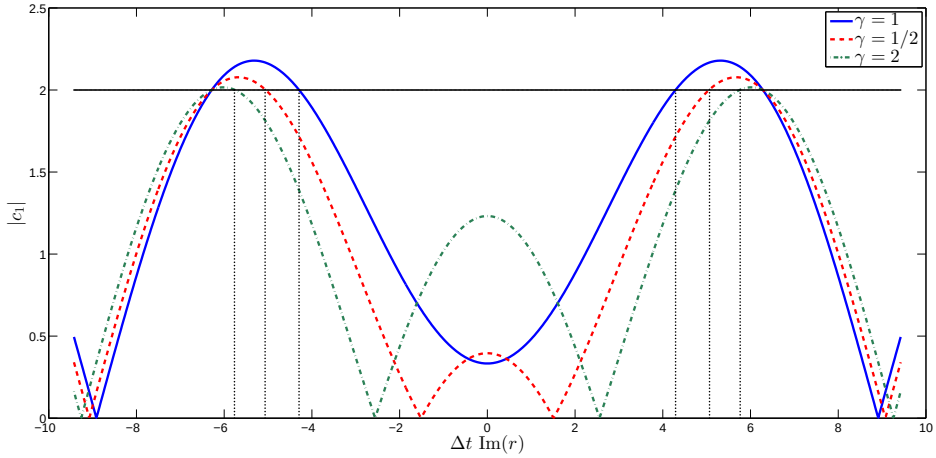

FIGURE 6.3: Here we show the maximum of $|\beta_1|$ when $r = \mathrm{i}b$, $\min\{\nu_x, \nu_y\} = \frac{1}{2}$, and $\alpha \in \{1, 1/2, 2\}$. This suggests that the condition $|\Delta t \mathrm{Im}(r)| \ll 1$ may be overly restrictive as the method should be stable for relatively poor resolution of a given mediums resonance frequency.

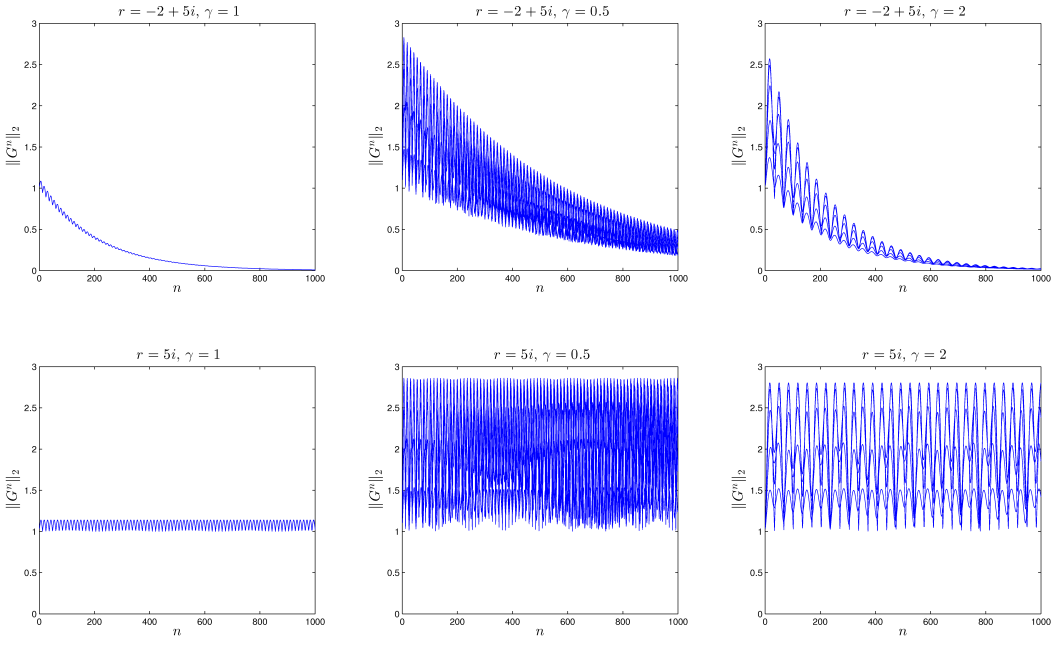

FIGURE 6.4: Illustrates that the norm of the amplification matrix stays bounded over a large number of time steps. Here the Courant number is chosen as $\min\{\nu_x, \nu_y\} = \frac{1}{2}$, $h = 10^{-2}$, and k is chosen so that there are 12 points per wavelength. Ten directions of propagation are chosen in each plot with angle $\theta \in (-\pi/2, \pi/2)$. Note that the norms of the matrix powers stay bounded, although the value of this bound depends upon material parameter r as well as mesh parameter α.

7 MAGNETOHYDRODYANMIC GENERATORS

A fundamental technique for generating electricity is the moving of a conductor in the presence of a magnetic field. For example, a simple electric turbine works by spining a magnet near a coil of wire which produces electricity. In essence the magnet pushes electrons in the wire inducing a current. A magnetohydrodynamic generator operates on much the same principle with a major difference – instead of a solid we choose our conductor to be a plasma.

An MHD generator consists of several components. First is the channel– for example a long tube or rectangular cylinder. The wall of the tube is composed of both electrically insulating material and electrode material. The copper electrodes will be highly conductive ($\sigma \approx 10^7 \frac{\mathrm{S}}{\mathrm{m}}$) while the insulators will ideally be perfect dielectrics. The cross section of this generator will exapand helping to mitigate the growth of boundary layers in the fluid. A magnet is positioned above the channel. While this could be a permanent magnet, typically one considers a high temperature super conducting magnet in order to apply a magnetic field on the order at least 1 tesla(T) to the flow. A combustor and nozzle are affixed to the upstream end of the channel while the downstream end either empties into a void space or could be piped to a secondary electrical power generator – for example a steam cycle. When used in this configuration – MHD generation followed by steam generation– we refer to the MHD generator as a *topping cycle*. Electrodes will be wired together through a resistive load. This will cause a potential difference across the generator and allow the extraction of current from the plasma.

This topping cycle approach is desirable in part because modern clean burning oxyfuel combustors – i.e. burners which mix liquid or gaseous oxygen with their fuel in order to combust as much of the fuel as possible – produce a working fluid significantly

hotter than most traditional turbines can be safely operated at. Example temperature ranges for oxyfuel combustion range from 2500 to 3000 K. MHD power generation operates well at higher temperatures due to the increased electrical conductivity of the working fluid. The topping cycle application is what we consider here. MHD power generation from a combustion product on its own may be only about 20% efficient, although estimates change depending on specific application. However, when used as a topping cycle on a high efficiency steam cycle, the efficiency of the MHD generator and the turbine is theoretically 52% compared to the efficiency of just the turbine which is only 40%. This dramatic increase in thermodynamic efficiency is the primary reason to consider MHD power generation.

The conductivity of the plasma is due primarily to temperature. In essence the hotter the gas the more likely it is to ionize – or have electrons freed from their constituent atoms. In order to aid in ionization, alkali or alkaline earth metals are added to the flow and vaporized. These *seed* ions allow for higher ionization of the gas by reducing the *ionization potential* of each chemcial component in the flow. For our problem of interest we are considering oxyfuel fired kerosene seeded with potassium carbonate.

However, MHD technology has high life cycle costs due in part to the high material failure rate of the generator. At 2500 K the walls of the channels need to be cooled or they could melt. Consider an example where a working fluid at 2500 K while the water cooled casing will be held at 500 K. This will result in sharp temperature gradients at the plasma wall interface. Given that conductivity is linked strongly to temperature– this results in a sharp decrease in electrical conductivity. Despite this drop in conductivity, the potential difference still remains across the channel. In order to resolve this difference, arcs form at the electrode fluid interface to create a conductivity "bridge" across which current can flow. When large, these arcs can vaporize the surface of the electrode resulting in material damage.

One of the major goals of the research presented here is to produce a computational assessment of the feasibility of detecting when arcs occur. As measurement inside the channel is impossible, and as the literature suggests that no change in current density or potential difference is detected despite the effects of arcing being observed, we will instead consider the magnetic field perturbations due to the high current densities at the arc. An important first step is to determine the sensitivity of the magnetic fields outside of the channel to *arc-like* current densities inside the channel. If external magnetic fields are not very sensitive then they would not a good indicator of arcing.

In Section 7.1 we will develop a model for an equilibrium MHD generator. In Section 7.2 we will prove the well-posedness of the electromagnetic fields in this model and show that the magnetic field depends continuously on the electrical conductivity of the fluid. In Section 7.3 we will perform numerical experiments exploring the sensitivity of magnetic fields to a heuristic arcing model. In Section 7.4 we present numerical solutions of the equilibrium MHD model presented in Section 7.1. Work in this section is an extension of results appearing in [8].

7.1 Equilibrium Generators

In this section we will develop a partial differential equation model for a Magneto-hydrodynamic Generator channel. Our modelling relies upon the following assumptions.

The Generator is in Equilibrium We make this assumption as we are interested in the long term behavior of the MHD generator system. Given that this particular power extraction scheme is ideally run continuously for long periods of time this assumption should give us a sense of the ideal performance of the machine. Further, given the large dissipative effects in place in the channel – for example electric fields being quickly dissipated – this analysis may have use for linearization around the

equilibrium.

This assumption is most likely *not* valid for in the case of arcing which is intuitively a *far from equilibrium* effect. However, we see this non-physical model as a first step in a more accurate approach.

Low Magnetic Reynolds Number The Magnetic Reynold's number is defined as

$$R_{\text{mag}} = \sigma \mu_0 U L \tag{7.1.1}$$

where U is a characteristic velocity of the flow, L is the characteristic length of the geometry, σ is the electrical conductivity of the material, and μ_0 the permeability material. The magnetic Reynold's number measures the relative ratio of induction (UL) to magnetic diffusivity $(\sigma\mu)^{-1}$. For our geometries and boundary conditions the reference length is $L = \mathcal{O}(100\text{mm})$ the length of the channel, $U = \mathcal{O}(200\frac{\text{m}}{\text{s}})$, $\sigma = 60\frac{\text{S}}{m}$, and given the permeability of free space is $\mu_0 = \pi 2.5 \times 10^{-5}\frac{\text{N}}{\text{A}}$ then the Magnetic Reynolds number is $R_{\text{mag}} \approx 10^{-2}$.

Since our estimate of the magnetic Reynolds number is significantly less then unity we assume that if the magnetic field $\mathbf{B}$ can be decomposed into $\mathbf{B} = \mathbf{B}_0 + \mathbf{B}_i$, where $\mathbf{B}_0$ is the applied magnetic field and $\mathbf{B}_i$ is the induced magnetic field, then we have $|\mathbf{B}_i| \ll |\mathbf{B}_0|$.

This assumption will linearize some effects as $\mathbf{B}_0$ will be fixed: reducing the influence of the electromagnetics on the fluid flow.

7.1.1 Generator Geometry

To develop a model of a generator in equilibrium we will first consider the physics of the actual MHD system – namely the coupling between fluid mechanics, electromagnetics, and thermodynamics. Before we delve into the equations with which we will model the system we must first develop some notation to describe the geometry. See Figure 7.1

for three simple configurations. We we will primarily focus on the segmented Faraday configuration 7.1.c.

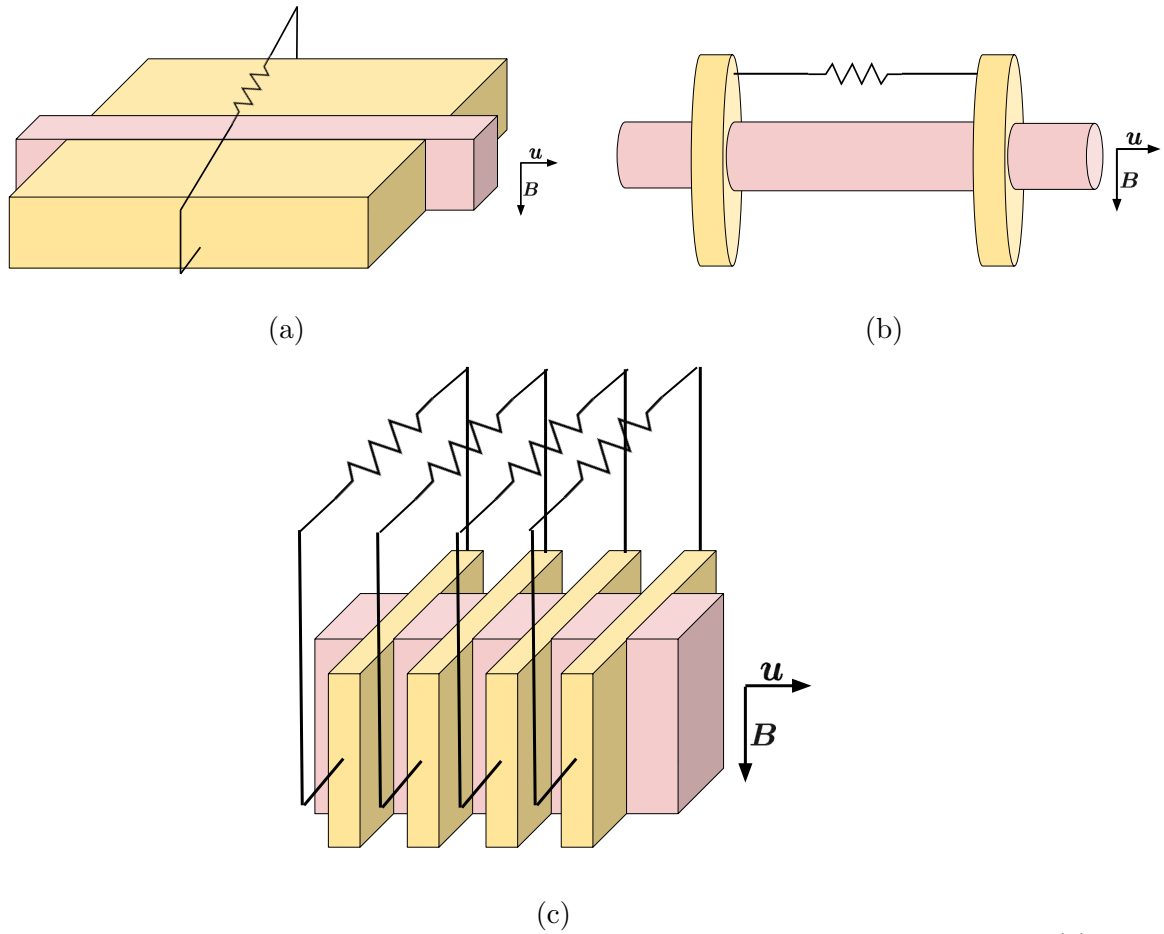

(a) (b)

(c)

FIGURE 7.1: Here we show three prototypical MHD generator configurations – (a) a Faraday channel, (b) a Hall channel, and (c) a segmented Faraday Generator. Pink areas denote the channel which contains the working fluid. Yellow areas are the conductors. Black lines represent wiring connections and resistors. The resistive parts of the casing are not pictured.

The channel is an open tube with either a round or square cross section. We call the space within the channel Ω_{chan}. Fluid will flow into the channel through the inflow boundary Γ_{in} and out through the outflow boundary Γ_{out}. The wall-channel interface will be referred to as Γ_{wall}. We refer to the generator casing– which is comprised of electrodes as Ω_{case}. See Figure 7.2 for an illustration. If we were to model the heat transfer in the entire

generator casing we would consider insulating segments their own subdomain. Inncluding electrical effects in this region as well is non trivial as jumps in electrical conductivity amy remove all precision for a naive approach.

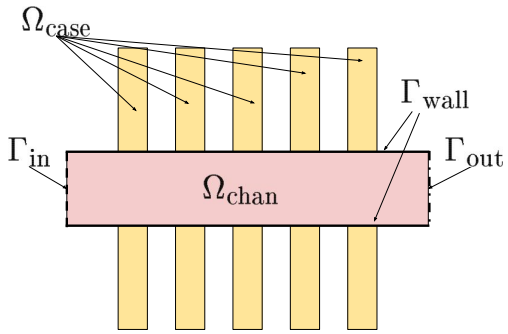

FIGURE 7.2: We show a cross section of a segmented Faraday channel. Boundaries, interfaces, and subdomains are labeled.

7.1.2 Model Formulation

We consider a generator whose working fluid is the product of oxyfuel combustion– namely a gas which is a mixture of the chemical species resulting from burning methane (or natural gas or kerosene) in an extremely oxygen rich environment. This fluid is compressible and non-isothermal as inflow gas is assumed to be much hotter than the walls of the channel which are cooled. A model of this flow is given as follows:

$$\begin{cases} \dfrac{\partial}{\partial t}\rho\mathbf{u} + \rho\mathbf{u}\cdot\nabla\mathbf{u} = \text{div}\boldsymbol{\tau} - \nabla p + \mathbf{F} & \text{Conservation of Momentum} \\ \dfrac{\partial}{\partial t}\rho = -\text{div}(\rho\mathbf{u}) & \text{Conservation of Mass} \\ \rho C\left(\dfrac{\partial}{\partial t}T + \mathbf{u}\cdot\nabla T\right) = \text{div}K\nabla T + Q & \text{Heat Transfer} \end{cases} \tag{7.1.2}$$

In typical developments of MHD equations instead of heat transfer one considers an equation of *energy conservation* , c.f. [51]. Unfortunately, COMSOL, the commercial software we use to simulte the fully coupled fluid flow and electromagnetic model we will develop

in this chapter, does not provide functionality for energy conservation. Therefore we consider the heat transfer as a proxy for energy conservation – especially as $\rho C_\rho T$ has units of energy density (given that the volumetric heat flux has units power density). The fluid mechanical variables are given by $\mathbf{u}$ the fluid velocity, $\boldsymbol{\tau}$ the stress tensor, p the pressure, and $\mathbf{F}$ external volume force density. The thermodynamic variables are T the temperature, ρ the gas density, C the heat capacity, K the heat conductivity, and Q is the internal heat flux (rather than the boundary flux which may be described by specific boundary conditions). The equilibrium assumption removes all time derivatives:

$$\begin{cases} -\mathrm{div}\boldsymbol{\tau} + \rho\mathbf{u}\cdot\nabla\mathbf{u} + \nabla p = \mathbf{F} & \text{Conservation of Momentum} \\ \mathrm{div}(\rho\mathbf{u}) = 0 & \text{Conservation of Mass} \\ -\mathrm{div}K\nabla T + \rho C\mathbf{u}\cdot\nabla T = Q & \text{Heat Transfer} \end{cases} . \tag{7.1.3}$$

The model is presently incomplete – namely we are lacking a constitutive model for ρ and $\boldsymbol{\tau}$. We use the linear correction to the strain tensor for compressible flows

$$\boldsymbol{\tau} = \nu(\nabla + \nabla^T)\mathbf{u} - \frac{2}{3}\nu\mathrm{div}\mathbf{u}\mathbb{I}. \tag{7.1.4}$$

The simplest constitutive law which relates ρ to T and p by the ideal gas assumption

$$\rho = \frac{p}{RT} \tag{7.1.5}$$

where R is the temperature dependent specific gas constant which is roughly the amount of energy added to a gas by heating the gas by a particular temperature. More sophisiticated models will require chemical calculations for every species in the flow in order to generate a numerical gas law. We recognize that the use of ideal gas is a modelling error and look to include more sophisticiated models in the future.

Additional coupling between fluid mechanics and thermodynamics is imposed by the heat flux Q. We wish to couple heating with gas expansion, frictional heating viscosity of

the fluid, and Joule heating from the presence of currents.

$$Q = Q_p + Q_\nu + Q_j, \tag{7.1.6}$$

$$Q_p = -\frac{T}{\rho}\frac{\partial \rho}{\partial T}\Big|_p \mathbf{u} \cdot \nabla p, \tag{7.1.7}$$

$$Q_\nu = \boldsymbol{\tau} : \nabla \mathbf{u} \tag{7.1.8}$$

$$Q_j = \mathbf{J} \cdot \mathbf{E} \tag{7.1.9}$$

The first heat flux is the heat due to the expansion of the gas. We will deal with the pressure term. We calculate the derivative of the ideal gas law with respect to T.

$$\frac{\partial p}{\partial T} = \rho T \frac{\partial R}{\partial T} + RT\frac{\partial \rho}{\partial T} + R\rho. \tag{7.1.10}$$

As we are assuming fixed pressure the right hand side is zero. Solving for $\frac{\partial}{\partial T}\rho$ we arrive at

$$\frac{\partial \rho}{\partial T} = -\frac{\rho}{R}\frac{\partial R}{\partial T} - \frac{\rho}{T}. \tag{7.1.11}$$

Applying this identity to the definition of Q_p we have

$$Q_p = \left(\frac{T}{R}\frac{\partial R}{\partial T} + 1\right)\mathbf{u} \cdot \nabla p. \tag{7.1.12}$$

The heating due to viscosity uses the double dot product (the Fröbenius inner product). We therefore have

$$\boldsymbol{\tau} : \nabla \mathbf{u} := \sum_{i=1}^{3}\sum_{j=1}^{3} \boldsymbol{\tau}_{ij}\frac{\partial \mathbf{u}_i}{\partial x_j} \tag{7.1.13}$$

$$= \sum_i \sum_j \nu\left(\frac{\partial \mathbf{u}_i}{\partial x_j} + \frac{\partial \mathbf{u}_j}{\partial x_i} + \frac{2}{3}\delta_{ij}\nabla \cdot \mathbf{u}\right)\frac{\partial \mathbf{u}_i}{\partial x_j}. \tag{7.1.14}$$

While the scalar equation may be useful for implementation, intuitively the term $\boldsymbol{\tau} : \nabla \mathbf{u}$ states that we create heat when viscosity slows the flow. The Joule heating term roughly accounts for the heat flux due to currents flowing through a resistor.

Lastly we need to provide a model for $\mathbf{F}$. As we are discussing **magneto**hydrodynamics we also include electromagnetic effects. In the channel we will have both current densities

J and magnetic fields **B**. We use the classical **Lorentz Force** to account for interactions between the electromagnetic and fluid components:

$$\mathbf{f} = \rho_c \mathbf{u} \times \mathbf{B} = \mathbf{J} \times \mathbf{B} \tag{7.1.15}$$

where **f** is the volumetric force density, **u** is the conductor velocity, and ρ_c is the charge density.

For the variables which are not governed by equations, namely R, ν, C, K, ρ the gas constant, viscosity, heat capacity, heat conductivity, and gas density we assume empirical relations that describe these variables as functions of temperature and pressure.

We use stationary Maxwell's equations to describe the electromagnetic fields present in the generator:

$$\begin{cases} \mathbf{curl}\mathbf{H} = \mathbf{J} & \mathrm{div}\mathbf{B} = 0 \\ \mathbf{curl}\mathbf{E} = 0 & \mathrm{div}\mathbf{D} = \rho_c \end{cases} \tag{7.1.16}$$

We equip this formulation with the following constitutive laws:

$$\mathbf{B} = \mu\mathbf{H} \qquad \text{No Magentization,} \tag{7.1.17}$$

$$\mathbf{D} = \epsilon\mathbf{E} \qquad \text{No Polarization,} \tag{7.1.18}$$

$$\mathbf{J} = \sigma(\mathbf{E} + \mathbf{u} \times \mathbf{B}) + \eta\mathbf{J} \times \mathbf{B} \qquad \text{Generalized Ohm's Law.} \tag{7.1.19}$$

Here σ is the electrical conductivity and η is the electron mobility. In addition we assume that $\mathbf{B} = \mathbf{B}_i + \mathbf{B}_0$ where $\mathbf{B}_i$ is the magnetic field induced by the currents in the generator and $\mathbf{B}_0$ is an applied, known, external field. We assume that these induced fields are negligible compared to the applied field.

We can formulate a magnetostatic system immediately where $\mathbf{B} = \mathbf{curl}\mathbf{A}$, assuming the Coulomb gauge condition $\mathrm{div}\mathbf{A} = 0$. Applying the Helmholtz decomposition to both

$\mathbf{B}_i$ and $\mathbf{B}_0$ we have

$$\mathbf{B}_i = \mathbf{curl}\mathbf{A}_i + \nabla\psi_i, \tag{7.1.20}$$

$$\mathbf{B}_0 = \mathbf{curl}\mathbf{A}_0 + \nabla\psi_0. \tag{7.1.21}$$

Combining these two formulas with the Coulomb gauge assumption we have

$$\mathbf{curl}\mathbf{A} = \mathbf{curl}\mathbf{A}_0 + \mathbf{curl}\mathbf{A}_i + \nabla\psi_0 + \nabla\psi_i. \tag{7.1.22}$$

This condition implies that $\nabla\psi_0 + \nabla\psi_i = 0$. We will now combine these conditions with Ampere's law,

$$\mathbf{curl}\mu^{-1}\mathbf{B} = \mathbf{curl}\mu^{-1}\Big(\mathbf{curl}\mathbf{A}_0 + \mathbf{curl}\mathbf{A}_i\Big). \tag{7.1.23}$$

This yields

$$\begin{cases} \mathbf{curl}\mu^{-1}\mathbf{curl}\mathbf{A}_i = \mathbf{J} - \mathbf{curl}\mu^{-1}\mathbf{A}_0 \\ \mathrm{div}\mathbf{A}_i = -\mathrm{div}\mathbf{A}_0. \end{cases} \tag{7.1.24}$$

A first impulse to determine $\mathbf{J}$ may be to solve an electrostatic problem for $\mathbf{E}$. However, give that the permittivity of strong conductors is approximately 0 this leads to problem which is very difficult to compute. Instead we will eliminate $\mathbf{E}$ from Ohm's Law and prescribe $\mathbf{J}$'s divergence from the continuity equation. Note that as $\mathbf{curl}\mathbf{E} = 0$ we have $\mathbf{E} = \nabla V$ where V is the voltage. We will now rewrite Ohm's law explicitly.

$$\mathbf{J} = \sigma(\mathbf{E} + \mathbf{u} \times \mathbf{B}) + \eta\mathbf{J} \times \mathbf{B} \tag{7.1.25}$$

$$\mathbf{J} \approx \sigma(\mathbf{E} + \mathbf{u} \times \mathbf{B}_0) + \eta\mathbf{J} \times \mathbf{B}_0 \tag{7.1.26}$$

$$(\mathbb{I} + \eta[\mathbf{B}_0]_\times)\mathbf{J} = \sigma(\mathbf{E} + \mathbf{u} \times \mathbf{B}_0) \tag{7.1.27}$$

$$\mathbf{J} = \sigma\frac{1}{1+\eta|\mathbf{B}_0|^2}(\mathbb{I} + \eta^2\mathbf{B}_0\mathbf{B}_0^T - \eta[\mathbf{B}_0]_\times)(\mathbf{E} + \mathbf{u} \times \mathbf{B}_0) \tag{7.1.28}$$

Where $[\mathbf{B}_0]_\times$ writes a cross product as a linear operator defined for an arbitrary vector

valued funciton by

$$[\mathbf{B}_0]_\times = \begin{pmatrix} & -B_z & B_y \\ B_z & & -B_x \\ -B_y & B_x & \end{pmatrix}, \qquad \mathbf{B}_0 = (B_x, B_y, B_z)^T. \tag{7.1.29}$$

This last statement can be proven using the identity $[\mathbf{B}_0]_\times^2 = \mathbf{B}_0\mathbf{B}_0^T - |\mathbf{B}_0|^2\mathbb{I}$. We now define the effective conductivity tensor for the Hall effect as

$$\underline{\sigma} = \frac{\sigma}{1+\eta^2|\mathbf{B}_0|^2}(1 + \eta^2\mathbf{B}_0\mathbf{B}_0^T - \eta[\mathbf{B}_0]_\times). \tag{7.1.30}$$

This formulation is similar to the standard development of generalized Ohm's Law, c.f. [48], but we have formulated it in purely vectoral form rather than componentwise. The continuity equation for charge states that

$$\frac{\partial}{\partial t}\rho_c = -\text{div } \mathbf{J}. \tag{7.1.31}$$

However, as $\frac{\partial}{\partial t}\rho_c = 0$ we have div $\mathbf{J} = 0$. Define the quantity $\mathbf{J}_i = \underline{\sigma}\nabla V$. Now apply the divergence condition to Generalized Ohm's law.

$$0 = \text{div}\mathbf{J} = \text{div } \underline{\sigma}(\nabla V + \mathbf{u} \times \mathbf{B}) \tag{7.1.32}$$

$$\text{div}\mathbf{J}_i = -\text{div } \underline{\sigma}\mathbf{u} \times \mathbf{B}. \tag{7.1.33}$$

We can then find the current $\mathbf{J}$ using the mixed Poisson equation

$$\mathbf{J} = \mathbf{J}_i + \underline{\sigma}\mathbf{u} \times \mathbf{B}, \tag{7.1.34}$$

$$\begin{cases} \underline{\sigma}^{-1}\mathbf{J}_i - \nabla V = 0 \\ \text{div}\mathbf{J}_i = -\text{div } \underline{\sigma}\mathbf{u} \times \mathbf{B} \end{cases}. \tag{7.1.35}$$

We now have a model for the bulk of the fluid flow, heat transfer, electric currents, and magnetic fields. We pose the fluid flow and heat transfer equations only in Ω_{chan}. We pose the electric currents model in $\Omega_{\text{case}} \cup \Omega_{\text{chan}}$. The magnetostatics are well posed on all of $\mathbb{R}^3$ however we will limit ourselves to a large box containing all of $\Omega_{\text{case}} \cup \Omega_{\text{chan}}$.

As most of our domains are finite we must introduce boundary conditions. To account for the inflow of gas into the channel we have

$$\mathbf{u} = \mathbf{u}_0 \text{ on } \Gamma_{\text{in}}. \tag{7.1.36}$$

In general we select $\mathbf{u}_0$ to point purely along the channel. In order to allow the fluid to leave the domain freely we prescribe

$$p = 1 \text{ atm on } \Gamma_{\text{out}}. \tag{7.1.37}$$

On the walls of the channel we apply the no-slip boundary condition on the walls.

$$\mathbf{u} = 0 \text{ on } \Gamma_{\text{wall}}. \tag{7.1.38}$$

On the both the walls and the inflow boundary we prescribe the temperature; namely

$$T = T_{\text{in}} \text{ on } \Gamma_{\text{in}}, \tag{7.1.39}$$

$$T = T_{\text{wall}} \text{ on } \Gamma_{\text{wall}}. \tag{7.1.40}$$

Our typical assumption is that $T_{\text{in}} = 2500$ K while $T_{\text{wall}} = 500$ K. For the outflow boundary we assume

$$\mathbf{n} \cdot \nabla T = 0 \text{ on } \Gamma_{\text{out}} \tag{7.1.41}$$

as $\mathbf{n} \cdot \nabla T \approx \mathbf{u} \cdot \nabla T$ at the outflow and we desire that no heat enter the domain against the fluid flow. For the current density on $\partial(\Omega_{\text{case}} \cup \Omega_{\text{chan}}) \setminus (\Gamma_{\text{in}} \cup \Gamma_{\text{out}})$ we prescribe an insulating boundary condition

$$\mathbf{J} \cdot \mathbf{n} = 0 \implies \mathbf{J}_i \cdot \mathbf{n} = -\underline{\sigma}\mathbf{u} \times \mathbf{B} \cdot \mathbf{n}. \tag{7.1.42}$$

At the inflow and outflow we prescribe that all the current entering the domain is given by

$$\mathbf{J} \cdot \mathbf{n} = \mathbf{n} \cdot \underline{\sigma}\mathbf{u} \times \mathbf{B}, \tag{7.1.43}$$

that is

$$\mathbf{n} \cdot \mathbf{J}_i = 0. \tag{7.1.44}$$

It should be mentioned that we have included wires with electrodes connecting loaded with resistors. These connections are also in essence boundary conditions although we will in general model them as wires connected by periodic boundary conditions coming out of the ends of our electrodes. Our resistors will be a box on the wire with a prescribed conductivity.

For the magnetostatic equations we solve on a super-domain which includes both the channel and casing. We prescribe a non-physical boundary condition $\mathbf{A} \times \mathbf{n} = 0$ and make the domain large enough that errors near the boundary do not pollute the magnetic field close to the channel.

We describe the full model for the equilibrium MHD generator as follows.

Fluid Mechanics (7.1.45)

$$\begin{cases} -\nabla \cdot \boldsymbol{\tau} + \rho \mathbf{u} \cdot \nabla \mathbf{u} + \nabla p = \mathbf{J} \times \mathbf{B}_0 & \in \Omega_{\text{chan}} \\ \boldsymbol{\tau} = \nu(\nabla + \nabla^T)\mathbf{u} + \nu \frac{2}{3} \text{div} \mathbf{u} \mathbb{I} & \\ \text{div}(\rho \mathbf{u}) = 0 \in \Omega_{\text{chan}} & \\ \rho = \frac{RT}{p} & \in \Omega_{\text{chan}} \\ -\text{div} K \nabla T + \rho C \mathbf{u} \cdot \nabla T = Q & \in \Omega_{\text{chan}} \\ Q = Q_p + Q_\nu & \\ Q_p = \left(\frac{T}{R} \frac{\partial R}{\partial T} + 1 \right) \mathbf{u} \cdot \nabla p & \\ Q_\nu = \boldsymbol{\tau} : \nabla \mathbf{u} & \end{cases} \tag{7.1.46}$$

Ohm's Law (7.1.47)

$$\begin{cases} \mathbf{J} = \mathbf{J}_i + \underline{\sigma}\mathbf{u} \times \mathbf{B}_0 & \\ \underline{\sigma}^{-1}\mathbf{J}_i - \nabla V = 0 & \in \Omega_{\text{chan}} \cup \Omega_{\text{case}} \\ \text{div}\mathbf{J}_i = -\text{div}\underline{\sigma}\mathbf{u} \times \mathbf{B}_0 & \in \Omega_{\text{chan}} \cup \Omega_{\text{case}} \\ \underline{\sigma} = \frac{\sigma}{1+\eta^2|\mathbf{B}|^2}(\mathbb{I} + \eta^2\mathbf{B}_0\mathbf{B}_0^T - \eta[\mathbf{B}_0]_\times) & \end{cases} \tag{7.1.48}$$

Magnetostatics (7.1.49)

$$\begin{cases} \mathbf{B}_i = \mathbf{curl}(\mathbf{A}_i + \mathbf{A}_0) - \mathbf{B}_0 & \\ \mathbf{B}_0 = \mathbf{curl}\mathbf{A}_0 + \nabla\psi_0 & \\ \mathbf{curl}\mu^{-1}\mathbf{curl}\mathbf{A}_i + \nabla\lambda = \mathbf{J} - \mathbf{curl}\mu^{-1}\mathbf{curl}\mathbf{A}_0 & \in \Omega \\ \text{div}\mathbf{A}_i = -\text{div}\mathbf{A}_0 & \in \Omega \end{cases} \tag{7.1.50}$$

Boundary conditions are collected in Table 7.1.

TABLE 7.1: Boundary conditions for an equilibrium MHD generator.

Condition	Boundary	Condition	Boundary
$\mathbf{u} = \mathbf{u}_0$	Γ_{in}	$\mathbf{u} = 0$	Γ_{wall}
$p = p_0$	Γ_{out}	$T = T_{\text{in}}$	Γ_{in}
$T = T_{\text{wall}}$	Γ_{wall}	$\mathbf{n} \cdot \nabla T = 0$	Γ_{out}
$\mathbf{J} \cdot \mathbf{n} = 0$	$\partial(\Omega_{\text{channel}} \cup \Omega_{\text{case}})$	$\mathbf{J} \cdot \mathbf{n} = \underline{\sigma}\mathbf{u} \times \mathbf{B}$	$\Gamma_{\text{in}} \cup \Gamma_{\text{out}}$
$\mathbf{A}_i \times \mathbf{n} = 0$	$\partial\Omega$		

7.2 Well Posedness of Elliptic Electromagnetic Problems

In this section we will prove well-posedness of the stationary electric current and magnetic field models developed in the previous section. We rely heavily on the mixed space theory – famously referred to as the Babushka-Brezzi-Kovalevskaya theory. Further we will show that induced magnetic fields $\mathbf{B}_i$ depend continuously on electrical conductivity.

Theorem 7.2.1. *Let $\mathcal{A} : V \to V'$ and $\mathcal{B} : V \to W'$ be continuous operators from the Hilbert spaces V, W to their duals. In addition*

- *$\mathcal{A}$ is non-negative and V-coercive on Ker$\mathcal{B}$: there is an $\alpha > 0$ such that*

$$\mathcal{A}v(v) \geq \alpha \|v\|_V^2, \quad v \in Ker\mathcal{B} \tag{7.2.1}$$

- *$\mathcal{B}$ is bounding, i.e. it is injective and*

$$\inf_{q \in W} \sup_{v \in V} \frac{|\mathcal{B}v(q)|}{\|v\|_V \|q\|_W} \geq \beta > 0 \tag{7.2.2}$$

Given these conditions then $\forall f \in V'$ and $g \in W'$ there exists a unique pair $(v, p) \in V \times W$ s.t.

$$\begin{aligned} \mathcal{A}u + \mathcal{B}'p &= f \quad \in V' \\ \mathcal{B}u &= g \qquad\quad \in W' \end{aligned} \tag{7.2.3}$$

Which obey the following a priori *estimate.*

$$\|u\|_V \leq \frac{1}{\alpha}\Big(\|f\|_{V'} + \frac{1}{\beta}(\|\mathcal{A}\|_{\mathcal{L}(V,V')} + \alpha)\|g\|_{W'} \Big) \tag{7.2.4}$$

$$\|p\|_W \leq \frac{1}{\beta}(\|f\|_{V'} + \|\mathcal{A}\|_{\mathcal{L}(V,V')}\|u\|_V) \tag{7.2.5}$$

Proof. A comprehensive proof may be found in Boffi, Brezzi, Fortan [5]. **Q.E.D.**

We will now use this formulation to prove existence and uniqueness of our electric current and magnetostatic models.

7.2.1 Well-Posedness of Electric Currents

Define the following subspace of H^1. Let $\Gamma = \partial\Omega$.

$$U = \{f \in H^1(\Omega) : \int f = 0\} \tag{7.2.6}$$

We will seek our voltage $V \in U$. The variational formulation of the stationary electric current system is posed as follows:

$$\begin{cases} \int_\Omega \underline{\sigma}^{-1}\mathbf{J}\cdot\boldsymbol{\Psi} - \int_\Omega \nabla V\cdot\boldsymbol{\Psi} = \int_\Omega \mathbf{F}\cdot\boldsymbol{\Psi} & \forall \boldsymbol{\Psi}\in\mathbf{L}^2(\Omega) \\ -\int_\Omega \mathbf{J}\cdot\nabla\phi = \int_\Omega f\phi + \int_\Gamma g\phi & \forall \phi \in U \end{cases} \qquad \text{(Mixed-Electric Currents)}$$

Lemma 7.2.2. *The bilinear form $A(\mathbf{F},\mathbf{G}) = \int_\Omega \underline{\sigma}^{-1}\mathbf{F}\cdot\mathbf{G}$ is coercive and continuous on $\mathbf{L}^2(\Omega)$ for σ essentially positive and bounded and for $\boldsymbol{\beta}\in\mathbf{L}^\infty(\Omega)$.*

Proof. We define the vector field $\boldsymbol{\beta} = \eta\mathbf{B}_0$. *Coercive:* Fix $\mathbf{F}\in\mathbf{L}^2(\Omega)$.

$$A(\mathbf{F},\mathbf{F}) = \int_\Omega \frac{1}{\sigma}(I + [\boldsymbol{\beta}]_\times)\mathbf{F}\cdot\mathbf{F} \tag{7.2.7}$$

$$= \int_\Omega \frac{1}{\sigma}|\mathbf{F}|^2 + \int_G \frac{1}{\sigma}(\boldsymbol{\beta}\times\mathbf{F})\cdot\mathbf{F} \tag{7.2.8}$$

$$= \int_\Omega \frac{1}{\sigma}|\mathbf{F}|^2 \tag{7.2.9}$$

$$\geq \|\sigma\|^{-1}_{L^\infty(\Omega)}\|\mathbf{F}\|_{\mathbf{L}^2(\Omega)} \tag{7.2.10}$$

This relies on $\boldsymbol{\beta}\times\mathbf{F}\cdot\mathbf{F} = 0$ pointwise a.e. and $\sigma\in L^\infty(\Omega)$.

Continuous: Fix $\mathbf{f},\mathbf{g}\in\mathbf{L}^2(\Omega)$.

$$|A(\mathbf{f},\mathbf{g})| \leq \left|\int_\Omega \frac{1}{\sigma}\left(\mathbf{f}\cdot\mathbf{g} + \boldsymbol{\beta}\times\mathbf{f}\cdot\mathbf{g}\right)\right| \tag{7.2.11}$$

$$\leq \frac{1}{\operatorname{ess\,inf}\sigma}\left(\left|\int_\Omega \mathbf{f}\cdot\mathbf{g}\right| + \left|\int_\Omega \boldsymbol{\beta}\times\mathbf{f}\cdot\mathbf{g}\right|\right) \tag{7.2.12}$$

$$\leq \frac{1}{\operatorname{ess\,inf}\sigma}\left(\|\mathbf{f}\|_{\mathbf{L}^2(\Omega)}\|\mathbf{g}\|_{\mathbf{L}^2(G)} + \left|\int_\Omega \boldsymbol{\beta}\times\mathbf{f}\cdot\mathbf{g}\right|\right) \tag{7.2.13}$$

Note that $|\boldsymbol{\beta}\times\mathbf{f}|^2 \leq |\boldsymbol{\beta}|^2|\mathbf{f}|^2$ point-wise a.e. Therefore if we desire $\boldsymbol{\beta}\times\mathbf{f}\in\mathbf{L}^2(\Omega)$ it is sufficient to require require $\boldsymbol{\beta}\in\mathbf{L}^\infty(G)$.

$$|A(\mathbf{f},\mathbf{g})| \leq \frac{1+\|\boldsymbol{\beta}\|^2_{\mathbf{L}^\infty(\Omega)}}{\operatorname{ess\,inf}\sigma}\|\mathbf{f}\|_{\mathbf{L}^2(\Omega)}\|\mathbf{g}\|_{\mathbf{L}^2(\Omega)} \tag{7.2.14}$$

As the bilinear form is bounded and linear, we have shown continuity. **Q.E.D.**

Lemma 7.2.3. *Let* $\mathbf{W} = \mathbf{L}^2(\Omega)$. *The bilinear form* $C : V \times \mathbf{W} \to \mathbb{R}$ *defined by* $C(v, \mathbf{f}) = \int_G \nabla v \cdot \mathbf{f}$ *is continuous and obeys the famous inf-sup conduction.*

Proof. Inf-Sup We wish to show that $\exists c$ such that

$$\inf_{u \in U} \sup_{\mathbf{f} \in \mathbf{W}} \frac{C(u, \mathbf{f})}{\|u\|_U \|\mathbf{f}\|_{\mathbf{W}}} \geq c > 0. \tag{7.2.15}$$

Fix $u \in U$.

$$\sup_{\mathbf{f} \in \mathbf{W}} \frac{C(u, \mathbf{f})}{\|f\|_{\mathbf{W}}} \geq \frac{C(u, \nabla u)}{\|\nabla u\|_{\mathbf{W}}} \tag{7.2.16}$$

$$= |u|_{H^1(G)}. \tag{7.2.17}$$

On ths space U a Poincare-Friedrich's estimate holds, i.e. $C_{p.f.}^{-1} \|v\|_{H^1} \leq |v|_{H^1} \leq C_{p.f.} \|v\|_{H^1}$ for some $C_{p.f.} > 0$. This follows from the fact that $u \in U \implies \int_\Omega u = 0$. As functions with the same gradient form an equivalence class which differ by a constant, the average value condition imposes that on U all those equivalence classes must have that constant equal to zero,

$$\inf_{u \in U} \sup_{\mathbf{f} \in \mathbf{W}} \frac{C(u, \mathbf{f})}{\|f\|_{\mathbf{W}}} \geq \frac{1}{C_{p.f.}}. \tag{7.2.18}$$

Therefore the inf-sup condition holds.

Continuity: Fix $u \in U$ and $\mathbf{f} \in \mathbf{W}$.

$$C(u, f) = \int_G \nabla u \cdot \mathbf{f} \tag{7.2.19}$$

$$\leq |u|_{H^1} \|\mathbf{f}\|_{\mathbf{W}} \tag{7.2.20}$$

$$\leq C_{p.f.} \|u\|_V \|\mathbf{f}\|_{\mathbf{W}} \tag{7.2.21}$$

Therefore the map is continuous. **Q.E.D.**

Theorem 7.2.4. *The variational electric currents for an equilibrium MHD generator are well posed when* $\mathbf{u} \times \mathbf{B}_0 \in \mathbf{H}(div, \Omega)$. *In addition the strong equations hold,* (7.1.48), *in the sense of* L^2

Proof. Let $\mathbf{F} = 0$, $f = -\nabla \cdot \mathbf{u} \times \mathbf{B}_0$, and $g = 0$. By Lemma 7.2.2, Lemma 7.2.3, and Theorem 7.2.1 $\mathbf{J}_i$ is the unique solution to the problem

$$\begin{cases} \int_\Omega \underline{\sigma}^{-1}\mathbf{J}_i \cdot \mathbf{\Phi} + \int_\Omega \nabla V \cdot \mathbf{\Phi} = 0 \quad \forall \mathbf{\Phi} \in \mathbf{L}^2(\Omega) \qquad (a) \\ \int_\Omega \mathbf{J}_i \cdot \nabla \psi = \int_\Omega \text{div}\underline{\sigma}\mathbf{u} \times \mathbf{B}_0 \psi \quad \forall \psi \in U. \qquad (b) \end{cases} \tag{7.2.22}$$

Further we have $\|\mathbf{J}_i\|$ depending continuously on $\|\text{div}\sigma\mathbf{u} \times \mathbf{B}_0\|$. The function $\mathbf{J}_i$ trivially equals $\underline{\sigma}\nabla V$ in the sense of $\mathbf{L}^2$ by (a). We will now show that given $\text{div}\underline{\sigma}\mathbf{u} \times \mathbf{B}_0 \in L^2$ we have $\mathbf{J}_i \in \mathbf{H}(\text{div}, \Omega)$ with its gradient given by $\text{div}\underline{\sigma}\mathbf{u} \times \mathbf{B}_0$. Let $\psi \in C_0^\infty \cap U$. Then

$$\int_\Omega \mathbf{J}_i \cdot \nabla \psi = -\int_\Omega \text{div}\mathbf{J}_i \cdot \psi = \int_\Omega \text{div}\underline{\sigma}\mathbf{u} \times \mathbf{B}_0 \psi. \tag{7.2.23}$$

Therefore we must have $\text{div}\mathbf{J}_i = -\text{div}\underline{\sigma}\mathbf{u} \times \mathbf{B}_0$ in the sense of L^2. Now testing against a general $\psi \in U$ we have

$$\int_\Omega \mathbf{J}_i \cdot \nabla \psi = \int_\Omega \text{div}\underline{\sigma}\mathbf{u} \times \mathbf{B}_0 \psi, \tag{7.2.24}$$

$$\int_\Gamma \mathbf{J}_i \cdot \mathbf{n} \psi = 0. \tag{7.2.25}$$

Therefore we have that $\mathbf{J}_i$ has zero normal component on all boundaries.

We have the function $\mathbf{J} = \mathbf{J}_i + \underline{\sigma}\mathbf{u} \times \mathbf{B}_0 \in \mathbf{H}(\text{div}, \Omega)$ by closure of the space. Further, $\text{div}\mathbf{J} = 0$ and $\mathbf{J} \cdot \mathbf{n} = \mathbf{n} \cdot \underline{\sigma}\mathbf{u} \times \mathbf{B}_0$ on $\Gamma_{\text{in}} \cup \Gamma_{\text{out}}$. **Q.E.D.**

Theorem 7.2.5. *Solutions to the electric current model depend continuously on σ. I.e. the mapping from the convex subset of*

$$\mathscr{C}_j : K = \{c \in L^\infty(\Omega^\sigma) : \liminf c \geq c_0\} \to \mathbf{L}^2(\Omega^\sigma), \tag{7.2.26}$$

where $\mathscr{C}_j(\sigma)$ is the solution to the PDE

$$\begin{cases} \int_\Omega \underline{\sigma}^{-1}\mathbf{J}_i \cdot \mathbf{\Psi} - \nabla V \cdot \mathbf{\Psi} = 0 \quad \forall \mathbf{\Psi} \in \mathbf{L}^2(\Omega^\sigma) \\ \int_\Omega \mathbf{J} \cdot \nabla \varphi = \int_\Omega div\underline{\sigma}\mathbf{u} \times \mathbf{B}_0 \varphi \quad \forall \varphi \in U \end{cases} \tag{7.2.27}$$

is continuous for $\mathbf{B}_0 \in \mathbf{L}^\infty(\Omega)$ and $div\underline{\sigma}\mathbf{u} \times \mathbf{B}_0 \in \mathbf{H}(div, \Omega)$.

Proof. Let $(V(\cdot:\sigma), \mathbf{J}(\cdot:\sigma))$ be the unique solution to

$$\begin{cases} \int_\Omega \underline{\sigma}^{-1}\mathbf{J}\cdot\mathbf{\Psi} - \nabla V\cdot\mathbf{\Psi} = 0 \qquad \forall \mathbf{\Psi}\in\mathbf{L}^2(\Omega) \\ \int_\Omega \mathbf{J}\cdot\nabla\varphi = \int_\Omega \mathrm{div}\underline{\sigma}\mathbf{u}\times\mathbf{B}_0\varphi \quad \forall\varphi\in U \end{cases} \tag{7.2.28}$$

Consider the difference between a solution with data $\sigma+\Delta\sigma$ where $\operatorname{ess\,inf}\Delta\sigma \geq -\frac{c_0}{2}$. Let $\Delta\mathbf{J} = \mathbf{J}(\cdot:\sigma+\Delta\sigma) - \mathbf{J}(\cdot:\sigma)$ and $\Delta V = V(\cdot:\sigma+\Delta\sigma) - V(\cdot:\sigma)$. The functions $\Delta\mathbf{J}$ and ΔV are the unique solution to the following variational problem

$$\begin{cases} \int_\Omega \frac{1}{\sigma+\Delta\sigma}(\mathbb{I}+[\boldsymbol{\beta}]_\times)\Delta\mathbf{J}\cdot\mathbf{\Psi} - \nabla\Delta V\cdot\mathbf{\Psi} = \int_\Omega \frac{\Delta\sigma}{\sigma(\sigma+\Delta\sigma)}(\mathbb{I}+[\boldsymbol{\beta}]_\times)\mathbf{J}(\cdot:\sigma)\cdot\mathbf{\Psi} \\ \int_\Omega \Delta\mathbf{J}\cdot\nabla\varphi = -\int_\Omega \mathrm{div}\frac{\Delta\sigma}{\sigma(\sigma+\Delta\sigma)}(\mathbb{I}+\boldsymbol{\beta}\boldsymbol{\beta}^T-[\boldsymbol{\beta}]_\times)\mathbf{u}\times\mathbf{B}_0\varphi \end{cases} \tag{7.2.29}$$

Applying the *a priori* estimate of the mixed space formulation we have

$$\|\Delta\mathbf{J}\|_{\mathbf{L}^2(\Omega)} \leq \|\Delta\sigma\|_\infty \frac{1+\|\boldsymbol{\beta}\|_\infty^2}{\operatorname{ess\,inf}\sigma}\Big(\|\mathbf{J}(\cdot:\sigma)\|_{\mathbf{L}^2(\Omega)} \tag{7.2.30}$$

$$+\frac{1}{C_{pf}}\left(\frac{1+\|\boldsymbol{\beta}\|_\infty^2}{\operatorname{ess\,inf}\sigma} - C_{pf}\right)\frac{\|\mathrm{div}\|_{\mathbf{H}(\mathrm{div},\Omega)}}{\operatorname{ess\,inf}\sigma}\|\mathbf{u}\times\mathbf{B}_0\|_{\mathbf{L}^2(\Omega)}\Big). \tag{7.2.31}$$

Therefore by letting $\|\Delta\sigma\|_\infty \to 0$ we force $\|\Delta\mathbf{J}\|_2 \to 0$. Note that dependence on ΔV is built into the a-priori estimate on $\Delta\mathbf{J}$.

Q.E.D.

7.2.2 Well Posedness of Magnetostatics

We consider a variational formulation of the Magnetostatics problem (7.1.50)

$$\begin{cases} \int_\Omega \mu^{-1}\mathbf{curl}\mathbf{A}_i\cdot\mathbf{curl}\mathbf{\Phi}_i + \int_\Omega \nabla\lambda\cdot\mathbf{\Phi}_i = \int_\Omega \mathbf{J}\cdot\mathbf{\Phi}, & \forall\mathbf{\Phi}\in\mathbf{H}_0(\mathbf{curl},\Omega) \\ \int_\Omega \mathbf{A}_i\cdot\nabla\psi = \int_\Omega f\psi, & \forall\psi\in\mathbf{H}_0^1(\Omega) \end{cases}. \tag{7.2.32}$$

We will prove the well-posedness using a mixed space approach. Define operators

$$\mathcal{H} : \mathbf{H}_0(\mathbf{curl}, \Omega) \to \mathbf{H}_0(\mathbf{curl}, \Omega)', \tag{7.2.33}$$

$$\mathcal{H}\mu^{-1}u(\mathbf{v}) = \int_\Omega \mathbf{curlu} \cdot \mathbf{curlv}, \tag{7.2.34}$$

$$\mathcal{G} : \mathbf{H}_0^1 \to \mathbf{H}_0(\mathbf{curl}, \Omega)', \tag{7.2.35}$$

$$\mathcal{G}v(\mathbf{u}) = \int_\Omega \mathbf{u} \cdot \nabla v. \tag{7.2.36}$$

Lemma 7.2.6. *The operator $\mathcal{H}$ is coercive on the kernel of $\mathcal{G}$ and continuous on $\mathbf{H}(\mathbf{curl}, \Omega)$ for $\mu^{-1} \in L^\infty(\Omega)$ and essentially positive.*

Proof. **Coercive:** The condition $\mathbf{A} \in \mathrm{Ker}(\mathcal{G})$ is exactly that $\mathbf{A}$ has weak divergence equal to zero a function in L^2. Therefore $\mathbf{A} \in \mathbf{H}_0(\mathbf{curl}, \Omega) \cap \mathbf{H}(\mathrm{div}, \Omega)$. As $\mathbf{n} \times \mathbf{A} \in \mathbf{L}^2(\Gamma)$ we have the estimate

$$\|\mathbf{curlA}\|_{\mathbf{L}^2(\Omega)} + \|\mathrm{div}\mathbf{A}\|_{\mathbf{L}^2(\Omega)} + \|\mathbf{n} \times \mathbf{A}\|_{L^2(\Gamma)} \geq C_{p.f.}\|\mathbf{A}\|_{\mathbf{L}^2(\Omega)}. \tag{7.2.37}$$

This result is discussed in detail in Monk's book [39]. We know that $\mathrm{div}\mathbf{A} = 0$ and $\mathbf{n} \times \mathbf{A} = 0$ therefore we have

$$\|\mathbf{curlA}\|_{\mathbf{L}^2(\Omega)} \geq C_{p.f.}\|\mathbf{A}\|_{\mathbf{L}^2(\Omega)}. \tag{7.2.38}$$

This is sufficient to show $\mathcal{H}$ is coercive on Ker$\mathcal{G}$ as

$$\mathcal{H}\mathbf{A}(\mathbf{A}) \geq \mathrm{ess\,inf}\,\mu^{-1}\|\mathbf{curlA}\|_{\mathbf{L}^2(\Omega)} \geq \mathrm{ess\,inf}\,\mu^{-1}\frac{C_{pf}}{1 + C_{pf}}\|\mathbf{A}\|_{\mathbf{H}(\mathbf{curl},\Omega)}. \tag{7.2.39}$$

Continuity Is immediate,

$$\mathcal{H}\mathbf{A}(\mathbf{B}) \leq \|\mu^{-1}\|_{L^\infty}\|\mathbf{curlA}\|_{\mathbf{L}^2(\Omega)}\|\mathbf{curlB}\|_{\mathbf{L}^2(\Omega)} \tag{7.2.40}$$

$$\leq \|\mu^{-1}\|_{L^\infty(\Omega)}\|\mathbf{A}\|_{\mathbf{H}(\mathbf{curl},\Omega)}\|\mathbf{B}\|_{\mathbf{H}(\mathbf{curl},\Omega)}. \tag{7.2.41}$$

Q.E.D.

Lemma 7.2.7. *The operator $\mathcal{G}$ is continuous and obeys the inf-sup condition.*

Proof.

Continuity : Again this property is immediate,

$$\mathcal{G}v(\mathbf{u}) \leq \|\mathbf{u}\|_{\mathbf{L}^2}\|\nabla v\|_{\mathbf{L}^2} \leq \|\mathbf{u}\|_{\mathbf{H}(\mathbf{curl},\Omega)}\|v\|_{\mathbf{H}^1(\Omega)}. \tag{7.2.42}$$

Inf-Sup: This proof follows from the immediately from the case where our domain is $\mathbf{L}^2(\Omega)$. Note that from the Hilbert complex we know that $\nabla u \in \mathbf{H}(\mathbf{curl},\Omega)$ for every $u \in \mathbf{H}^1(\Omega)$ as $\mathbf{curl}\nabla = 0$. Fix $u \in \mathbf{H}^1(\Omega)$.

$$\sup_{\mathbf{u}\in\mathbf{H}(\mathbf{curl},\Omega)} \frac{\mathcal{G}v(\mathbf{u})}{\|\mathbf{u}\|_{H(\mathbf{curl})}} \geq \frac{\mathcal{G}(v,\nabla v)}{\|\nabla v\|_{\mathbf{L}^2}} \tag{7.2.43}$$

$$= \|\nabla v\|_{L^2} \tag{7.2.44}$$

As $H_0^1(\Omega)$ has a Poincare Friedrich's $|v|_{H^1(\Omega)} \geq C_{p.f}\|v\|_{H^1(\Omega)}$ we have

$$\frac{\mathcal{G}(v,\nabla v)}{\|\nabla v\|_{\mathbf{L}^2}} \geq C_{p.f.}\|v\|_{H^1(\Omega)} \tag{7.2.45}$$

which implies that

$$\inf_{v\in H^1(\Omega)} \sup_{\mathbf{u}\in\mathbf{H}(\mathbf{curl},\Omega} \frac{\mathcal{G}v(\mathbf{u})}{\|v\|_{H^1}\|\mathbf{u}\|_{H(\mathbf{curl})}} \geq C_{p.f.} \tag{7.2.46}$$

Q.E.D.

Theorem 7.2.8. *The magnetostatics problem for equilibrium MHD generators* (7.1.50) *assuming* $\mathbf{A}_0 \in \mathbf{H}(\mathbf{curl},\Omega) \cap \mathbf{H}(div,\Omega)$ *and* $\mathbf{A}\times\mathbf{n}$ *is in* $\mathbf{L}^2(\Omega)$.

Proof. Choosing $\mathbf{J} = \mathbf{J} - \mathbf{curlA}_0$ and choosing $f = \mathrm{div}\mathbf{A}_0$ we have $\mathbf{A}_i$ is the unique solution of the following variational problem,

$$\begin{cases} \displaystyle\int_\Omega \mathbf{curlA}_i \cdot \mathbf{curl}\boldsymbol{\Phi} + \int_\Omega \nabla\lambda\cdot\boldsymbol{\Phi} = \int_\Omega (\mathbf{J} - \mathbf{curlcurlA}_0)\cdot\boldsymbol{\Phi} & \forall\boldsymbol{\Phi}\in\mathbf{H}_0(\mathbf{curl},\Omega) \\ \displaystyle\int_\Omega \mathbf{A}_i\cdot\nabla\psi = \int_\Omega \mathrm{div}\mathbf{A}_0\psi & \forall\psi\in H_0^1(\Omega) \end{cases} \tag{7.2.47}$$

by Lemmata 7.2.6 and 7.2.7 and Theorem 7.2.1. **Q.E.D.**

Theorem 7.2.9. *If* $\mathbf{J}$ *is defined as in Theorem 7.2.4 and* $\mathbf{B}_i = \mathbf{curl}\mathbf{A}_i$ *as defined in 7.2.8, the* $\mathbf{B}_i$ *depends continuously on* $\mathbf{J}$.

Proof. We have constructed $\mathbf{J}_i$ such that $\mathbf{J}$ is divergence free. This gives us that $\mathbf{curlcurlA}_i = \mathbf{J} - \mathbf{curlcurlA}_0$. Consider $\mathbf{A}_i(\sigma)$ being the induced magnetic potential from $\mathbf{J}(\sigma)$. Define $\Delta\mathbf{A}_i = \mathbf{A}_i(\sigma + \Delta\sigma) - \mathbf{A}_i(\sigma)$ and $\Delta\mathbf{J}$ similarly and $\Delta\mathbf{B}_i = \mathbf{curl}\Delta\mathbf{A}_i$. As every $\mathbf{J}$ is divergence free we have $\Delta\mathbf{J}$ is divergence free. The change $\Delta\mathbf{A}_i$ obeys the following variational problem

$$\begin{cases} \mathcal{H}\Delta\mathbf{A}_i(\mathbf{\Phi}) = \langle \Delta\mathbf{J}, \mathbf{\Phi} \rangle_{\mathbf{H}_0(\mathbf{curl},\Omega)} \\ \mathcal{G}'\Delta\mathbf{A}_i(\psi) = 0 \end{cases} . \tag{7.2.48}$$

We have dropped the Lagrange multiplier λ as we know it to be zero. The a-priori error estimate for mixed space systems then implies that

$$\|\Delta\mathbf{B}_i\|_{\mathbf{L}^2(\Omega)} \leq \|\Delta\mathbf{A}_i\|_{\mathbf{H}(\mathbf{curl},\Omega)} \leq \alpha\|\Delta\mathbf{J}\|_{\mathbf{L}^2(\Omega)}. \tag{7.2.49}$$

As $\Delta\mathbf{J}$ depends continuously on σ taking $\Delta\sigma \to 0$ will result in $\Delta\mathbf{B}_i \to 0$. **Q.E.D.**

7.3 Heuristic Arcing

In MHD Generators a major challenge is the formation of arcs at the electrode-fluid interface. These arcs can be attributed to a boundary layer effect: namely that sharp drop in fluid temperature from the bulk flow to the electrode (which is cooled) causes a sharp drop in electrical conductivity. Because the electrical conductivity is low but there is still a potential difference being forced across the channel, currents seek a way to resolve this potential by "jumping the conductivity gap" resulting in arc formation. These arcs in essence gather ions from the fluid, vaporize the electrode, or most likely will locally ionize gaseous seed (for example potassium carbonate) in the boundary layer in order

to create the conductivity necessary to sustain the discharge. If the electrode surface is vaporized then we are clearly damaging the electrode – resulting in expensive damage to the generator.

Finding an accurate model for arcing is complicated and may be computationally impractical except on a very large computer. For this reason we will consider **heuristic arc models**. The heuristic that we use is the addition of artificial conductivity in the boundary layer. This approach is relatively sensible in that arcs create their own conductivity. In this section we will analyze the sensitivity of magnetic fields to these heuristic arcs as a proof of concept of the detection of arcs from perturbations in the magnetic field outside of the channel.

7.3.1 Magnetic Fields and Parameterized Currents

In our first investigation of the sensitivity of magnetic fields to arcing we have implemented a lowest order 3D MFD discretiztion of the magnetostatics equations. Here we have solved the following discrete variational problem:

$$\begin{cases} [\mathbf{curl}_h \mathbf{A}_h, \mathbf{curl}_h \mathbf{\Phi}_h]_{\mathscr{F}} + [\nabla_h \lambda_h, \mathbf{\Phi}_h]_{\mathscr{E}} = [\mathbf{J}_h, \mathbf{\Phi}_h]_{\mathscr{E}} & \forall \mathbf{\Phi}_h \in \mathscr{E}_h \in \mathscr{E} \\ [\mathbf{A}_h, \nabla_h \psi_h] = 0 & \forall \psi_h \in \mathscr{V}_h \end{cases} \tag{7.3.1}$$

Using a uniform cubic mesh of a cube and imposed Dirichlet type boundary conditions on both $\mathbf{A}_h$ and λ_h for simplicity. In order to determine the viability of the response of the induced magnetic flux density to changes in the current density we will perform a sensitivity analysis. There are number of features of current densities which are suspected to occur in MHD Generator channels which we would like to be able to detect.

Total Current Given that the current is extracted from the channel by the load applied across the electrodes, this will be a design parameter for the generator.

Current Density Experimental evidence from legacy MHD research suggests that the destructive macro-arcs which form at electrodes will have much denser current pro-

files than the diffuse state. As our long term goal is to detect the location of the arcs inside the generator and facilitate an understanding of their dynamics, this is perhaps the most critical parameter for sensitivity.

Direction of Current Density It is known from earlier MHD work that the Hall effect causes a tilt to the current density, pointing the current slightly in the direction of the fluid flow [23]. Sensitivity to this parameter would allow one to estimate the magnitude of the Hall effect near the sensor.

Given these three features, we have developed the following parameterized current profile

$$\mathbf{J}(\mathbf{x}; J_m, s, \theta) = \mathbf{v}\frac{J_m}{\sqrt{2\pi s^2}} \exp\left(\frac{1}{2s^2}\left|\left(\mathbb{I} - \mathbf{v}\mathbf{v}^T\right)\mathbf{x}\right|^2\right), \quad \mathbf{v} = \begin{bmatrix}\cos\theta \\ \sin\theta \\ 0\end{bmatrix}. \tag{7.3.2}$$

This current density is a Gaussian around the line passing through the origin pointing in the direction $(\cos\theta, \sin\theta, 0)^T$. The parameter J_m (A/m^2) controls the total current in the system, the parameter s (m) controls the spread of the density profile, and θ controls the tilting of the arc due to the Hall effect. A significant feature of this formulation is that the profile is naturally divergence free as all variation happens orthogonally to the direction the vector field is pointing.

To perform our sensitivity analysis we fix two parameters and vary the third. We compute actual magnetic flux density values instead of derivatives in order to additionally inform the necessary specifications of measurement equipment. We assume our domain is $[-1, 1]^3$, the magnetic permeability is constant and on the order of 10^{-6} (which is on the order of magnitude of air at STP) and we measure the magnetic flux density at the origin and at $(0, 0.25, 0)$. The center result is to estimate the magnitude of fields very close to the arc, while the short distance away is to demonstrate the effect of measuring outside the

channel near where sensors would be placed. The sensitivity results are depicted in Figure 7.3. Figure 7.3(a) shows high sensitivity to J_m, while Figure 7.3(b) shows an increasing sensitivity to s in the limit toward smaller diameter, i.e., dense arcs. Finally, Figure 7.3(c) shows some interesting phenomenon. Namely when we measure the magnetic flux density inside the arc we see that increasing the intensity of the arc as s decreases. A short distance away however we see that when the s decreases past some critical value ($s \approx 0.2$) the magnetic flux will decrease as well. This is consistent with exact solutions of the magnetic field using a Biot-Savart law for current along an infinite line which is the limit of this current distribution as $s \to 0$.

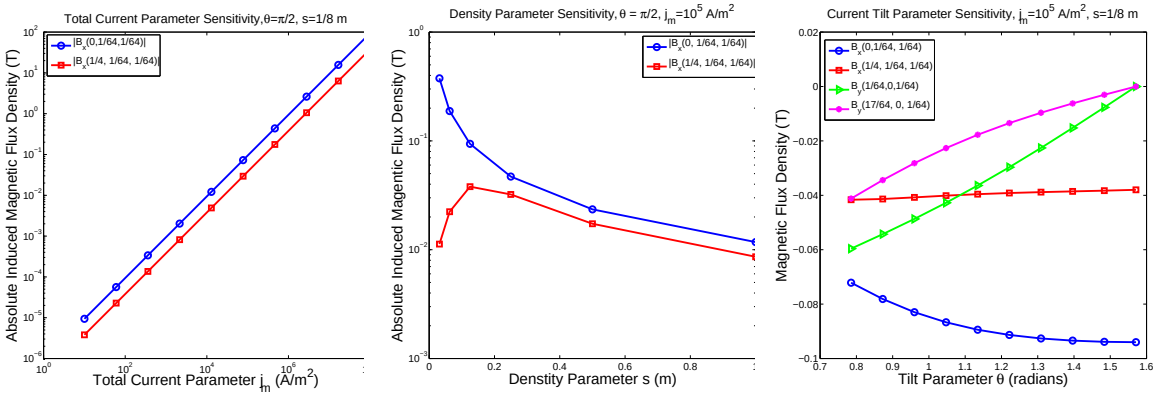

(a) (b) (c)

FIGURE 7.3: Analysis of the sensitivity of the induced magnetic flux density to the three current density parameters: J_m, s, and θ.

7.3.2 Back-powered Channel with Artificial Conductivities

In order to increase the complexity of our underlying model we have used an equilibrium MHD model for a generator assuming that $\mathbf{B}_0 = 0$. In addition, as this experiment will be adding an arcing heuristic rather than examining areas where arcs are likely to form in the generator we neglected the effect of Joule heating in this model. To simulate the current paths which might lead to arcing, we pump current into the system through a non-homogeneous boundary condition on $\mathbf{J}_i$ in two electrodes.

To create a heuristic for arcing we will add a parameterized artificial conductivity to a physical conductivity $\sigma_b(T, p)$. This physical conductivity was produced by solving for the chemical equilibrium for the combustion products of oxyfuel-methane combustion using a code provided by collaborators at the National Energy Technology Laboratory. The arc conductivity is parameterized as

$$\sigma_a(\mathbf{x}) = \sigma_{\max} \exp(-s\|(\mathbb{I} - \mathbf{v}\mathbf{v}^T)(\mathbf{x} - \mathbf{x}_c)\|^2 - \ell\|\mathbf{x} - (\mathbf{x}_c + r\mathbf{v})\|), \tag{7.3.3}$$

$$\mathbf{x}_c = (x_c, 0, 0)^T, \tag{7.3.4}$$

$$\mathbf{v} = (0, \cos\theta, \sin\theta)^T. \tag{7.3.5}$$

For this experiment we solve the non-isothermal hydrodynamics in order to generate the conductivity profile σ_b. All of our solutions in this section were computed using COMSOL Multiphysics commercial software.

For our simulations we choose our inflow velocity to be $\mathbf{u}_0 = (300\frac{\mathrm{m}}{\mathrm{s}}, 0, 0)$, our inflow temperature to be 2500 K, our wall temperature to be 500 K. We add 15 A of current in through the inflow wire and ground the outflow wire. In Figure 7.4 we show the temperature profile across the channel (in the y direction) and along the channel (x direction). The temperature distribution appears to have a "top hat profiles" along every cross section and the temperature drops along the length of the channel – although non-linearly. This non-linear decrease may be non-physical but the general cooling trend can be attributed to the non-physical cooled wall boundary condition that we are applying. Figure 7.5 shows the cross sectional conductivity of the channel in the absence of the arc conductivity and with it present. Figure 7.6 shows the log of the current density norm and several stream lines. The inflow current enters through the wire on the left while the ground is on the right.

We seek to determine how the parameterization of σ_a will perturb the magnetic field. To do so we solve for $\mathbf{J}$ and $\mathbf{B}$ on a grid in the x_c, θ plane and generating many distinct arc configurations. We choose $\sigma_{\max} = 10^7$ (as if the arc were vaporizing the electrode), and

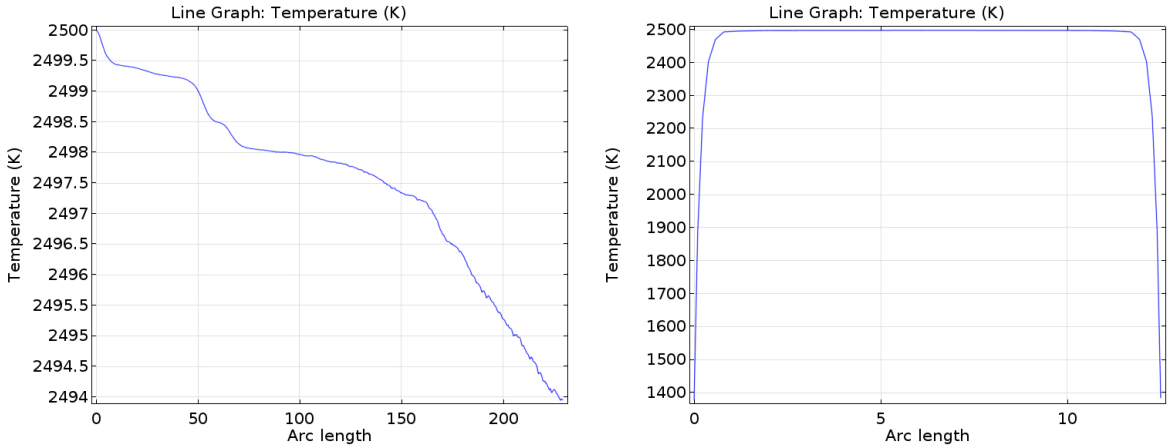

(a) (b)

FIGURE 7.4: Temperature profiles for a back-powered channel: (a) is the profile along the centerline of the channel while (b) temperature profile across the channel

.

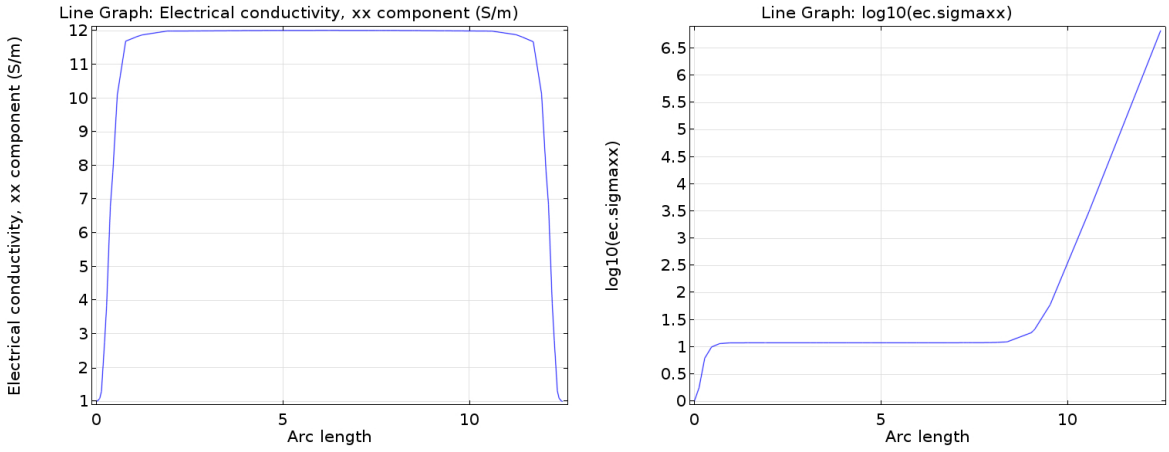

(a) (b)

FIGURE 7.5: Conductivity profiles in the case of no arcing (a) and heuristic arcing (b). Figure (b) shows the $\log_{10}(\sigma)$.

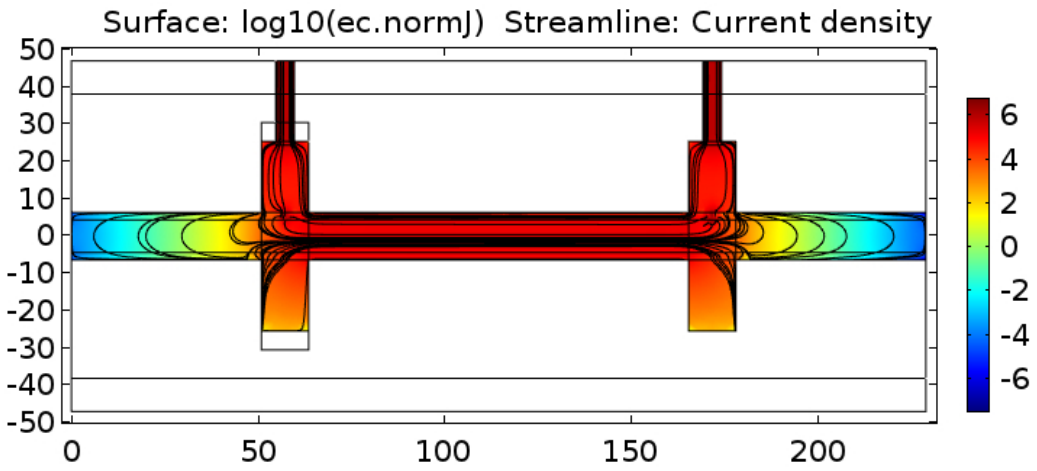

FIGURE 7.6: Current densities and streamlines in a back-powered channel. 15 A are added by in the left wire while the right wire is grounded at 0 V. This figure shows a heuristic arc at both electrodes.

.

we choose $\ell = 5$ and $s = 20$. We measure the magnetic field at 5 equally spaced points around the outer boundary of the electrode. See Figure 7.7 for the configuration.

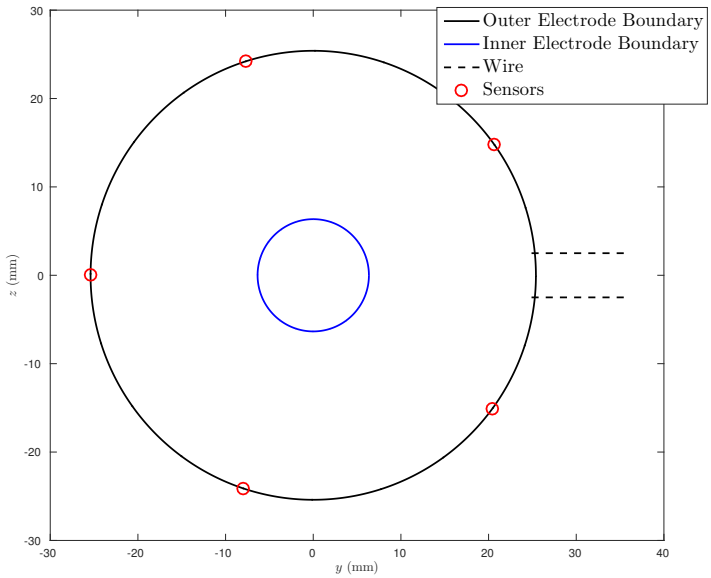

FIGURE 7.7: Magnetic field measurement configuration for the back-powered channel.

Having established both our measurements and our model parameters we will now

show sensitivities for the grid of x_c, θ values. We show the difference between a magnetic field with arcing at a particular location and a generator without arcing. Call $\mathbf{B}_i(\cdot; \mathbf{x}_c, \theta)$ the induced field from an arc at $(\mathbf{x}_c, \theta)$ and define the induced field without arcing $\mathbf{B}_{i,0}$. At each sensor we will plot the quantity

$$\Delta B_{x_i}(\cdot; \mathbf{x}_c, \theta) = \mathbf{e}_i \cdot (\mathbf{B}_i(\cdot; \mathbf{x}_c, \theta) - \mathbf{B}_{i,0}) \tag{7.3.6}$$

which is the difference in the x_i direction.

Figure 7.8 shows the sensitivity of ΔB_{x_i}. This experiment shows that in general the magnetic field is more perturbed by increasing x_c. Further, we see that by changing the angle θ we can change the sign of the perturbation. This is true for all sensors and roughly states that the direction of the magnetic field is sensitive to the position of the arc. This may suggest moving forward that features like the Hall effect– which distort the orientation of the current density paths, should also distort the magnetic field. It is also worth noting that we expect, in this case, that an increase in the inflow current will linearly scale the magnitude of the magnetic flux.

7.4 3D Currents in Equilibrium Generators

In this section we will create numerical simulations of current densities arising in equilibrium MHD generators, namely by finding approximate solutions to equations (7.1.46) and (7.1.48). The purpose of this section is to provide qualitative validation for the model – namely by showing that the model captures qualitative features which are well known in the field. We will consider a segmented Faraday generator geometry. We used COMSOL to generate the numerical solutions in this section.

This situation is different from the backpowered channel experiment primarily from the introduction of the applied field $\mathbf{B}_0$. We chose $\mathbf{B}_0 = (0, 0, B_0)^T$ and select B_0 as a

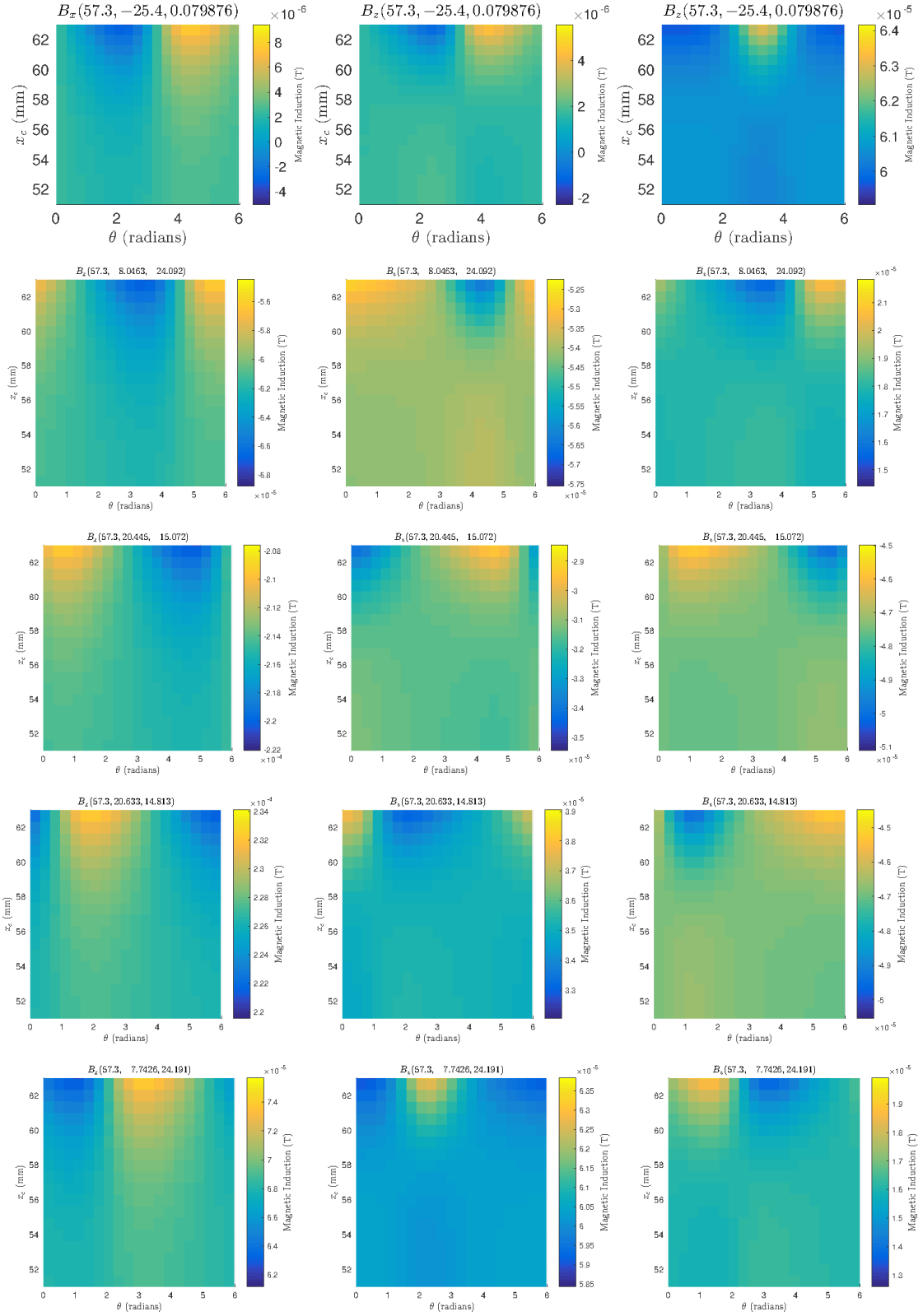

FIGURE 7.8: Sensitivity of magnetic fields to σ_a in a back-powered channel. First column is component x, second is component y, third is component z. Rows represent sensors moving counter clockwise starting opposite the wire.

difference of logistic curves:

$$B_0 = \frac{B_{\max}}{2}\left(\frac{1}{1+\mathrm{e}^{-k(x-x_\ell)}} - \frac{1}{1+\mathrm{e}^{-k(x-x_r)}}\right) \tag{7.4.1}$$

where $B_{\max} = -2$ T and k, x_r, x_ℓ are tuned so that the magnetic field is "on" before the first segment begins and "off" before the channel ends. In the presence of the magnetic field produces two major effects – first it creates current in the channel due to the flow, it introduces the Lorentz force thus strongly coupling the magnetic fields and currents to the fluid flow, and finally it introduces the Hall effect which makes the effective conductivity anisotropic. In this experiment, in contrast with the backpowered channel, we do not neglect Joule-heating effects introducing another dimension of coupling between the fluid flow (through the heat equation) and electromagnetics.

We will begin by investigating some cross sectional properties of the channel. First let ℓ_1 be the line pointing in the $+x$ direction passing through the center of the channel and let ℓ_2 be the line pointing in the $+y$ direction likewise centered in the channel. On these lines we will show physical quantities normalized by their maximum value. This is done to emphasize qualitative properties rather than specific values. In Figure 7.9 we show quantities on ℓ_1. We see that along the length of the channel quantities such as velocity, temperature, pressure, and gas density are almost constant. All of the values appear correlated with constant behavior in the end regions and approximately linear behavior along the length of the channel. This may be due to the very short length of the channel (120 mm). This figure also shows that both heat flux and the x component of the Lorentz force are strongly activated in the inter-electrode space. However, we see interesting jumps in the end regions – for example heating in the end regions. This heating may be due to end-region eddy currents. In addition these two quantities both exhibit numerical oscillations suggesting that sophisticated stabilization strategies may be necessary for low resolution realizations of these quantities.

In Figure 7.10 we show variables on along ℓ_2. We see that the x component of

velocity exhibits a strong top hat behavior. We also see a somewhat sinusoidal behavior or in the y component of velocity. We see strong boundary layer features in the gas density, effective conductivity, temperature, and heat flux.

Next we will explore current paths with early two-dimensional modelling of MHD generators, c.f. [16, 47]. In Figure 7.11 we show the voltage and current density paths in

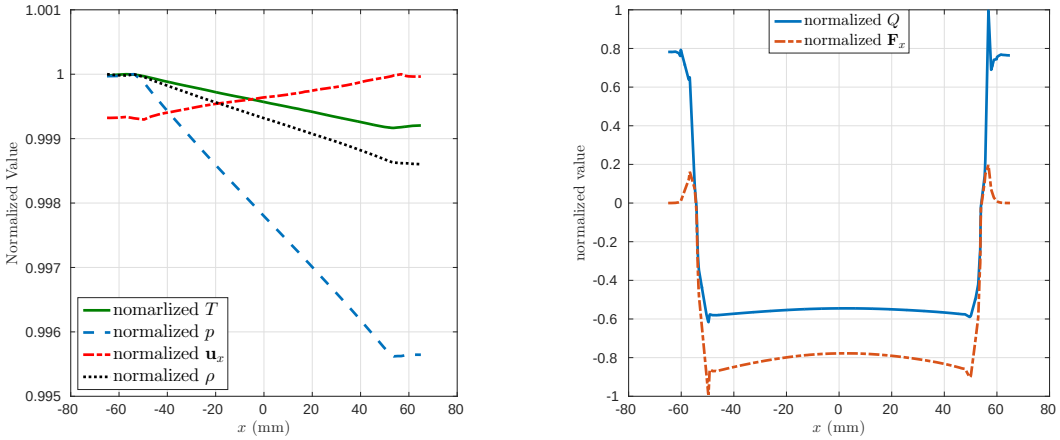

FIGURE 7.9: Normalized values on an line in the x direction centered in the channel. (Left) We show temperature, x component of velocity, and gas density. (Right) We show the x component of the Lorentz Force and heat flux.

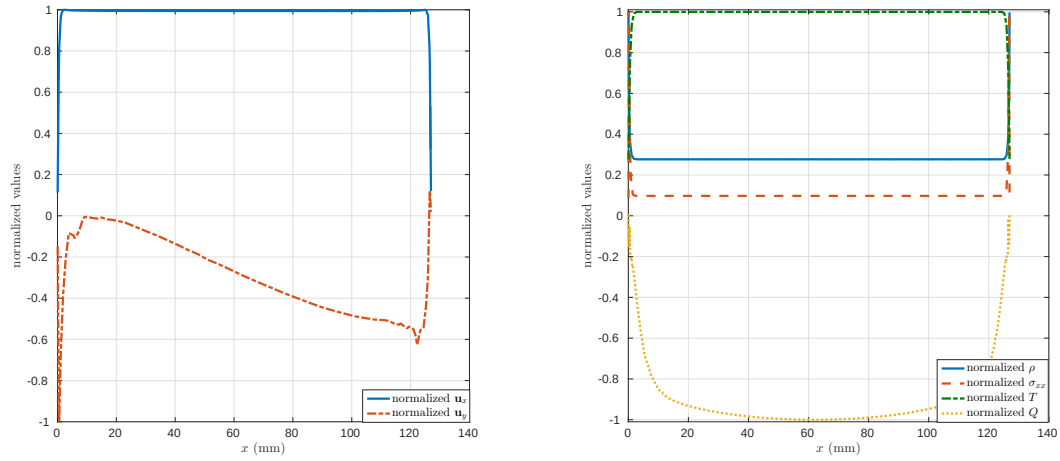

FIGURE 7.10: Noramlized values on a line in the y direction centered in the channel. (Left) We show x and y components of velocity. (Right) we show gas density, the xx component of effective conductivity, temperature, and heat flux.

an xy plane passing through the center of the generator. We see that there is a voltage difference in both the x and y direction of the channel. Interestingly we see a roughly uniform change in voltage across every electrode (roughly 20 V). In addition we see the current concentration at the corners of the electrodes. This agrees qualitatively with [16, 47]. In addition we see strong eddies in the end regions– large vortical structures outside of the electrodes. This phenomenon is referred to in the literature, c.f. [16], as a *end region eddy*. See Figure 7.12 for a 3D realization of this feature. Note the strong non-uniformity in all directions. These features may be the reason for the positive heating observed in the end regions, c.f. Figure 7.9. In two dimension these features have been observed in [16].

In addition we want to highlight some of the advantages of a 3 dimensional simulation rather than reduced dimensional models of the generator. In particular we show normalized current density and normalized heat fluxes at the electrode-fluid interface in Figure 7.13. We observe that both the current densities and heat flux concentrated at one end of the electrode instead of being uniformly distributed across the electrode. This suggests where arcing is most likely to occur–namely at the edge of the electrode. In addition, the anisotropic heat flux makes it clear that the Dirichlet type boundary conditions for temperature are *non-physical*. For an accurate model it may be necessary to also solve the heat transfer in the casing in order to more accurately represent the temperature in the fluid.

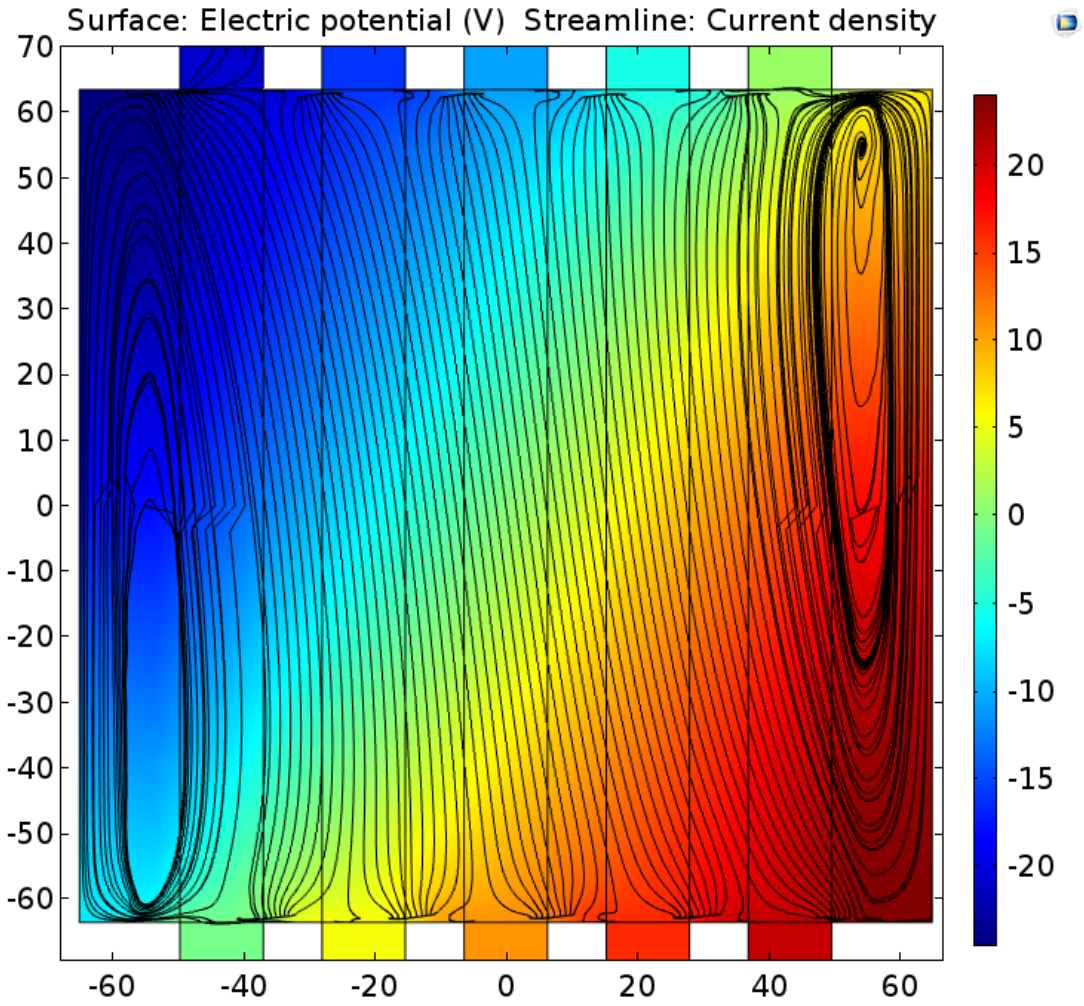

FIGURE 7.11: Surface coloring is the voltage while stream lines are current paths. Note concentration of currents at edges of electrodes.

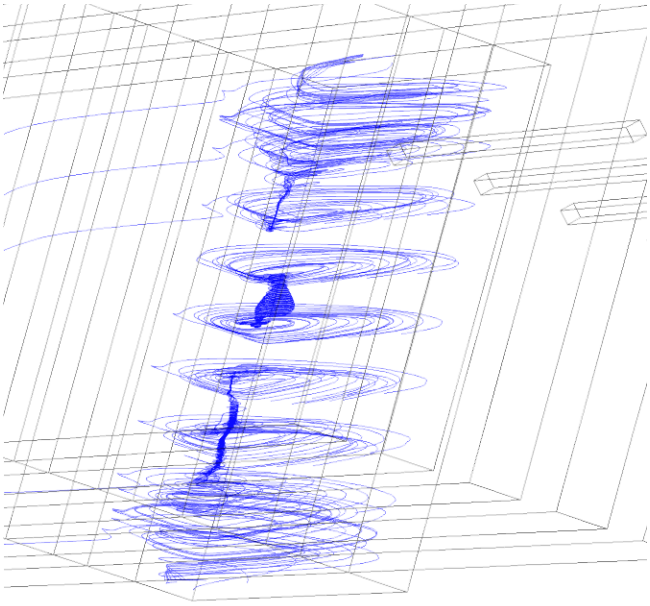

FIGURE 7.12: 3D current path in end region eddy. Vortical structures may reduce efficiency do to Joule heating

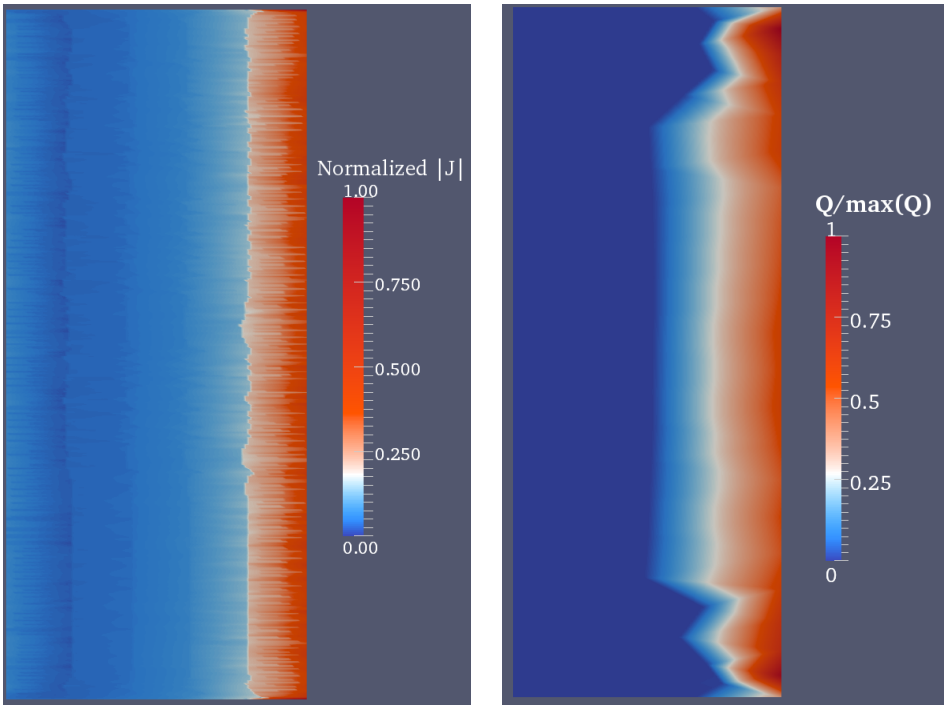

FIGURE 7.13: Normalized current densities $|\mathbf{J}|/\max|\mathbf{J}|$ at fluid-electrode interface. Current densities concentrated at the edges of the electrode rather than being uniformly distributed. Further the heat source Q appears to concentrate where $\mathbf{J}$ is concentrated suggesting that the Joule heating is dominant in the boundary region.

8 CONCLUSIONS

The products of this thesis are as follows. We have introduced the theory of low order mimetic finite difference methods in a way which highlights the simlarities of the MFD to the VEM. We have developed a framework for creating M-adapted MFD discretizations for Maxwell's Equations with general linear polarization laws. These schemes are truly explicit, relying on a generalization of mass lumping which simultaneously eliminates the need to solve a linear system at every time step and preserves a set of free parameters for optimization. These M-adapted schemes have super convergent dispersion error at fourth order rather than second order guaranteed by MFD family. Further we have found that the optimal parameters for free space and for polarization media are identical as long as one employs exponential time differencing. We have also found that M-adaptation is not possible for time averaged differencing.

We found that the error of the M-adapted schemes is very senstive to initial conditions but were able to demonstrate theoretically optimal convergence and dispersion errors by discretely eliminating a variable. We hypothesize that this sensitivity is due to the fact that we have optimized for plane waves which do not truly have initial conditions. Our numerical demonstrations have shown that the reduction of dispersion also reduces the numerical anisotropy of the method compared to the Yee scheme. We have proven that these schemes obey conditional stability constraints identical to the Yee scheme on rectangular meshes. Numerical experiments illustrate that these stability estimates are sufficient as well as necessary.

Lastly, we have developed a model for equilibrium MHD generators. We have proven that the electromagnetic fields in this model are well posed and that magnetic fields depend continuously on electric currents, which in turn depend continuously on electrical conductivity. We developed a simple heuristic for arcing – namely the addition of non-

physical conductivity. By parameterizing this heuristic we have quantified the sensitivity of magnetic fields to this heuristic. We found that for a heuristic arc magnetic fluxes are most sensative to an increase in the arc location deeper into the channel and geometrically sensitive to the orientation of the arc.

8.1 Open Probems

In this section we pose several open problems that can guide future research in the construction and analysis of MFD methods and the modeling and analysis of MHD generators.

1. The M-Adapted MFD discretizations are very sensitive to initial conditions in first order formulation. Can a quadrature for calculating initial conditions, or some more sophisticated method, be developed to guarantee optimal order convergence?

2. The stability analysis technique provided only necessary conditions. However, one could prove necessary and sufficient conditions for stability if one employed **energy analysis**. Consider Leap frog time staggering and MFD applied to Maxwell's equations in free space. The following quantity is provable constant at every time step

$$\mathcal{E}_h^n = \|\mathbf{E}_h^n\|_{\mathscr{E}}^2 + [H_h^{n+1/2}, H_h^{n-1/2}]_{\mathscr{F}}. \tag{8.1.1}$$

   By proving conditions under which $\mathcal{E}_h^n$ is a norm, i.e. by proving that $[H^{n+1/2}, H^{n-1/2}]_{\mathscr{F}}$ is positive, then we would have necessary and sufficient conditions for stability. This argument requires an exact calculation or a very tight estimate of

$$\|\mathbb{W}_{\mathscr{E}}\mathrm{curl}_h^T\mathbb{M}_{\mathscr{F}}\mathrm{curl}_h\|_{\mathscr{E}} \tag{8.1.2}$$

   where the above norm is the operator norm induced by $[\cdot,\cdot]_{\mathscr{E}}$.

Once this problem is solved it will be interesting to investigate stability for the ETMFD. While this energy estimate proof essentially follows the proof for the Yee scheme it is unclear how to define the discrete energy for the ETMFD. Can this be done for a general polarization law or will we have to consider a case by case approach?

3. In this thesis we developed M-adaptation to increase the accuracy of methods. However, there are two equally obvious other objectives – namely stability and computational complexity. The stability optimization problem would require necessary and sufficient conditions for stability for the entire mimetic family. Once developed is there an optimal member? Can this approach be extended to unstructured polyhedral meshes?

   In terms of computational efficiency, we already know that on square and rectangular meshes there exists a choice of parameters which diagonalizes the matrix $\mathbb{W}_{\mathscr{E},f}$. Can an algorithm be developed which creates diagonal $\mathbb{W}_{\mathscr{E},f}$ for a general polygonal mesh? Will the degeneracy of the mesh effect stability? What are the computational trade offs between the optimization (which seems like it will be done at compute time rather than off line) and the improvement in the efficiency of the scheme? For what size problem would this approach be practical?

4. Can the M-adaptation procedure be extended to non-commuting meta-materials? In this case Maxwell's equations are posed as

$$\begin{cases} \mathbf{u} = \mathbb{X}\mathbf{u} + D\mathbf{v} \\ \mathbf{v} = \mathbb{Y}\mathbf{v} - D\mathbf{u} \end{cases} \tag{8.1.3}$$

   where

$$\mathbf{u} = \begin{pmatrix} \mathbf{E} \\ \mathbf{P}_m \end{pmatrix}, \quad \mathbf{v} = \begin{pmatrix} \mathbf{H} \\ \mathbf{M}_\ell \end{pmatrix}, \quad D = \begin{pmatrix} \mathbf{curl} & 0 \\ 0 & 0 \end{pmatrix}. \tag{8.1.4}$$

I am calling the material non-commuting as I assume that $\mathbb{X}$ and $\mathbb{Y}$ do not commute.

5. An answer to the previous question would allow for the development of M-adapted uniaxial perfectly matched layers. Does dispersion reduction improve the performance of the PML?

6. Can an immersed interface method be created which allows for dispersion reduction using M-adaptation in a domain with piecewise constant material models? This would allow for accurate solutions and also offset the inability of square and rectangular meshes to accurate model complex geometry.

7. Are the theoretical optimal geometries for MHD generators, which were developed with 0 dimensional calculations, actually optimal? This problem is a topology optimization problem on the MHD generator. Here the objective function would be the generator efficiency

$$\text{EFF} = \frac{\displaystyle\int_{\text{resistors}} \sigma^{-1}\mathbf{J}\cdot\mathbf{J}}{\displaystyle\int_{\text{channel}} (\mathbf{u}\times\mathbf{B})^T\underline{\sigma}(\mathbf{u}\times\mathbf{B})} = \frac{P_{\text{available}}}{P_{\text{ideal}}} \tag{8.1.5}$$

This quantity is related to a zero dimensional design parameter called the *loading factor*. The parameter space might be the ratio of electrode thickness to insulator thickness and the conductivity in the resistors. In addition, an important design parameter for the MHD generators is the maximum current density at the electrode-fluid interface.

8. When we developed our MHD model we focused on the use of heat transport rather than energy conservation. Our modeling decision was made primarily to best use the features readily available in COMSOL. A thorough investigation of the similarities and differences between the two possible models is an important next step.

   In addition, if heat transport rather than energy conservation is a reasonable model,

heat transfer in the casing may be very important in accurately modelling the temperature in the channel.

9. Can a multi-fluid description of the plasma in an MHD generator be used to explain arc formation on short time scales? In this formulation we would assume all the species in the flow, as well electrons and ions, are miscible but simulate each with an independent formulation of Navier-Stokes

$$\begin{cases} \rho_i \dfrac{D\mathbf{u}_i}{Dt} = -\nabla \cdot \boldsymbol{\tau}_i + \nabla p_i + \alpha_i \rho_i (\mathbf{E} + \mathbf{u} \times \mathbf{B}) \\ \dfrac{\partial}{\partial t} \rho_i = -\nabla \cdot (\rho_i \mathbf{u}_i) + R(\rho_i, \rho_j, T) \end{cases} \tag{8.1.6}$$

Here α_i is a proportionality between mass density and charge density of each species. Here we would for account for both the entire Lorentz force acting on each species and would account for the Hall effect very naturally. The function R is a reaction term which would account for non-equilibrium chemistry and the conversion of one specie to another. We would then couple these n fluid terms to Maxwell's Equations as follows.

$$\begin{cases} \dfrac{\partial}{\partial t}\mathbf{E} = -\dfrac{1}{\epsilon}\mathbf{J} + c^2 \mathbf{curl}\mathbf{B} \\ \dfrac{\partial}{\partial t}\mathbf{B} = -\mathbf{curl}\mathbf{E} \\ \mathbf{J} = \sum_i \alpha_i \rho_i \mathbf{u}_i. \end{cases} \tag{8.1.7}$$

In addition we would need to describe the thermodynamics of the system to extract temperatures for use in the reaction term. This would rely on the following heat equation.

$$\begin{cases} \rho C_p \left(\dfrac{\partial}{\partial t} T + \mathbf{u} \cdot \nabla T \right) = -\mathrm{div} K \nabla T + Q \\ \rho = \sum_i \rho_i \end{cases} \tag{8.1.8}$$

Correctly formulating the function $\mathbf{u}$ is not immediately obvious. Will the temperature advect with mean of the velocity or the sum of the velocities of all species?

This model is obviously significantly more complex. However, it may be able to account to describe significantly more complex physics at the electrode wall -fluid flow interface. Perhaps this formulation would allow the description of arcing as a boundary layer instability.

BIBLIOGRAPHY

1. D. N. Arnold, R. S. Falk, and R. Winther, *Finite element exterior calculus, homological techniques, and applications*, Acta Numerica, 15 (2006), pp. 1–155.

2. L. Beirão da Veiga, K. Lipnikov, and G. Manzini, *The Mimetic Finite Difference Method for Elliptic Problems*, Springer, 2014.

3. L. Beirao da Veiga, F. Brezzi, A. Cangiani, G. Manzini, and A. Marini, L. D. an Russo, *Basic priniciples of virtual element methods*, Math. Mod. Meth. Appl. S., 23 (2013), pp. 199–214.

4. L. Beirao da Veiga, F. Brezzi, and A. Russo, *Mixed virtual element methods for general second order elliptic problems on polygonal meshes.* `http://arxiv.org/abs/1506.07328`, 2015.

5. D. Boffi, F. Brezzi, and M. Fortin, *Mixed Finite Element Methods and Applications*, Springer, 2013.

6. V. A. Bokil and N. L. Gibson, *Analysis of Spatial High-Order Finite Difference Methods for Maxwell's Equations in Dispersive Media*, IMA J. Numer. Anal., 32 (2012), pp. 926–956.

7. V. A. Bokil, N. L. Gibson, V. Gyrya, and D. A. McGregor, *Dispersion reducing methods for edge discretizations of the electric vector wave equation*, J. Comput. Phys., 287 (2015), pp. 88–109.

8. V. A. Bokil, N. L. Gibson, D. A. McGregor, and C. R. Woodside, *Toward estimating current densities in magnetohydrodynamic generators*, J. Phys. Conf. Ser., 640 (2015), p. 012032.

9. V. A. Bokil, V. Gyrya, and D. A. McGregor, *A dispersion minimized mimetic method for a cold plasma model*, Submitted to ECCOMAS, (2016).

10. F. Brezzi and A. Buffa, *Innovative mimetic discretizations for electromagnetic problems*, Journal of Computational and Applied Mathematics, 234 (2010), pp. 1980 – 1987.

11. G. C. Cohen, *Higher-Order Numerical Methods for Transient Wave Equations*, Springer, 2002.

12. G. C. Cohen, *Higher Order Numerical Methods for Transient Wave Equations*, Springer, 2002.

13. S. M. Cox and P. C. Matthews, *Exponential time differencing for stiff systems*, J. Comput. Phys., 176 (2002), pp. 430–455.

14. S. A. Cummer, *An Analysis of New and Existing FDTD Methods for Cold Plasma and a Method for Improving Accuracy*, IEEE Trans. Antennas Propag., 45 (1997), pp. 392–400.

15. A. Fisher, R. N. Rieben, G. H. Rodrigue, and D. A. White, *A generalized mass lumping technique for vector finite-element solutions of the time-dependent maxwell equations*, IEEE Trans. on Antennas Propag., 53 (2005).

16. P. Fritzer, L. L. Lengyel, and K. J. Witte, *Self consistent calculation of the gasdynamic and electrical properties of a two-dimensional mhd flow*, Proc. 12th Symp. on Engineering Spects on MHD, Argonne, Ill., (1972).

17. N. L. Gibson, *A polynomial chaos method for dispersive electromagnetics*, Communications in Computational Physics, 18 (2015), pp. 1234–1263.

18. D. J. Griffiths, *Introduction to Electrodynamics (3rd Edition)*, Benjamin Cummings, 1998.

19. M. Guddati and B. Yue, *Modified integration rules for reducing dispersion error in finite element methods*, Comput. Methods Appl. Mech. Engrg., 193 (2004), pp. 275–287.

20. V. Gyrya and K. Lipnikov, *High-order mimetic finite difference method for diffusion problems on polygonal meshes*, J. Comput. Phys., 227 (2008), pp. 8841–8854.

21. V. Gyrya and K. Lipnikov, *M-Adaptation method for acoustic wave equation on square meshes*, J. Comput. Acoust., 20 (2012), pp. 1250022–1 – 1250022–23.

22. Y. Hao and R. Mittra, *FDTD Modeling of Metamaterials: Theory and Applications*, Artech House, 2008.

23. J. D. Huba, *Hall Magnetohydrodynamics: A Tutorial*, vol. LNP 615, Springer, 2003.

24. J. M. Hyman and M. Shashkov, *Mimetic finite difference methods for maxwell's equations and the equations of magnetic diffusion*, Prog. Electromagn. Res., 32 (2001), pp. 89–121.

25. J. D. Jackson, *Classical Electrodynamics*, John Wiley & Sons, 3 ed., 1999.

26. B. Jiang, J. Wu, and L. Povinelli, *The origin of spurious solutions in computational electromagnetics*, J. Comp. Phys., 125 (1996), pp. 104–123.

27. C. Jo, C. Shin, and J. H. Suh, *An optimal 9-point, finite difference, frequency-space, 2-D scalar wave extrapolator*, Geophysics, 61 (1996), pp. 529–537.

28. S. Krenk, *Dispersion-corrected explicit integration of the wave equation*, Comput. Methods Appl. Mech. Engrg., 191 (2001), pp. 975–987.

29. J. Lee, D. K. Sun, and Z. J. Cendes, *Tangential vector finite elements for electromagnetic field computation*, IEEE Trans. Magn., 27 (1991), pp. 4032–4035.

30. J. M. Lee, *Introduction to Smooth Manifolds*, Springer, 2003.

31. R. J. LeVeque.

32. J. Li and Y. Huang, *Time-Domain Finite Element Methods for Maxwell's Equations in Metamaterials*, Springer, 2013.

33. K. Lipnikov, G. Manzini, F. Brezzi, and A. Buffa, *The mimetic finite difference method for the 3d magnetostatic field problems on polyhedral meshes*, J. Comput. Phys, 230 (2011), pp. 305–328.

34. K. Lipnikov, G. Manzini, and M. Shashkov, *Mimetic finite difference method*, J. Comput. Phys., 257 (2014), pp. 1163–1227.

35. V. R. Malghan, *History of mhd power plant development*, Energy Convers. Mgmt., 37 (1996), pp. 569–590.

36. H. K. Messerle, N. L. Ho, and L. P. Heffernan, *Electrical breakdown of electrode boundary layers*, Proc. 12th Symp. on Engineering Aspects of MHD, Argonne Ill., (1972).

37. P. Monk, *An Analysis of Nédélec's method for the Spatial Discretization of Maxwell's Equations*, J. Comput. Appl. Math., 47 (1993), pp. 101–121.

38. ——, *Finite element methods for Maxwell's equations*, Oxford University Press, 2003.

39. P. Monk, *Finite Element Methods for Maxwell's Equations*, Clarendon Press, 2003.

40. R. Mullen and T. Belytschko, *Dispersion analysis of Finite Element semidiscretizations of the two-dimensional wave equation*, Int. J. Numer. Meth. Eng., 18 (1982), pp. 11–29.

41. G. Mur, *The finite-element modeling of three-dimensional electromagnetic fields using edge and nodal elements*, IEEE Trans. Antennas Propag., 41 (1993), pp. 948–953.

42. ——, *Edge elements, their advantages and their disadvantages*, IEEE Trans. Magn., 30 (1994), pp. 3552–3557.

43. G. Mur and I. E. Lager, *On the causes of spurious solutions in electromagnetics*, Electromagnetics, 22 (2002), pp. 357–367.

44. J. C. Nédélec, *Mixed finite elements in* $\mathbb{R}^3$, Numer. Math., 35 (1980), pp. 315–341.

45. ——, *A new family of mixed finite elements in* $\mathbb{R}^3$, Numer. Math, 50 (1986), pp. 57–81.

46. N. S. Novich, W. Unkel, M. Martinez-Sanchez, and E. Harmon, *Voltage drop and arcing characteristics of non-slagging metallic electrodes in mhd generators*, 19th Symp. on Engineering Aspects of MHD, Tullahoma, TN, (1981).

47. D. A. Oliver and M. Mitchner, *Nonuniform electrical conduction in magneto-hydrodynamic channels*, Am. Inst. Aeronautics Astronautics J., 8 (1967), pp. 1424–1432.

48. B. Parent, M. N. Shneider, and S. O. Macheret, *Generalized ohm's law and potential equation in computational weakly-ionized plasmadynamics*, J. Comput. Phys., 230 (2011), pp. 1439–1453.

49. P. G. Petropoulos, *The wave hierarchy for propagation in relaxing dielectrics*, Wave Motion, 21 (1995), pp. 253 – 262.

50. P. G. Petropoulos, *Analysis of exponential time-differencing for FDTD in lossy dielectrics*, IEEE Trans. Antennas Propag., 45 (1997), pp. 1054–1057.

51. R. Rosa, *Magnetohydrodynamic energy conversion*, McGraw-Hill, second ed., 1987.

52. R. J. Rosa and R. J. Pollina, *Corrosion and arc erosian in mhd channels*, Tech. Rep. DE-FG22-88PC88928, Montana State University, 1992.

53. I. e. a. Sadovnik, *Electrode arcing phenomena in mhd generatros*, 19th Symp. on Engineering Aspects of MHD, Tullahoma, TN.

54. A. Sescu, R. Hixon, and A. A. Afjeh, *Multidimensional optimization of finite difference schemes for Computational Aeroacoustics*, J. Comput. Phys., (2008), pp. 4563–4588.

55. W. S. Smith, A. Razmadze, X. Shao, and J. L. Drewniak, *A hierarchy of explicitly low-dispersion FDTD methods for electrically large problems*, IEEE Trans.Antennas and Propag., 60 (2012), pp. 5787–5800.

56. I. Stekl and R. G. Pratt, *Accurate viscoelastic modeling by frequency-domain finite difference using rotated operators*, Geophysics, 63 (1998), pp. 1779–1794.

57. D. Sun, J. Manges, X. Yuan, and Z. Cendes, *Spurious modes in finite-element methods*, IEEE Antennas Propag Magazine, 37 (1995), pp. 12–24.

58. A. Taflove and S. C. Hagness, *Computational Electrodynamics: The Finite-Difference Time-Domain method*, Artech House, Norwood, MA, 3rd ed., 2005.

59. D. A. White, *Orthogonal vector basis functions for time domain finite element solution of the vector wave equation [em field analysis]*, IEEE Trans. Magn., 35 (1999), pp. 1458–1461.

60. C. R. Woodside, *Direct power extraction with oxy-combustion: An overview of magnetohydrodynamic research activites at the NETL-Regional University Alliance.* Pittsburgh Coal Conference, 2012.

61. C. R. Woodside and P. King, *Characterizing arc motion and distribution during vacuum arc remelting*, in TMS2009 International Symposium on Liquid Metal Processing and Casting. Santa Fe: TMS Publications, vol. 75, 2009.

62. K. Yee, *Numerical solution of initial boundary value problems involving maxwell's equations in isotropic media*, IEEE Trans. Antennas Propag., 14 (1966), pp. 302–307.

63. K. S. Yee, *Numerical solution of initial boundary value problems involving maxwell's equations in isotropic media*, IEEE Trans. Antennas and Propag., 14 (1966), pp. 302–307.

64. B. Yue and M. N. Guddati, *Dispersion-reducing finite elements for transient acoustics*, J. Acoust. Soc. America, 118 (2005), p. 2132.